

Role of the Intermediate Filament Protein Nestin in Modulating Growth Cone
Morphology and Behavior

Christopher Joseph Bott
Rock Hill, South Carolina

B.S., Clemson University, 2009

A Dissertation presented to the Graduate Faculty
of the University of Virginia in Candidacy for the Degree of
Doctor of Philosophy

Department of Cell Biology

University of Virginia
November, 2019

Abstract

Axonal patterning in the neocortex requires that responses to an individual guidance cue vary among neurons in the same location, and within the same neuron over time, to establish the varied and diverse sets of connections seen in the developed brain. The growth cone is the structure at the tip of a growing axon that interprets these guidance cues and translates them into morphological rearrangements. Different brain regions often reuse the same individual guidance cue molecules. Consequently, the sensitivity or type of response the growth cone has to various guidance cues varies over the course of maturation of the neuron, as the growth cone weaves its way into and out of different brain regions in order to reach its target. In addition there are different responses between different parts of the same neuron: the dendritic growth cones respond very differently compared to axonal growth cones to the same guidance cue using the same basic cytoskeletal proteins. How a growth cone responds to a guidance cue is thus a complex cell biological question and the molecular mechanism are not well understood. I propose that the atypical intermediate filament protein nestin, in its role as a kinase modulator, functions in this manner to change responsiveness to the same guidance cue in time and space.

Nestin is expressed highly in neural progenitors and is thus used widely as a progenitor marker. In my work, I discovered a subpopulation of mouse embryonic cortical neurons which transiently express nestin in their axons, but not in their dendrites. Since the prevailing view contends that intermediate filaments are not present in growth cones, intermediate filaments are understudied in developing axons, with very few studies looking into the role of intermediate filaments in axon guidance. Many studies, on the other hand, investigate the role of actin and microtubule dynamics in growth cones. I used high resolution imaging to demonstrate that nestin containing filaments are present in the distal axon and the growth cone and even extend into peripheral regions of the growth cone including filopodia. Nestin expression is thus not restricted to neural progenitors but persists for 2-3 days at lower levels in newborn neurons. Since protein expression level in progenitors is far greater than in axons, without careful and technically challenging analysis axonal nestin may be easily (although incorrectly) dismissed as background staining- particularly *in vivo*.

This early period of neuronal maturation, in which nestin protein can be detected, is a critical period that establishes the orientation of the axon and its future trajectory. I initially found that nestin-expressing neurons have smaller growth cones, suggesting that nestin affects cytoskeletal dynamics. Nestin, unlike other intermediate filament subtypes, regulates Cdk5 kinase via binding the Cdk5 activator p35. Cdk5 is a critical kinase that operates during early neuronal development, and is part of the downstream signaling machinery of the repulsive axon guidance cue, Sema3a. Sema3a is important for initial axon positioning and organization within the intermediate zone of the developing cortex. I find that nestin selectively facilitates the phosphorylation of the lissencephaly-linked protein doublecortin (DCX) by Cdk5/p35, but surprisingly the phosphorylation of other Cdk5 substrates is not affected by nestin. DCX is a microtubule binding protein, which stabilizes microtubules. Phosphorylation of DCX by Cdk5 decreases microtubule binding and thus induces microtubule instability. DCX and DCX phosphorylation have previously been shown to be important for axon guidance. I uncover that the Cdk5 substrate selectivity imparted by nestin is based on the ability of

nestin to specifically interact with DCX, but not with other Cdk5 substrates. In addition, I find that other intermediate filaments do not interact with DCX. Nestin thus creates a selective scaffold for DCX with activated Cdk5/p35 to facilitate robust phosphorylation. Neurons that express nestin are more sensitive to the repulsive effects of Sema3a, and nestin siRNA reduces growth cone sensitivity to Sema3a. A nestin mutant that does not interact with DCX or p35 and does not affect DCX phosphorylation, does not have the same effects on growth cone morphology as WT nestin. Lastly, I use cortical cultures derived from DCX knockout mice to show that the effects of nestin on growth cone morphology and on Sema3a sensitivity are DCX-dependent, thus suggesting a functional role for the specific DCX-nestin complex in neurons. DCX null neurons are more sensitive to Sema3a in a nestin-independent manner. This observation suggests that DCX is operating as a brake or buffer to resist the cytoskeleton destabilizing effects induced by Sema3a. Nestin-enhanced Cdk5 phosphorylation of DCX removes the DCX brake on microtubules and thus DCX dissociates from microtubules in WT neurons.

I propose that nestin changes growth cone behavior by regulating subsets of substrates that are phosphorylated by intracellular kinase signaling downstream of guidance cues in developing neurons. Thus, the transient expression of nestin could allow for temporal and/or spatial modulation of a neuron's response to Sema3a, particularly during early axon guidance. Temporally, at 2-3 days, when nestin expression can no longer be detected *in vitro*, is the same time period *in vivo* in which cortico-cortical axons are growing into a Sema3a rich region- and these are insensitive to the repulsive effects of Sema3a. This is consistent with the loss of nestin during that time period. Spatially, nestin's absence from dendrites may play a role in the lack of sensitivity of dendrites to the repulsive effects of Sema3a.

This is one example of how generalized signaling pathways can have variable signaling outcomes depending on which signaling modifying proteins are present. For example, the absence or presence of signaling modifying proteins, such as nestin, which can alter the subsets of substrates that are phosphorylated, may provide a mechanism how Cdk5 can be involved in both the attractive response of dendrites to Sema3a, and the repulsive response of axons to the same guidance molecule. This raises the question if other intermediate filaments may be playing similar roles. The exquisite developmental and cell type variability of intermediate filament expression could in principle provide unique signaling chemistries depending on which intermediate filaments are expressed. Intermediate filaments may thus have functions beyond mechanically providing a structure or skeleton to cells, but modify signaling networks.

Acknowledgments

I would first like to thank my advisor Bettina Winkler. Her enthusiasm inspired me, and her pragmatism kept me grounded. Bettina has provided me with an ideal amount of support, independence, and at times, patience. I truly appreciate her permitting me to pursue ideas and concepts wherever they led, and never bounding me by the lab's expertise. I will always be grateful to her for allowing me to pursue this degree in her lab.

I want to thank all the members of the Winckler lab for so much help along the way. First of all, Chan Choo is one of the most knowledgeable scientists that I have ever worked with, and I am thankful that she was able to remind and inform me of the limitations of our techniques, as well as best practices. I want to thank my fellow graduate student lab mate Kelly Barford, who started in this lab with me and finished her degree well ahead of me, and in doing so provided me inspiration to keep going. Laura Digilio was just so very helpful with so many day to day tasks, and helped me keep my mouse colony down to reasonable numbers. Lloyd McMahon was a fantastic bench mate, whose knowledge of the finer points of the chemistries of our techniques provided frequent and often heated conversation. I think we both helped each other optimize our experimental techniques. Finally, I want to thank our undergraduates in the lab, Meheret Kinfe and Isabelle Witteveen, for their help in processing data, and more importantly, providing a fresh dose of enthusiasm in the lab.

I am thankful to the members of my committee, Noelle Dwyer, Xiaowei Lu, Doug DeSimone, and the frequently added member Judy White. Other members of the cell biology department that both inspired, encouraged, or helped me in various ways are David Castle, Jim Casanova, and Mary Hall.

Finally I want to thank my encouraging family and supportive Wife. My parents have always been an inspiration for doing hard work and the importance of completing a task. Their support gave me the confidence to pursue the goals that I was passionate about, even though it was not always a linear path. My sister provided me much needed encouragement along the way. And finally, I want to thank my wife Emily, who has faced the challenges of us both pursuing degree's in higher education, and I think it has strengthened our bond. I have been truly inspired by her accomplishments, and I could not have done this without her.

Table of Contents

Abstract

Acknowledgements

Table of Contents

List of Figures

Chapter 1: Introduction intermediate filaments, the Doublecortin, and the growth cone

- 1.1 A brief introduction to intermediate filaments
 - 1.1.1 IF proteins possess conserved structural features which underlie their ability to assemble into filaments.
 - 1.1.2 IF proteins are encoded by a large multi-gene family subdivided into assembly classes.
 - 1.1.3 IF proteins are expressed in a highly cell-lineage restricted manner.
 - 1.1.4 Human diseases are linked to IFs.
 - 1.1.5 IF networks are dynamic.
- 1.2 Roles of intermediate filaments – old truths and new concepts
 - 1.2.1 IFs provide structural support to cells.
 - 1.2.2 Beyond structure - IFs modulate signaling cascades.
 - 1.2.3 Integrating structure and signaling – mechanosensitive signaling roles of IFs.
- 1.3 Intermediate filaments in neurons
 - 1.3.1 The neurofilament class of IFs are the main structural IF in mature axons.
 - 1.3.2 Neurofilaments – still many surprises and open questions!
 - 1.3.3 Intermediate filaments in developing neurons are structurally and functionally diverse.
- 1.4 Nestin: an unconventional intermediate filament protein.
 - 1.4.1 Roles for nestin in NPCs
 - 1.4.2 Nestin knockout mice – great confusion from different mouse models.
 - 1.4.3 Nestin – a potent regulator of Cdk5 signaling cascades.
 - 1.4.4 Nestin – a potent scaffold for other signaling molecules.
- 1.5 Doublecortin and its role in the growth cone
- 1.6 Research Objectives

Figures

Chapter 2: Nestin in immature embryonic neurons affects axon growth cone morphology and Semaphorin3a sensitivity

- 2.1 Introduction
- 2.2 Material and methods
- 2.3 Results
- 2.4 Discussion

Figures

Chapter 3: Nestin selectively facilitates the phosphorylation of the Lissencephaly-linked protein doublecortin (DCX) by Cdk5/p35 to regulate growth cone morphology and Sema3a sensitivity in developing neurons.

- 3.1 Introduction

3.2 Materials and Methods:

3.3 Results

3.4 Discussion

Figures

Chapter 4: Overview and summary of major findings

4.1 Overview

4.2 Nestin cell type expression, localization, and functional relevance

4.3 Nestin selectively facilitates phosphorylation of DCX by Cdk5 through scaffolding

4.4 Summary

References

Appendix 1: Different doublecortin (DCX) patient alleles show distinct phenotypes in cultured neurons: evidence for divergent loss-of-function and “off-pathway” cellular mechanisms.

List of Figures

Chapter 1

Figure 1: Assembly of intermediate filaments

Figure 2: Neuronally expressed IF's throughout development

Figure 3: Intermediate filaments are enriched in the distal regions of growing axons.

Figure 4: DCX phosphorylation in growth cone in response to guidance cues

Figure 5: Contralateral projecting cortical axons grow into a region containing repulsive cues

Chapter 2

Figure 6: Nestin protein expression persists in immature primary cortical neurons in culture.

Figure 7: Nestin protein antibody controls and cell population comparisons

Figure 8: Nestin-expressing neurons are observed in multiple rodent and human culture models

Figure 9: Nestin is expressed in sub-populations of cortical axons in developing cortex

Figure 10: Identical staining pattern seen in E16 mouse cortical axons with two different anti-Nestin mouse monoclonal antibodies

Figure 11: The level of nestin expression in neurons influences growth cone morphology and response to Semaphorin3a

Figure 12: Nestin depletion results in abnormal growth cone morphology and resistance to Semaphorin3a

Figure 13: Multiple single nestin siRNA's lead to nestin depletion and associated morphological changes

Chapter 3

Figure 14: Nestin selectively augments phosphorylation of DCX by Cdk5, but not of other Cdk5 substrate proteins

Figure 15: Nestin, but not α -internexin, promotes phosphorylation of DCX by Cdk5

Figure 16: Nestin forms a complex specifically with DCX

Figure 17: Nestin co-localizes with DCX-MT bundles

Figure 18: Nestin colocalizes with DCX in the axons of newly born neurons *in vitro* and *in vivo*

Figure 19. Nestin scaffolds Cdk5 and DCX to promote DCX phosphorylation

Figure 20: The T316D mutation in nestin affects p35 and DCX binding, as well as DCX phosphorylation, but not incorporation into vimentin filaments

Figure 21: Binding to p35 and/or DCX is required for nestin's effect on growth cone size

Figure 22: In the absence of DCX, nestin overexpression does not result in small growth cones

Figure 23: DCX is a Cdk5 substrate downstream of Sema3a, and DCX null neurons respond to Sema3a in a nestin independent manner.

Chapter 1: Intermediate filaments in neurodevelopment: from structure to signaling scaffolds and back again.

Adapted from review for “Cytoskeleton”

1.1 A brief introduction to intermediate filaments

Intermediate filaments (IFs) together with actin-based microfilaments and microtubules constitute the vast majority of the cellular cytoskeleton. Cytoplasmic IFs were first described in the late 1960s, and elegant biochemistry *in vitro* with purified proteins led to important insights into their assembly. Unlike actin filaments and microtubules, IFs assemble in the absence of nucleotides and are largely insoluble *in vitro*, although some aspects of their dynamics may require ATP (Robert *et al.*, 2015). Cloning of the IF genes allowed probing of how they assemble not only *in vitro* but also inside cells and has led to substantial progress in understanding their roles in cellular physiology. Because IFs are very stable *in vitro* and largely insoluble in cells, they were mostly thought of as the stable “skeleton” in cytoskeleton. In contrast to microtubules and microfilaments, most IFs do not disassemble and reassembly rapidly, and their high stability provides mechanical support to cells. By some estimates, subunit exchange occurs only at the rate of about 1 tetramer per 200 tetramers per hour (Köster *et al.*, 2015; Herrmann and Aebi, 2016). Excellent reviews already exist that discuss the many aspects of IF structure and function, and we will first summarize the main themes that have emerged from an extensive body of work over many years in many labs.

1.1.1 IF proteins possess conserved structural features which underlie their ability to assemble into filaments.

IF proteins consist of an N-terminus (typically ~ 100 amino acids, but both longer and shorter head domains also occur), a central α -helical rod domain (~310 amino acids), and a C-terminus of variable lengths (from ~ 15 amino acids to > 1400 amino acids). The central rod domain allows formation of coiled-coil dimers which then assemble into higher order filaments. The N-terminal head domains and C-terminal tail domains are non-helical and contain intrinsically unstructured segments. The head domain is required for assembly whereas the tail domain protrudes laterally from the assembled filament, but is not required for assembly.

The first step in assembly is the formation of parallel dimers which then form anti-parallel tetramers (Figure 1). The tetramer is apolar and forms the basis for an apolar assembled filament. Unlike microtubules and actin filaments, therefore, the two ends of assembled IFs are identical. Dimers and tetramers of many IF proteins are exceptionally stable and can form *in vitro* in 5M urea (Kreplak, Aebi and Herrmann, 2004; Köster *et al.*, 2015). *In vitro*, eight tetramers can laterally associate to form unit length filaments (ULF) which then join end-to-end to form filaments of increasing lengths (Figure 1). The ULF can thus be envisioned as being the assembly-competent subunit in this model (Köster *et al.*, 2015). *In vitro* assembled IF preparations readily show filaments of various lengths as well as smaller particles, and evidence for stable tetramers and ULFs *in vitro* is overwhelming. There is also increasingly good evidence that tetramers and small particles (likely ULFs) can exist inside cells (Soellner, Quinlan and Franke, 1985; Herrmann, Aebi and Mu, 2004; Bernot, Lee and Coulombe, 2005; Kim and Coulombe, 2007), but overall there is a strong energetic driving force towards assembled filaments *in vitro* and *in vivo*. IFs thus largely exist as insoluble species (filaments of various lengths) with only a small proportion of soluble subunits which likely correspond to tetramers and ULFs (Soellner, Quinlan and Franke, 1985; Chang and Goldman, 2004; Kim and Coulombe, 2007), although the actual ratio of soluble to insoluble IFs varies between cell

types, IF species, and conditions. The initial filament ultimately undergoes a complex conformational change to compact to the ~10 nm diameter of the mature filament commonly observed inside cells. For a recent review on assembly, see Herrmann Aebi, also Robert.

1.1.2 IF proteins are encoded by a large multi-gene family subdivided into assembly classes.

Cytoplasmic IF genes were initially only identified in vertebrate genomes (except for lamins- which are universal in metazoans), but IF-like genes have more recently been identified in some invertebrate genomes as well (Herrmann and Strelkov, 2011; Herrmann and Aebi, 2016). For instance, *C. elegans* has 11 genes encoding IF proteins. Of these 11 genes, four are essential genes (Karabinos *et al.*, 2001). Notably, no IF-related genes have been identified in *Drosophila*, although some intermediate filament-like proteins have been described (Cho *et al.*, 2016). Vertebrate genomes contain an even larger number of IF genes. For instance, there are over 70 genes encoding IF proteins in the human genome, giving rise to an astounding isotype variety. IF genes are classified into distinct classes based on sequence homology, some of which can form heteropolymers whereas others cannot (Chang and Goldman, 2004). The largest class by far are the keratins (54 functional genes in humans) which are subdivided into acidic (class I) and basic (class II) keratins. Keratins can only assemble via obligate heterodimers of one acidic and one basic keratin. Class III IFs include vimentin (VIM), desmin, peripherin, and glial fibrillary acidic protein (GFAP). Class III IF proteins are capable of forming homo-oligomers. Class IV includes all of the neuronally expressed IF genes, such as the triplet neurofilament proteins, NF-L, NF-M, and NF-H, as well as α -internexin (INA)- which is sometimes considered a 4th neurofilament (Yuan *et al.*, 2006). INA and NF-L are in principle capable of homo-oligomerization *in vitro* whereas NF-M and NF-H require heterodimerization with NF-L. Nestin is an unconventional IF protein and is sometimes classified with Class IV or in a separate class VI (Lendahl, Zimmerman and McKay, 1990). Because of its particularly short head domain, nestin is incapable of forming homo-polymers and usually co-assembles with VIM or INA (Steinert *et al.*, 1999). NFM and NFH also cannot form homo-polymers (Lee *et al.*, 1993). This review will focus primarily on the neuronally expressed IF proteins, but will draw on insights gleaned from work on keratins and VIM, in particular, to illustrate certain points. Class V is comprised of the nuclear lamins which will not be discussed in this review.

1.1.3 IF proteins are expressed in a highly cell-lineage restricted manner.

One of the striking features of IFs is that they are expressed in a highly cell-lineage specific manner and are thus often used as convenient markers for specific lineages. For instance, keratins are expressed overwhelmingly in epithelial cells whereas the triplet NF proteins are restricted to expression in neurons. Within the nervous system, the peripheral nervous system contains peripherin while the central nervous system does not. α -internexin is present in adult central nervous system, but absent from adult peripheral nerves (Yuan *et al.*, 2012). Desmin is highly expressed in muscle whereas GFAP is expressed in astrocytes. This tight regulation of IF subtype expression, which has the potential to give each cell type a “unique cytoskeletal architecture” (Chang and Goldman,

2004; Mitew *et al.*, 2013), begs the question of what cell type-specific functions the IF proteins carry out and to what degree IF proteins are functionally interchangeable.

There are two obvious ways to think about the potential functional relevance of the cell-lineage specificity of IF protein expression. The first is to ask how assembled filaments made from different IF proteins might be different from each other to impart cell type-specific functions (stiffness, dynamics, etc), and the second is to ask if different IF subtypes have different binding partners that would change the functionality of the filament in different cell types. This review will be focusing on the latter scenario. With regard to the first question of whether filaments made from different subtypes are structurally distinct, whether they are more stable or more dynamic, and whether their assembly or disassembly is regulated differently dependent on the IF subtype, the answer is clearly yes. For example, vimentin and INA filaments have very similar axial length dimensions, but INA filaments are more stable than VIM filaments *in vitro* (Steinert, Marekov and Parry, 1999). In addition, there are differences in the head domains which can lead to differential assembly or disassembly since phosphorylation of head domain residues are particularly important in slowing assembly inside cells. Secondly, the tail domains can be as short as 15 amino acids (in human keratin 19; (Herrmann and Aebi, 2016)) or as long as 1497 amino acids (in rat nestin; (Lendahl, Zimmerman and McKay, 1990)) and the tails protrude laterally from the filament. If the protruding tail is long, it gives some IFs a “bottle brush” appearance by EM (Kornreich *et al.*, 2015; Herrmann and Aebi, 2016). Inside cells, the protruding long tails are thought to change the spacing of filaments and/or the interaction with other cytoskeletal components. In addition, there are a large number of phosphorylation sites on the repeat motifs present in the tail domains of a subset of IF proteins, which substantially change the charge distribution and conformation of the protruding tails. These IFs are thus structurally distinct based on their tails. Regarding the second possibility of recruiting distinct binding partners to create functional diversity, the divergent tail domains are a prime candidate since they vary greatly among the subtypes and can bind to different IF associated proteins (IFAPs). There is thus much interest in divergent structural features, post-translational modifications, and binding interactions of the distinct tail domains in different IF proteins. We will discuss IF binding proteins and their roles below.

Another poorly understood aspect of IF subtype diversity relates to cell types that express more than one IF protein subtype at the same time and could thus make distinct IFs that contain a mixture of subunits. This is certainly true for neural progenitors which express vimentin and nestin, but also for neurons which express many IF proteins at the same time (such as NF-L, -M, -H, and INA). For example, differences in the rod domains of nestin and vimentin change the stability and ease of subunit exchange of filaments made of pure vimentin compared to a nestin-vimentin hetero-polymer (Steinert *et al.*, 1999). Nestin containing vimentin IF networks can more quickly disassemble when modified by cyclin dependent kinases (Chou *et al.*, 2003). It has been postulated that this is important during cell division, when the IF cytoskeleton must be disassembled to allow for cytokinesis. In support of this claim, nestin is often associated with rapidly dividing cell types, both developmentally (various tissue progenitors; (Bernal and Arranz, 2018)) and in cancers (Rani *et al.*, 2006; Neradil and Veselska, 2015). Thus, this is an example of how a heteropolymer can behave and function very differently than a homo-polymer in the same context. Some of the intriguing questions relate to whether all IF filaments in

such cells have the same IF composition or if regional differences occur as to the relative incorporation of one or the other IF protein into the IF filament locally. Existing examples of IF protein types segregating into subdomains within a single polymer (Leduc and Manneville, 2017) illustrates how this type of segregation can only be seen with careful, high resolution/magnification, multi-channel/color microscopy. Immunolabeling experiments of cell lines (Hela, PtK2) showed that there can even be two distinct, non-intermixing IF networks comprised of keratins and vimentin (Osborn, Franke and Weber, 1980; Eriksson *et al.*, 2009). This serves as the basis for another way to classify the different IF species, i.e. by assembly group: IF proteins are grouped together if they can assemble together into hetero polymers. The acidic (class I) and basic (class II) keratins comprise assembly group 1, which are cytosolic and generally the most stable/static. Assembly group 2 is comprised of Class III and class IV IF proteins, which are also cytosolic but generally more dynamic in terms of assembly and rearrangement. Assembly group 3 is comprised of the nuclear associated lamins, which are also very stable. These three groups can exist as structurally distinct filament systems within a single cell (Herrmann, Aebi and Mu, 2004). This local diversity could additionally diversify the roles IFs play in each cell type.

1.1.4 Human diseases are linked to IFs.

IFs in many cell types play critical roles which manifest by the devastating diseases linked to mutations in these genes. Examples include dysfunctional epidermal keratins (keratins 5 and 14, in particular) which lead to fragile skin with extensive blistering (epidermolysis bullosa simplex; (Kim and Coulombe, 2007; Omary, 2009)). Keratins are among the most stable IFs with only a small soluble pool and the phenotypes associated with keratin mutations suggest that keratins are responsible for mechanical integrity of the epithelium. Another example is the muscle-specific IF desmin which enables muscle cells to withstand the mechanical stress of contractility. Mutations in desmin thus manifest as cardiomyopathies. Several of the neuronally expressed IF genes are linked to Amyotrophic Lateral Sclerosis (ALS) or Charcot-Marie-Tooth disease which cause neurodegeneration in the peripheral nervous system (Brownlee *et al.*, 2002; Omary, 2009). Again, one obvious interpretation is that neurofilaments contribute to the mechanical integrity of peripheral nerves by providing protection from stretching and deformation. About half of the human IF genes (Omary, 2009) have so far been genetically linked to human diseases, but many have not. This suggests either that these non-linked genes play essential roles (with no live human births) or, alternatively, that they play more subtle roles that can be compensated for by other pathways, and their absence does not lead to mechanical lability of the expressed cell. Thirdly, links to human diseases for these IF genes might still be discovered in the future.

Disease-associated mutations in neurofilament (NF) genes are frequently not loss-of-function, but act dominantly. The proposed mechanism for such dominant pathology is based on the observation that abnormal aggregates of NF species form and accumulate in neurons (Didonna and Opal, 2019). These might be toxic and lead to the dominant phenotypes of these disease-associated alleles. Abnormal accumulation of IF proteins has also been noted in multiple degenerative diseases (Alzheimer's, Parkinson's, Huntington's, spastic paraplegia, spinal muscular atrophy, giant axonal neuropathy), neuropsychiatric disorders (drug addiction, schizophrenia, bipolar disorder), and others

(cancer, diabetic neuropathy, traumatic brain injury)(Omary, Coulombe and Mclean, 2004; Godsel, Hobbs and Green, 2008; Perrot *et al.*, 2008; Eriksson *et al.*, 2009; Omary, 2009; Perrot and Eyer, 2009; Mahammad *et al.*, 2013; Yuan and Nixon, 2016; Didonna and Opal, 2019; Sharma *et al.*, 2019). These diseases and disorders can often occur even in the apparent absence of mutations in the neuronal IF genes. These aggregates are presumably the result of changes in expression, post-translational modification, or dysregulation of assembly/disassembly of IFs as a secondary consequence of the pathological process. To what degree these IF aggregates contribute to the observed pathologies is not clear.

Knockout mice have also contributed importantly to establishing a basic understanding of what roles IFs might be playing in tissues. An extensive discussion of mouse knockout phenotypes can be found in (Galou *et al.*, 1997; Toivola *et al.*, 2005; Perrot *et al.*, 2008; Battaglia *et al.*, 2019). Cell culture work had demonstrated defects in cell migration, mitosis, suppression of apoptosis, and other critical processes when IFs are impaired or depleted, so it was expected that most IF genes would be essential genes. When the first IF knockouts were generated, there was therefore much surprise that many of them were viable and fertile. For instance, the VIM KO mouse has no striking developmental defects. The lack of apparent phenotypes have led to the assessment that IFs are either redundant or play subtle and non-critical roles, especially in development (Eriksson *et al.*, 2009; Sanghvi-shah and Weber, 2017). Since these first reports, more extensive phenotypic analysis has uncovered multiple problems arising in some of the KO animals, demonstrating roles of IFs in later stages of tissue morphogenesis or in tissue maintenance and recovery from injury (Zhu, 1997; Eckes *et al.*, 2000; Weber, Bjerke and DeSimone, 2013). These phenotypes highlight the importance of IF proteins in imparting structural integrity to multicellular assemblies. It is of note that in *Xenopus* loss of keratin expression leads to early developmental abnormalities at the gastrulation stage more pronounced and earlier than those observed in mice (Baribault *et al.*, 1993; Sonavane *et al.*, 2017), raising interesting questions about redundancy among IF classes in mammals. In addition, IF proteins have emerged as important players during cell stress and after injuries. For instance, VIM KO mice show defects in injury responses and in wound healing (Eckes *et al.*, 2000; Cheng *et al.*, 2016). Phenotypes such as these may not be as apparent in mice that are kept in stress-, disease-, and predator-free laboratory vivarium where food and water are in abundance, but could become important to a mouse under strenuous conditions in the wild (thrive vs. survive). In addition, these more subtle defects might be accounted for by redundancy among IF subtypes or point to other functions which are not primarily related to imparting structural integrity to cells. We will discuss the mounting evidence for non-structural roles of IFs below.

1.1.5 IF networks are dynamic.

New tools have now demonstrated clearly that many IF networks are more dynamic than initially thought (Robert, Hookway and Vladimir I. Gelfand, 2016). Despite their stability, IF networks can undergo undulating movements, and can contract and rearrange without complete disassembly. For instance, in addition to long assembled filaments, smaller oligomers such as tetramers and small “particles” as well as short filaments (called “squiggles”) can be observed by live imaging which undergo dynamic behaviors such as lateral subunit exchange along filaments, annealing of short filaments

to make longer filaments, and transport along microtubules. In addition, severing of long filaments into shorter filaments has been observed. It is currently not understood how annealing or severing of IFs is regulated and if auxiliary proteins are required (Colakoglu and Brown, 2009).

How the assembly dynamics of IFs are regulated in time and space inside cells is not yet fully understood. There are clear indications that particles and non-filamentous pools of vimentins and keratins are more common at the periphery of cultured cell lines and that assembly is spatially regulated (Robert, Hookway and Vladimir I Gelfand, 2016). There is thus a striking non-homogeneous distribution of IFs in many cells. For example, when cells migrate collectively (as is the case in many instances of developmental tissue morphogenesis), keratin filaments need to be assembled from newly synthesized keratin subunits in a polarized fashion to coordinate polarization, directionality of motility, and communication across many cells (Sanghvi-shah and Weber, 2017). It has been known for a long time that IFs connect to a subset of cell contact sites, such as desmosomes and hemidesmosomes, where they are associated with specialized adhesion receptors and impart not only resistance to deformation for an individual cell, but also structural integrity across sheets of connected epithelial cells. Force transduction across cell-cell junctions is in fact required for reorganizing keratin networks from a radially symmetric “wagon wheel” configuration into a network which is polarized towards the rear of the cell. This polarized network of keratin IFs then in turn regulates actin dynamics and assembly in a polarized manner (Sonavane *et al.*, 2017)(see below for more details).

In addition to differential assembly of filaments to ensure directional motility, oligomeric forms of IFs might also be playing functional roles in dynamic cellular processes (Robert, Hookway and Vladimir I Gelfand, 2016), including cell motility. The preferential localization of oligomeric IF pools near the cell periphery of motile cells suggests that local disassembly might be critically involved in changing the mechanical properties and allowing local actin-driven motility (Robert, Hookway and Vladimir I Gelfand, 2016). In addition, IF proteins have been shown to be involved in some signaling pathway, both as filaments and as oligomers (Robert, Hookway and Vladimir I Gelfand, 2016). There are only a handful of such examples (see below), but our current understanding of the possible dynamic roles of oligomeric IF species is very likely to be quite incomplete. In fact, many of the early studies and characterization of neurofilaments was (and continue to be) performed on an insoluble fraction of bovine brain- which contains a very stable population of neurofilaments. The more soluble and probably dynamic population of neurofilaments were discarded in these preparations- yet observations on the insoluble pool have been generalized to all IF networks.

Another striking example of dynamic rearrangements of IFs is mitosis where VIM IFs completely disassemble prior to M phase (Sahlgren *et al.*, 2001; Chou *et al.*, 2003). This disassembly is triggered by phosphorylation of the head domain by cyclin-dependent kinases and is thus a highly regulated process. The importance of the intricate connections of signaling pathways impinging on IFs as a downstream target are increasingly obvious. The best documented IF connection with signaling proteins are kinases that phosphorylate IF protein head domain residues, resulting in disassembly of IFs. These kinases are often downstream of growth factor pathways and drive disassembly of IF networks. A separate signaling link to IFs which is only emerging and less well documented is the reverse causality: IF proteins are upstream in some signaling

cascades to affect the signaling output. This signaling modality of IFs will be discussed in more detail below.

1.2 Roles of intermediate filaments – old truths and new concepts

What roles do IFs play in cells? The best established role is one of providing structural support. This is an “old truth” and evidence supporting structural roles for IFs is overwhelming. New concepts for additional roles of IFs beyond structural support have arisen based on new tools that allow observation of IFs live inside cells and monitoring of their dynamic behaviors and signaling roles. We will highlight examples below.

1.2.1 IFs provide structural support to cells.

Based on extensive evidence, IFs have come to be viewed as forming a stable filament network that extends throughout the cytoplasm to provide structural support in many cell types. IFs have very unusual mechanical properties compared to MTs and MFs. IFs can be stretched (to 2.5 times their initial length) without breaking and can thus provide elastic support to cells under mechanical strain (Kreplak *et al.*, 2005). Cellular stiffness is also influenced by IFs, so the responses of cells to both compression as well as to stretching are dependent on the viscoelastic properties of IFs. Since IFs interact with cell-cell adhesion sites, IFs impart mechanical integrity not just to individual cells but also across multicellular assemblies (Sanghvi-shah and Weber, 2017).

In addition to acting as mechanical stabilizers in the context of their own filament system, IFs interact in complex ways with microtubules and microfilaments (Chang and Goldman, 2004). It has been known for a long time that when drugs are used in cultured cell lines to disassemble microtubules, IF networks will ultimately also collapse in a tight cage around the nucleus. Interdependent interactions have also been observed between IFs and microfilaments, especially for the keratin IF networks. One mechanism to account for the interdependence of the three cytoskeletal elements is the presence of linker proteins which bind IFs and also microtubules or microfilaments. The best known such example is plectin which binds to IFs (such as keratins, VIM, and desmin) as well as to actin and microtubules. Loss of plectin leads to mechanical instability of muscle and other tissues and thus phenocopies loss of the IF protein itself. Another IF binding protein which also binds microtubules and actin is BPAG1 (bullous pemphigoid antigen). Loss of BPAG1 in mice is associated with major defects in the skin as well as with sensory neuron degeneration (Leung *et al.*, 2001), again reminiscent of phenotypes associated with mutations in the IF genes themselves. More recently, Rudhira/BCAS3 (Breast Carcinoma Amplified Sequence 3) binds to intermediate filaments and microtubules. Loss of BCAS3 in mice results in an embryonic lethal (E9.5) phenotype due to severe disruption of vascular patterning and is important for endothelial cell migration (Shetty *et al.*, 2018; Joshi, Inamdar and Forscher, 2019). IFs operate thus in close functional crosstalk with microtubules and microfilaments to integrate cellular space and provide structural integrity (Chang and Goldman, 2004). Vimentin IFs can also provide “memory” to template microtubule regrowth after microtubule depolymerization (Gan *et al.*, 2017). Various IF species can interface with other cellular components via linker proteins, such as with adhesions (Filamin C), the plasma membrane (Spectrins), and the nucleus (Nesprin and SUN-KASH proteins) via additional linker type proteins (Bridges, Starr and Fridolfsson, 2010; Goldmann, 2018; Liem, 2019).

The viscoelastic properties of cells (i.e. their stiffness and their resilience to withstand stretching) could thus be a function of both IF networks independently as well as of IF networks which are dynamically interconnected to other cytoskeletal elements. In either scenario, IFs are often also anchored at cell-cell and cell-matrix junctions in order to act as mechanical integrators in cells. Again, the exact response of any given cell type to mechanical forces could be tailored to its specific needs by the cell type-specific expression of a particular IF protein which can impart different cytoskeletal crosstalk and regulation (Chang and Goldman, 2004).

1.2.2 Beyond structure - IFs modulate signaling cascades.

We discussed above the roles of phosphorylation of head domain residues in changing assembly and disassembly kinetics of IFs, making IFs a downstream target of kinase signaling cascades. The reverse is also true: binding of signaling components to IFs changes signaling outcomes. Some of the known signaling processes affected by IFs are cell cycle, apoptosis, and stress responses (Pallari and Eriksson, 2006). IF binding interactions with signaling components occur within both the head and tail domains of IF proteins. Many of the known binding partners of individual IF proteins are signaling proteins and their binding to IFs changes their localization and possibly their activity. Since the different IF proteins have very divergent tail domains, the binding interactions are very much dictated by the IF isotype expressed and are one likely reason for cell type specificity of IF proteins. Given how many distinct IF proteins exist, we have barely scratched the surface of the possible roles that IFs play in different cell types to modulate signaling. The observations that many IF KO mice have subtle defects is overall consistent with many of them modulating signaling rather than being required solely for structural support. There are several different ways in which IF proteins can influence signaling outcomes. These include IFs providing binding scaffolds for signaling components along assembled filaments, regulating the positioning of organelles, and acting as mechanosensitive signal transducers. Secondly, some evidence is also accumulating that oligomeric, non-filamentous IF pools can play active signaling roles.

One example of IFs scaffolding signaling components is the binding of 14-3-3 proteins to the phosphorylated head domain of VIM or keratin (Liao and Bishr, 1996; Ku, Liao and Omary, 1998; Tzivion, Luo and Avruch, 2000; Ku *et al.*, 2002; Paramio and Jorcano, 2002). This regulates how available 14-3-3 is to its many other binding partners which include cell cycle control proteins (such as cdc25), signaling factors (such as Raf, PI3K), and apoptosis regulators (such as BAD). Absence of keratin K8, as an example, causes changes in cell cycle regulation by driving cells into S phase. This might be due to lack of sequestering of 14-3-3 by keratin K8. Other signaling pathways besides 14-3-3 are also modulated by direct binding to IFs. Keratin K10 binds the kinases Akt/PKB and PKC α via its head domain which sequesters them away from their membrane binding sites and keeps them inactive. This again affects cell cycle progression. These examples highlight one mechanism of signaling roles for IFs, which is to remove an active signaling component from its site of action by scaffolding it to IFs. Conversely, scaffolding by an IF can also increase rather than decrease signaling output of a particular pathway (see below).

Are non-filamentous IF oligomers also capable of modulating signaling? The modulation of 14-3-3 signaling discussed above might be one such example since

phosphorylation of head domains disfavors assembly and 14-3-3 binds preferentially to phosphorylated residues in the head domain. There are several well documented examples in which cellular stress responses are changed when IF proteins are depleted. As an example, it has been shown that axonal injury leads to upregulation of vimentin in the injured axonal stump. This occurs by local translation of preexisting axonal vimentin mRNA and is coupled to calpain-mediated cleavage of vimentin in the rod domain which renders it assembly-incompetent. This injury-induced non-filamentous vimentin pool is required for injury signaling to the soma: neurons derived from VIM KO mice have a blunted injury response. The exact oligomeric form of vimentin involved in injury signaling is not known. Mechanistically, axonal injury signaling requires the retrograde transport of pERK via dynein. It was shown that vimentin binds to the nuclear import factor importin β as well as to dynein. Importin β in turn, binds to pERK and the complex of vimentin-importin β -pERK is transported back to the soma via dynein. Once it reaches the soma, pERK dissociates from the vimentin complex and signals transcriptional changes to mount an injury response. One of the roles of vimentin is thus to create the bridge between pERK and dynein motors. A second role is that pERK is stabilized when bound to the vimentin complex, which allows active pERK to be maintained for the journey back to the soma (Perlson *et al.*, 2004, 2005). Ndel1 generated de novo at the crush site facilitates the formation of a multi-protein vimentin-dynein complex, and is associated with more robust axon regrowth (Shi *et al.*, 2008; Toth *et al.*, 2008). Binding to vimentin thus scaffolds an active signaling component away from deactivating phosphatases and links it to a microtubule motor for long-distance transport (Perlson *et al.*, 2005, 2006). NFL null mice also exhibit delayed axon regeneration, but it is not known if NFL is functioning in a filamentous or non-filamentous form (Zhu, 1997).

1.2.3 Integrating structure and signaling – mechanosensitive signaling roles of IFs.

Another emerging concept in IF biology is that assembled IFs can change signaling inside cells by virtue of sensing mechanical forces via cell-cell and cell-matrix junctions. This new concept thus combines a purely mechanical role for IFs with a signaling role and profoundly changes the way we think about mechanical integration of complex cellular behaviors. One striking example is the molecular mechanisms of collective cell migration, using *Xenopus* embryos as a model system. In explants of collectively migrating embryonic tissue, tension on cadherin cell-cell contact sites recruits local keratin filaments to the rear of a migrating cell via the adaptor plakoglobin. The keratin network assembled at the rear of the cell in turn suppresses Rac activation and thus the assembly of actin filaments. In turn, activated Rac at the front of the cell not only organizes actin assembly to drive lamellipodial protrusion but also leads to local disappearance of keratin IFs. There is thus a reciprocal feedback regulation of actin and keratin filaments which is spatially organized by the force transduced across junctions at the cell's rear in a migrating cell sheet. Singly migrating cells in culture, on the other hand, rely on cell-matrix contacts, such as focal adhesions, which are cross-regulated by vimentin filaments. Interestingly, vimentin can bind to β 1 Integrin (Kreis *et al.*, 2005), and also regulates FAK (Dave *et al.*, 2013). Migratory cells in many different contexts are thus likely to engage mechanosensing, IF-based mechanisms to regulate signaling to the actin cytoskeleton, to cell junctions, and possibly as well to MTs (Sanghvi-shah and Weber, 2017). The molecular details of how mechanical tension, IFs, and actin networks are

integrated to modulate cell polarity and directional migration are only starting to be understood, and much more will be learned in the future.

1.3 Intermediate filaments in neurons

Neurons, like other cell types, express IFs and do so in a cell type-specific manner. In fact, the neuronal-restricted expression of the neurofilament (NF) class of IF proteins is commonly used to identify neurons by immunostaining. Immature neurons initially do not express NFs, but express vimentin, nestin, and INA. The early expressed neuronal IFs are rapidly replaced with NFs (Figure 2)(Cochard and Paulin, 1984; Bennett, 1987; Nixon and Shea, 1992; Benson, D. L., Mandell J. W., Shaw G., 1996; Grant and Pant, 2000; Yabe *et al.*, 2003), although in some cells these early IF's can persist into adulthood (Gu *et al.*, 2002; Hendrickson *et al.*, 2011; Guo *et al.*, 2014). The complex changes in IF expression as neurons mature beg the question of what roles the early neuronal IFs play and what roles the NFs play that are uniquely needed in either developing or mature neurons, respectively.

1.3.1 The neurofilament class of IFs are the main structural IF in mature axons.

Mature neurons express specific subsets of IF proteins, most notably the neurofilament subunits NF-L (light), NF-M (medium), and NF-H (heavy) which are often referred to as the “triplet” NFs. During development, other subunits are initially expressed, such as nestin, vimentin, α -internexin (INA), and in the PNS, peripherin. Both vimentin and nestin are largely downregulated as axons reach their target areas and make synaptic connections (Cochard and Paulin, 1984; Yabe *et al.*, 2003). INA expression is maintained throughout adulthood, as triplet NF expression increases with time, with NF-H being expressed last (Figure 2)(Shaw, G., Banker, G., Weber, 1985). Triplet NFs have been extensively studied, and we refer the interested reader to the many excellent reviews.

The IF network of mature axons was initially thought to be composed of the triplet of NF-L, -M, and -H, but it has now been demonstrated that either INA (in the CNS) or peripherin (in the PNS) are stable components of NFs, making them thus “quadruplet” NF networks. NF subunits assemble as obligate heteropolymers. Only NF-L is capable of homo-oligomerization *in vitro*. Both NF-M and NF-H require heterodimerization with NF-L for assembly and transport. In mature optic nerve, NF filaments were determined to have a subunit composition of 4:2:2:1 (NF-L:INA:NF-M:NF-H)(Perrot *et al.*, 2008).

In mature axons, NFs fill the entirety of the axons along their lengths. Since NF-H in particular has a very long tail domain with many phosphorylation sites, it protrudes laterally from the surface of the filament and is thought to increase spacing between NFs as well as between microtubules. NF KO mice show disruption of axon morphology. Most strikingly, axon diameters are decreased, particularly in NFL and NFM knockout mice. This affects conduction velocity in these axons and leads to sensorimotor deficits. In addition, axon numbers are decreased by 10 - 20% in NFL and NFM knockouts (Perrot *et al.*, 2008). The phenotypes of NF KO mice are consistent with NFs playing structural roles in the axon as stably assembled filaments (Hoffman *et al.*, 1987). The roles of NFs in axons thus include maintaining cytoskeletal spacing's and creating a viscoelastic cytoplasm in the axon which resists deformation (Leterrier *et al.*, 1996; Rammensee,

Janmey and Bausch, 2007). However, there is some evidence that the changes in axon diameter is not the only factor causing the decreases in conduction velocity. For instance, NFH knockout mice, which only have a minor changes in axon caliber, conduction velocity of individual neurons was decreased up to 40% compared to WT in axons that are similar in diameter to WT axons (Kriz *et al.*, 2000).

Even though NFs are often used to label axon tracts, their distribution in axons may not be as uniform as frequently assumed (Goldstein, Sternberger and Sternberger, 1983; Chan, Peng and Chiu, 1997). In the adult guinea pig and rat neocortex only about 10-20% of mainly pyramidal neurons can be labeled with any combination of NF-L, NF-M, or NF-H directed antibodies, or with the NFM/NFH reactive SMI-32 antibody, and intensity of immunolabeling can vary by brain region (Vickers and Costat, 1992; Hiscock, Mackenzie and Willoughby, 1996; Kirkcaldie *et al.*, 2002; Ouda, Druga and Syka, 2012). Studies of monkey and human cortices came to a similar conclusion, although the proportion was slightly higher in human brain (20-30%) (Campbell and Morrison, 1989). The consequence of NF deletion include alterations in axon caliber in PNS axons, but in CNS axons, changes of axon caliber due to NF deletion are far less pronounced than in the PNS, suggesting that they are performing other functions in the CNS, such as roles in development and/or synapse modulation. For instance, genetic deletion of INA, NFL, and NFH (which completely eliminates any NFs in the hippocampus) results in a significant decrease in hippocampal long term potentiation without altering synapse morphology (Yuan *et al.*, 2015).

NFs are also subject to phosphorylation by many stress-induced kinases and are often described as “phosphate sponges” or “sinks”, capable of buffering the detrimental effects of over-activated kinases (Rao *et al.*, 2002; Lobsiger *et al.*, 2005; Omary *et al.*, 2006; Kim and Coulombe, 2007). Not surprisingly, NFs have been found to be associated with neurodegenerative diseases (Barry *et al.*, 2007; Hyder *et al.*, 2008) and these defects are often associated with abnormal NF phosphorylation (Perrot *et al.*, 2008). NFs can also be found in aggregates after injury. This is likely due to the influx of calcium at the injury site with activates calpain and leads to massive cleavage of IFs and abnormal aggregate formation (Schlaepfer, 1974; Perrot *et al.*, 2008).

NFs are extraordinarily stable with turnover being on the order of weeks in adult nerves (Yuan *et al.*, 2009). It was unknown for a long time how NFs assemble and are transported to fill the whole axon, but much excellent work has now clearly established that NFs are moved as short (“squiggles”) or long filaments bidirectionally in axons at all times. This occurs by association with both kinesin and dynein motors (Yabe, Pimenta and Shea, 1999; Roy *et al.*, 2000; Helfand *et al.*, 2003; Chang and Goldman, 2004; Yan, 2005; Manuscript, 2007; Uchida, Alami and Brown, 2009; Uchida *et al.*, 2018). The Brown lab in particular has demonstrated with beautiful live imaging that NFs in mature axons continue to move, anneal, and sever (Uchida and Brown, 2004; Wang, Monsma and Brown, 2013; Uchida *et al.*, 2018). They are thus more dynamic than initially thought. NFs in mature axons are now often viewed as “bottle brushes” that move up and down the axon and maintain spacing of cytoskeletal elements. There is also a stationary pool of assembled and crosslinked NFs which contribute to the viscoelastic properties of the axoplasm to maintain structural integrity (Leterrier *et al.*, 1996).

1.3.2 Neurofilaments – still many surprises and open questions!

It is very clear that NFs in axons play structural roles as stationary filaments to provide viscoelastic buffering of mechanical forces. But new tools, such as live imaging of fluorescently labeled neurofilaments, have discovered that NFs are unexpectedly dynamic in mature axons. In the soma and dendrites, non-phosphorylated NFs predominate whereas axonal NFs are highly phosphorylated on their tail domains with increasing phospho-content more distally. In the soma, NF is phosphorylated on the head domain which prevents assembly into filaments and prevents tail phosphorylation (Grant and Pant, 2000). As a consequence, oligomeric species and shorter filaments are more abundant in the proximal axon and filaments can assemble and grow in length during axonal transport. With increasing maturity, tail phosphorylation increases, leading to more stable and more stationary phases of NFs along axons. Even with this stationary stable pool, motile shorter filaments can always be observed (Grant and Pant, 2000).

As discussed above, many IFs have been implicated in signaling. It is less clear to what degree NFs in axons participate as signaling scaffolds in the same way as has been described for VIM or keratins. The phosphorylation events on NF tail domains are usually viewed as changing tail conformation to maintain spacing or to sponge up phosphates of hyperactivated kinases, rather than as specific regulators of signaling outcomes. It is known, though, that NF-M binds to 14-3-3 proteins when phosphorylated in its head domain, similarly to VIM and keratins, and might thus also modulate local signaling. In addition, NFs likely serve as “docking platforms” for organelles and vesicles (Wagner *et al.*, 2003; Toivola *et al.*, 2005; Potokar *et al.*, 2010; Rao *et al.*, 2011; Lowery *et al.*, 2015; Yuan, Rao and Nixon, 2017). Much of this is still unknown, and exciting new discoveries will likely be made in this area in the future.

Lastly, whereas NF assembly, transport, and function in axons of the PNS are well studied, the roles of NFs in dendrites and in the CNS are less well understood. Dendritic NFs are less dense and less phosphorylated, and deletion of NF genes has less noticeable effects on CNS architecture. Interestingly, NF KO mice present with both axonal and dendritic defects raising the question of whether NFs in dendrites play similar structural roles as in axons or carry out dendrite-specific functions. Recent evidence has revealed NFs in synaptic boutons, but also at postsynapses and even in spines, both by immunofluorescence and electron microscopy. INA in particular has been shown to localize inside synaptic spines by immunofluorescence (Benson, D. L., Mandell J. W., Shaw G., 1996; Yuan *et al.*, 2015; Bragina, Conti and Duffy, 2018), and biochemically purified PSD fractions contain all the three neurofilament proteins and INA (Jordan *et al.*, 2004). Neurofilament proteins in the synapse are likely of non-filamentous forms such as tetramers or protofibrils due to the rarity of neurofilaments detected in synapses by classic EM studies, although some carefully done studies do show that some ~10nm filaments (IFs) are in synaptic spines. (Landis and Reese, 1983; Sumio *et al.*, 1996; Yabe, Pimenta and Shea, 1999; Yuan *et al.*, 2003, 2015; Perrot *et al.*, 2008). IFs in synapses could be of particular importance due to associations of NFs with synaptic signaling machinery, including receptors, kinases, phosphatases, and scaffolding machinery. For example, NFL binds to the cytoplasmic tail of the GluN1/NR1 subunit of the NMDA receptor and to protein phosphatase 1 (PP1) (Ehlers *et al.*, 1998; Terry-Lorenzo *et al.*, 2000; Ratnam and Teichberg, 2005). Indeed NFL knockout neurons exhibit reduced spine density and length with schizophrenia-like behavioral defects (Yuan *et al.*, 2018). α -Internexin interacts with the PP1 scaffold spinophilin in an age dependent manner- i.e. more α -internexin co-IPs

with spinophilin in adult brain compared to post-natal (Baucum *et al.*, 2010; Baucum, Strack and Colbran, 2012). NFM binds to the cytoplasmic loop of D1 dopamine receptor and influences the receptor distribution. (Kim *et al.*, 2002). Another study demonstrated that complete loss of NFs in the hippocampi of mice dramatically disrupts synaptic plasticity and social memory without altering the structural integrity of synapses. Moreover, deletion of NFM in mice showed an enhanced response to dopaminergic drugs such as cocaine and amphetamines (Yuan *et al.*, 2015). The synapse is thus likely a whole new locale where NFs can act in neurons. Since altered NF distribution and phosphorylation have been implicated in neuropsychiatric and neurodegenerative disease models, NFs at synapses might have clinical relevance (Yuan and Nixon, 2016). This role of NFs at synapses is well reviewed in Yuan and Nixon 2016. Even after many years of intensive research, much remains to be learned about the roles of mature NF networks in neurons!

1.3.3 Intermediate filaments in developing neurons are structurally and functionally diverse.

Given the striking temporal progression of IF subtype expression patterns in neurodevelopment (Figure 2), one wonders what the functional consequences are of such complex expression changes. Heterogeneity of IF expression could change the mechanical characteristics of neurons and the signaling scaffolds of neurons as they mature (Robert, Hookway and Vladimir I Gelfand, 2016). The full extent of IF heterogeneity in developing neurons is currently poorly understood, as most existing data rely on comparative single or double labeling of IF subtypes, and comparisons between different sections stained with different antibodies. Many of these studies are older and were performed before quadruple or even triple labeling was possible. Thus IF diversity among individual cells may be underappreciated. There is clear evidence already that developing neurons transiently express different IF subtype filament systems (Nixon and Shea, 1992) which progressively mature with age to the stable NF network. Therefore, it would be quite interesting to see how neuronal IF proteins express differently among different neuronal cell types over time in specific brain regions.

The exact expression profiles of IFs in developing neurons are not well established even in culture, and studies labeling more than one IF protein type at a time are rare. It was initially shown that early axons are mainly composed of MTs with only low levels of NF-M and NF-L before axons reach their synaptic targets (Perrot *et al.*, 2008). Cortical neurons express VIM and nestin at 24 hours in culture, but expression of these IF subtypes is transient, although some adult neurons continue to express vimentin and nestin (Yan *et al.*, 2001; Walker *et al.*, 2007). INA is already expressed at DIV1 (DIV = days *in vitro*) in culture and expression is maintained. The majority of hippocampal neurons express some NF (both NF-L and NF-M) by DIV3, but expression patterns are heterogeneous. Interestingly, IFs are enriched in the distal regions of growing neurites in cultured neurons, suggesting possible roles of IFs in axon growth and growth cone responses (Figure 3)(Yabe *et al.*, 2001; Yan *et al.*, 2001; Uchida and Brown, 2004). What then is the evidence for IF roles in neurodevelopment, including axon growth? VIM KO mice are viable, but do show some neurological deficits, including hyperactivity, impaired balance, and increased anxiety (Colucci-Guyon *et al.*, 1999), which might stem from neurodevelopmental or synaptic alterations. Downregulation of VIM with antisense

oligonucleotides in cultured hippocampal neurons decreased neurite outgrowth (Shea, Beermann and Fischer, 1993; Boyne, Fischer and Shea, 1996), implicating VIM in some aspect of axon growth. Interestingly, during axon regeneration after injury in the PNS, IF networks are rearranged with NF being replaced by VIM (Leon *et al.*, 1991; Gillen *et al.*, 1995; Vita *et al.*, 1998; Perlson *et al.*, 2005). This return to a more immature IF network might help in the dynamic cytoskeletal processes required for regeneration. INA KO have no reported phenotypes to date, suggesting that other IFs may compensate for INA function in the nervous system (Levavasseur, Zhu and Julien, 1999). A role for INA in axon outgrowth is not well documented. There is evidence from PC12 cells and neuroblastoma cell lines that INA plays a role in neurite outgrowth (Shea and Beermann, 1999), but newer approaches have not been used to investigate a role for INA in axon growth or growth cone behavior. A number of studies have demonstrated a role for NFs themselves in axon outgrowth in cultured neurons. In *Xenopus* neurons, decreased rates of axonal growth are observed when embryos are microinjected with anti-NFM antibodies (Szaro *et al.*, 1991; Walker *et al.*, 2001). In addition, NF content in *Xenopus* neurons correlates with the length of a particular neurite branch (Smith, Gervasi and Szaro, 2006). In mice, *in vivo* analysis of axon growth during development in the NF knockouts has not been carried out extensively at early time points, so subtle or transient defects might not have been detected.

The overall notion is thus that the early expressed IF proteins contribute to IF networks which are more dynamic and which are replaced with the very stable NF network as axon growth completes and stable synaptic connections are formed. The molecular pathways in which early expressed IF proteins might be important are not well established. We recently discovered an unexpected role for the early expressed IF protein nestin in responsiveness to axon guidance cues. We will discuss the functions of nestin below.

1.4 Nestin: an unconventional intermediate filament protein.

One of the earliest expressed IFs in the brain is the unconventional IF protein nestin. Nestin is a unique member of the cytosolic IF family, with an extremely long C-terminal tail and a truncated head domain (Hockfield and McKay, 1985; Lendahl, Zimmerman and McKay, 1990; Dahlstrand *et al.*, 1992; Dahlstrand, Lardelli and Lendahl, 1995a). The truncated head domain is thought to prevent homo-oligomerization of nestin, so it is dependent on other similar type of IFs (Assembly group 2 IF proteins such as VIM, INA, and NFs) for hetero-polymerization (Steinert *et al.*, 1999). The C-terminal tail of nestin has unique binding interactions that are critical to its function. Most notably, the nestin tail binds the Cdk5 activator p35, and is thus able to scaffold activated Cdk5 (Sahlgren *et al.*, 2003, 2006; Yang *et al.*, 2011). During development, nestin expression in the brain is highest in neural progenitor cells (NPCs). It is thus commonly used in the field as a marker for NPCs (Dahlstrand, Lardelli and Lendahl, 1995a). Nestin expression is by no means restricted to NPCs, though, and it is broadly associated with many types of proliferative cells, including myoblasts and cancer cells, as well as their vascular networks (Bernal and Arranz, 2018; Calderone, 2018). The cellular roles of nestin are far from fully understood, but it regulates a variety of signaling pathways. These pathways include inducing proliferative signaling (cdc2, MapK, EGFR pathways) (Chou *et al.*, 2003; Xue and Yuan, 2010; Hu *et al.*, 2016), as well as downregulating apoptotic pathways and

providing protection from oxidative stress (Sahlgren *et al.*, 2006; Su *et al.*, 2013; Wang *et al.*, 2019). The modulation of oxidative stress responses by nestin occurs in part via its regulation of Cdk5/p35 (Sahlgren *et al.*, 2006; Su *et al.*, 2013), but if all roles of nestin are Cdk5-dependent has not been established. In addition to being present in proliferating cells, nestin is also present in postmitotic neurons for a short time (Yan *et al.*, 2001; Walker *et al.*, 2007), possibly representing a transition state between progenitor and neuron.

1.4.1 Roles for nestin in NPCs

Given the prominent expression of nestin in NPCs, much effort has been made to uncover the molecular roles of nestin in NPCs. A number of defects have been reported for nestin knockdown in neural stem cells in culture, including increased cell death and reduced proliferation (Sahlgren *et al.*, 2006; Park *et al.*, 2010; Hu *et al.*, 2016). In Zebrafish, microcephaly and small eyes were reported after KD of nestin with morpholinos (Chen, Yuh and Wu, 2010). Again, NPC cell death was increased. There were also some defects in axon tracts, but it was not clear if these were a consequence of NPC phenotypes or independently arising in neurons. Another paper used in utero electroporation of nestin directed shRNA into rat embryos and found fewer migratory neurons. This was reported to be due to cell cycle arrest of NPCs in G1. Cell death was not increased. The shNestin phenotype could be rescued with WT nestin, lending additional validity to this phenotype (Xue and Yuan, 2010).

1.4.2 Nestin knockout mice – great confusion from different mouse models.

In 2010/2011, the first mouse nestin KO papers were published. One paper reported embryonic lethality with severe brain defects due to increased NPC cell death (Park *et al.*, 2010). The reported phenotype thus appeared similar to the Zebrafish phenotype (Chen, Yuh and Wu, 2010) and possibly also the rat shNestin phenotype (Xue and Yuan, 2010). A different study generated an independent knockout line (Mohseni *et al.*, 2011), and another used lentivirus to express nestin RNAi in developing embryos (Yang *et al.*, 2011). From both of these studies nestin appeared not essential for neural development, but was important for myogenesis and NMJ formation, and behaviorally resulted in poor performance in the rota-rod test due to decreased muscle coordination. Surprisingly, adult neurogenesis was found to be impaired in the viable nestin KO strain by an unexpected non-cell autonomous mechanism where nestin-expressing astrocytes regulate Notch signaling in progenitors to maintain stemness (Wilhelmsson *et al.*, 2019). In addition, some behavioral defects were described in the same paper, in particular with respect to long term memory in an object recognition test (Wilhelmsson *et al.*, 2019). A role for nestin in maintaining embryonic NPC pools are thus controversial. It is not at all clear how to reconcile the diametrically opposed results from these differing mouse models. However, since nestin has been linked to stress responses, perhaps variance in environmental stress (environment, background strain, microbiome, stress) in different facilities contributes to these different outcomes. This is consistent with knockout models of other IF proteins, whose functions only become apparent after injury (Eckes *et al.*, 2000).

1.4.3 Nestin – a potent regulator of Cdk5 signaling cascades.

We discussed above the vast amount of accumulating evidence that many IF proteins have roles in regulating signaling cascades. Nestin is clearly also active in signaling regulation, and in fact, some of the best examples of IF protein signaling come from studies of nestin. Nestin has been shown to promote or inhibit several signaling pathways through different mechanisms. Most notably, Cdk5 activity is regulated by scaffolding of Cdk5/p35 onto nestin. This scaffolding of active Cdk5 reportedly leads to either increased or decreased phosphorylation of different Cdk5 substrates, creating contradictory conclusions.

For example, in differentiating myoblasts the proper level of Cdk5 activity is critical for differentiation. In this cellular model, the level of Cdk5 activity is modulated by controlled cleavage of the Cdk5 activating protein, p35, into its hyperactive form p25 (Pallari *et al.*, 2011). In Alzheimer's models, p25 is often associated with disease progression, although this is controversial (Giese, 2014). However in myoblasts, p25 generation occurs during physiological muscle development (Thonel *et al.*, 2010). Nestin via its direct interaction with p35 can protect p35 from calpain-mediated cleavage into p25, and thus modulate the rate of differentiation of myoblasts. Depletion of nestin in myoblasts thus resulted in hyperactivation of Cdk5/p25 which led to transcriptional changes promoting increased muscle cell differentiation (Pallari *et al.*, 2011). In a cancer context, nestin was also shown to dampen Cdk5 activity towards a nuclear Cdk5 substrate. A study using two lung cancer cell lines showed that nestin depletion increased nuclear lamin A/C phosphorylation by Cdk5, which induced tumor cell senescence and reduced proliferation (Zhang *et al.*, 2018). Interestingly, this group identified a nuclear localization motif on nestin which may modulate how nestin affects nuclear targets in some cell types (Zhang *et al.*, 2018).

Cdk5 has both cytosolic and nuclear pools and nestin might localize Cdk5 activity in the cytosol. For instance in NPCs, nestin expression increased the cytosol to nuclear ratio of Cdk5 localization and Cdk5 activity, without affecting the total level of Cdk5 activity when assayed *in vitro* on the exogenous Cdk5 substrate histone H1 (Wang *et al.*, 2017). Nestin depletion decreased Cdk5 mediated phosphorylation of the mitochondrial organization protein, DRP1 (which is localized in the cytosol), and thus affects mitochondrial organization (Wang *et al.*, 2017). In other models of muscle differentiation using C2C12 myotubes, nestin RNAi reduced overall Cdk5 activity of lysates, particularly on membrane fractions, on the exogenous Cdk5 substrate histone H1 *in vitro* (Yang *et al.*, 2011). This affected muscle development and NMJ formation, in a way that phenocopies Cdk5 deletion, knockdown, or inhibition. Whether nestin increased or decreased Cdk5 activity is thus context-dependent (Lindqvist, Wistbacka and Eriksson, 2016).

These findings could be reconciled if one proposed that nestin can increase the phosphorylation of cytosolic Cdk5 substrates, while decreasing phosphorylation of nuclear Cdk5 substrates. As a consequence, depletion of nestin would increase nuclear Cdk5 activity, but decrease cytosolic Cdk5 activity. The effect of nestin on inhibiting or promoting substrate phosphorylation would thus depend on the localization of the substrate. Conclusions on this matter are complicated and conflicting, as most studies rely on exogenous, non-physiological Cdk5 phosphorylation assays of histone H1, a nuclear protein, instead of phosphorylation of endogenous relevant substrates. Albeit, some studies do distinguish and compare the activity of Cdk5 on histone H1 in nuclear

vs cytosolic cellular extracts. One could imagine cytosolic localized nestin/kinase complex (Cdk5/p35) could be modified in some other way (or in a complex) in that it prefers cytosolic substrates after lysis, and not nuclear substrates such as histone H1.

1.4.4 Nestin – a potent scaffold for other signaling molecules.

Nestin has been shown to affect fate signaling in some cellular systems. The underlying mechanism is by altering the distribution of fate-inducing molecules to affect results of cell divisions - be it differentiation, continued proliferation, or cell death. Depletion of nestin in neural stem cells and myoblasts has been shown to induce premature differentiation (Pallari *et al.*, 2011; Wilhelmsson *et al.*, 2019), but the NPC pathway is not thought to be via Cdk5 regulation, but via affecting numb segregation. Again, confusion exists because the effects are not the same in all systems. Nestin was found to segregate away from the cell fate determinant Numb in dividing mouse NPCs in culture (Shen *et al.*, 2002). In contrast, in chicken, the nestin analog transitin was found to interact with numb and segregate together with numb into daughter cells (Wakamatsu *et al.*, 2007). A very different model again has been proposed in an adult neural stem cell model where nestin in astrocytes of the adult neural stem cell niche resulted in changed processing of Notch. Absence of nestin led to pre-mature differentiation of neuroblasts into neurons in a non-cell autonomous manner (Wilhelmsson *et al.*, 2019). The mechanism by which nestin might regulate Notch signaling and Numb localization is thus not clear and will require additional work.

In a different example, nestin interacts with and alters the subcellular localization of unliganded glucocorticoid receptor GR (Reimer *et al.*, 2009). GR is associated with nestin in the cytosol, and upon ligand stimulation, GR dissociates from the nestin IF network and translocates into the nucleus to induce cell cycle arrest. Nestin depletion phenocopies ligand stimulation and leads to constitutive accumulation of GR in the nucleus. In this way, anchoring of GR by nestin is important for robust cell proliferation by sequestering GR in the cytosol (Reimer 2009). This study highlights and visually demonstrates well how nestin can sequester or scaffold signaling molecules in the cytosol, and its loss results in increased activity of that signaling molecule in the nucleus-which is similar to what is seen with Cdk5 activity.

These different examples highlight the emerging notion that scaffolding by nestin can change signaling outcomes related to cell cycle exit and differentiation, but the direction of change and the molecular mechanisms depend on the cell type. It is currently impossible to predict the ultimate effect of nestin on any given signaling pathway, and it will have to be tested separately for each different context.

The appreciation of different functions of individual IF protein types is an important step in understanding neuronal diversity. Unlike other filament systems, the building blocks of IF's impact more than just the physical properties of the resulting filament, but can provide a scaffold with novel chemistries in specific locations within a cell. The ability to localize specific reactions within a neuron suggests that the study of how IFs are localized and transported throughout the cell will yield insights into what signaling process an IF is involved in. The varied expression of IF proteins over time, between cells, and between brain regions might be one factor that alters functions and behavior of individual neurons. In addition to acting as a monomer in a filament, the appreciation of functions of soluble intermediate filament species (from monomer to protofilaments) is an important

consideration going forward. Finally, more experiments to uncover the different interacting proteins with neurofilaments are important to elucidate more signaling functions of IF proteins. Even though the first knockouts were made over 20 years ago, the study of the cell biological functions of intermediate filaments still has much room for future research.

1.5 Doublecortin and its role in the growth cone

Understanding mechanisms of neural development are critical to understanding the underlying causes of deleterious and severe neurodevelopmental pathology (such as lissencephaly) as well as milder but more prevalent neuropsychiatric disorders (such as schizophrenia). From another perspective, the identified causative alleles in such disorders are informative to understand the basic mechanisms of neurodevelopment, as well as higher order developmental paradigms that allow for a healthy functioning adult brain.

Doublecortin (DCX) is a microtubule associated protein originally identified as a major causative allele in the neurodevelopmental disorder lissencephaly (Pilz *et al.*, 1998). Lissencephaly is a neurodevelopmental disorder characterized by a normal sized brain which lacks fold, or “smooth brain”. Individuals with lissencephaly have multifocal epilepsy and results in death by teenage years (Bahi-Buisson *et al.*, 2013). DCX is a microtubule binding protein, and its binding to microtubules stabilizes them and can bundle them together (Gleeson *et al.*, 1999; Moores *et al.*, 2006). DCX’s affinity for microtubules is regulated by a number of kinases, but most relevant here is cyclin dependent kinase 5 (Cdk5)(Tanaka, Finley F. Serneo, *et al.*, 2004).

CDKs are cyclin-dependent kinases which regulate the cell cycle in proliferating cells and which are activated by binding to cyclins. Interestingly, Cdk5 is a critical kinase in post-mitotic neurons. Unlike the mitotic CDKs, Cdk5 is not activated by cyclins, but by distinct activators, p35 and p39. The majority of Cdk5 knockout mice die in utero with severe neurodevelopmental defects and cortical malformation, highlighting the importance of Cdk5-regulated pathways in early brain development (Ohshima *et al.*, 1996; Shupp, Casimiro and Pestell, 2017). Cdk5 regulates cytoskeletal dynamics downstream of signaling pathways via phosphorylation of several critical proteins, including FAK, CRMP2, tau, drebrin, and DCX, but the exact mechanism by which Cdk5 affects normal brain development are largely still unknown. A number of Cdk5 substrates have been identified as causative of or associated with neurodevelopmental, neuropsychiatric, and neurodegenerative disorders. Among them are DCX (lissencephaly)(Pilz *et al.*, 1998), Lis1 (lissencephaly)(Pilz *et al.*, 1998), Ndel1 (lissencephaly)(Sasaki *et al.*, 2005), Disc1 (depressions/autism), Dixdc1 (depression)(Singh *et al.*, 2010), Fak (schizophrenia/epilepsy)(Murphy, Park and Lim, 2016), Crmp2 (Alzheimer’s)(Williamson *et al.*, 2014), Drebrin (Down Syndrome/Alzheimer’s)(Shim and Lubec, 2002), Map1B (ADHD/Alzheimer’s)(Ulloa *et al.*, 1994; Walters *et al.*, 2018), tau (Alzheimer’s)(Ballatore, Lee and Trojanowski, 2007), Pak1 (Alzheimer’s)(Ma *et al.*, 2012), and neurofilaments (Alzheimer’s)(Sternberger, Sternberger and Ulrich, 1985). Thus Cdk5 and its substrates are important players in the development and maintenance of a functioning central nervous system, particularly the cortex.

DCX knockout mice have only mild problems in cortical development, and are viable, but exhibit epilepsy and memory defects (Nosten-Bertrand *et al.*, 2008; Germain *et al.*, 2013). While mutations in DCX are associated with severe malformations of the cortex, hippocampus and the corpus callosum in humans, the relatively mild problems in the DCX knockout mice were initially unexpected but have several possible explanations. First, there is evidence that some of the human disease causing mutations are not null alleles, but are neomorphs and may have off target deleterious gain-of-function mechanisms (Yap *et al.*, 2016). In addition, mice may not be the best model to study lissencephaly in particular, as WT mice are essentially lissencephalic- they lack cerebral folds (Wynshaw-Boris *et al.*, 2010). So the defects resulting from DCX loss in neural migration may be less pronounced in mice compared to humans. Time lapse imaging of mouse developing cortex has uncovered some abnormalities in neuronal migration in DCX null mice, but these defects are temporary and ultimately the cortex shows normal layering (Tanaka, Finley F Serneo, *et al.*, 2004; Kappeler *et al.*, 2006; Pramparo *et al.*, 2010). However, DCX null mice do have some well characterized defects of neurodevelopmental processes, particularly in axon targeting. In vivo, cortical projections are delayed, are fewer in number in DCX null mice, and often there is no corpus callosum (Bielas *et al.*, 2007). In culture, DCX null neurons are insensitive to the attractive cue netrin (Fu *et al.*, 2013), and more sensitive to the repulsive cue Semaphorin 3A (C.J. Bott *et al.*, 2019). However, DCX null neurons show normal responses to the repulsive cue Slit (Koizumi *et al.*, 2006), so this is not a general problem with axon responsiveness. DCX is well positioned to participate in axon guidance, as it is enriched in distal, most dynamic segments of the axon, and can be detected in all regions of the growth cone, from central to peripheral. Interestingly, DCX null mice and humans with mutations in the DCX gene also have NMJ defects- a phenotype that is shared with nestin knockout mice (Yang *et al.*, 2011; Bourgeois *et al.*, 2015).

Cdk5 is downstream of Semaphorin 3A, although the mechanisms downstream of Semaphorin 3A that lead to Cdk5 activation are not clear. The Semaphorin 3A receptor Neuropilin 1, and co-receptor PlexinA4, are not kinases themselves, but lead to the downstream activation of a number of kinases, including Src family kinases, Cdk5, and FAK, among others. Fyn, a Src family kinase, complexes with Neuropilin1 upon ligand stimulation, which activates Cdk5 by phosphorylation at pY15 (Sasaki *et al.*, 2002). However, this proposed mechanism, which was worked out in heterologous cells, is controversial, as the equivalent pY15 site on other Cdk's is inhibitory, and subsequent studies have failed to show any phosphorylation at Y15 of Cdk5 upon Semaphorin 3A stimulation. In addition, the pY15 site was shown to decrease its association with the activator p35, suggesting that it is indeed inhibitory (Kobayashi *et al.*, 2014). Nevertheless, Cdk5 is important for the downstream signaling of Semaphorin 3A as shown by several studies (Brown *et al.*, 2004; Uchida *et al.*, 2005; Ng *et al.*, 2013), although the exact mechanism for activation remains unclear.

DCX's best described role is as a microtubule regulator and microtubules are likely a major effector of DCX downstream of guidance cues. DCX also interacts with F-actin through the actin binding protein spinophilin, and therefore DCX's interaction with and regulation of both filament systems are most likely important in axon guidance (Bielas *et al.*, 2007; Fu *et al.*, 2013). When DCX is bound to microtubules, microtubules are strengthened and more resistant to depolymerization. When DCX is phosphorylated by

Cdk5, DCX has decreased affinity for microtubules, and dissociates (Tanaka, Finley F. Serneo, *et al.*, 2004; Bielas *et al.*, 2007)- providing conditions permissive for regressive cytoskeleton remodeling, like what is seen in response to repulsive axon guidance cues such as *Sema3a* (Figure 4).

1.6 Research Objectives

Sema3a is commonly considered a repulsive guidance cue, and indeed axons of many neurons will retract when exposed to *Sema3a*. Curiously, dendritic growth cones do not collapse in response to *Sema3a*, but instead are attracted to it. The response, and presumably the intracellular signaling, to *Sema3a* can thus vary depending on the particular cellular structure in both time and space, such that *Sema3a* leads to axon repulsion, but dendrite attraction at some times in development but not others. Temporally, sensitivity to *Sema3a* must change due to the inherent bi-lateral symmetry of the cortex. Axons that cross the midline through the corpus collosum, and project to the other hemisphere need to grow into a region that contains axon repulsive signals (such as *Sema3a*) which repels axons of their contralateral counterparts (Figure 5). Thus, the response to *Sema3a* varies by both intracellular location and over time within the same neuron.

How intercellular signaling varies spatiotemporally is thus a critical underlying question for organization of the brain. Identifying and understanding the mechanisms behind signaling modifiers that vary in expression by both time and space is critical to solving this biological question. I propose that the expression and localization of nestin is well suited to provide this variance. Mechanistically, nestin's ability to modulate Cdk5 activity and localization could place it right in the center of the downstream signaling of the repulsive cue *Sema3a*.

Chapter 2 provides the initial observation that nestin expression persists in early cortical neurons, but is lost after 2-3 days after the start of differentiation. Nestin in these early neurons localizes to the distal regions of the axon, but is absent from dendrites. By carefully categorizing neurons with nestin expression, we found that the morphological characteristics of nestin expressing neurons was different from nestin negative neurons, and the differing characteristics suggest differences in cytoskeletal dynamics. Finally, we found that nestin expressing neurons are more sensitive to *Sema3a*, in a Cdk5 dependent manner

Chapter 3 dissects the mechanism behind how nestin modulates Cdk5 signaling downstream of *Sema3a*. Our finding of this mechanism were spurred by an initial finding that DCX and nestin interact from an unbiased mass spectrometry screen of DCX binding proteins in embryonic mouse brain. We found that the interaction between nestin and DCX is specific, and that other Cdk5 substrates do not bind nestin, nor do other intermediate filaments bind to DCX. Nestin expression leads to more efficient phosphorylation of DCX by Cdk5, by binding to both the kinase and the substrate-increasing phosphorylation through a scaffolding mechanism. We find that nestin mutants that are deficient in their ability to bind to DCX and affect DCX phosphorylation fail to have effects on growth cone morphology that WT nestin has. Finally, we show that nestin expression has no effect on growth cone morphology or *Sema3a* responsiveness of DCX null neurons.

The appendix contains some additional published data. Appendix 1 is adapted from a published study where a surprising gain of function mechanism is discovered for disease related DCX mutant alleles.

In summary: This work identifies a novel role for the intermediate filament protein nestin in neurons, where it unexpectedly modulate the phosphorylation of DCX by Cdk5, and thus responsiveness to the repulsive axon guidance cue Semaphorin3a. Modulation of signaling cascades by intermediate filaments is an emerging concept in other cell types. My work is the first to demonstrate such a signaling role for an intermediate filament in neurons. These findings have important implications for how signaling outcomes might be modulated not only by the ligand-receptor complex, or by the substrates, but additionally by the intermediate filament subtype present at certain times and locations as the brain develops.

Figure1: Assembly of intermediate filaments

Diagram of intermediate filament assembly and the various intermediate species of intermediate filament oligomers that can exist *in vivo*. Long tailed intermediate filaments have their tails exposed to the cytosol, permitting interactions with various binding proteins and post-translational modification.

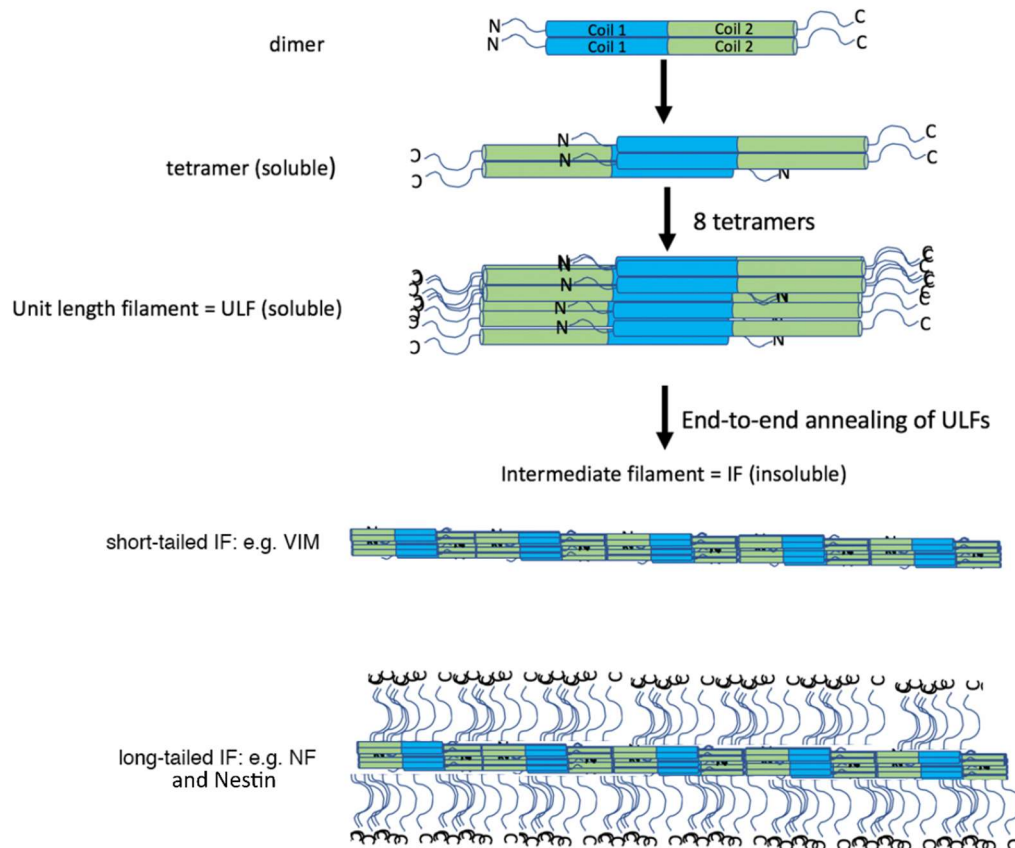


Figure 2: Neuronally expressed IF's throughout development

Intermediate Filaments, including the neurofilaments that expressed during the course of neuronal development. Tail domains are highly divergent in length, and suggests a large capacity for potential binding by many binding partners.

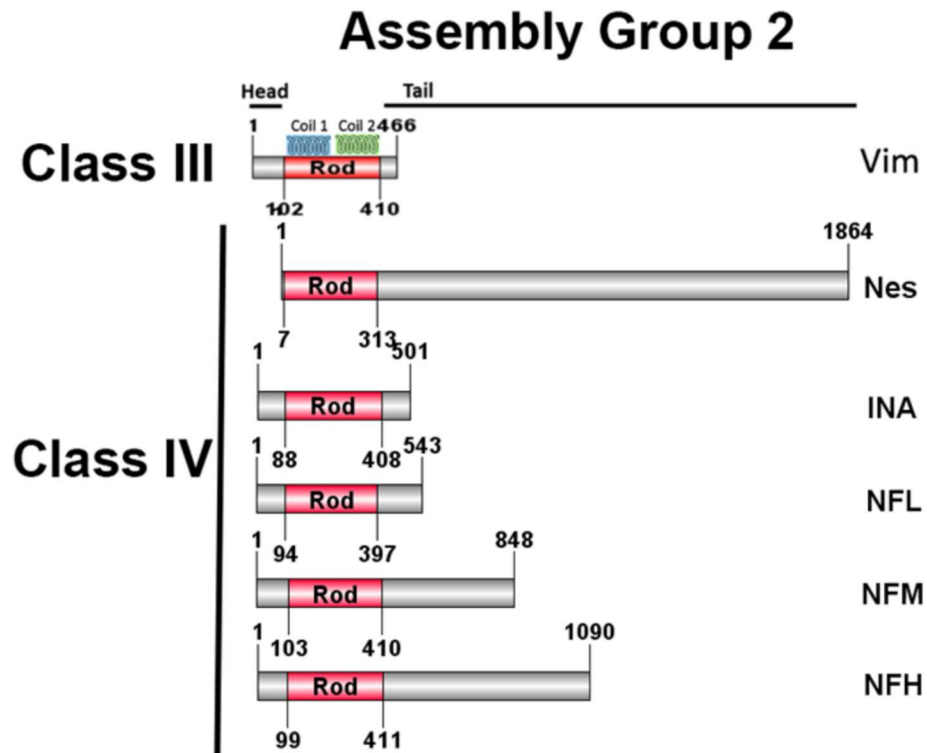


Figure3: Intermediate filaments are enriched in the distal regions of growing axons.

A. The intermediate filament nestin is enriched in distal regions of the axon (arrowhead) but absent from other secondary neurite emanating from the cell body (arrows). Other intermediate- and neuro-filaments also have this localization in early growing axons. B. Super resolution STED image of the filamentous nature of nestin in the distal region and growth cone of developing axons.

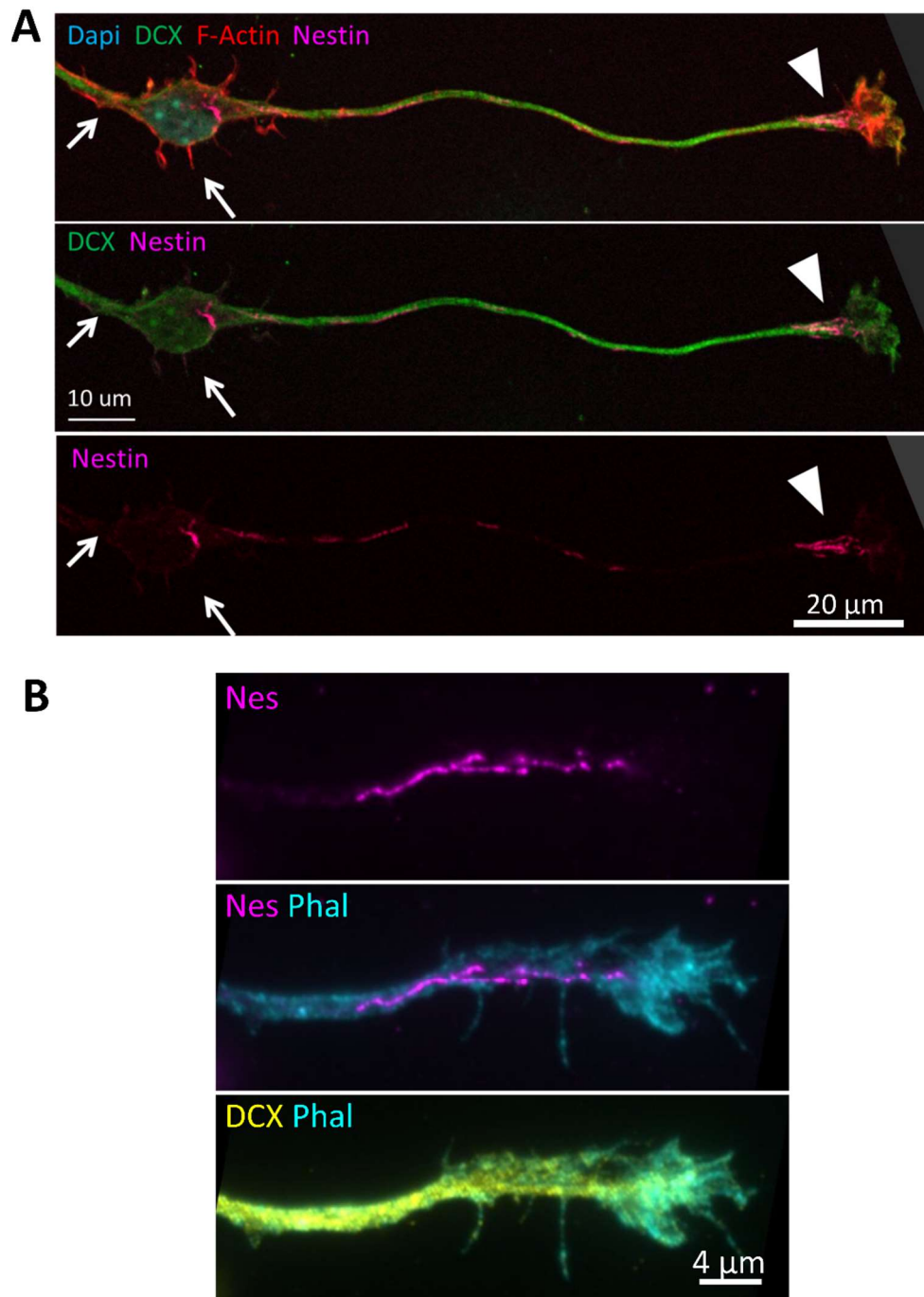


Figure4: Model of DCX phosphorylation in an axon growth cone

DCX is phosphorylated by Cdk5 downstream of Semaphorin3a, and results in microtubule destabilization and filopodia retraction in a cultured cortical neuron.



 Phospho DCX

 Non-Phospho DCX


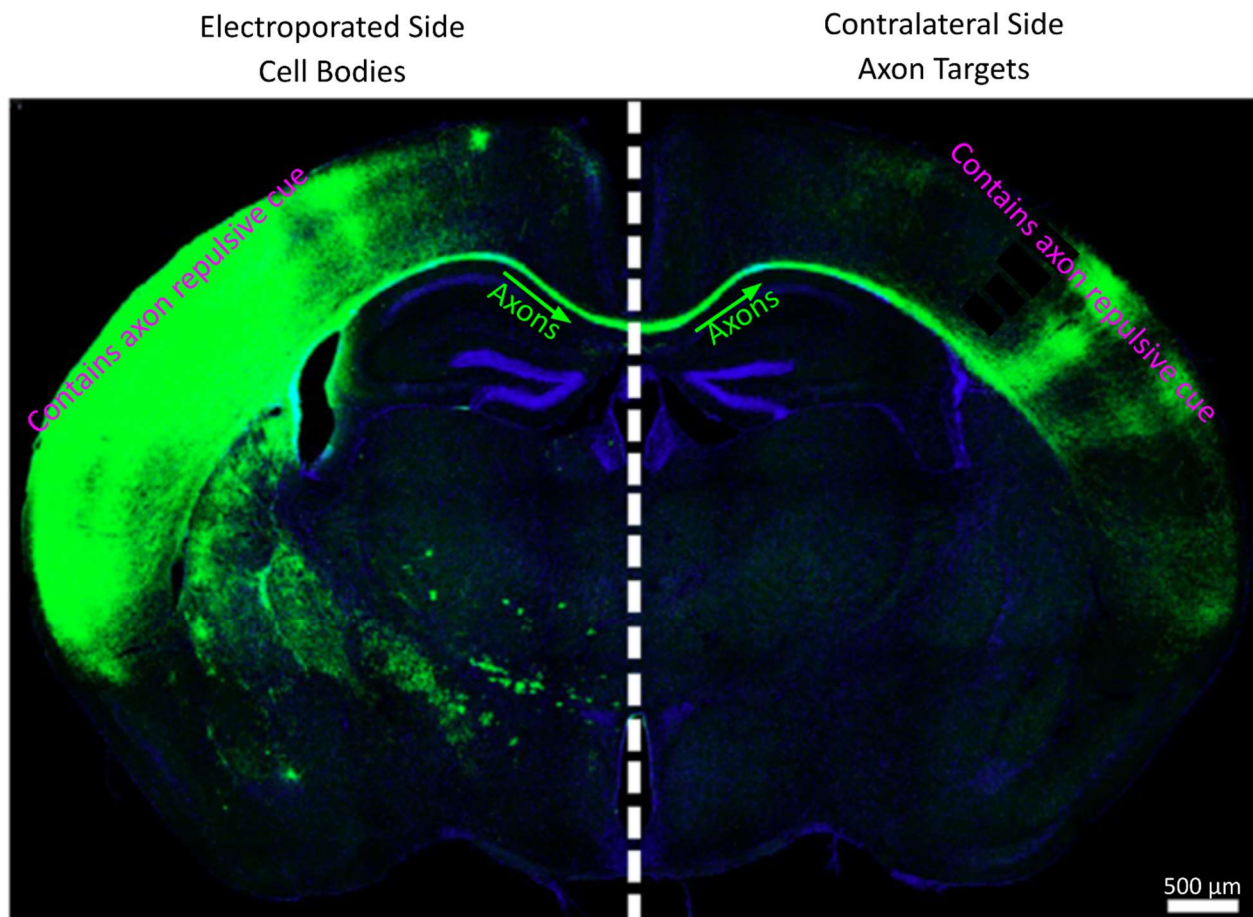
 Collapsing factors
(stathmin2, drebin/eb1)

Figure5: Contralateral projecting cortical axons grow into a region containing repulsive cues

In cortical developments, axons are initially repelled by the repulsive cue Semaphorin3a located in superficial regions of the cortex. After crossing the midline through the corpus callosum, cortical projecting axon grow into a Semaphorin3a rich region to reach their targets. Thus these axons are no longer repelled by the repulsive cue Semaphorin3a, thus their sensitivity to this cue must have changed. Adapted from Rodríguez-Tornos, FM. et. al. Neuron 2016.



Chapter 2: Nestin in immature embryonic neurons affects axon growth cone morphology and Semaphorin3a sensitivity

Adapted from: Bott, C. J., Johnson, C. G., Yap, C. C., Dwyer, N. D., Litwa, K. A., & Winckler, B. (2019). Nestin in immature embryonic neurons affects axon growth cone morphology and Semaphorin3a sensitivity. *MBOC*, 30(10), 1214–1229.

2.1 Introduction

Proper wiring of the nervous system requires that axonal growth cones respond to a variety of extracellular guidance cues to find their correct targets (Kolodkin and Tessier-Lavigne, 2011). Semaphorin 3a (Sema3a) is one of many diffusible developmental cues and has been shown to repel axons of responsive neuronal populations (Sibbe *et al.*, 2007). Addition of Sema3a to cortical neuron cultures causes rapid filopodial retraction (within 5 minutes) and ultimately collapse of many axonal growth cones (Dent *et al.* 2004). Binding of Sema3a to its receptor neuropilin1 and co-receptor PlexinA4 leads to downstream activation of the neuronal serine/threonine kinase cyclin dependent kinase 5 (Cdk5) (Sasaki *et al.*, 2002; Chen *et al.*, 2008; Perlini *et al.*, 2015). Cdk5 is critical for early neuronal development as a regulator of cytoskeleton, trafficking, and membrane dynamics and, thus, cell morphology (Kawauchi, 2014). Sema3a-activated Cdk5 phosphorylates multiple substrates to affect the assembly and dynamics of both the actin and microtubule cytoskeleton, and of adhesion components which results in filopodial retraction and growth cone collapse *in vitro* (Sasaki *et al.*, 2002; Ng *et al.*, 2013). Not all cortical neurons are repelled by Sema3a, and the molecular mechanisms for this differential responsiveness are under active investigation (Carcea *et al.* 2010; Mintz *et al.* 2008; Ip *et al.* 2011; Wang *et al.* 2014).

Intermediate filaments are generally thought to provide structure and stability to a cell. In adult neurons, neuronal intermediate filaments, the neurofilaments, play such a structural role to maintain axon caliber (Lariviere and Julien, 2003). In addition to the classic neurofilaments, other intermediate filament subunits are expressed during neural development. Vimentin and nestin are both highly expressed in neural progenitor cells (NPCs), so much so that nestin expression is widely used as a marker for NPCs. α -internexin (INA) and neurofilament proteins expression, on the other hand, is upregulated only after neurons differentiate. Neurofilaments, INA, and vimentin (all expressed in CNS neurons) have also been shown to play additional but poorly understood roles in early neuritogenesis (Shea *et al.* 1993; Shea & Beermann 1999; Lee & Shea 2014; Walker *et al.* 2001). The function of nestin in neurons has not been investigated since nestin is not thought to be expressed in neurons.

Little is known about nestin's function, even in NPCs, where it is highly expressed (Sahlgren *et al.*, 2006), but it appears to offer some protection from cellular stress. In addition, nestin is often expressed in cancer cells, and has well documented effects on cancer cell migration and invasion by influencing cytoskeletal dynamics and kinase activity (Zhao *et al.* 2014; Liang *et al.* 2018; Yan *et al.* 2016; Hyder *et al.* 2014). Nestin's developmental function is best understood in muscle where it acts as a scaffold and regulator for Cdk5 at the neuromuscular junction (NMJ). At the NMJ, nestin deletion phenocopies Cdk5 deletion (Lin *et al.*, 2005), and nestin is required for the acetylcholine agonist carbachol-induced Cdk5 activity (Yang *et al.* 2011; Pallari *et al.* 2011; Mohseni *et al.* 2011). The binding site for the p35/Cdk5 complex has been mapped to the unique, long C-terminal tail of nestin (Sahlgren *et al.*, 2003, 2006) which is much larger than conventional intermediate filaments (57 kd vimentin vs ~300kd nestin).

In this work, we show for the first time that nestin has a function in postmitotic newborn cortical neurons. We first characterized the patterns of endogenous nestin expression. As expected, we find that nestin is highly expressed in NPCs.

Unexpectedly, nestin protein can be detected during early, but critical, periods of axon formation and is subsequently lost. Secondly, we found that depletion of nestin affects growth cone morphology of immature cortical neurons. Lastly, we discovered that nestin depletion from cultured neurons decreases their sensitivity to Sema3a in a roscovitine-dependent manner. Based on our data, we propose that nestin acts as a “gain control” modulator of Sema3a growth cone signaling during early neuronal differentiation. Since neurons can encounter the same cue at different developmental stages, but respond differently (Kolodkin and Tessier-Lavigne, 2011), nestin’s modulation of Sema3a responsiveness might be one mechanism to temporally and spatially regulate differential axon guidance decisions in the cortex.

2.2 Material and methods

Antibodies

Mouse anti-Nestin Rat401- recognizes the unique C-terminal tail region of nestin (Su *et al.*, 2013)—All experiments shown with 2q178 were also repeated with this antibody.

Note this antibody and the other antibodies recognize full length nestin. 1:200 IF, 1:500 IHC, 1:500 WB **DSHB Cat# Rat-401 also rat-401 RRID:AB_2235915**

Mouse anti-Nestin 2Q178 This clone and RAT401 produce indistinguishable staining patterns. All staining and blotting is done with this antibody unless otherwise noted.

1:200 IF, 1:500 IHC, 1:500 WB **Santa Cruz Biotechnology Cat# sc-58813**

RRID:AB_784786

Goat anti-Nestin R-20: Raised against peptide in the unique C-terminal tail region of nestin 1:500 IF, 1:200 IHC **Santa Cruz Biotechnology Cat# sc-21249**

RRID:AB_2267112

Chicken anti-Nestin- three peptide directed antibodies combined to the unique C-terminal tail region of nestin 1:300 IF, 1:400 IHC, 1:3000 WB **Aves Labs Cat# NES**

RRID:AB_2314882

Rabbit anti-Nestin AB92391: Raised against peptide in the unique C-terminal tail region of nestin 1:500 IF **Abcam Cat# ab92391, RRID:AB_10561437**

Rabbit anti-DCX- 1:1200 IF, IHC, 1:4000 WB **Abcam Cat# ab18723 RRID:AB_732011**

Mouse anti- β III Tubulin Tuj1- 1:800 IF A generous gift from the Deppman Lab YVA A. Frankfurter, University of Virginia; Department of Biology Cat# TuJ1 (beta III tubulin) **RRID:AB_2315517**

Chicken anti- β III tubulin- 1:200 IF **Aves Labs Cat# TUJ RRID:AB_2313564**

Rat anti α -tubulin- 1:2000 WB **Santa Cruz Biotechnology Cat# sc-53030**

RRID:AB_2272440

Rabbit anti-Vimentin- 1:100 IF, 1:100 IHC, 1:1000 WB **Bioss Inc Cat# bs-0756R**

RRID:AB_10855343

Rat anti-Myc tag 9E1- 1:1000 WB ChromoTek Cat# 9e1-100, **RRID:AB_2631398**

Mouse anti-NeurofilamentM 2H3- 1:200 IF **DSHB Cat# 2H3 RRID:AB_531793**

Mouse anti- α Internexin 2E3- 1:100 IHC **Sigma-Aldrich Cat# I0282 RRID:AB_477086**

Rat anti-L1- 1:150 IHC **Millipore Cat# MAB5272 RRID:AB_2133200**

Mouse anti-Tag1-4D7 (DSHB) 1:150 IHC **DSHB Cat# 4D7 RRID:AB_2315433**

Rabbit anti-Calretinin- 1:600 IHC **Millipore (chemicon) Cat# PC254L-100UL**

RRID:AB_564321

Goat anti-Sox2- 1:250 IF **Santa Cruz Biotechnology Cat# sc-17320, RRID:AB_2286684**
 Rat anti-CTIP2- 1:400 IF **BioLegend Cat# 650601 RRID:AB_10896795**
 Rabbit anti-SatB2- 1:400 IF **Abcam Cat# ab92446 RRID:AB_10563678**
 GFP booster nanobody- 1:600 IF **ChromoTek Cat# gba488-100 RRID:AB_2631434**
 Phalloidin 568 1:150 Invitrogen

Neuronal Culture

Primary cultures of cortical neurons were obtained from embryonic day 16 (E16) mouse cortex of either sex as described. The protocol follows institutional ACUC protocols (approved animal protocol #3422). Cells were plated on poly-L-lysine coverslips and incubated with DMEM medium with 10% fetal bovine serum. After 8 hrs, the cells were transferred into serum-free medium supplemented with B27 (Invitrogen) and glutamine and cultured for a total of the indicated time periods *in vitro* (DIV). Cells were plated at ~100,000 cells per 15mm coverslip, and at 50,000 in the Low Density experiment, or 125,000/coverslip in electroporation experiments. Cortical neurons for culture were harvested at E16 prior to gliogenesis. Thus non-neuronal glia are rare in these cultures, but occasional nestin/Sox2 positive, GFAP negative persisting neural stem cells were found.

2D explants were acquired from E16 cortex, but only partially dissociated before plating as described above.

Cells for Semaphorin 3A treatment assay were prepared as described above. At 24 or 36 hours, cells were treated with mouse Semaphorin 3A (R&D systems) diluted in growth media for 5 minutes at 1nM, or 15 minutes at 2nM as indicated prior to fixation. In some experiments, cells were pre-treated with 10 μ M Roscovitine (Cayman Chemical) for 30 minutes prior to Semaphorin 3A treatment. Time course experiments were fixed at the indicated time points after plating.

Immunofluorescence

Cells were fixed in 4% Paraformaldehyde-PHEM-Sucrose (PPS: 60mM PIPES, 25mM HEPES, 10mM EGTA, 2mM MgCl₂ (PHEM), 0.12M sucrose, 4% paraformaldehyde pH 7.4) for preservation of the cytoskeleton and cellular morphology with prewarmed fixative (37°C) and fixed at 37°C for 20 min. Thorough permeabilization was required for nestin/intermediate filament visualization in neurons. Coverslips were permeabilized with 0.4% Triton-X 200 in 1% BSA/PBS for 20 min for nestin and intermediate filament staining, or 0.2% Triton-X when no intermediate filaments were being immunostained, and then blocked for 30 min in 10%BSA, 5% normal donkey serum (NDS) in PBS. Primary antibodies were diluted in 1% BSA in PBS, and secondary antibodies in 1%BSA, 0.5% NDS in PBS. Primary antibodies were incubated overnight at 4° C, and secondary antibodies for 90 min at room temperature. Appropriate species specific Alexa-350, -488, -568, or -647 labeled secondary antibodies raised in Donkey (Invitrogen) were used for fluorescent labeling. Phalloidin-568 (Invitrogen) at 1:150 was used to visualize F-actin and DAPI to visualize nuclei. For peptide blocking negative control experiments, the goat anti-nestin antibody was diluted at 1:500 with the corresponding immunizing peptide (Santa Cruz) at 1:50 and incubated at room temperature for 3 hours. The goat anti-nestin antibody for the non-blocked condition

was diluted and incubated similarly but in the absence of peptide. Coverslips were mounted with ProLong Gold (Invitrogen) and imaged with a Zeiss Z1-Observer with a 40x (for population counting) or 63x (for morphology analysis) objective. Images were captured with the Axiocam503 camera using Zen software (Zeiss) and processed identically within experiments. No non-linear image adjustments were performed.

Histology

Human iPSC derived Cortical Organoids (minibrains) or embryonic E16 mouse brain were dissected and placed in 4% PFA and 6% sucrose in PBS at 4°C overnight. Tissue was then cryo-protected by sinking overnight in 30% sucrose. Tissue was imbedded in OCT, and brains cut by coronal cryosection at 16 µm sections (Zeiss Confocal imaging) or 10 µm sections (Abberior super-resolution). Sections were mounted directly on slide, permeabilized with 3% NDS + 0.2% Triton-X 100 in PBS for 1 hour, and blocked with 10% BSA for 30 min. Antibodies were diluted in permeabilization buffer with indicated primary antibodies overnight at 4°C, and secondary antibodies 2 hours at room temperature following thorough washing with PBS. Sections were mounted with Prolong Gold. For peptide blocking negative control experiments, the goat anti-nestin antibody was diluted at 1:100 with the corresponding immunizing peptide (Santa Cruz) at 1:10 and incubated at room temperature for 3 hours. The goat anti-nestin antibody for the non-blocked condition was diluted and incubated similarly but in the absence of peptide. The antibody was then used as described above. Of note, the anti-Tag1 IgM antibody has cross reaction with mouse IgG secondary antibodies, so staining with mouse IgG and mouse IgM antibodies were done sequentially. Confocal imaging of cryosections was carried out on an inverted Zeiss LSM880 confocal microscope using a 63X objective. Super-resolution STED imaging utilized Abberior STED confocal with 100X objective at the Keck Microscopy Center (University of Virginia). A donkey anti-goat-488 (Invitrogen) secondary antibody was imaged using a 595 nm extinction laser.

Neuron nucleofection

After cell were dissociated from cortex, but prior to plating, cells were electroporated by Amaxa 4d nucleofection, according to manufacturer's protocols. 800,000 cells were electroporated in the small volume (20µl) cuvettes using P3 primary cell solution and EM-100, CL-133, and CU-100 programs variably between experiments. All three of these programs worked similarly in our hands. 0.1µg of GFP plasmid (pCMV-GFP-Clontech) as a transfection marker, and 100nM siRNA (siCON-SCBT sc-37007, siNes smart-pool Dharmacon siGenome M-057300-01-0010, consisting of 4 individual siRNA's (D-057300 -01,-03,-04, and -17) with target sequences: siRNA #1-AAAGGUGGAUCCAGGUUA, siRNA #3 D-AGACAAGACUCAUGAGUC, siRNA #4 CAGCAGGCAUUUAGACUUC, siRNA #17 GCGACAACCUUGCCGAAGA). All 4 target the region in the mRNA corresponding the unique C-terminal tail of nestin protein, which is unlike other IFs.

Molecular biology

Circular mouse nestin cDNA was obtained as a gift from Bruce Lahn (U. Chicago). Briefly, PCR was used to generate EcoR1 and HindIII sites on the 5' or 3' end

respectively of full length mouse nestin. Both the insert and vector were treated with EcoR1 and HindII, the cut insert was ligated into pCDNA3.1 Myc-His(+) B.

Cell culture and transfection.

HEK293 cells were maintained in DMEM+10% fetal bovine serum, and all transfections were conducted using Lipofectamine 2000 (Invitrogen) according to the manufacturer's protocol. mNestin-myc and respective control or nestin siRNAs were transfected simultaneously according to the recommended instructions.

Western Blot

Cells were washed with ice cold PBS, and lysed directly on the plate (6cm) into lysis buffer (400 μ l); 50mM Tris HCl, 150mM NaCl, 1% NP-40, 1mM EDTA, 1mM DTT, 1mM PMSF, 1X HALT protease/phosphatase inhibitor cocktail. After rotisserie at 4° C for 30 minutes, lysate were cleared by centrifugation at 21K X g for 15 min at 4° C. Supernatants were diluted with 5X Laemmli buffer and equivalent amounts were run on a 4-20% polyacrylamide gel. After transfer onto nitrocellulose with the BioRad Transblot, membrane was blocked with Licor TBS blocking buffer for 1 hours at room temp. Primary and secondary antibodies were diluted in 50% blocking buffer, 50% PBS, 0.1% Tween-20. Peptide blocked was performed on diluted primaries in blocking buffer for 8 hrs at room temperature with a 10x excess of peptide to antibody ratio prior to incubation with blots. Primary antibodies were incubated overnight at 4° C, followed by near-infrared secondary antibodies for 1 hour at room temperature. Blot were imaged with the Licor Odyssey CLx imager.

Image analysis

Image J was used for all image analysis

Neuron morphology and nestin expression analysis. Neuron staging was performed according to the Banker neuron staging method, and neurites were designated as axons if it is 2X longer than the next longest neurite (dendrite). Nestin positivity in the axons of neurons was assessed by outlining the distal region of the axon and measuring the maximum nestin immuno-staining in the region. If this value was at least 1.5x above average background, then a cell would be considered positive for nestin. In siRNA experiments, only green GFP+ (transfection indicator) cells were imaged and counted for both for morphology and nestin siRNA efficiency analysis. All counts were confirmed by blinded analysis. Depiction of how morphology measurements were made is in Figure 13.

Filopodial protrusion were counted using the phalloidin channel, and any actin rich protrusion from the growth cone was counted.

Axon length was the length of the axon from the cell body to the growth cone tip.

Growth cone area and perimeter were assessed by measuring traced outlines the growth cone not counting the filopodial protrusions, and extending down to the point where the splayed growth cone microtubules consolidate into bundles in axon shaft.

Mouse Neural stem cell marker expression. DCX, nestin, and DAPI stained differentiated neural stem cells were manually counted for immunopositivity in any part of the cell above background levels.

Human IPSC Nestin and β III tubulin co-localization was assessed per image using the ImageJ co-localization plugin.

Mouse neural stem cell culture

Embryonic (E16) cortical neural stem cells were prepared as described (Pacey *et al.*, 2006) and grown as neurospheres for at least 3 passages prior to use for dissociated and differentiating cell experiments to ensure purity. For these experiments, neurospheres were dissociated using Stem Cell chemical dissociation kit, and plated in poly-L-lysine coated coverslips for 1 day and fixed and immunostained as described. For 4DIV, proliferative media was replaced with media lacking EGF and FGF growth factors until 4 DIV, fixed and processed for immunostaining as described.

Neural Differentiation of Human Induced Pluripotent Stem Cells

Human induced pluripotent stem cells from neurotypic control 9319 were generated by Kristen Brennand in the laboratory of Dr. Fred Gage (Salk Institute). Neural progenitor cells (NPCs) were generated through an embryoid body protocol as described by Brennand et al. (2011). For neuronal differentiation, we plated 75,000 control NPCs on each poly-ornithine and laminin-coated 18mm glass coverslip. After 24 hours, cells were switched to neuronal differentiation media consisting of DMEM F12 + Glutamax and supplemented with N2 and B27 with retinoid acid and 20 ng/ml BDNF, 20 ng/ml GDNF, 400 μ M cyclic AMP, and 200 nM ascorbic acid. Half of the media was replaced with fresh media every 3 days. Neurons were fixed with 4% formaldehyde with 4% sucrose on the days indicated in the text and used for subsequent immunofluorescence analysis.

Generation of Cortical Organoids

Human fibroblasts from neurotypic control 7545 were obtained from the Coriell Institute and reprogrammed into induced pluripotent stem cells by the laboratory of Dr. Mike McConnell (UVA) using the CytoTune Reprogramming Kit (Life Technologies) and maintained in Essential 8 media (Life Technologies). Cortical organoids were grown using a low-attachment protocol. Briefly, we used dispase to detach hIPSC colonies from matrigel dishes. These colonies were placed in ES/DMEM media (GlobalStem) supplemented with 20% Knockout Serum Replacement (Life Technologies) and treated with 5mM Dorsomorphin and 10mM SB-431542 for the first 5 days. The ROCK inhibitor, 10mM Y-27632, was added for the first 48 hours. From day 6-24, spheroids were fed with Neuronal Media consisting of Neurobasal A with B27 without Vitamin A, GlutaMax, penicillin/streptomycin (Life Technologies), and supplemented with 20 ng/ml EGF and FGF2 (Peprotech). From day 25-42, the growth factors were replaced with 20 ng/ml BDNF and NT3 (Peprotech). From Day 43 onwards, BDNF and NT3 were removed and organoids were grown solely in Neuronal Media.

Statistical analysis

Human IPSC Nestin and β 3 tubulin colocalization was performed using Sigma Plot 13.0. All other statistical analysis was carried out using Prism software. The datasets were first evaluated as parametric versus nonparametric using the Shapiro-Wilk normality test. The corresponding one way ANOVA test was used when there were multiple

comparisons, and the t-test was used when only two conditions were compared. This is specified for each figure in the figure legends.

2.3 Results

Nestin protein expression persists in immature primary cortical neurons in culture.

Nestin protein is expressed at high levels in cortical radial glia/neural progenitor cells (NPCs) (Lendahl, Zimmerman and McKay, 1990). In contrast, doublecortin (DCX) and β III-tubulin expression is low/absent in NPCs but upregulated in postmitotic neurons (Francis *et al.*, 1999). Nestin and DCX/ β III-tubulin are thus routinely used as markers to distinguish these mutually exclusive cell types. E16 mouse dissociated cortical neurons were cultured for 1 day *in vitro* (DIV) and immunostained against nestin and DCX. To our surprise, many DCX-positive cells were also positive for nestin (Figure 6A). These DCX/nestin-double positive cells had the morphology of stage 3 immature neurons (using Banker staging, see methods (Dotti, Sullivan and Banker, 1988)) (Figure 6A) and were positive for neuronal-specific β III-tubulin (see Figure 8D), indicating that they had differentiated into neurons. In addition, GFAP (a marker of astrocytes) was not detected at this early stage of development (not shown), in agreement with studies that show gliogenesis, i.e. formation of astrocytes or oligodendrocytes, does not begin until E17/18 or postnatally, respectively (Miller and Gauthier, 2007). We note that cells lacking neurites were generally nestin-positive and likely correspond to NPCs and some early stage 1 neurons (see Figure 6D). Cells with short processes which might correspond to stage 2 neurons or to non-neuronal cell types had variable nestin expression.

Because nestin is considered a marker of NPCs, we performed a series of rigorous controls to validate the observed staining. We obtained two additional nestin antibodies (raised in chicken (Chk) or goat (Gt)), all against different epitopes in the C-terminal region of nestin. Both antibodies produced immunostaining patterns similar to the mouse anti-nestin antibody (Figure 6A,B). A blocking peptide was available for the goat anti-nestin antibody which allowed testing the specificity of the observed axonal nestin staining. Pre-incubation of the goat anti-nestin antibody with the immunizing peptide prior to labeling specifically reduced immunostaining with the goat antibody, but nestin was still detected in distal axons with the mouse anti-nestin antibody in the same cell (Figure 6B). Both of these antibodies appear highly specific to nestin since they detected single bands (~300kd) by immunoblot (consistent with the expected size of nestin) in DIV1 E16 cortical mouse neuron lysate (Figure 5B).

As an additional validation of antibody specificity, we performed nestin knockdowns with either control, non-targeting siRNA (siCon) or a nestin-specific pool of 4 siRNAs (siNes-pool) using Amaxa nucleofection prior to plating dissociated neurons. GFP was co-electroporated to visualize transfected cells (Figure 6C). Cultures were fixed after 36 hrs and stained for nestin. The intensity of axonal nestin was then quantified. At 36 hrs, approximately 1/3 of GFP-positive stage 3 neurons stained positive for nestin after siCon electroporation, similar to untransfected cells (see below Figure 8D), whereas nestin staining was significantly reduced and essentially undetectable in GFP-positive cells electroporated with siNes-pool (Figure 6C). The

specificity of the three nestin antibodies was also assessed by western blot after siRNA knockdown in neurons (Figure 7A). Electroporation is not very efficient in neurons and the knockdowns were not complete after only 36 hours, but decreased nestin levels were found after siNes-pool nucleofection for all three antibodies confirming that the antibodies were specific for nestin. When mouse nestin-myc was transfected into HEK293 cells together with either siCon or siNes-pool siRNA, a near complete loss of nestin signal was observed in the siNes-pool treated condition, while the related IF vimentin was not affected (Figure 5A'). We conclude that nestin protein is indeed expressed in immature neurons in culture. Close reading of the literature revealed that nestin protein has been detected in neurons in human and mouse, both in early differentiating neurons (Cattaneo and McKay, 1990; Messam, Hou and Major, 1999; Yan *et al.*, 2001; Messam *et al.*, 2002; Walker *et al.*, 2007; Crews *et al.*, 2011), and in subpopulations of adult neurons (Gu *et al.*, 2002; Decimo *et al.*, 2011; Hendrickson *et al.*, 2011; Guo *et al.*, 2014; Liu *et al.*, 2018). Recent advances in single cell western blotting have revealed persistent nestin expression in β III tubulin positive differentiated neural stem cells (Hughes *et al.*, 2014).

Despite the evidence that nestin protein expression is not exclusive to neural stem cells, nestin continues to be used as a specific neural stem cell marker. We thus performed a side by side comparison (Figure 7C) of nestin staining in cultures counterstained with the NPC marker Sox2 and the neuronal marker DCX to compare the relative levels of nestin protein. This comparison within a single imaging field demonstrates that the nestin protein immunofluorescence level seen in axons (high DCX, but low Sox2 expression) was many times lower than nestin expression in an NPC cell body (high Sox2, but low DCX expression). High levels of anti-nestin antibody staining was thus confirmed to be a reliable NPC marker, when used as a tool to label NPCs and is clearly distinguishable from the lower axonal levels of nestin.

Nestin is present in filaments in distal axons and growth cones.

Having validated the nestin antibodies, we next characterized endogenous neuronal nestin distribution. Nestin was not uniformly distributed, but primarily localized to the distal region of the growing axon (pink arrowheads) and was rarely observed in secondary neurites (white arrows) (Figure 6A). Variable levels of nestin were often also detected in the cell body. In addition to the distal axon accumulation of nestin, short linear nestin profiles (called squiggles) were often found distributed along the length of the axon (white arrowhead) (Figure 6A), which is typical of neurofilaments in young neurons (Benson *et al.* 1996; Wang *et al.* 2000). Nestin is an obligate heteropolymer and requires another cytosolic IF type to assemble into filaments (Steinert *et al.*, 1999). If nestin existed as assembled filaments in neurons, it should be part of a filament composed of other IF subunits in addition to nestin. Indeed, we found that nestin colocalized with vimentin, neurofilament-medium (NF-M) (Figure 6D), α -internexin (INA) and neurofilament-light (NF-L) (not shown). Neurofilament heavy (NF-H) was not detected at these early time points, as NF-H is expressed in more mature neurons (Benson *et al.* 1996). A magnification inset and a linescan show that nestin and NF-M occupy subdomains within a heteropolymer, as has been demonstrated with nestin filaments in other cell types (Leduc and Manneville, 2017).

In addition to assembled nestin-containing filaments (squiggles) along the axon, we also see nestin staining in the growth cone central domain which extends more peripherally to various degrees. A typical pattern is represented by the growth cone shown enlarged at the bottom of Figure 6A. Nestin staining appears consolidated at this magnification and resolution. Individual filaments cannot easily be discerned. This staining may represent a tight bundle or tangle of short nestin-containing intermediate filaments (squiggles). In more spread growth cones (such as the growth cone shown enlarged in the bottom left of Figure 6B) nestin staining appears clearly filamentous, suggesting that nestin in neurons can exist at least partially as an assembled heteropolymer filament.

Nestin-expressing neurons are observed in multiple rodent and human culture models

Since neurons are not usually thought to express nestin, we looked at other neuronal models to see if we observed DCX/nestin double positive neurons in other contexts. When we prepared neuronal cultures from embryonic rat cortex, we also observed DCX/nestin double positive neurons (not shown). Next, we grew mouse NPCs as neurospheres and then differentiated them into neurons in culture in order to determine whether neurons differentiated from NPCs continued to express nestin. Differentiation into neurons takes several days using this protocol. One day after neurosphere dissociation and plating, >95% of cells were nestin-positive, but did not express DCX, consistent with them being NPCs (Figure 8A). The remainder had started to differentiate into neurons and expressed both DCX and nestin. After 4 days of differentiation in dissociated culture, ~50% of cells had differentiated into neurons (DCX-positive). A large proportion of the DCX-positive neurons also expressed nestin. The DCX/nestin double positive cells had a morphology similar to stage 2 or stage 3 cultured primary neurons and cells with a stage 3 morphology had nestin localized to the tips of neurites (Figure 8A inset). Only around 10% of cells had no detectable nestin immunopositivity (Figure 8A) and expressed only DCX, consistent with being more differentiated neurons. Differentiating NPCs after 4 days became too crowded to assess on a cell-by-cell basis.

To test whether human neurons similarly express nestin during early differentiation, we assessed nestin expression in cultures derived from human neural progenitor cells derived from induced pluripotent stem cells (IPSCs). At 1 day, nestin expression is high and β III tubulin expression is low, resulting in low co-localization of nestin and β III tubulin. After 4 days of differentiation, nestin colocalization with β III tubulin peaked, and nestin staining was clearly detected at the tips of β III-tubulin positive axons (Figure 8B), confirming nestin expression also in cultures of human neurons. Co-localization again drops at ~ 1 week due to decreasing nestin expression, however nestin is still expressed at the tips of some neurites. To assess if nestin expression occurred in neurons that are differentiating in a more tissue-like context, we also grew human NPCs as large cortical spheroids, often referred to as “minibrains” (Figure 8C). Minibrains recapitulate several developmental processes which are also observed during *in vivo* development. Nestin staining was clearly detected in neurons (identified by β III-tubulin expression). Nestin staining was most prominent in neuronal processes with lower β III-tubulin expression (less mature neurons), while cells expressing higher levels of β III-tubulin (more mature neurons) were mostly negative for

nestin. We conclude that nestin is transiently expressed in neurons in both human and rodent neurons, and can be observed in a model that recapitulates some aspects of human cortical development.

Nestin protein is transiently expressed broadly among cortical neuron cell types but decreases with maturation

Typical techniques to culture primary neurons select for cells that just recently completed mitosis, or are undergoing migration at the time of dissociation (Banker and Cowan, 1977). We thus wondered if nestin-positive neurons represent a transition state between nestin-positive neural progenitor cells (NPCs) and nestin-negative neurons. Alternatively, nestin-positive neurons could be a stable neuronal cell type which maintain nestin expression over longer times in culture. Since cultured cortical neurons maintain cell type fates after dissociation (Romito-DiGiacomo et al. 2007; Digilio et al. 2015), we used two cell-type specific transcription factors to distinguish cortical-projecting (Satb2-positive) from subcortical-projecting (Ctip2-positive) neurons. Nestin expression in DCX-positive neurons did not correlate with either Ctip2 or Satb2 expression (Figure 7D). Similarly, when cultures were prepared from E14, E15 or E16 embryos (representing different cortical layer fates), about 2/3 of DCX-positive neurons were nestin-positive after 24 hours in culture (data not shown), regardless of embryonic age at dissection. These data suggest that nestin is expressed by immature neurons of all cortical layers.

Since nestin-positivity was not skewed by neuronal cell type, we next assessed if nestin expression was correlated with time after differentiation. To this end, we utilized an *in vitro* time course of neurons dissociated from E16 mouse cortex (Figure 8C), since time in culture represents the maturity of the cell. For the first 12- 24 hours, around two-thirds of stage 3 neurons expressed nestin in the axon. Plating density had no effect on the percentage of neurons that express nestin (not shown). Nestin expression dropped steadily after 24 hours, with only one third remaining nestin-positive at 36 hours, one quarter by 48 hours, and less than a tenth by 72 hours (Figure 8C). The change in axonal nestin staining is easily appreciated in axon bundles growing from a cortical explant. At 36 hours, nestin expression was clearly seen mostly in the distal region of some axons, but was reduced to near background levels at 72 hours (Figure 8D). These data demonstrate that nestin is expressed transiently in a substantial subpopulation of differentiating cortical axons, and subsequently downregulated as differentiation proceeds.

Nestin is expressed in subpopulations of developing cortical neurons in vivo.

We next sought to determine if there was an *in vivo* correlate to the axonal nestin expression we observed in cultured neurons. Others have shown that developing cortical neurons in the intermediate zone (IZ) consist of a mixture of axons of variable states of maturation- pre-existing axon tracts laid down by earlier pioneer neurons, and later born neurons which initiate axon projections during migration through the IZ (Namba, Kibe, Funahashi, Nakamuta, Takano, Ueno, Shimada, Kozawa, Okamoto, Shimoda, Oda, Wada, Masuda, Sakakibara, Igarashi, Miyata, Faivre-Sarrailh, *et al.*, 2014). We thus imaged axons in the lower intermediate zone (IZ) of E16 mouse developing cortex, similarly to where nestin mRNA was detected by Dahlstrand (1995).

In vitro, nestin was not present in all axons and did not fill the whole length of an individual axon. We thus predicted that nestin positive axons would be detected as a subpopulation of axons in the IZ. We also predicted that axonal nestin would be lower than nestin in NPCs/radial glia.

A low magnification overview of one hemisphere of the cortex showing vimentin and α -internexin (INA) expression is shown in Figure 9A, along with a schematic to orient the reader. The boxed region in Figure 9A indicate the lateral lower IZ which is the region in the schematic imaged in the following panels. All panels in Figure 9B-E have the radial glia oriented vertically and axon tracts oriented horizontally. INA is an intermediate filament expressed early in neuronal development, but not expressed in radial glia (Kaplan *et al.*, 1990; Fliegner *et al.*, 1994; Dahlstrand, Lardelli and Lendahl, 1995a; Benson, D. L., Mandell J. W., Shaw G., 1996). As expected, INA is readily detected in axons of the IZ (Figure 9A,B). Vimentin is expressed in both radial glia and, at a lower level, neurons (Cochard and Paulin 1984; Boyne *et al.* 1996; Toth *et al.* 2008; Yabe *et al.* 2003).

As expected, nestin staining intensity in the radial glia (arrowheads in Figure 9C,D,E) was high, which made evaluation of nestin staining in axon tracts challenging. However high resolution confocal microscopy, the use of distinct axonal markers, and sequential imaging of four channels permitted us to resolve and distinguish between the segregated but interwoven cellular processes of radial glial and IZ axons. Staining with chicken and goat anti-nestin antibodies labeled the bright radial glia fibers (INA negative) oriented vertically (arrowheads) (Figure 9D). Similarly to nestin mRNA (Dahlstrand *et al.* 1995), INA is present in early cortical axon tracts (arrows), and nestin immunoreactivity was clearly detected in these axon tracts, albeit at lower levels compared to radial glia fibers. This staining pattern is similar to what is seen with *in vitro* axon bundles (Figure 8E). Early defining work had observed low nestin staining on spinal cord axons, but attributed it to background staining by the antibody (Hockfield and McKay, 1985). To assess the specificity of nestin staining on IZ axons, we repeated the peptide blocking assay used in Figure 6 for the goat anti-nestin antibody on E16 cryosections (Figure 9D). The staining by the goat nestin antibody was completely blocked by pre-incubation with the immunizing peptide, both on radial glia fibers and on axon tracts, indicating specific staining of nestin on axons *in vivo*. Both radial glia fibers and axons were still stained with the chicken nestin antibody. In addition, specificity of both the mouse 29178 antibody and the goat antibody to nestin was assessed by immunoblot of E16 mouse cortex lysate, and resulted in clearly labeled single bands that corresponds to the expected size of the nestin protein (Figure. 5B'). Furthermore, the ~300kd band recognized by the goat nestin antibody could be specifically reduced by preincubation with the immunizing peptide, arguing that the observed staining of IZ axons can be attributed to nestin (Figure. 7B').

To further characterize the IF content of the lower IZ axons, co-staining for nestin and vimentin was performed (Figure 10A,B). Vimentin was found to have a similar staining pattern to nestin, with high levels in radial glia, and low levels in axons. The nestin- and vimentin-positive IZ fibers were also positive for the axon marker L1-CAM (Figure 10A,B), confirming their identity as axons. The same axonal nestin staining pattern was seen with the mouse anti-nestin Rat401 monoclonal antibody, the initial antibody used to characterize and define nestin (Hockfield and McKay, 1985) (Figure

10B). Thus, multiple pieces of evidence demonstrate that nestin is expressed in axons in the IZ at E16 in mouse cortex.

To better visualize the axonal nestin, we performed STED super-resolution microscopy on goat anti-nestin immunostained E16 mouse cortex. The bright nestin-positive radial glia fibers were again the most prominently stained feature, but individual axons with less bright nestin staining could be unambiguously resolved. Nestin is clearly present on a subset of axons of the IZ (Figure 9C). In addition to the axons of cortical neurons (Tag-1 positive) of variable maturity, the IZ contains axons of neurons projecting from the thalamus, calretinin-positive thalamo-cortical neurons (Shinmyo *et al.*, 2015). We thus used these markers to further define the nestin expressing subpopulations (Figure 9E): L1-CAM for all axons, TAG-1 for cortical axons, and calretinin for thalamocortical axons. Intriguingly, we observed that a subpopulation of cortical (TAG-1 positive) axons had detectable nestin staining whereas the calretinin-positive (thalamo-cortical) axons lacked nestin staining (Figure 9E). However, we note that this could be due to differences in the cell type, and/or maturity level of cortical vs thalamic originating axons.

The level of nestin expression in neurons influences growth cone morphology and response to Sema3a.

An important question is whether nestin plays a functional role in axons, or is simply left over from the mother NPC and no longer plays a role. As a starting point for probing whether nestin still has a function in neurons, we determined if axons and growth cones were the same or different in neurons with (+) and without (-) nestin (representative images in Figure 11A). We measured axon length, growth cone area, and number of growth cone filopodia (diagram in Figure 13F). Nestin levels were not correlated with any variance in axon length (Figure 11E), but interestingly growth cone area was significantly smaller when nestin was present (Figure 11F). This finding is consistent with previous reports in frog neurons, where the neurons expressing the nestin homolog, tannabin, had smaller blunted growth cones (Hemmati-Brivanlou, Mann and Harland, 1992). How growth cone size is regulated and what effect growth cone size has on growth cone functions is unknown, but other molecules that regulate the actin and microtubule cytoskeleton display a similar phenotype. Growth cone size therefore may be representative of the underlying overall cytoskeletal dynamics, where a more stable cytoskeleton leads to larger growth cones, and a more dynamic cytoskeleton leads to smaller growth cones (Poulain and Sobel, 2007; Khazaei *et al.*, 2014). Others have noted a correlation between axon growth rates and growth cone size, however our measurements of axon length do not show any significant differences (Argiro *et al.* 1984; Ren and Suter 2016).

Since nestin regulates Cdk5-dependent processes in muscle cells (Yang *et al.* 2011), we wondered if nestin could affect Cdk5-dependent processes in neurons as well. Sema3a is upstream of Cdk5 in neurons (Kobayashi *et al.*, 2014), and we thus utilized an *in vitro* bath application “Sema3a collapse assay” to test this idea. In cultured neurons, phosphorylation of Cdk5 substrates and morphological changes in growth cones (Dent, 2004; Perlini *et al.*, 2015) start within minutes of Sema3a exposure with the loss of growth cone filopodia, resulting ultimately in a collapsed growth cones with no filopodia. Therefore, prior to complete growth cone collapse Sema3a leads to

retraction of individual filopodia (Dent, 2004). Given nestin's role in promoting Cdk5 activity at the neuromuscular junction, we hypothesized that growth cone filopodial retraction in response to Semaphorin 3A occurred in a nestin-sensitive manner. In order to quantitatively address this, we counted actin-rich filopodial protrusions of the growth cones (Figure 11G). In untreated cells, filopodia number was inversely correlated to axonal nestin levels (Figure 11G). After a low dose of Semaphorin 3A treatment (1nM for 5 minutes) (Perlini *et al.*, 2015), nestin-positive cells retracted growth cone filopodia significantly, whereas nestin-negative growth cones were not significantly affected by Semaphorin 3A during the 5 minute timeframe (shown in Figure 11B, quantified in Figure 11G). Area of the growth cone was not significantly altered in this short time frame as expected (Dent, 2004), so we relied on the retraction of filopodia as our most sensitive measurement of Semaphorin 3A sensitivity. Because Semaphorin 3A is known to act in part through Cdk5, we added 10 μ M of the Cdk inhibitor roscovitine for 30 minutes prior to Semaphorin 3A application. Roscovitine pretreatment inhibited the decrease in filopodia number after Semaphorin 3A treatment (Figure 11C,G). Roscovitine inhibits Cdk5 potently, but it also inhibits some of the mitotic Cdks (Cdk2 and cdc2), albeit less effectively. Since neurons are post-mitotic, they have little to none of the mitotic Cdk activities. It is thus likely that the roscovitine inhibition of the Semaphorin 3A effect is due to Cdk5 inhibition.

Lastly, nestin is not absolutely required for Semaphorin 3A sensitivity since higher and longer Semaphorin 3A stimulation (2nM for 15 minutes) resulted in filopodial retraction even in nestin negative cells (Figure 11D,G). Together these data demonstrate a strong correlation between axonal nestin expression and growth cone size, and Semaphorin 3A mediated filopodial retraction.

Nestin depletion results in abnormal growth cone morphology and decreased sensitivity to Semaphorin 3A.

To test for nestin dependent sensitivity to Semaphorin 3A directly, we used nestin siRNAs to deplete nestin protein from neurons and assess growth cone morphology and response to Semaphorin 3A. Neurons electroporated with the siNes-pool and GFP (to visualize transfected cells) (Figure 6C, Figure 7A, Figure 12A,E) were analyzed for differences in morphology. Neurons that received the siNes-pool had no variance in axon length (Figure 12C), but had large growth cones (Figure 12D) and more growth cone filopodia (Figure 12F) compared to siCon, mirroring the effects seen from analysis of endogenous variation of nestin expression (Figure 11). To confirm that this effect was specific to nestin depletion and not an off-target effect, the 4 siRNAs that make up the siNes-pool were tested individually. Two of them (#1 and #17) were effective for both depleting nestin as well as for increasing growth cone size and filopodial number (Figure 13A-E). More than one distinct siNes thus resulted in the same phenotype as the siNes-pool, consistent with specificity of the phenotype to nestin depletion. Consistent with this conclusion, siNes #4 failed to reduce nestin levels and did not affect growth cone morphology, similar to siCon (Figure 13A-E).

As expected, siCon transfected neurons had a significant reduction in filopodia number following 1nM Semaphorin 3A treatment for 5 minutes. Neurons transfected with the siNes pool and then treated with Semaphorin 3A (1nM 5 minutes), in contrast, showed no change in filopodia number (Figure 12E) and they were thus insensitive to this dose of

Sema3a. These results demonstrate, surprisingly, that nestin increases the sensitivity of axonal growth cones to Sema3a.

2.4 Discussion

Neural development requires that axonal growth cones respond to a variety of extracellular guidance cues to change their direction of growth for proper wiring of the nervous system (Kolodkin and Tessier-Lavigne, 2011). Importantly, not all growth cones traversing the same environment respond the same way to the same cues at the same time (Carcea et al. 2010; Mintz et al. 2008; Wang et al. 2014). Even more remarkably, the same growth cone often responds differently to the same axon guidance cue when encountering it at a different point in time and space (Kolodkin and Tessier-Lavigne, 2011). As an axon grows into new brain regions, it must therefore not only respond to new cues, but often differently to the same, previously encountered cue. The molecular mechanisms underlying this variable response to the same cue are poorly understood. We propose that nestin acts as a sensitizer and might provide a gain control mechanism, such that axons lacking nestin are less repelled by Sema3a than axons expressing nestin.

Nestin is highly expressed in NPCs but expression persists in young neurons.

We made the surprising discovery that nestin, the most commonly used marker for NPCs, is also found in young neurons. Our conclusion that nestin is in fact expressed in neurons is based on multiple lines of evidence, including multiple antibodies to distinct epitopes, multiple distinct siRNAs to knockdown expression, and peptide blocking of nestin immunostaining.

We find that nestin localizes predominantly to the distal axon, and is not found enriched at dendritic tips. This is an intriguing observation, given the importance of neuronal polarity (Takano et al. 2015) and of the opposite growth directions of the future axons and apical dendrite in early cortical neurons (Wang et al. 2014). In the distal axon, nestin is found in tightly bundled filaments which co-distribute with other neuronal IFs at the wrist region of the growth cone, but individual nestin filaments can also be seen to extend into the central region of the growth cone and even sometimes into the periphery. Nestin is thus well positioned to regulate growth cone dynamics.

A remaining question is if the nestin protein detected in neurons is a remnant that was translated when the cell was a NPC, or is made from nestin mRNA in neurons. Our ability to knock down nestin with siRNA following dissociation suggests that nestin mRNA is present after dissociation and actively translated in early neurons. Several papers have described nestin mRNA in neurons in developmental, normal adult, and pathological/injury contexts (Crino and Eberwine, 1996; Kuo *et al.*, 2005; Zhu *et al.*, 2011; Perry *et al.*, 2012; Arner *et al.*, 2015; Bigler *et al.*, 2017; Dey *et al.*, 2017; Farzanehfar *et al.*, 2017; Farzanehfar, Horne and Aumann, 2017). Nestin expression is thus not excluded from neurons. Nestin's presence in subpopulations of adult neurons suggests that some neurons may never lose nestin expression or may regain it later. The best evidence for nestin mRNA in early post-mitotic cortical neurons arises from a single cell RNA-seq experiment in which flash tag labeling was used to birthdate newborn cells in the cortex of an E14 mouse embryo *in utero*, followed by dissociation

and single cell RNA-seq 6 to 48 hours after labeling (Telley *et al.*, 2016). This unbiased single cell approach *in vivo*, revealed that nestin mRNA does persist in some newborn neurons of the embryonic mouse cortex 24-48 hours after cell division. This suggests that early neurons continue to make new nestin. We propose that newly made neuronal nestin still plays a functional role. Furthermore, the initial nestin mRNA localization study did detect nestin mRNA in the intermediate zone (Dahlstrand, Lardelli and Lendahl, 1995a), where early axons are located.

A role for neuronal nestin *in vivo*?

Little is known about nestin function in the developing brain overall and existing reports of nestin phenotypes are conflicting. A number of defects have been reported for nestin knockdown in neural stem cells in culture, including increased cell death, but proliferation and differentiation were reportedly normal (Hu *et al.* 2016; Di *et al.* 2014). Downregulation of nestin also augmented sensitivity to oxidative stress (Sahlgren *et al.*, 2006), implicating nestin in cellular stress pathways. In Zebrafish, microcephaly and small eyes were reported after knockdown of nestin expression with morpholinos (Chen *et al.*, 2010). Again, NPC cell death was increased. There were also some defects in axon tracts, but it was not clear if these were a consequence of NPC phenotypes or independently arising in neurons. Another paper used in utero electroporation of shNestin into rat embryos and found fewer migratory neurons (Xue and Yuan, 2010). This was reported to be due to cell cycle arrest of NPCs in the G1 phase of the cell cycle. Cell death was not increased. The shNestin phenotype could be rescued with WT nestin (Xue and Yuan, 2010). The same year, the first mouse nestin KO papers were published. One paper reported embryonic lethality with severe brain defects due to increased NPC cell death (Park *et al.* 2010). The reported phenotype thus appeared similar to the Zebrafish phenotype and possibly also the rat shNes phenotype. A second nestin KO paper, in contrast, reported viable and fertile mice showing only mild motor deficits (Mohseni *et al.* 2011). The motor deficits were traced to defects in myoblasts, resulting in abnormal NMJ formation with impaired AChR clustering. Adult (but not embryonic) neurogenesis was found to be impaired in the viable nestin KO strain by a surprising non-cell autonomous mechanism where nestin-expressing astrocytes regulate Notch signaling in progenitors to maintain stemness (Wilhelmsson *et al.* 2019). In addition, some behavioral defects were described in the same paper, in particular with respect to long term memory in an object recognition test (Wilhelmsson *et al.* 2019). A role for nestin in maintaining NPC pools is thus likely, but data are contradictory and controversial. Furthermore, the mechanism by which nestin might regulate embryonic NPC pools is not known.

A role for nestin in neurons during embryonic development is completely unknown. We provide evidence that nestin modulates responsiveness to Sema3a in cultured cortical neurons. What role could the neuronal nestin play *in vivo*? At these early developmental time points, Sema3a is important for initial axon positioning and fasciculation (Zhou *et al.* 2013; Beher *et al.* 1996). Since Sema3a exists *in vivo* as a gradient emanating from the ventricular zone and cortical plate, it is conceivable that nestin mediated Sema3a sensitivity could dictate the position of the axon within the IZ (Ruediger *et al.*, 2013). We were unable to deplete nestin *in vivo* acutely, because nestin depletion by *in utero* shRNA electroporation, results in loss of migratory neurons

in the cortex. Since nestin expression is much higher in NPCs, the authors conclude this phenotype is likely due to impaired cell division of NPCs (Xue and Yuan, 2010), precluding analysis of nestin function in postmitotic neurons. More detailed analysis of the nestin-positive axons *in vivo* will be needed to more precisely predict what guidance defects might be found if neuronal nestin expression was disrupted. Given our results, this is something of great interest to do in the future, but a conditional KO might be needed to avoid depleting nestin in NPCs, in order to separate any effects of nestin in NPCs versus in early neurons.

Nestin as a novel gain control element in Sema3a signaling

Several other molecules have been shown to modulate responsiveness to guidance cues (Kaplan *et al.*, 2014), including types of co-receptors (Dang, Smythe and Furley, 2013), lipid raft components (Carcea *et al.*, 2010), second messengers (such as cAMP/cGMP and calcium) (Henley *et al.* 2004; Tojima *et al.* 2014; Shelly *et al.* 2011), and modification of downstream signaling cascades by ERM (Mintz *et al.*, 2009), α 2-chimaerin (Brown *et al.* 2004; Ip *et al.* 2011), and 14-3-3 proteins (Kent *et al.*, 2010; Yam *et al.*, 2012). Our results now add the IF protein nestin to this category of proteins that can variably regulate responsiveness to Sema3a. The previously identified modulators often serve to vary the degree of signaling output to alter the cytoskeleton and adhesive properties of the growth cone (Vitriol and Zheng, 2012). Nestin might similarly modulate cytoskeletal responses to Sema3a, but the molecular mechanism is currently not known. Multiple cytoskeletal proteins are known substrates for Cdk5 and act downstream of Sema3a. They are obvious candidates for being nestin effectors in this cascade and mediating the increased Sema3a sensitivity of nestin-expressing neurons. Studies on the role of nestin in cancer cells has demonstrated the importance of nestin for migration/invasion, proliferation, and survival of cancer cells- which are reduced after nestin depletion by altering cell signaling pathways (Zhao *et al.* 2014; Hyder *et al.* 2014; Narita *et al.* 2014; Liang *et al.* 2018; Wei *et al.* 2007; Zhang *et al.* 2017). How nestin promotes higher sensitivity to low doses of Sema3a remains unknown, and future investigation will assess how phosphorylation of Cdk5 substrates are affected by the presence or absence of nestin.

One other remaining question is how nestin, which is primarily localized to the distal parts of the axon and to the central domain and/or wrist of the growth cone, affects the stability and dynamics of peripherally localized filopodia. Other examples of proteins initially described as being wrist localized, have been found to affect filopodial morphology but is an open question how actin-based structures and microtubule networks coordinate growth cone morphology and axon growth (Astle *et al.* 2011; Grabham *et al.* 2007). In fact, intermediate filaments are known to crosslink and interact with these other cytoskeletal elements (Chang and Goldman, 2004). Nestin might similarly affect the other structures of the growth cone by structural or regulatory crosstalk. This is currently not known, but an exciting future direction for further research.

In summary, we have identified nestin intermediate filament protein at the axonal growth cone where it plays a role in regulating growth cone morphology. In addition, we identify nestin as a novel downstream effector of Sema3a signaling. Nestin intermediate filament protein could thus play critical regulatory roles in axon guidance responses by

serving as a “gain control” element to increase responsiveness of a subset of axons to a common guidance cue. The mechanism by which nestin sensitizes growth cones to Sema3a in a Cdk5 dependent manner will be discussed in the following chapter.

Figure 6: Nestin protein expression persists in immature primary cortical neurons in culture.

A. Nestin expression in cultures derived from E16 mouse cortex grown for one day (1DIV). Doublecortin (DCX) immunostaining and a stage 3 morphology was used to identify neurons. Nestin is enriched near the axonal growth cone (pink arrowheads), but largely absent from growth cones of minor dendrites (white arrows) using both mouse and chicken anti-nestin antibodies. White arrowheads indicate short nestin IF segments found along the axon shaft. Bottom panel is enlarged inset of growth cone, rotated, from within the white box. Growth cone outline drawn from the phalloidin stain shown in the panels with phalloidin and in the enlargement.

B. Validation of nestin antibody staining on stage 3 neurons with mouse and goat anti-nestin antibodies with immunizing peptide antibody blocking. Both antibodies again show a distal axon enrichment of nestin (pink arrowheads) while the dendrites again are not labeled (white arrows). Pre-incubation of the goat anti-nestin antibody with the immunizing peptide abolishes all staining but staining in the distal axons is still detectable with the mouse anti-nestin antibody which was raised against a different epitope. Shown are E16 mouse cortical neurons 1DIV. Bottom panel is enlarged inset of growth cone from within the white box. Growth cone outline drawn from the phalloidin stain shown in the panels with phalloidin and in the enlargement.

C. Nestin siRNA results in loss of immunostaining, validating that the axonal growth cone staining is due to nestin protein. GFP was co-transfected as a transfection indicator. After 36 hours in culture, cells were fixed and immunostained for nestin and DCX. The number of GFP positive cells positive for nestin in the axon as a fraction of the number of cells counted was quantified.

D. Nestin is co-localized with other intermediate filaments in the same assembly group (vimentin and Neurofilament-Medium NF-M) in the distal axon (pink arrowheads) of E16 mouse cortical neurons 1DIV. N-FM expression was low in immature cortical neurons cultured for only 1DIV. High magnification of the boxed region and linescans reveal that nestin and N-FM appear to decorate the same filament structure in partially co-localizing subdomains, as expected for nestin containing intermediate filaments. Pink arrowheads indicate nestin positive axonal intermediate filament heteropolymers.

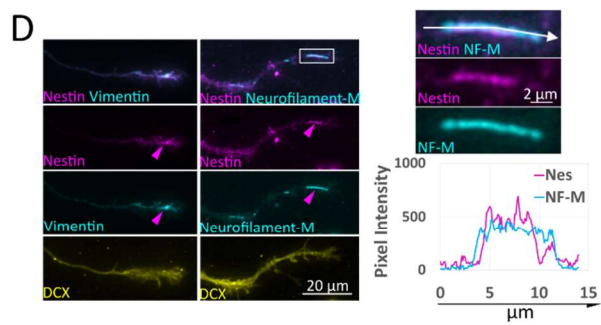
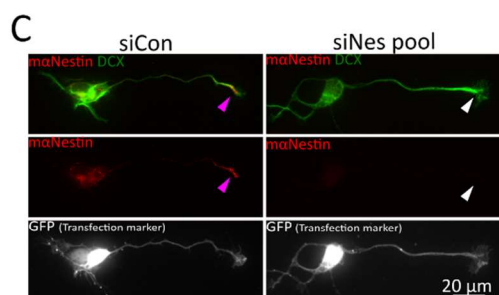
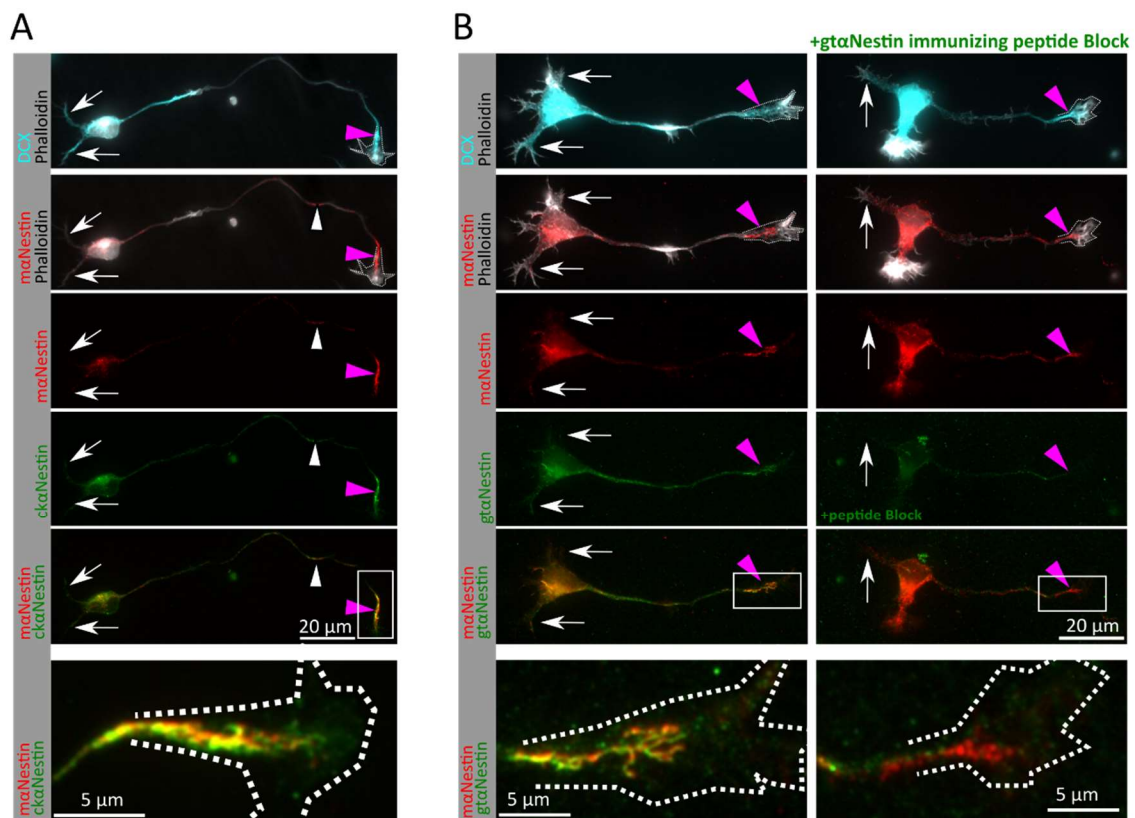


Figure 7: Nestin protein antibody controls and cell population comparisons

A. Nestin knockdown was also qualitatively assessed by western blotting of whole cell lysates of cortical cultures (1 DIV) with Mouse, Goat, and Chicken nestin antibodies. A band of the expected size was detected with all 3 antibodies in siCon but decreased levels are seen after siNes expression. The knockdown was partial. This is likely due to lower transfection efficiencies in cultured neurons where less than 50% of cells are transfected. The related intermediate filament vimentin was unaffected, and DCX was blotted as a loading control.

A'. Myc-tagged nestin was overexpressed in HEK293 cells and co-transfected using lipofectamine2000 with siCon or siNes siRNA. Lysates were blotted for the myc-tag and for nestin, demonstrating near complete knockdown in the high transfection efficiency HEK293 cells. The related intermediate filament vimentin was unaffected, and alpha-tubulin is loading control.

B and B'. Full blots demonstrating specificity of nestin antibodies used in IF studies as a single band above 250 kd (~300kd). Protein lysate from cultured 1DIV E16 mouse neurons (B), and E16 mouse cortex (B'), both probed with the goat anti-Nestin antibody and the mouse anti-Nestin clone 2q178 antibody. In addition, E16 brain lysates were probed in the presence or absence of the immunizing peptide to the goat nestin antibody. This preincubation specifically diminished the ~300kd immunoreactive band recognized by the goat antibody.

C. Side by side comparison of nestin levels in a Sox2 positive neural progenitor cell (NPC) and a primary differentiating DCX positive neuron. E16 mouse cortical cultures at 1DIV were stained with antibodies to the indicated proteins. They contain mostly neurons but an occasional NPC can still be found at 1 DIV. Nestin levels in the in the primary neurite and cell body of DCX+ neurons are many fold lower than in the NPC, but is still detectable.

D. Both nestin negative and nestin positive have a range of Ctip2 and Satb2 nuclear intensities. Pink arrowheads indicate nestin in the distal axon. A total of 68 DCX+ neurons (24 nestin negative, 44 nestin positive) were quantified in terms of nuclear intensity of either Ctip2 or Stab2 immunostaining. No correlation was found. (Unpaired t-test)

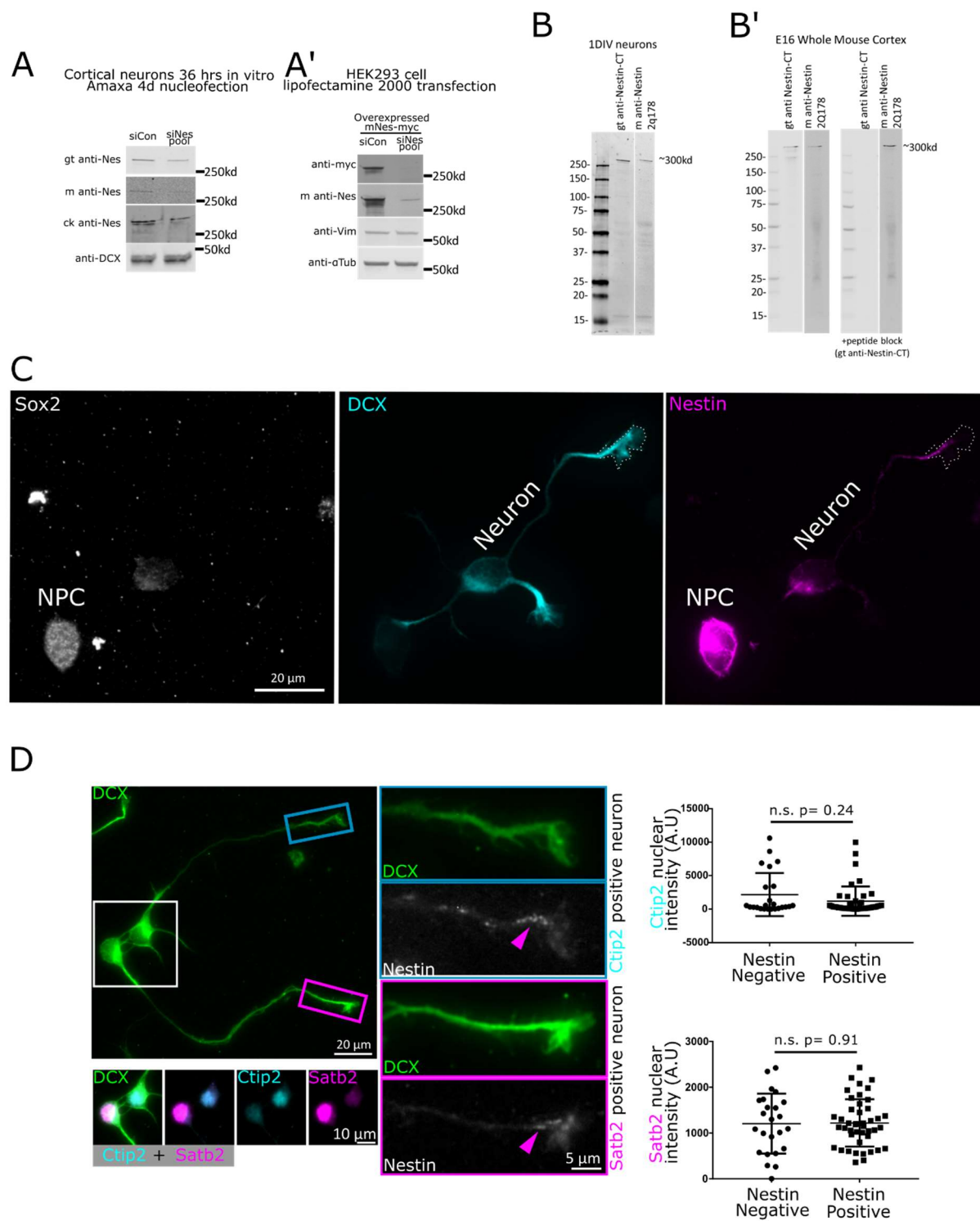


Figure 8: *Nestin-expressing neurons are observed in multiple rodent and human culture models*

A. Mouse Neurosphere NPC cultures: Nestin expression was assessed in differentiating dissociated neural progenitor cells (mouse NPC) after 4 days of neuronal differentiation. DCX-positive neurons frequently stain positive for nestin (yellow asterisk), especially in axon tips (pink arrowheads). An example of axon positive for DCX but not nestin is marked with a series of white arrowheads along the length of the long and thin axon, and a large white arrowhead indicating the growth cone. Nestin single positive cells are marked with a pink asterisk. One example of a double-positive cell is shown in the middle panels to highlight its neuronal morphology and tip-enriched nestin staining (pink arrowhead). The proportion of cells positive for only nestin (red bar), only DCX (green bar) or double-positive for DCX and nestin (yellow bar) was quantified for NPCs cultured under differentiation conditions from 1 or 4 days. Yellow dotted lines highlight the expanding double positive population (yellow bar). 323 cells were counted at 1 DIV, and 219 cells counted at 4 DIV.

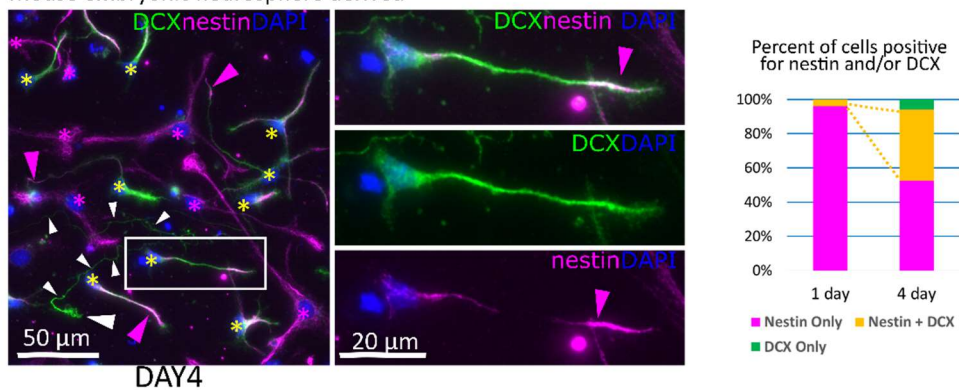
B. Human IPSC derived neuronal cultures: Nestin is expressed in human (IPSC) differentiating neurons derived from NPCs in dissociated cultures under differentiating conditions from 1, 4 and 6 days. The distribution of nestin is similar to the mouse NPC-derived neurons described above. Percent co-localization with the neuronal-specific β III tubulin was quantified. A close-up of a nestin-positive axon tip in the boxed region is shown in the panels below the respective image. n=14 (day 1), 10 (day 4), and 14 (day 6-8). (Statistics: Mann-Whitney t test)

C. Nestin is expressed in β III tubulin-positive neurons in human IPSC derived mini-brains. The boxed regions 1-3 are shown larger in the insets, and arrowheads indicate nestin β III tubulin doublepositive cells. Nestin positive radial glia like cells span the spheroid, while high β III tubulin cells are located to the periphery. Low β III tubulin expressing cells can also be found in the central ventricular-like region representing differentiating neurons not yet migrated, and insets analyzed are outside of this region. Nestin can be detected in the tips of some of the β III tubulin processes (arrowheads).

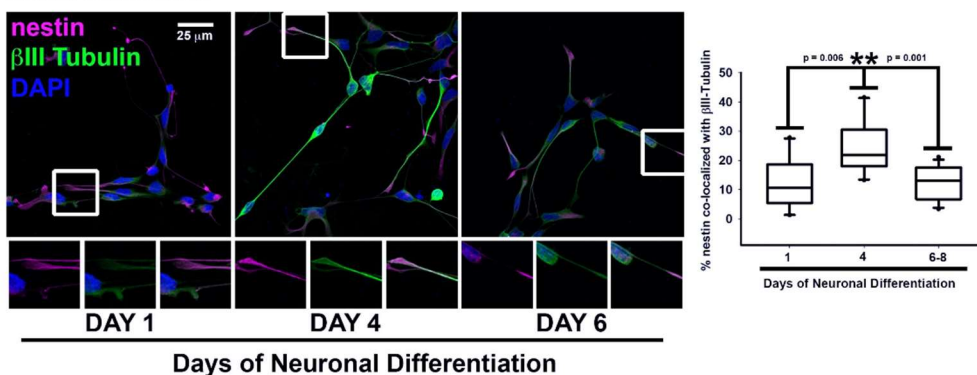
D. Mouse primary neurons cortical neuron cultures: Percentage of nestin-positive neurons rapidly decreases with time in culture. (30-60 stage 3 neurons were counted per time point for 3 to 5 experiments as shown as the n). Cortical neuron cultures were prepared from E16 mice embryos and culture times are indicated.

E. Mouse primary explants: Axonal nestin expression is progressively lost between 36 to 72hours in culture. Significant axonal nestin immunostaining is no longer detected by 72 hours. E16 mouse cortex was explanted by incomplete dissociation and cultured. Axon fascicles emerging from the explant are shown. Arrowheads point at axon tips.

A Mouse embryonic neurosphere derived-

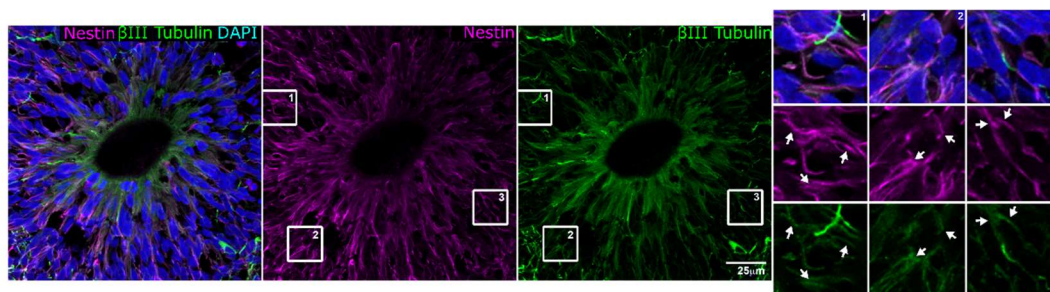


B Human IPSC derived

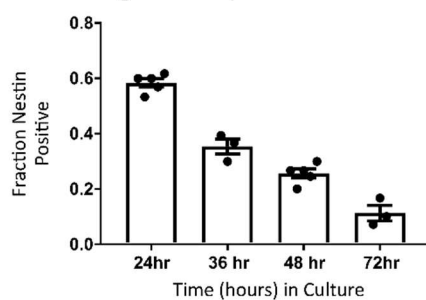


C

Nestin in Human IPSC derived minibrains



D E16 Stage 3 axons per time in culture



E 36hr 72hr

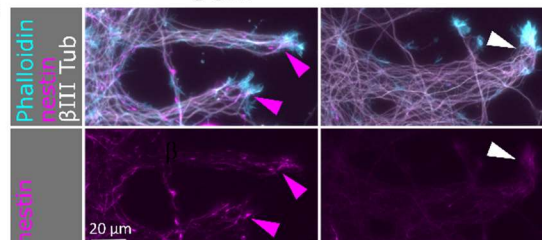


Figure 9: *Nestin is expressed in sub-populations of cortical axons in developing cortex.*

A. A low magnification of a coronal cortical section (E16 mouse) is shown for orientation (top) and showing α -internexin localization to the axon rich intermediate zone. The white box (lateral lower Intermediate Zone) is the region imaged in the following panels, and is (B) diagrammed below illustrating the vertically oriented radial glia, and horizontal IZ axon bundles.

C. Super resolution microscopy (STED) of nestin immunostaining reveals bright staining of radial glial fibers (arrowheads) as well as fainter staining of axons (arrows) in mouse E16 cortex. Many axons in the axon fascicle do not express nestin, so only a subset of axons in the intermediate zone express nestin at this time point. Arrow heads indicate radial glia and arrows indicate nestin-positive axons.

D. Nestin staining of the lower intermediate zone of E16 mouse cortex using chicken anti-nestin (cyan) and goat anti-nestin (magenta) antibodies. Axon tracts are visualized with α -internexin antibody (white). Nestin staining is found in radial glia fibers (arrowheads) as well as in α -internexin-positive axon tracts (arrows). The goat anti-nestin antibody was preincubated with immunizing peptide on sequential cryosections in the lower panels. All staining with the goat anti-nestin antibody was blocked by peptide preincubation, including the axon tract staining, demonstrating that the axon staining was specific and not background staining. All images correspond to higher magnification of the lower intermediate zone of the lateral E16 mouse cortex (boxed regions in A). Radial glia are oriented vertically (arrowheads) and axon tracts are oriented horizontally (arrows).

E. Identification of nestin-positive axons in mouse cortex. The L1-CAM-positive axons (white) contain mixed populations of both cortical and thalamic projections in this brain region. Nestin (magenta) is specifically expressed in axons originating from the cortex (Tag-1-positive; cyan), but not in axons with thalamic origin (calretinin-positive, yellow). Arrow heads indicate radial glia and arrows indicate nestin-positive and Tag1-positive axons.

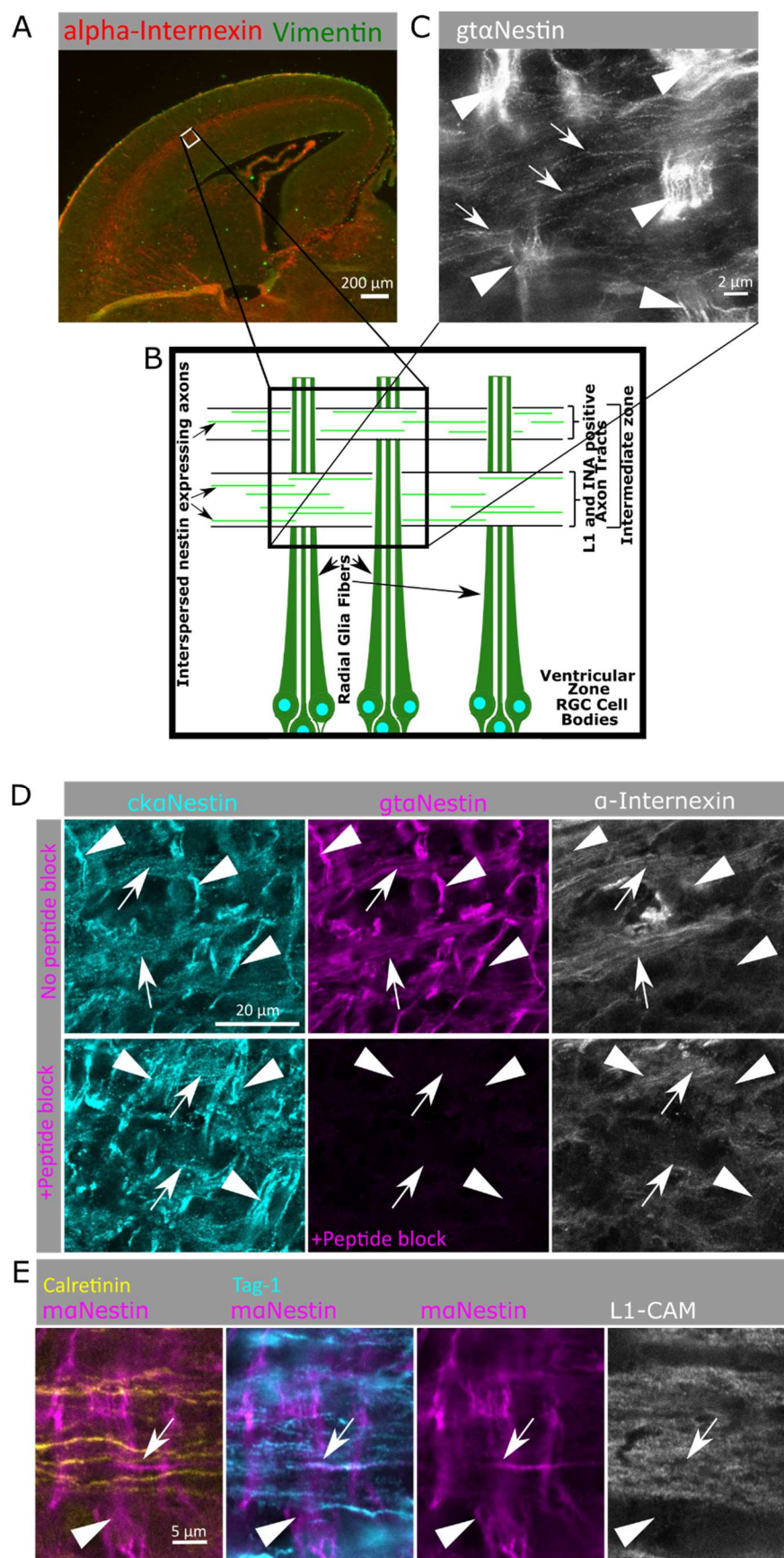


Figure 10: Identical staining pattern seen in E16 mouse cortical axons with two different anti-Nestin mouse monoclonal antibodies

A,B. Nestin (multiple antibodies) is found together with its polymerization partner vimentin along axons (identified by the axonal cell adhesion molecule L1-CAM). Arrow heads indicate radial glia and arrows indicate nestin-positive axons.

Both the mouse anti-nestin antibody 2q178 (A) and rat401 (B) produce similar axon immunostaining in E16 mouse cortex, as do the other nestin antibodies used in this study (Figure 9B).

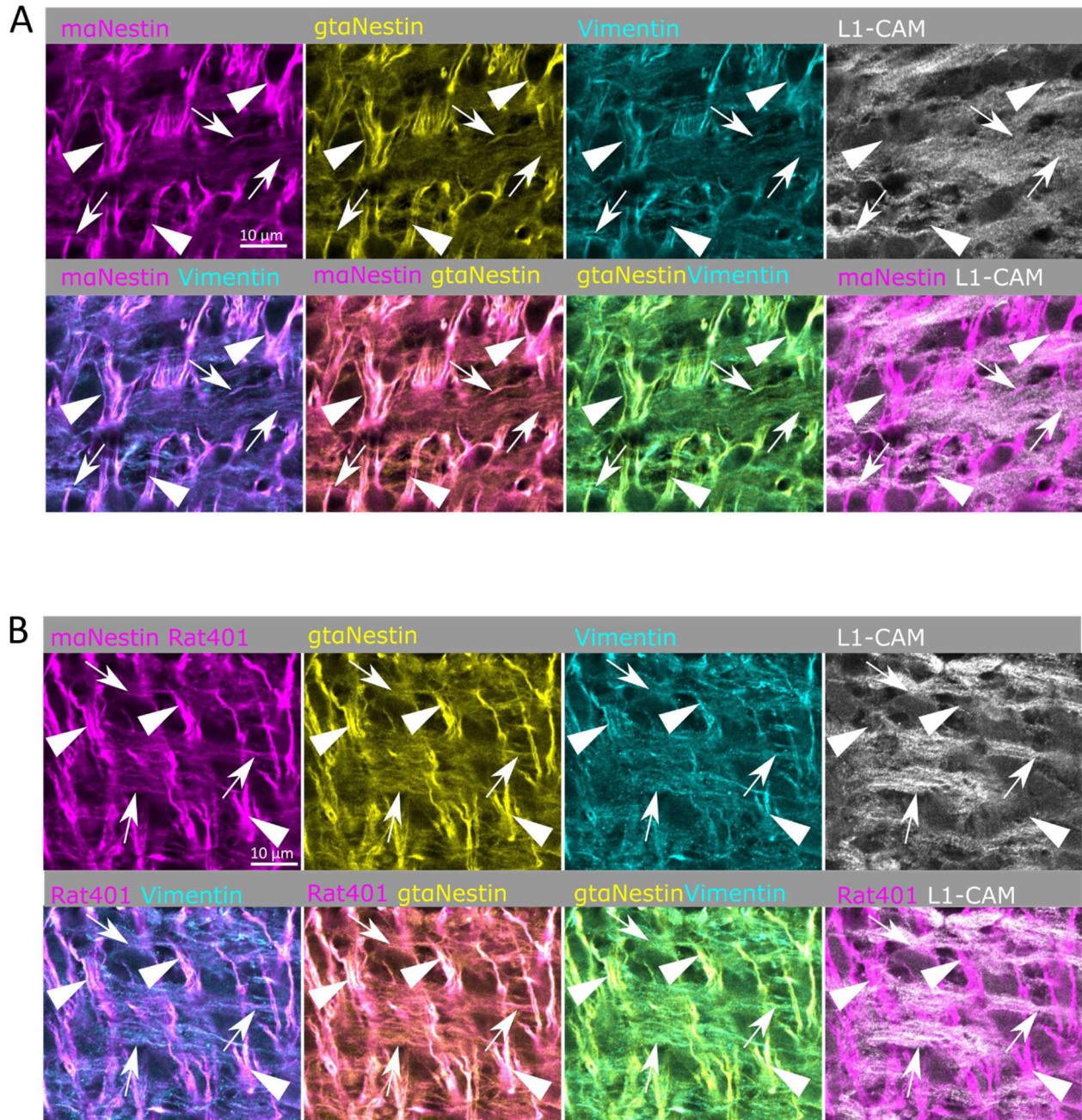


Figure 11: The level of nestin expression in neurons influences growth cone morphology and response to Semaphorin3a

A. E16 mouse cortical neurons 1DIV (stage 3) were immunostained against DCX (to confirm neuronal identity), phalloidin (to visualize the growth cones), and nestin. Cells were characterized based on nestin immunoreactivity in the distal axon nestin as Nes(-)-not detected, Nes(+)-nestin positive. Conditions are untreated (A), 1nM Sema3a 5 minutes (B), pretreatment with 10 μ M Roscovitine 30 minutes prior to 1nM Sema3a treatment for 5 minutes (C), and a Sema++ treatment of 2nM Sema3a for 15 minutes (D). Insets allow for appreciation of the filamentous nature of the nestin immunostaining and proximity to the growth cone. Channel intensity is adjusted equally for nestin and DCX. In the low magnification, phalloidin labeling has been adjusted variably to show morphology, but in the insets the phalloidin channel was adjusted in an equal manner.

E,F. Nestin expressing neurons are not significantly different by axon length (E), but have significantly smaller axon growth cones (F). Neuron morphology was quantified (30-40 cells per experiment for 6 (E), or 5 (F) independent experiments). Mean of each experiment and SEM are indicated. Statistical test was t-test with n=6 (E), or n=5 (F).

G. Neurons with nestin have fewer filopodia compared to those without nestin. In cells treated with 1nM Sema3a for 5 minutes, the nestin positive cells had a significant reduction in filopodia compared to untreated nestin positive cells, whereas the nestin negative cells did not. Conditions have been color-coded for ease of comparison. Roscovitine inhibited the decrease in filopodia number after Sema3a treatment. When a high dose (2nM) and longer treatment (15minutes) of Sema3a is used, both nestin negative and positive neurons retract filopodia and significantly so, indicating nestin is not absolutely required for Sema3a induced filopodial retraction, but increases Sema3a sensitivity. Filopodia number were quantified for 6 (vehicle, Sema3a), 4 (roscovitine + Sema3a), or 3 (Sema++) independent experiments. The average of 30-40 cells quantified per experiment is shown. Mean of each experiment and SEM are indicated. Normality was confirmed with the Shapiro-Wilk normality test. Statistical test was one way ANOVA with Tukey's multiple comparison correction, with n= number of experiments. Each condition was compared to every other condition.

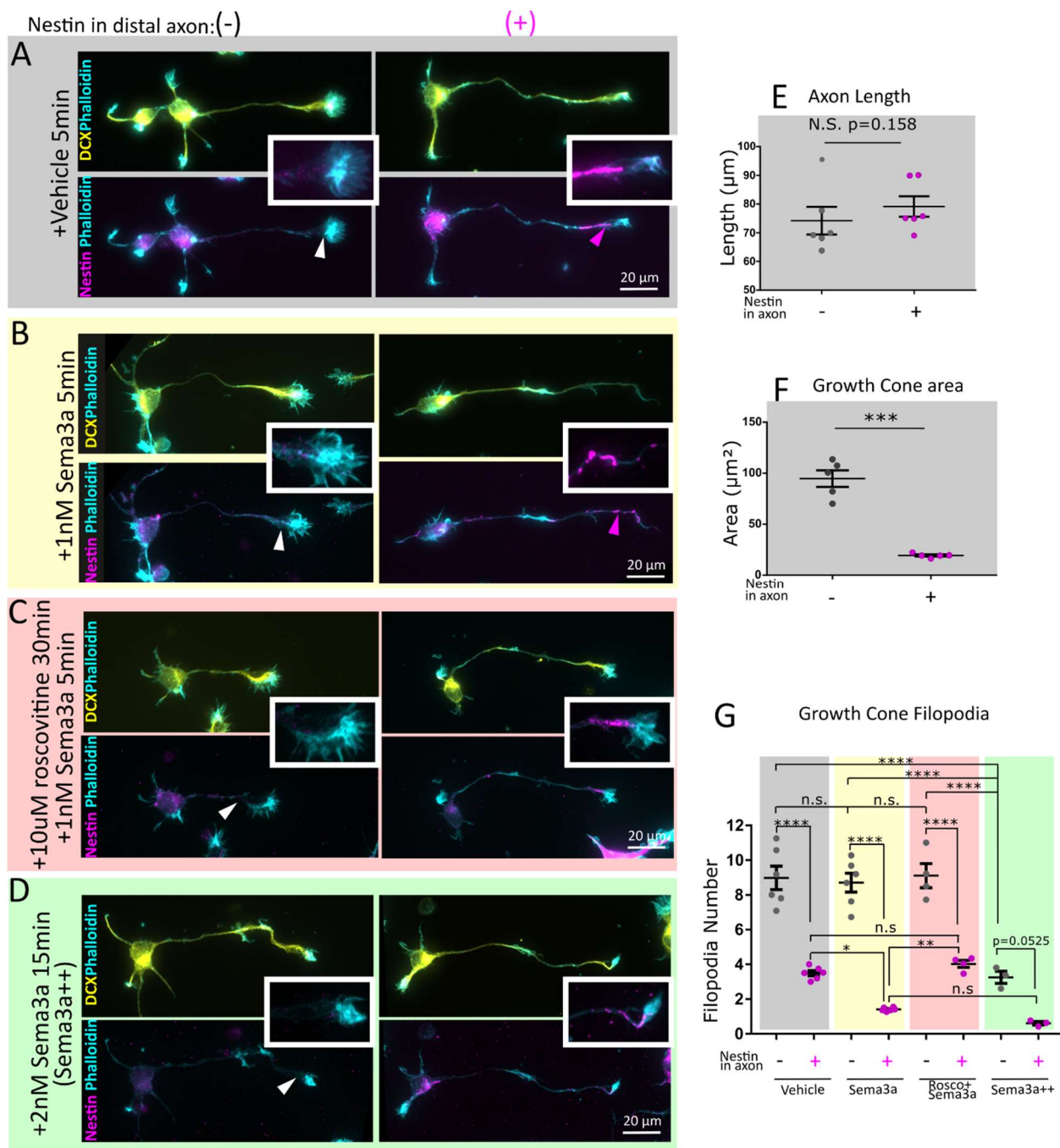


Figure 12: Nestin depletion results in abnormal growth cone morphology and resistance to Semaphorin3a

Representative images of primary E16 Mouse cortical neurons that were co-transfected with a plasmid encoding GFP and either control siRNA (siCon) or nestin siRNA (siNes) and cultured for 36hrs. GFP booster was used to visualize transfected cells, Tuj1 (β III-tubulin) was used to confirm neuronal identity and for cell morphology, and phalloidin to visualize growth cones (A,E). The efficiency of nestin knockdown was quantified (B) by counting GFP (transfected) and nestin positive cells by immunostaining was quantified in stage 3 neurons. ~1/3 of siCon neurons express nestin at 36 hrs in the axon. Very few transfected neurons showed nestin expression in the axon under siNes conditions. 120-140 cells per condition were counted in n=5 independent experiments. $p < 0.001$ (Paired t-test). In vehicle treated conditions (A), siNes treated cells had no significant difference in axon length (C) but resulted in significantly larger growth cones (D). n= ~100 cells (plotted on the graph) were measured for each condition and significance measured by unpaired Mann-Whitney rank comparison test. Shapiro-Wilk normality test indicated the data were not normal. A t-test was also performed (to be consistent with other analysis) for the growth cone area data separately with each experimental average, n=4 (each a different color on graphs), and resulted in a significant p value of 0.025. siCon or siNes transfected neurons were treated for 5 minutes with 1 nM Sema3a (E). siNes resulted in more filopodia per growth cone, and these filopodia were resistant to Sema3a retraction (F). ~100 or cells in 4 independent experiments were averaged and n=4 was used for statistical analysis (one way ANOVA with Sidak correction –only the pairs shown were compared). Normality was confirmed with the Shapiro-Wilk normality test.

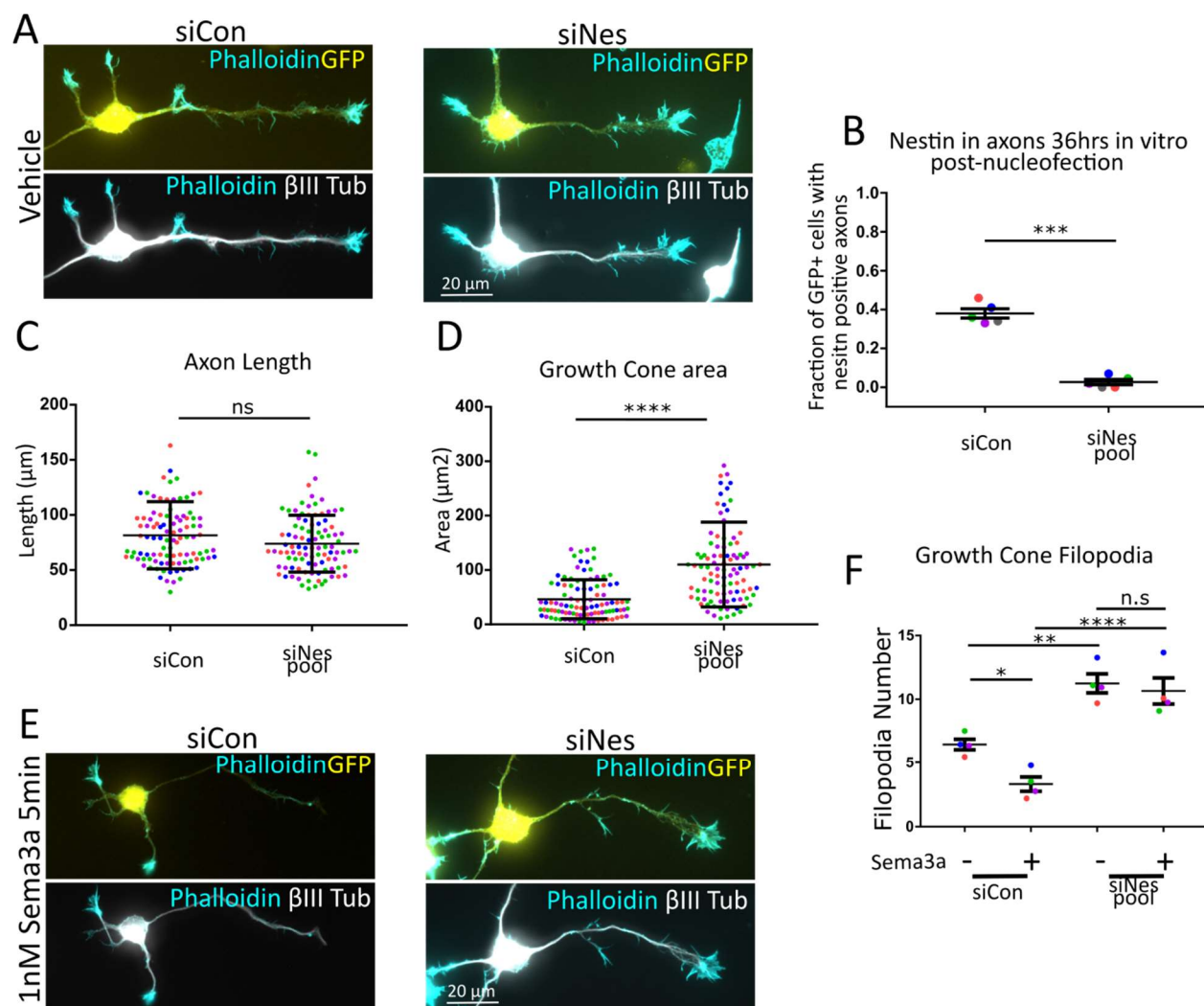


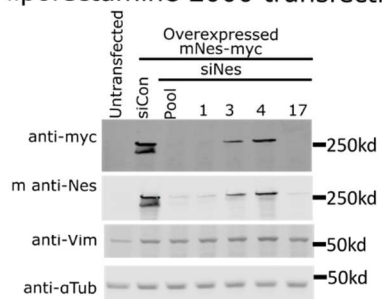
Figure13: Multiple single nestin siRNA's lead to nestin depletion and associated morphological changes

A. Relative efficiency of nestin silencing of the 4 individual siRNA's from the siNes pool. Myc-tagged nestin was overexpressed in HEK 293 cells and co-transfected using lipofectamine 2000 with siCon or various siNes siRNA. Lane 1 is untransfected HEK293 cell lysate. Lysates were blotted for the myc-tag and for nestin, demonstrating again complete knockdown with the siNes pool, as well as efficient knockdown by siNes #1 and 17. siNes #3 had an intermediate effect, while siNes #4 was the least effective, and is used as an additional control in the following experiments in neurons. The related intermediate filament vimentin was unaffected, and α -tubulin is used as a loading control.

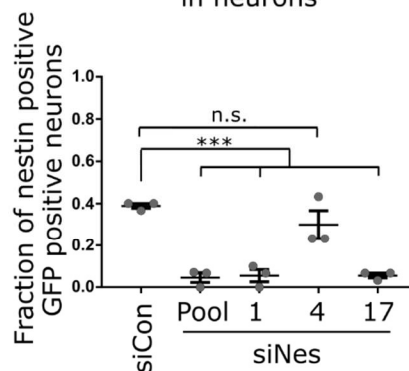
B-E. 3 individual siNes siRNA's were transfected into neurons to confirm efficiency (B) and confirm morphological phenotypes (C,D,E) seen after nestin depletion by siNes pool. Both effective siNes #1 and #17 (and the siNes-pool) resulted in a significant depletion of nestin positive neurons after 36 hours, while the non-effective siNes #4 did not significantly reduce the number of nestin positive cells. None of the transfection conditions altered the average axon length (C), while siNes #1 and #17 phenocopied the pool by growth cone area (D) and growth cone filopodia number (E), while siNes #4 had no significant effect. Error bars are SEM. N=3 experiments, with the means of each plotted on the graph. Normality was confirmed with the shapiro-Wilk normality test. Each condition was compared to control with a one way ANOVA with Dunnet's correction.

F. A labeled version of the cell in Figure 12E diagraming how morphological measurements were made.

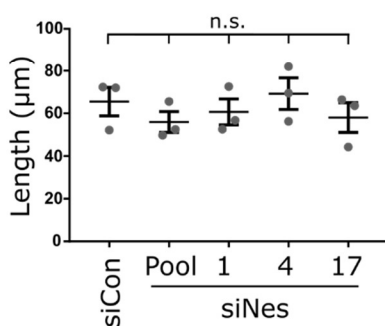
A HEK293 cells lipofectamine 2000 transfection



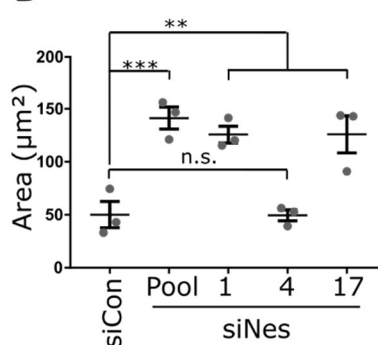
B Nestin siRNA efficiency in neurons



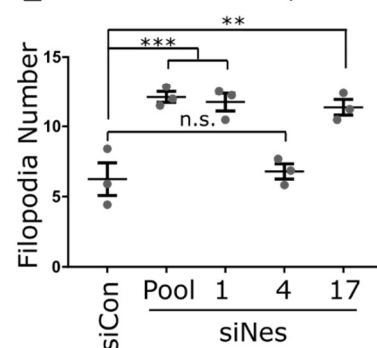
C Axon Length



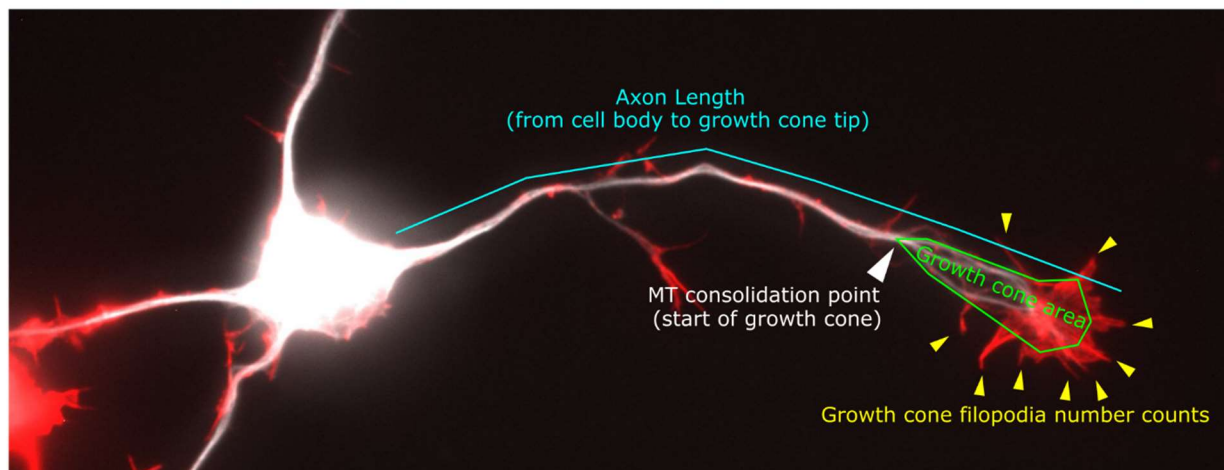
D Growth Cone Area



E Growth Cone Filopodia



F Diagram of morphology measurements



Chapter 3: Nestin selectively facilitates the phosphorylation of the Lissencephaly-linked protein doublecortin (DCX) by Cdk5/p35 to regulate growth cone morphology and Sema3a sensitivity in developing neurons.

Adapted from: Bott, C. J., Keil, J. M., McMahon, L. P., Yap, C. C., Kwan, K. Y., & Winckler, B. (2019). Nestin selectively facilitates the phosphorylation of the Lissencephaly-linked protein doublecortin (DCX) by Cdk5/p35 to regulate growth cone morphology and Sema3a sensitivity in developing neurons. *Bioarxiv Preprint*.

-submitted to and under revision at Journal of Neuroscience

3.1 Introduction

Correct wiring of the brain requires the targeting of growing axons to their future target fields. The outgrowth of axons is driven by the growth cone (GC) which is an actin- and microtubule (MT)-rich motile structure at the tip of growing axons (Menon and Gupton, 2016; Miller and Suter, 2018). GCs also respond directionally to a large number of extracellular guidance cues (Petrovic & Schmucker, 2015; Yamamoto et al., 2003). Guidance cues elicit local signaling responses which result in rearrangement of the GC cytoskeleton to give directional growth (Vitriol & Zheng, 2012; Dent et al., 2011), especially via guidance cue-activated kinases and their downstream substrates (Dent, Gupton and Gertler, 2011). Phosphorylation of cytoskeleton-associated proteins downstream of guidance cues is thus an important mechanism by which incoming guidance cue information is converted into morphological rearrangements of the GC.

Most work on the cytoskeleton of axonal GCs has focused on actin filaments and MTs (Dent & Gertler, 2003; Geraldo & Gordon-Weeks, 2009; Kapitein & Hoogenraad, 2015; Tamariz & Varela-Echavarría, 2015; Yamada et al., 1970). Distinct roles for the third main cytoskeletal filament system, the intermediate filaments (IFs), during early axon formation and GC guidance are not extensively studied, despite early promising studies in *Xenopus* neurons (Lin & Szaro, 1995, 1996; Szaro et al., 1991; Walker et al., 2001). IFs are sparsely expressed in growing axons and are composed of vimentin and α -internexin prior to expression of the neurofilament class of IFs (NF-L, NF-M, and NF-H) (Benson et al., 1996; Brown, 2013; Chang & Goldman, 2004; Pennypacker & Fischer, 1991; Shaw et al., 1985; Uchida & Brown, 2004; Wang et al., 2000). Once axons reach their targets, neurofilaments are greatly upregulated (Laser-Azogui et al., 2015; Nixon & Shea, 1992; Yabe et al., 2003).

The atypical IF protein nestin is highly expressed in neuronal progenitor cells. We recently found lower levels of nestin protein in post-mitotic cortical neurons, especially in the distal axon. Depletion of axonal nestin leads to increased GC size and blunts sensitivity to the Cdk5-dependent axonal guidance cue Sema3a (C Bott *et al.*, 2019). Our previous study thus was the first to discover a role for nestin in neurons (C Bott *et al.*, 2019), but the molecular pathways by which nestin affects growth cones remains unknown. Nestin binds the Cdk5/p35 heterodimer complex (Sahlgren *et al.*, 2003, 2006; Yang *et al.*, 2011), but the Cdk5 substrates affected by nestin are not known. The best studied example of nestin-mediated regulation of Cdk5 is at the neuromuscular junction (Yang *et al.*, 2011), but even there the physiological substrates of Cdk5 affected by nestin are still unknown. In this work, we discover a neuronal nestin-regulated Cdk5 substrate, namely DCX, and show that nestin's effect on GC morphology is DCX-dependent.

DCX is a multifunctional cytosolic protein expressed in developing neurons (Ge et al., 2006; Gleeson, et al 1999; Moslehi, et al, 2017; Sapir et al., 2000; Tanaka et al., 2004; Tsukada et al., 2005; Yap et al., 2018, 2012). Mutations in human DCX cause lissencephaly, a disease characterized by defects in neuronal migration and axon outgrowth that results in profound cortical malformations (Bahi-Buisson *et al.*, 2013). Patients exhibit intellectual disability and intractable epilepsy and often die in childhood. *In vitro*, DCX promotes MT assembly, and DCX-bound MTs are less dynamic (Moores *et al.*, 2004). Multiple kinases regulate DCX phosphorylation (Schaar, 2004; Tanaka et al., 2004), including Cdk5 (Nishimura, et al, 2014; Xie et al., 2006). Phosphorylation of

DCX by Cdk5 decreases the affinity of DCX for MTs and thus leads to decreased MT stability and increased MT dynamics (Bielas et al., 2007; Tanaka et al., 2004).

In this work, we identify DCX as a novel nestin-associated protein and demonstrate that Cdk5 potently phosphorylates nestin-scaffolded DCX. In addition, we show that nestin's effects on growth cone morphology and Sema3a sensitivity are DCX-dependent, thus demonstrating a functional role for the DCX-nestin complex in neurons.

3.2 Materials and Methods:

293 Cell culture and transfection.

HEK293 cells were maintained in DMEM+10% fetal bovine serum, and all transfections were conducted using Lipofectamine 2000 (Invitrogen) according to the manufacturer's protocol. Phosphorylation assays and IPs were performed on low passage HEK 293s in 6cm plates. Cells in low serum (4%) were transfected for 24-26hrs, and serum starved for 10-14 hours prior to lysis, to reduce background activity of mitotic kinases. Total transfection time 34 to 40 hours.

Cos-7 cell culture and transfection.

Cos-7 cells were maintained in DMEM + 10% fetal bovine serum and all transfections were conducted using Lipofectamine 2000 (Invitrogen) according to the manufacturer's protocol. Cells were plated on , ethanol soaked, washed, round glass cell gro Fisherbrand coverslip in each 12 well plate well, at a density of 40k per well/coverslip. 2µg total of plasmid was used per transfection, and were carried out with equivalent amounts of GFP or GFP tagged construct, and empty vector myc or myc-tagged construct. The empty vector myc control is for a c-terminal myc tagged protein, thus has no start codon and is not expected to make any myc protein. Cells in low serum (4%) were transfected for 24-26hrs, and serum starved for 10-14 hours prior to lysis, to reduce background activity of mitotic kinases. Total transfection time was 34 to 40 hours.

Western Blot

HEK 293T cells were washed with ice cold PBS, and lysed directly on the plate (6cm) into lysis buffer (500 µl); 50mM Tris HCl, 150mM NaCl, 1% NP-40, 1mM EDTA, 1mM DTT, 1mM PMSF, 1X HALT protease/phosphatase inhibitor cocktail. Extra NaF and NaOV was added in the lysis buffer for phosphorylation experiments in addition to that already in the cocktail. After incubating lysates on a rotisserie at 4° C for 30 minutes, lysate were cleared by centrifugation at 21k x g for 15 min at 4° C. We note that SPN is not well solubilized under these lysis condition, and we find that most of the SPN protein is in the pelleted material (not shown). Supernatants were diluted to 1x with 5X Laemmli buffer for western blot. Neuron cultures for Sema3a treatments where lysed directly in the 12 well plate well into 80-100 µl 1.5x laemmli sample buffer for western blot. Samples were vortexed, boiled, and spun at 18k x g for 10 minutes prior to loading. For neurons, the protein equivalent to 100-150k neurons was loaded per lane. Equivalent amounts of cells within each experiment were run on a 4-20% polyacrylamide gel. After transfer onto nitrocellulose with the BioRad Transblot Turbo, membrane was blocked with Licor TBS blocking buffer for 1 hour at room temp.

Primary and secondary antibodies were diluted in 50% blocking buffer, 50% TBS, final 0.1% Tween-20. Primary antibodies were incubated overnight at 4° C, and after washing, followed by near-infrared secondary antibodies for 1 hour at room temperature. Blots were imaged with the dual color Licor Odyssey CLx imager, so each phospho-probe could be directly compared to the total protein in the same band. Densitometry of western blots was performed with Licor Image Studio software, the same software used to acquire the fluorescent blot images. The phospho antibody signal was divided by the total protein level (GFP tag or non-phospho specific antibody), and normalized to control. Positions of molecular weight ladders (in KD) are indicated next to the blot when there was room, otherwise the value of the approximate position in KD is shown.

Immunoprecipitation

Cell lysates were prepared as though for western blotting- 500ul of lysis buffer per 6cm dish of confluent cells. After the 21k x g spin, cells were precleared with 50ul of Thermo fisher control agarose for 4-6 hours. All incubations and washes were performed on the rotisserie at 4°C. For IP's for myc-tagged proteins, 12ul Bethyl goat anti-myc pre-conjugated beads were added to the pre-cleared lysate overnight.

Lambda phosphatase dephosphorylation experiments were prepared from transfected 10cm dishes of confluent cells, and lysed with 1ml of lysis buffer (0.4% NP-40) minus the phosphatase inhibitors in the GFP-DCX condition. Following clearing by centrifugation (21k x g 15min), GFP-DCX lysates were split into two Eppendorf's, and to one, phosphatase inhibitors were added, and to the other 3200 units (8ul) of lambda (λ) phosphatase (SCBT) and a final concentration of 2mM MnCl₂. Both conditions were incubated at 30°C for 30 minutes, and the λ phosphatase containing sample was quenched with EDTA and phosphatase inhibitors. Each sample was separately combined each with half of the nestin-myc lysate, and incubated overnight at 4°C with 12ul Bethyl goat anti-myc beads.

For IP's for other proteins (nestin, dcx, p35), 2μg of the relevant antibody was added to the precleared lysate for 4-6 hours, followed by addition of 12ul A/G beads overnight. Experiments using protein A/G beads for IP also used them for pre-clearing instead of the control agarose. After overnight incubation, all IPs were washed 6 times in 500ul IP buffer. For GFP nano-body precipitations for phosphorylation assays, in order to minimize time and thus loss of phospho-epitopes, no pre-clearing was performed, the GFP-trap beads were immediately added to post-21k x g spin lysates for 1hr, and washed 2x. All IPs were eluted by addition of 2x sample buffer and immediate western blotting.

Neuronal Culture

Primary cultures of cortical neurons were obtained from embryonic day 16 (E16) mouse cortex of either sex as described in Bott et al., 2019. The protocol follows institutional ACUC protocols (approved animal protocol University of Virginia #3422). Cells were plated on acid-washed poly-L-lysine coated coverslips and incubated with Neurobasal medium with 10% fetal bovine serum and Penn/Strep. After 8 hrs, the cells were transferred into serum and antibiotic-free neurobasal medium supplemented with B27 (Invitrogen) and glutamax and cultured for a total of the indicated time periods *in*

vitro (DIV). When WT vs DCX null neurons were compared within an experiment, mice were dissected and cultures prepared at the same time for consistency of comparison. For imaging purposes, cells were plated at ~100,000 cells per 15mm coverslip or at 130,000/coverslip in electroporation experiments. Cortical neurons for culture were harvested at E16, just prior to gliogenesis. Thus non-neuronal glia are rare in these cultures, but occasional nestin/Sox2 positive, GFAP negative persisting neural stem cells were found. Cells were fixed at 24 hours (for non-transfection experiments) or 42-48 hours for overexpression experiments.

For co-IP experiments in neurons, cells were prepared similarly as described above. Six million untransfected cells were plated per 6 cm dish. At 24 hours, the cells in the 6cm dish were lysed and subjected to DCX immunoprecipitation as described above. Cells for Sema3a treatments and western blot, cells were prepared similarly as described above. Untransfected cells were plated at a density of 1 million cells per 12 well plate well. After 24 hrs, cells were treated with mouse Sema3a (R&D systems) diluted in growth media for 5, 15, or 30 minutes at 1nM as indicated. All conditions were subjected to 25nM calyculinA treatment 3 minutes prior to lysis to inhibit relevant phosphatase activity prior to lysis. After treatments, media was removed thoroughly and cells were quickly lysed directly into 1.5x laemmli sample buffer and subjected to western blotting as described above. In some experiments as indicated, cells were pre-treated with 10 μ M Roscovitine (Cayman Chemical) for 30 minutes prior to Sema3a treatment.

Neuron nucleofection

After cells were dissociated from E16 mouse cortex, cells were electroporated by Amaxa 4d nucleofection, according to manufacturer's protocols. 800,000 cells were electroporated in the small volume (20 μ l) cuvettes using P3 primary cell solution and CL-133 program. 0.1 μ g of GFP plasmid (pCMV-GFP-Clontech) as a transfection marker, and 0.15 μ g of relevant myc-tagged construct was used in each nucleofection condition. The cells were then all plated in a 6cm dish containing 6 poly-L-lysine coated coverslips.

Immunofluorescence

Cells were fixed in prewarmed 4% Paraformaldehyde-PHEM-Sucrose (PPS: 60mM PIPES, 25mM HEPES, 10mM EGTA, 2mM MgCl₂ (PHEM), 0.12M sucrose, 4% paraformaldehyde pH 7.4) for preservation of the cytoskeleton and cellular morphology and fixed at room temp for 16 min. Thorough permeabilization was required for nestin/intermediate filament visualization in neurons. Coverslips were permeabilized with 0.25% Triton-X 100 in 1% BSA/PBS for 20 min and then blocked for 30 min in 10% BSA, 5% normal donkey serum (NDS) in PBS all at room temperature. Primary antibodies were diluted in 1% BSA in PBS, and secondary antibodies in 1% BSA, 0.5% normal donkey serum in PBS. Primary antibody were incubated overnight at 4° C, and secondary antibodies for 90 min at room temperature. Appropriate species specific Alexa-350, -488, -568, or -647 labeled secondary antibodies raised in Donkey (Invitrogen and Jackson Immuno Research) were used for fluorescent labeling. Phalloidin-568 (Invitrogen) at 1:150 was used to visualize F-actin. Coverslips were mounted with ProLong Gold (Invitrogen). Widefield images for quantification were

captured with a Zeiss Z1-Observer with a 40x objective. Images were captured with the AxioCam503 camera using Zen software (Zeiss) and processed identically within experiments. Confocal images of the whole neurons were captured with inverted Zeiss LSM880 confocal microscope using a 63X objective. Enhanced resolution images of growth cones were captured using a Nikon TiE with A1 confocal microscope with a 100x objective and NA 1.49. Images were deconvolved using Landweber for 10 iterations. No non-linear image adjustments were performed.

In utero electroporation with CRISPR

The IUE CRISPR/Cas9 strategy is as follows: A gRNA sequence targeting the c-terminus of the Actb coding sequence (5'- AGTCCGCCTAGAAGCACTTG) was cloned into eSpCas9Opt1.1, expressing enhanced-specificity Cas9 and utilizing an optimized gRNA scaffold. To construct Actb_3xHA, tandem HA tag sequences were cloned between two Actb gRNA recognition sequences in the same orientation. Timed-pregnant dams were anesthetized with Ketamine (100 mg/kg) and Xylazine (10 mg/kg) via intraperitoneal injection, and given carprofen (5 mg/kg) via subcutaneous injection for analgesia. Uterine horns of an E13.5 pregnant CD-1 dam were exposed by midline incision. Lateral ventricles of embryos were injected with plasmid mix, composed of eSpCas9opt1.1-Actb_gRNA (1 µg/µl), Actb_3xHA (1.5 µg/µl), and CAG-Lifeact3xBFP (1 µg/µl), and 0.1% Fast Green FCF to visualize solution during intraventricular injection. Successful genome editing and repair in a subset of transfected cells yielded an HA-tagged Actb locus and led to sparse expression of ACTB-3xHA in individual cells. Electroporation paddles were positioned on opposing sides of the ventricle and 4 - 5 pulses of 27 volts (45 milliseconds each) were delivered, with 950 milliseconds between pulses, delivered using a BTX Harvard Apparatus ECM 830 power supply. Brains were isolated 3 days after electroporation, at E16.5, and fixed overnight in 4% PFA. These experiments were carried out in compliance with ethical regulations for animal research. The study protocol was reviewed and approved by the University of Michigan Institutional Animal Care & Use Committee.

Histology

Fixed *in utero* electroporated E16.5 mouse brains were then washed with PBS, embedded in agarose and vibratome sectioned into 100 µm sections. Sections were stained as floating sections- permeabilized and blocked with 3% normal donkey serum + 0.3% Triton-X 100 in PBS for 1 hour at room temperature. Antibodies were diluted in the same permeabilization buffer with indicated primary and secondary antibodies sequentially overnight at 4°C. Sections were thoroughly washed over a period of 10hrs at room temperature with 0.5% BSA and 0.1% Triton-X 100 in PBS after primary and secondary antibody incubations. Sections were mounted on slides with Prolong Gold using 22X22mm 1.5 fisher brand coverslips. Confocal and Airyscan imaging of cryosections was carried out on an inverted Zeiss LSM880 confocal microscope (available in the UVA microscopy core facility) using a 63X objective.

Molecular biology

Plasmids

GFP-DCX (Yap *et al.*, 2016)

Negative control substrates-GFP tagged:

DCLK1 (Shin *et al.*, 2013)

Drebrin (addgene)

FAK (addgene)

Tau-YFP (George Bloom)

P35 (addgene)

HA-Cdk5 (addgene)

HA-Cdk5-DN (D145N) (addgene)

Myc-SPN Lawrence Brass (UPenn)(Yap *et al.*, 2016)

INA-myc (Sino biological)

Nestin-myc (Bott2019 via original cDNA Bruce Lahn) PCR was used to generate EcoR1 and HindII sites on the 5' or 3' end respectively of full length mouse nestin. Both the insert and vector were treated with EcoR1 and HindII, the cut insert was ligated into pCDNA3.1 Myc-His(+) B.

Myc EV 3.1 B (stratagene)

GFP (Clontech)

CMV-HA EV- (addgene)

New constructs made for this study:

Nestin mutants:

Nestin-myc T316A- We used to traditional primer mutagenesis for this plasmid derived from the pcDNA 3.1 B Nestin(wt)-myc plasmid. Only one nucleotide change was needed to mutate T(946ACA) to A(946GCA). Primer: 5'-gaacttctccaggtgcctgcaagcgagagttc-3'

Nestin-myc T316D- Could not be obtained via traditional mutagenesis and was made, instead via gene synthesis from genscript of a large >1kb piece of nestin that included the three nucleotide changes- T(946ACA) to D(946GAT). The 5' end had a HINDIII site for incorporation into the MCS of pcDNA 3.1 B nestin(wt)-myc plasmid. An ECOR1 site present in WT nestin was used for the 3' end.

Image analysis

All image analysis was performed on ImageJ blinded to experimental conditions.

Transfected cells were identified by having a prominent GFP fluorescence. Stage3 neurons were identified (according to Banker staging) by having one neurite (the future axon) at least 2x longer than the next longest neurite. The distal portion of the future axon was analyzed for morphological measurements as the "axon growth cone". Images were analyzed as in Bott et al. 2019.

Filopodial protrusions were counted using the phalloidin channel, and any protrusions from the growth cone were counted.

Axon length was the length of the axon from the cell body to the growth cone tip as in Bott et al. 2019.

Growth cone area were assessed by measuring traced outlines the growth cone not counting the filopodial protrusions, and extending down proximally to the point where the splayed growth cone microtubules consolidate into bundles in axon shaft as in Bott et al. 2019.

Statistical analysis

All data was statistically analyzed using Prism software. Datasets were first evaluated for normality by using the Shapiro-Wilk normality test. This result was used to decide if parametric or non-parametric tests were to be used. When more than one comparison was made, the corresponding ANOVA test was used. When only two conditions were compared, we used a t-test. Figure legends specify details- for each set of experiments we made an effort to show precise p-values when shown. p-values reaching statistical significance of at least <0.05 are in **bold**.

Microscope image acquisition

Widefield images for quantification were captured with a Zeiss Z1-Observer with a 40x objective. Images were captured with the Axiocam503 camera using Zen software (Zeiss) and processed identically within experiments.

Confocal images of the whole neurons or brain sections were captured with inverted Zeiss LSM880 confocal microscope using a 63X objective with Zen software.

Airyscan was used for some brain section imaging.

Enhanced resolution images of growth cones were captured using a Nikon TiE with A1 confocal microscope with a 100x objective and NA 1.49. Images were deconvolved using Landweber for 10 iterations. No non-linear image adjustments were performed.

Reagents

Antibodies

Mouse anti-Nestin 2Q178 1:200 IF, 1:500 IHC, 1:500 WB **Santa Cruz Biotechnology Cat# sc-58813 RRID:AB_784786**

Goat anti-Nestin R-20: Raised against peptide in the unique C-terminal tail region of nestin 1:200 IHC **Santa Cruz Biotechnology Cat# sc-21249 RRID:AB_2267112**

Rabbit anti-DCX- 1:1200 IF, IHC, 1:4000 WB **Abcam Cat# ab18723 RRID:AB_732011**

Mouse anti- β III Tubulin Tuj1- 1:800 IF A generous gift from the Deppman Lab YVA A. Frankfurter, University of Virginia; Department of Biology Cat# TuJ1 (beta III tubulin) **RRID:AB_2315517**

Chicken anti- β III tubulin- 1:200 IF **Aves Labs Cat# TUJ RRID:AB_2313564**

Rat anti α -tubulin- 1:2000 WB **Santa Cruz Biotechnology Cat# sc-53030 RRID:AB_2272440**

Rabbit anti-Vimentin- 1:100 IF, 1:100 IHC, 1:1000 WB **Bioss Inc Cat# bs-0756R RRID:AB_10855343**

Rabbit anti-Vimentin 1:1000 IF **Abcam Cat# ab92547, RRID:AB_10562134**

Mouse anti-Myc tag 9E10: 1:1000 WB, 1:200 IF **Santa Cruz Biotechnology Cat# sc-40, RRID:AB_627268**

Rat anti-Myc tag 9E1- 1:1000 WB **ChromoTek Cat# 9e1-100, RRID:AB_2631398**

Rat anti-HA 1:2000 WB **ChromoTek Cat# 7c9, RRID:AB_2631399**

Rabbit anti-GFP D5.1 1:5000 WB **Cell Signaling Technology Cat# 2956, RRID:AB_1196615**

Mouse anti-GFP N86/8 1:5000 WB **UC Davis/NIH NeuroMab Facility Cat# 73-131, RRID:AB_10671444**

Rabbit anti-CDK substrate multiMab 1:1000 WB **Cell Signaling Technology Cat# 9477, RRID:AB_2714143**
 Rabbit anti-pS297 DCX 1:1000 WB **Cell Signaling Technology Cat# 4605, RRID:AB_823682**
 Rabbit anti-pS334 DCX 1:2000 WB **Cell Signaling Technology Cat# 3453, RRID:AB_2088485**
 Mouse anti-Cdk5 1:2000 WB **1H3 Cell Signaling Technology Cat# 12134, RRID:AB_2797826**
 Rabbit anti-p35/p25 1:2000 WB **C64B10 Cell Signaling Technology Cat# 2680, RRID:AB_1078214**
 Mouse anti-Spinophilin (Neurabin II) 1:2000 WB **Santa Cruz Biotechnology Cat# sc-373974, RRID:AB_10918794**
 Mouse anti-Drebrin 1:2000 WB **Santa Cruz Biotechnology Cat# sc-374269, RRID:AB_10990108**
 Mouse anti- Phf1 tau- supernatant 1:50 WB **P. Davies Albert Einstein College of Medicine; New York; USA Cat# PHF1, RRID:AB_2315150. A gift from George Bloom.**
 Rabbit anti-pS522 Crmp2a 1:1000 WB **Thermo Fisher Scientific Cat# PA5-37550, RRID:AB_255415**
 Mouse anti-pS732 FAK 1:1000 WB **Santa Cruz Biotechnology Cat# sc-81493, RRID:AB_1125825**
 Rabbit anti-pY397 FAK 1:1000 WB **Bioss Cat# bs-1642R, RRID:AB_10856939**
 Gt anti-myc agarose 1:50 IP **Bethyl Cat# S190-104, RRID:AB_66618**
 GFP trap agarose 1:100 IP **ChromoTek Cat# gta-20, RRID:AB_2631357**
 GFP booster nanobody- 1:600 IF **ChromoTek Cat# gba488-100 RRID:AB_2631434**
 Phalloidin 568 1:150 Invitrogen

Cell lines

Hek293 cell lines: **ATCC Cat# PTA-4488, RRID:CVCL_0045**
 Cos7 cell lines: **ATCC Cat# CRL-1651, RRID:CVCL_0224**

3.3 Results

Nestin selectively augments Cdk5-phosphorylation of DCX, but not of other Cdk5 substrates.

Our recent work (C Bott *et al.*, 2019) discovered an unexpected role for nestin in axonal growth cones: downregulation of nestin increases GC size and decreases Sema3a sensitivity. In other cell types, nestin has been shown to affect the activity of Cdk5. In neuromuscular junction (NMJ) development, for example, nestin deletion phenocopies Cdk5 deletion or treatment with the Cdk5 inhibitor roscovitine by altering levels and localization of Cdk5 activity (Lin *et al.*, 2005; Yang *et al.*, 2011). Since nestin binds the Cdk5 activator p35 (Sahlgren *et al.*, 2003, 2006; Yang *et al.*, 2011), and Cdk5 inhibition abrogates the effect of nestin-associated Sema3a-mediated GC collapse in

neurons (C Bott *et al.*, 2019), we reasoned that nestin might change the phosphorylation of one or more Cdk5 substrates to mediate the nestin-dependent changes in axonal GCs. We thus tested whether the phosphorylation of several known neuronal Cdk5 substrates was affected by the expression of nestin.

To this end, we utilized an “in-cell” phosphorylation assay in transfected HEK293 cells (Figure 14A-E). HEK293 cells endogenously express Cdk5, but not the Cdk5 activator p35 (see p35 immunoblot in Figure 15A). They thus have minimal Cdk5 activity under basal conditions. We focused on Focal Adhesion Kinase (FAK), Collapsin Response Mediator Protein 2 (Crmp2), tau, and DCX since phospho-specific antibodies are commercially available for these four Cdk5 substrates which are known to be phosphorylated in neurons downstream of Sema3a signaling (Figure 14A-E).

Transfection of HEK293 cells with p35 to activate Cdk5 led to increases in phosphorylation of GFP-tagged FAK, Crmp2, or tau, as expected (Figure 14A,C,D). Surprisingly, p35 expression was not sufficient to increase Cdk5-mediated phosphorylation of DCX in this context (Figure 14E). When nestin was expressed in addition to p35, FAK, Crmp2, or tau showed no further increase in phosphorylation. However, DCX phosphorylation became significantly increased when nestin was co-expressed with p35. A myc-empty vector (myc-EV) was used as a negative control. For quantification of all conditions, we used ratios of the phospho-protein signal to total expression of the GFP-tagged substrate protein (Figure 14A'-E'). As an additional control, we utilized an antibody to a phospho-tyrosine residue on FAK. As expected, pY397-FAK was not affected in any condition (Figure 14B, B'). We note that there was basal phosphorylation for some of these substrates even in the absence of overexpressed p35, which is likely due to activity of other kinases in HEK293 cells. We thus discovered a surprising substrate selectivity for nestin-enhanced phosphorylation by p35/Cdk5. This finding suggested the hypothesis that DCX could be a downstream effector for the nestin-dependent effects seen in the growth cones of young neurons.

Nestin, but not α -internexin, promotes phosphorylation of DCX by Cdk5.

In order to more fully characterize the effect of nestin on DCX phosphorylation, we repeated the phosphorylation assay of DCX with additional controls. As shown above, we saw a significant increase in pS297-DCX levels only when p35 and nestin are both co-expressed (Figure 15A,A', grey bars). In contrast to the phosphorylation of S297, the phosphorylation of S334 by JNK was not changed by co-expression of nestin (Figure 15A,A', red bars). In order to test specificity of the phospho-specific antibodies, we expressed spinophilin (SPN) (Figure 15A,A') which is a known PP1 phosphatase scaffold and promotes dephosphorylation of both the Cdk5 and JNK sites of DCX (Bielas *et al.*, 2007; Shmueli *et al.*, 2006; Tsukada *et al.*, 2006). The levels of both pS297-DCX and pS334-DCX were greatly diminished by SPN co-expression. We note that nestin co-expression with p35 consistently resulted in an increase in total DCX levels. Again, we used the ratio of the phospho-DCX signal to total expression of GFP-DCX to normalize for input levels of DCX.

We next carried out several controls to ascertain that the increased phosphorylation of DCX was attributable to Cdk5 activity and not to other endogenous kinases present in HEK293 cells. The Cdk5 inhibitor roscovitine reduced pS297-DCX phosphorylation, but neither SP600125 (a JNK inhibitor) nor Ro3306 (a Cdk1/cdc2 inhibitor with minimal

cross-reactivity with Cdk5) changed the pS297-DCX levels (Figure 15B,B'), supporting previous literature that S297 is a Cdk5 site on DCX (Tanaka et al., 2004). Multiple residues in addition to S297 are phosphorylated by Cdk5 on DCX, but specific antibodies to detect these phosphorylation events are not available. We obtained another antibody, which recognizes the general "K/H pSP" phospho-epitope consensus site for CDKs to confirm our results with the pS297-DCX antibody. GFP-DCX was precipitated from lysates with GFP-trap agarose beads to separate DCX from other reactive endogenous Cdk substrates in this experiment. Similar to our results using the anti-pS297DCX antibody, a significant nestin-dependent increase in Cdk5 phosphorylation of DCX could also be seen with this Cdk phospho-substrate antibody (Figure 15C and quantified in 2C'). Again, expression of SPN to recruit PP1 to DCX abolished the band on Western blot.

Lastly, we tested a different neuronal IF protein, α -internexin (INA) which is not known to bind to p35. INA did not promote DCX phosphorylation by p35/Cdk5, arguing for a specific enhancement of DCX phosphorylation by nestin (Figure 15A,A').

Nestin forms a complex specifically with DCX

Next, we asked by what mechanism nestin might selectively enhance Cdk5-phosphorylation of a specific Cdk5 substrate. We first tested if nestin formed a complex with any of the Cdk5 substrates. We co-transfected Nestin-myc or myc-empty vector (EV-negative control) with several GFP-tagged Cdk5 substrates (DCX, Doublecortin-like-Kinase 1 (DCLK1), CRMP2, Tau, Drebrin, and FAK) individually in HEK293 cells, followed by cell lysis and anti-myc tag immunoprecipitation (Figure 16A). The efficiency of co-IP with nestin-myc was quantified for each GFP-tagged substrate by densitometry analysis as a ratio of immunoprecipitated protein to the total amount of protein in the corresponding input. Only GFP-DCX significantly co-immunoprecipitated with nestin-myc (Figure 16A, A').

To determine if the nestin-DCX complex occurred endogenously in the relevant tissue, lysates from embryonic rodent brain were subjected to IP with either anti-nestin (Figure 16B) or anti-DCX (Figure 16B') antibodies and compared to non-immune IgG. An endogenous complex of nestin and DCX was recovered for both IPs. IP with anti-nestin antibody resulted in efficient co-IP of DCX. In contrast, relatively low amounts of nestin were recovered in the IP with an anti-DCX antibody, but when compared to the known DCX interacting protein SPN (a positive control), similar levels of co-IP efficiency were detected. This low efficiency is likely due to the fact that DCX is a multifunctional protein which has a multitude of binding interactions which might be mutually exclusive. The non-interacting protein drebrin was not detectable in the co-IP, serving as a negative control. In agreement with these findings, we also found nestin by mass spectrometry in DCX IPs of embryonic rat brain (Yap CC, unpublished data).

Since brain contains multiple cell types, we repeated the IP with lysates from E16 cortical neurons cultured for one day *in vitro* (DIV1). Indeed, nestin co-IP'ed with DCX (Figure 16C) in DIV1 cortical cultures. As a negative control, we carried out IPs from neuronal cultures prepared from DCX KO E16 cortex. The DCX KO neurons expressed similar levels of nestin as WT cultures, but no nestin was detected in the DCX IP (Figure

16C). We thus discovered a novel endogenous complex of DCX and nestin in immature cortical neurons.

Since DCX is MT-associated and nestin is an IF, we wondered where a complex of nestin with DCX would localize in cells. In order to test if DCX and nestin affected their respective cellular localizations, we transfected COS-7 cells which are large, well-spread cells which have spatially resolvable MT and vimentin IF filament systems. As shown previously by us and others, GFP-DCX decorates MTs (Gleeson *et al.*, 1999; Sapir *et al.*, 2000; Tsukada *et al.*, 2005; Ge *et al.*, 2006; Yap *et al.*, 2012, 2018; Moslehi, Ng and Bogoyevitch, 2017), but is not co-localized with vimentin (Figure 17A). Conversely, Nes-myc co-localized with endogenous vimentin in the absence of DCX (Figure 17B). When DCX was co-expressed, nestin became enriched on DCX-decorated MT bundles (Figure 17C). When a different MAP, YFP-tau, was expressed instead of DCX, nestin remained associated with vimentin IFs (Figure 17D). Other IFs, such as INA, did not enrich with DCX-MT bundles (Figure 17E). Nestin can thus be recruited to DCX-decorated MTs.

Nestin and DCX co-localize in the distal axon of cortical neurons *in vitro* and *in vivo*

We previously described a striking localization of nestin in the distal axon of cultured E16 mouse cortical neurons at 1 DIV that is rapidly lost as neurons matured (C Bott *et al.*, 2019). DCX is enriched in the distal axon, but is also present in dendrites (Friocourt *et al.*, 2003; Schaar, Kinoshita and McConnell, 2004). Simultaneous staining with antibodies against DCX and nestin revealed co-localization in the distal axon (Figure 18A; arrowhead), but not in dendrites. Enhanced resolution microscopy of the distal axon showed that nestin co-distributed with DCX in the “wrist” region of the axonal growth cone (Figure 18B) and appeared to be filamentous. Nestin staining also extended past the “wrist” into the central domain of the GC. Interestingly, we observed occasional nestin staining in some of the proximal filopodia of the growth cone which were also stained for DCX.

We previously showed nestin immunostaining in E16.5 mouse cortex in axon fascicles in the intermediate zone (IZ) which are interwoven among highly expressing radial glial processes (C Bott *et al.*, 2019). However, we were unable to discern single axons *in vivo*, let alone single growth cones, due to the high density of axons in the IZ. In order to visualize nestin localization in individual developing axons *in vivo*, we utilized *in utero* electroporation (IUE) to sparsely label individual neurons (Figure 18C). Using CRISPR/Cas9 genome editing, 3xHA tags were introduced into the endogenous β -actin locus which enabled us to label the actin cytoskeleton of developing neurons including the growth cone (diagram in Figure 18F). Three days after IUE, brains were fixed, sectioned and immunostained for the HA-tag in combination with staining for DCX and nestin (Figure 18C). This technique introduced the HA tag into a small number of newly born neurons, which were scattered throughout the IZ and cortical plate (CP) at multiple stages of maturation. We expected to find nestin-positive axon tips in only a subset of labeled neurons (C Bott *et al.*, 2019) and therefore focused on neurons that were migrating through the IZ and had not yet reached the cortical plate (Figure 18C, white asterisk “*”). These neurons are less mature and still in the early stage of axon extension (Namba, Kibe, Funahashi, Nakamuta, Takano, Ueno, Shimada, Kozawa,

Okamoto, Shimoda, Oda, Wada, Masuda, Sakakibara, Igarashi, Miyata, Faivre-sarrailh, *et al.*, 2014; Sakakibara and Hatanaka, 2015) and thus most analogous to the young neurons we used in culture. One such neuron (soma marked with red arrowhead, axon tip marked with white arrowhead) is shown enlarged in Figure 18C'. The nestin staining pattern in the IZ consisted of bright radial staining of the radial glial processes and fainter staining of axons running parallel to the ventricular surface, as we showed previously (C Bott *et al.*, 2019). The sparse labeling provided by the HA-tag knock-in strategy thus allowed us to identify individual neurons at the earliest stage of axon extension and positioning and to assess for nestin staining. A high magnification of a single section of a z-stack shows an example of nestin staining that clearly localized within the distal region of the extending axon (Figure 18D), but did not extend to the most distal regions of the growth cone. Orthogonal projections of the z-stack were used to allow for visualization of nestin within the HA-positive axon (Figure 18D'). Enhanced resolution Airyscan confocal imaging of the same growth cone in the same z-plane allowed for better appreciation of the axonal nestin (Figure 18D''). Nestin in distal axons was thus also observable *in vivo* and thus mirrors what was seen in culture (C Bott *et al.*, 2019). We observed nestin primarily in the smaller, more compact GCs of younger neurons whose cell bodies had not yet reached the cortical plate (Figure 18C “*” symbol). The growth cones of longer axons (presumably belonging to more mature neurons) did not have detectable nestin enrichment and were larger in size (Figure 18E, 18C “#” symbol). Even though we were able to observe examples of nestin-positive growth cones by this technique, the very low number of definable growth cones with traceable axons per electroporated brain made quantification from this preparation not feasible. Therefore, we looked at all the growth cones we could identify to see that they were indeed comparable to what we had observed *in vitro*.

Nestin does not increase global Cdk5 activity towards DCX.

What is the mechanism for nestin-mediated enhancement of Cdk5 phosphorylation of DCX? As was reported before in other systems, we observed that p35 levels were increased by nestin co-expression (Figure 15A), likely due to stabilization of p35 by nestin binding (Pallari *et al.*, 2011; Sahlgren *et al.*, 2003, 2006; Yang *et al.*, 2011). This stabilization of p35 has been proposed to constitute the mechanism by which nestin promoted Cdk5 activity, since more activator should result in more Cdk5 activity. To test this model directly, we expressed increasing amounts of p35 in HEK293 cells by increasing the amount of p35 plasmid used in the transfection from 1 to 4 µg. We saw an increased amount of p35 expressed with more p35 plasmid used (Figure 19A). We could thus directly compare the levels of pS297-DCX at similar p35 levels with or without nestin. Even with similar levels of p35, levels of pS297-DCX were not increased in the absence of nestin (Figure 19A,A', grey bars). This demonstrated that the increased p35 levels were not sufficient to account for the increased DCX phosphorylation by Cdk5 observed with nestin co-expression. Nestin thus did not increase global Cdk5 activity, but selectively increased Cdk5 activity towards DCX.

Nestin scaffolds Cdk5/p35 for DCX phosphorylation

We next asked how nestin can increase phosphorylation of DCX selectively. We hypothesized that nestin acted to scaffold the active kinase (Cdk5/p35) with the substrate by binding to both proteins simultaneously (see diagram top panel Figure 19B). Typically, interactions between a kinase and its substrate are transient, and phosphorylation of the substrate results in dissociation of the kinase from the substrate (Goldsmith et al., 2007; Manning & Cantley, 2002). Mutated kinases which are “kinase-dead” (KD) form more stable complexes with their substrates, thus “trapping” the substrate bound to the kinase. This will result in an increase in co-IP efficiency of the substrate with the kinase (bottom panel Figure 19B). In order to test for a multimeric complex of nestin with Cdk5/p35 and DCX, we compared the extent of DCX-nestin complex formation in cells co-expressing either HA-Cdk5-WT or HA-Cdk5-D145N (= kinase-dead KD) with p35 and nestin (Figure 19C). We could co-IP significantly more DCX with nestin-myc (using anti-myc IP) when the substrate-trapping Cdk5-KD was co-expressed, compared to low co-IP efficiency with Cdk5-WT (Figure 19C'). As a control, co-expression of INA-myc, which does not interact with p35 or DCX, resulted in only background levels of GFP-DCX co-IP in all conditions (Figure 19C). These results suggested that nestin was acting as a scaffold for Cdk5 and DCX.

To more directly test this idea, we pulled down the substrate-trapped Cdk5-KD complex via p35 IP, to test for differences in DCX co-IP in the absence or presence of nestin (Figure 19D). We found that nestin co-expression significantly increased the amount of DCX recovered in the co-IP by anti-p35 antibody, suggesting a complex of p35-Cdk5-KD with DCX and nestin (Figure 19D,D'). Nestin did not affect the abundance of Cdk5/p35 heterodimer, as there was not a significant difference in the amount of Cdk5 recovered by anti-p35 IP in the absence or presence of nestin (normalized average of 1 (no nestin) compared to 1.125 (with nestin), $p=0.88$, $n=3$).

Our model predicts that nestin would bind with higher affinity to dephosphorylated DCX (see diagram top panel Figure 19B). To test this, we treated GFP-DCX containing lysate, prepared from transfected HEK293 cells, with Lambda (λ) phosphatase, or with phosphatase inhibitors (inhibs.), to increase dephosphorylated or phosphorylated DCX, respectively (Figure 19E, inputs). These crude lysates were mixed with nestin-myc containing lysates, and nestin-myc was IP'ed. We found that the sample that had been treated with the exogenous λ phosphatase (containing more dephosphorylated DCX) was co-IP'ed more efficiently by nestin-myc than the sample that contained a higher level of pS297-DCX (Figure 19E).

Thus, we propose that nestin acts as a selective scaffold, which can bind to Cdk5/p35 and DCX simultaneously, and this results in increased efficiency of WT Cdk5-mediated phosphorylation of DCX (Figure 23C). Dephosphorylation of DCX was shown by others (Shmueli et al., 2006; Bielas et al., 2007) to be dependent on the recruitment of PP1 to DCX by the actin binding protein SPN. We confirmed this observation (Figure 15A,A'). Thus, we propose that the level of DCX phosphorylation is determined by the balance between these opposing reactions (see top half of model in Figure 23C), and that phosphorylation would be more dominant when nestin is present. We thus envision nestin to act like a “gain control” in growth cones, which sensitizes DCX to Cdk5 phosphorylation.

The T316D mutation in nestin affects p35 and DCX binding as well as DCX phosphorylation, but not incorporation into vimentin filaments.

We previously showed that nestin expression is associated with small compact GCs, whereas nestin negative-neurons have larger GCs (C Bott *et al.*, 2019). Is the effect of nestin on GC morphology dependent on its ability to scaffold Cdk5/p35/DCX? To test this, we aimed to create nestin mutants that lack Cdk5/p35 binding. Previous work showed that the threonine at position 316 (T316) on nestin is an important regulatory site for Cdk5/p35 binding and for Cdk5-dependent effects of nestin (Yang *et al.*, 2011; Su *et al.*, 2013). The T316 site can be phosphorylated, which affects binding to p35. The T316A phospho-dead mutant had increased binding to p35 in *in vitro* binding assays of purified recombinant protein (Yang *et al.*, 2011). In addition to making the T316A phospho-dead nestin mutant, we created a phospho-mimetic mutant (T316D-Nes), reasoning that it might be unable to bind p35. To test p35 binding of the T316 mutants, we used a co-IP strategy similar to that used in Figure 16 (Figure. 20A). In our hands, the T316A-Nes mutant showed only a slight increase in p35 binding. T316D-Nes, on the other hand, was greatly deficient in p35 binding (Figure 20A). We then tested if these nestin mutant proteins still formed a complex with DCX. We performed IPs with WT nestin or nestin mutants when GFP-DCX was co-expressed. Surprisingly, T316D-Nes exhibited decreased binding to DCX (Figure 20A), whereas T316A-Nes still co-IP'ed DCX. We note that T316D-Nes levels appeared consistently lower in the lysates compared to WT nestin or T316A-Nes.

In order to test the ability of T316 nestin mutants to associate with DCX by an additional assay, we also used the COS-7 cell immunofluorescence assay to determine if nestin mutants were still recruited to MTs by DCX. In agreement with the co-IP studies, both WT nestin and T316A-Nes still showed apparent enrichment with GFP-DCX MT bundles in COS-7 cells. T316D-Nes, on the other hand, localized more similarly to vimentin and did not appear enriched with DCX-decorated MTs (Figure 20C-E).

Our scaffolding hypothesis proposes physical associations between DCX, p35/Cdk5, and nestin. We thus reasoned that a nestin mutant deficient in p35 and DCX binding should also be deficient in promoting Cdk5-mediated phosphorylation of DCX. We tested if the pS297-DCX levels were altered in cells expressing WT or T316 nestin mutants (Figure 20B). T316A-Nes + p35 resulted in increased phosphorylation of DCX similar to WT nestin + p35, whereas T316D-Nes + p35 did not result in increased phosphorylation of DCX (Figure 20B, quantified in 20B'). This result is consistent with our scaffolding hypothesis.

Since nestin forms heteropolymers with vimentin, we also tested if the nestin T316 mutants still interacted with vimentin. The T316 site is just outside of the IF polymerization rod domain, so modification of this site is not expected to interfere with IF polymerization. Indeed, we observed WT nestin, T316A-Nes, and T316D-Nes co-IP'ing with vimentin effectively (Figure 20A), arguing that they still formed homo-oligomers/polymers with vimentin. In agreement, these mutants appeared to co-distribute with endogenous vimentin filaments similarly to WT nestin when co-expressed in COS-7 cells (Figure 20F-H). We thus conclude that T316D-Nes binds less well to both p35 and DCX whereas T316A-Nes still binds p35 and DCX, and that neither

mutation grossly disrupts vimentin binding. We use the T316D-Nes mutant to test the role of the nestin-p35-DCX complex in neurons below.

Binding to p35 and/or DCX is required for nestin's effect on growth cone size.

We previously reported that reducing neuronal nestin levels leads to larger GCs (C Bott *et al.*, 2019). We thus wondered if overexpression of WT nestin would do the opposite, i.e. lead to smaller GCs. We expressed myc-nestin in cultured cortical neurons for 2 days along with GFP to allow for detection of transfected cells. At this stage, the majority of neurons are nestin-negative (C Bott *et al.*, 2019), allowing us to assess the effects of re-expressing nestin. Overexpression of WT nestin-myc resulted in statistically smaller GCs on axons (arrows) with fewer filopodia, which is the opposite phenotype of downregulating nestin. Overexpression of INA-myc did not change GC size or filopodia number compared to myc-EV controls (Figure 21A, B, B'). Next we asked if p35/DCX binding by nestin was required for the effect on GC size. T316A-Nes, which retained binding to p35 and DCX (Figure 20A) and resulted in WT levels of DCX phosphorylation (Figure 20B), resulted in small GCs with fewer filopodia, similar to WT nestin (Figure 21A, B, B'). However, the T316D-Nes mutant, which did not interact with p35 or DCX (Figure 20A) and did not result in increased DCX phosphorylation (Figure 20B), did not significantly alter GC size or filopodia number (Figure 21A, B, B'). Therefore, binding to p35 and/or DCX is required for nestin's effect on GC size.

Nestin does not have any effect on GC size in the absence of its downstream effector DCX.

Since nestin selectively bound to DCX and affected its phosphorylation, we hypothesized that the effects of nestin overexpression on GCs were dependent on DCX. Therefore, we tested if nestin overexpression would affect GCs in the absence of DCX. We thus overexpressed nestin-myc, myc-EV, or myc-INA in WT or DCX KO neurons and determined GC size and filopodia number. We again observed decreased axonal GC size (arrows) and decreased filopodia number specifically with nestin-myc expression (Figure 22A,B,B'). However, in DCX null neurons, no decrease in GC size or filopodia number was seen with nestin-myc expression (Figure 22A,B,B'). When GFP-DCX was reintroduced together with nestin-myc into DCX null neurons, the nestin effect on GC size and GC filopodia was rescued (Figure 22A,B,B'). Axon length was not affected (Figure 22B''). We thus conclude that nestin acts via DCX to influence GC size.

DCX is a Cdk5 substrate downstream of Sema3a, and nestin-sensitivity to Sema3a is absent in DCX null neurons.

We previously showed that 1DIV cortical WT neurons respond to Sema3a by retracting their axon growth cone filopodia and that this response is blunted when nestin is downregulated. We wondered if DCX was also downstream of nestin for Sema3a responsiveness. S297-DCX phosphorylation has been reported to be induced by Sema3a in DRG neurons (Ng *et al.*, 2013), but this has not been shown in other neuronal cell types. We treated DIV1 E16 cortical mouse neurons with vehicle or 1 nM

Sema3A for 5, 15, or 30 minutes and determined the levels of DCX phosphorylation. We could detect phosphorylation of the S297-DCX epitope in cortical neurons, which was significantly increased after Sema3a treatment (Figure 23A,A' grey bars). The JNK site pS334 was not increased after Sema3a treatment (Figure 23A,A' red bars). pS297DCX, but not pS334DCX levels, were reduced by roscovitine, consistent with activation of Cdk5 downstream of Sema3a (Figure 23A,A").

In order to determine if nestin still affected the extent of Sema3a sensitivity in the absence of DCX, we compared the Sema3a response of nestin-positive and nestin-negative neurons in WT or DCX null cortical cultures. At 1DIV a little more than half of the stage 3 neurons are nestin-positive, while the remainder are nestin-negative (C Bott *et al.*, 2019), allowing us to compare Sema3a responsiveness in the same culture when stained against nestin. In WT neurons, we again saw a nestin-dependent decrease in growth cone size in untreated cultures, whereas the growth cone size of nestin-positive and nestin-negative neurons was not significantly different in DCX null cultures (Figure 23B), in agreement with the data in Figure 22. As we reported previously (C Bott *et al.*, 2019), we again observed a decrease in filopodia number in nestin-expressing neurons when treated with Sema3a whereas nestin-negative neurons were less Sema3a-responsive (Figure 23B'). When we treated DCX null neurons with Sema3a, however, we no longer observed decreased GC filopodia number in nestin-positive neurons. Nestin-positive and nestin-negative neurons derived from DCX null mice showed the same Sema3a sensitivity (Figure 23B'), indicating that DCX is required for nestin-dependent regulation of GC size and Sema3a sensitivity. Axon length was not significantly different (Figure 23B").

In our model (Figure 23C), we propose that basally, non-phospho DCX binding to MTs stabilizes the MTs, and in the absence of nestin-scaffolded Cdk5 phosphorylation, DCX provides resistance or buffering against Sema3a-mediated growth cone collapse and filopodial retraction. Activation of the pathway in nestin-positive WT neurons allows for DCX phosphorylation and removal of the MT stabilizing effects of DCX. When DCX is absent and is not there to provide resistance to Sema3a, growth cones are responsive to Sema3a in a non-nestin dependent manner.

3.4 Discussion

A number of IF subtypes are expressed in the brain, but their cell biological functions during development are incompletely understood (Yuan and Rao, 2012). One of the earliest expressed IFs in the developing brain is nestin, but little is known about nestin's function, even in NPCs where it is highly expressed (Park *et al.*, 2010; Mohseni *et al.*, 2011; Wilhelmsson *et al.*, 2019). We previously found that nestin protein expression persists at low levels in early neurons and that nestin expression influences growth cone size and responsiveness to Sema3a in a Cdk5-dependent manner (C Bott *et al.*, 2019), but the molecular pathways for this phenotype were not known. Nestin is known to directly interact with the Cdk5/p35 heterodimer. We thus hypothesized that nestin might also affect the activity of Cdk5 in neurons, similarly to what occurs during neuromuscular junction development (Yang *et al.*, 2011). Hence, we screened known neuronal Cdk5 substrate cytoskeletal proteins for nestin binding and identified DCX as a novel nestin-associated protein that is selectively phosphorylated in the presence of

nestin and Cdk5/p35. Mechanistically, we find that nestin selectively promotes robust phosphorylation of DCX by Cdk5/p35 through scaffolding. We show that DCX and nestin co-localize in the distal axon and growth cone, and that DCX is required for the effects of nestin on GC morphology and Sema3a sensitivity. In summary, our results uncover a novel signaling role for neuronal nestin in regulating GC morphology specifically via scaffolding the Cdk5 substrate DCX.

DCX is a substrate for nestin-scaffolded Cdk5 in neurons.

Earlier work identified nestin as a p35 binding protein and showed that nestin modulated both the level and localization of Cdk5 activity in C2C12 myotubes (Yang *et al.*, 2011). *In vivo*, nestin depletion phenocopies Cdk5 deletion or roscovitine treatment in maintaining acetylcholine receptor clustering in agrin (AGD) mutants (Lin *et al.*, 2005; Mohseni *et al.*, 2011; Yang *et al.*, 2011). However, the effect of nestin depletion on Cdk5 activity (promoting or inhibiting) has varied between reports and assay systems and has been a point of contention (Sahlgren *et al.*, 2006; Pallari *et al.*, 2011; Yang *et al.*, 2011; Huang *et al.*, 2017; Lindqvist *et al.*, 2017; Wang *et al.*, 2017; Zhang *et al.*, 2018). Since the relevant endogenous Cdk5 substrate in myoblasts remains unknown, exogenous substrates (such as recombinant H1 histone protein) are commonly used for phosphorylation assays. The different interpretations are thus likely due to the use of exogenous substrates in the phosphorylation assays. Our work for the first time identifies a biologically relevant substrate for nestin-scaffolded Cdk5, namely DCX (Figure 14 and 16). If DCX is also the relevant substrate in myoblasts is not known, but it is intriguing that DCX null mice also have developmental defects at the neuromuscular junction, as do human lissencephaly patients with DCX mutations (Bourgeois *et al.*, 2015). Our work suggests that nestin does not modulate Cdk5/p35 kinase activity per se since nestin did not affect Cdk5/p35 heterodimer formation and several other Cdk5 substrates were not affected by nestin (Figure 14 and 17D). Rather, we propose that in neurons nestin selectively increases Cdk5-mediated DCX phosphorylation by providing a scaffold.

DCX as a downstream effector of nestin: a model for regulation of GC size.

How does nestin affect GC size via DCX? Three major processes are necessary for axon growth and guidance - protrusion, engorgement, and consolidation (Dent and Gertler, 2003). Protrusions towards positive guidance cues are mediated by actin-based filopodia and lamella which serve as templates for subsequent MT infiltration and growth. These MTs stabilize the new actin-based structures and allow for transport of cell components through vesicular trafficking which leads to the filling and engorgement of the advancing growth cone. The absence of DCX results in decreased stability and extent of protruding MTs (Jean, Baas and Black, 2012). Lastly, the proximal part of the growth cone is consolidated, and MTs are bundled into new axon shaft. MT-binding proteins play essential roles in regulating the assembly dynamics and bundling extent of MTs in a spatially regulated manner and are critical regulators of axon growth. Phosphorylation and dephosphorylation are known to spatially regulate the activities of many MAPs, including DCX. We propose that nestin affects GC size by promoting the phosphorylation of DCX in the distal axon. Dephosphorylation of DCX has already been implicated in the consolidation step of axon growth (Bielas *et al.*, 2007). Specifically,

Bielas et al. (2007) showed that Cdk5-mediated phosphorylation of DCX is reversed by the phosphatase PP1 which is scaffolded by the DCX-binding protein SPN (Tsukada, Prokscha and Eichele, 2006). In extension of these earlier models, we propose that nestin scaffolds Cdk5 and thereby promotes the phosphorylation of DCX - thus completing the regulatory cycle of DCX phosphorylation and dephosphorylation (Figure 23C). The regulation of the phosphorylation of DCX is thus driven by the balance of nestin/Cdk5/p35 to increase phosphorylation and SPN/PP1 to decrease it - perturbation of either process results in abnormal MT organization (Bielas et al., 2007; Dehmelt & Halpain, 2007; Schaar et al., 2004). In our model, the level of phospho-DCX would be determined by the relative opposing activity of the two differently localized regulatory complexes (Figure 23C).

On a molecular level, we predict that the presence of nestin would result in more pS297-DCX in growth cones, which has a decreased affinity for MTs. We were unable to stain neurons with the pS297-DCX antibody reliably and could thus not test this idea directly. Since DCX binding to MTs stabilizes them (Moores *et al.*, 2004), growth cones with more pS297-DCX may have intrinsically less stable or more dynamic MTs. This notion is consistent with previous findings that GC size reflects MT dynamics. For instance, smaller growth cones have intrinsically more dynamic MTs than larger growth cones (Kiss et al., 2018). In addition, treatment with taxol, which stabilizes MTs, results in larger GCs (Gumy *et al.*, 2013). Thus we propose that a smaller growth cone represents a GC with more robust kinase/phosphatase activity which would result in more rapid cytoskeletal dynamics, morphological turnover, and GC sculpting via changes in the phosphorylation of cytoskeletal associated proteins, including DCX. A smaller GC would thus correlate with a more robust response to a given relevant guidance cue as it is able to remodel the existing cytoskeleton more rapidly.

A novel role for intermediate filaments in axon growth.

IFs have previously not been thought to be important for axon formation, much less axon guidance. Early studies had concluded that IFs were absent from the most distal and peripheral regions of the growth cone, and thus were ruled out early on as relevant players in regulating axon targeting (Dent and Gertler, 2003). However, the higher resolution and more sensitive imaging methods used here (Figure 18), reveal IFs in some peripheral regions of the GC, suggesting this question should be revisited. It remains thus an open question whether or not some IF proteins can affect axon guidance or outgrowth in some ways *in vivo*.

Nestin-containing IFs are indeed well localized to influence growth cone behavior. In support of our *in vitro* data, DCX and nestin co-express *in vivo* while neurons are in the stage of axon positioning and orientation (Namba et al., 2014)(Figure 18D) which are Cdk5 and Sema3a dependent processes (Oshima et al. 2007; Polleux et al., 1998). Our own work shows striking accumulation of nestin in the distal axon shaft and even in some peripheral regions of the axonal growth cone (Figure 18). Nestin co-localizes with a subset of DCX, but is not identically distributed. This raises interesting future questions about why nestin is not present in dendrites, and if this distribution is related to known differences in behavior of axonal and dendritic growth cones (i.e. differential guidance cue sensitivity) (Wang et al., 2014).

Summary

This work highlights how the IF composition of neurons can alter intracellular signaling pathways and thus alter the cell's morphology. IFs have long been implicated as mediators and regulators of "cytoskeletal crosstalk" (Chang and Goldman, 2004; Michalczyk and Ziman, 2005), and our findings here represent an example of cytoskeletal crosstalk between IFs and MTs and their associated proteins. Our previous work has found that nestin expression correlated with small GC size and greater responsiveness to Sema3a. Based on our new work, we implicate modulation of DCX phosphorylation by Cdk5 as a relevant molecular pathway downstream of neuronal nestin function. We thus posit that nestin sensitizes growth cones to Cdk5 activity by scaffolding DCX. Based on our data, we propose the model that nestin affects growth cone morphology as a kinase regulator. In addition to this signaling role, nestin could also play a structural role as a cytoskeletal filament, but more work will be required to more fully elucidate nestin's role in neurons during development.

Figure 14: Nestin selectively augments Cdk5-phosphorylation of DCX, but not other Cdk5 substrates.

A-E. Comparison of Cdk5-mediated phosphorylation of several Cdk5 substrates in the indicated transfection conditions: Myc-EV (empty vector) – left lane, Myc-EV + p35 – middle lane, Nes-myc + p35 – right lane. Cdk5-dependent phospho-sites on FAK (A), Crmp2 (C), tau (D) and DCX (E) were assessed for p35- and nestin-dependence. The pY397 site on FAK (B) is a negative control because Cdk5 is a Ser/Thr kinase.

A'-E'. The level of phosphorylation of each substrate was quantified by densitometry analysis of the phospho-signal compared to total (GFP) and graphed to the right of each blot. Error bars are SD. The statistical test used was one-way ANOVA with Tukey's correction. N= 3 or 4 independent experiments. *p* values of less than 0.05 are indicated in bold.

Immunoblot

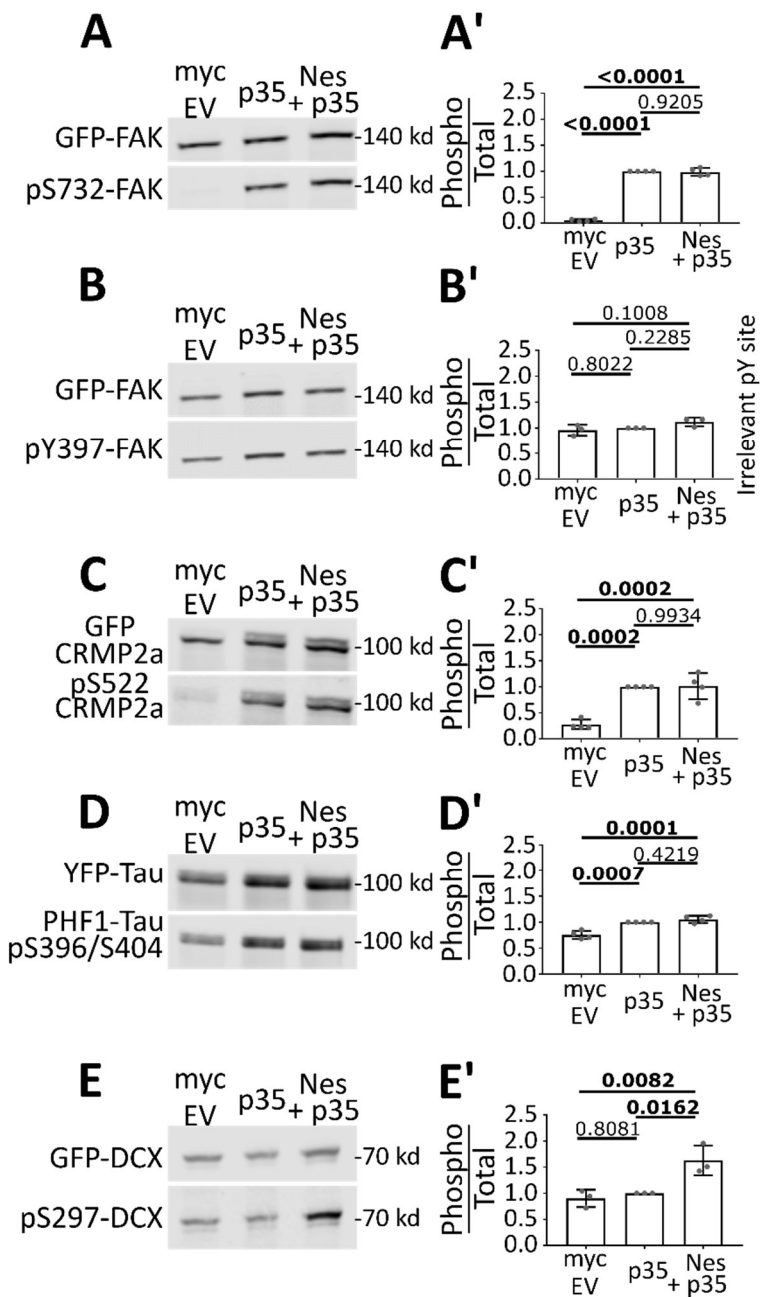


Figure 15: Nestin, but not α -internexin, promotes phosphorylation of DCX by Cdk5

A. Myc Empty Vector (EV), Nestin-myc, INA-myc, or myc-SPN were expressed in HEK293 cells with DCX alone (-), or with both p35 and DCX (+). Cell lysates were run on two replicate western blots and both blotted against GFP for total levels of GFP-DCX. Each was blotted with the relevant phospho-specific antibodies to pS297-DCX (a Cdk5 site) or pS334-DCX (a JNK site). The levels/presence of relevant proteins are shown, including cdk5 (endogenous), p35 (overexpressed), tubulin (endogenous, loading control), and the overexpressed myc-tagged constructs. Arrows point at the relevant myc-tagged protein bands. A'. Quantification of A by densitometry. Ratio of phospho-DCX to total DCX are plotted. Black bars represent pS297-DCX/total DCX, and red bars represent pS334-DCX/total DCX- colors correspond to the outline around the relevant blot. Error bars are SD. N = 4 to 6 independent experiments. Every condition was compared to every other condition with an ordinary one way ANOVA test with Tukey correction. P-values compared pairwise to control (CON) are shown. Additional comparisons not shown are pS297 level in Nestin + p35 condition is significantly different than p35 alone ($p < 0.0001$) and nestin alone ($p = 0.0004$), while pS334 is not significantly different (> 0.9999 and 0.8979 respectively) for the same comparisons. *p* values of less than 0.05 are indicated in bold. The values for DCX phosphorylation are from additional independent experiments separate from those shown in Fig. 14E.

B. HEK293 cells transfected simultaneously with p35, nestin-myc, and GFP-DCX were treated with inhibitors (i) of Cdk5 (roscovitine), JNK (SP600125), Cdk1 (Ro2206), or vehicle (UNT) for 6h before lysis. Only roscovitine significantly decreased levels of pS297-DCX. B'. Quantification of the blots in B. Error bars shown are SD, ordinary one-way ANOVA with Dunnett's correction was performed and the pairwise *p*-values are shown for each condition compared to untreated control (UNT). N=3-5 independent experiments. *p* values of less than 0.05 are indicated in bold.

C. HEK293 cells were transfected similarly to Figure 15A and total Cdk5-mediated phosphorylation of GFP-DCX was assessed using an antibody to a generic K/H SP Cdk5 phosphorylation motif to detect. Because many proteins in HEK293 cell lysates can be recognized with this antibody, cell lysates were subjected to GFP-trap incubation and precipitation to isolate GFP-tagged DCX from other reactive proteins and subsequently subjected to western blot. C'. Densitometry quantification of C where levels of signal to the phospho-reactive antibody is ratio-ed to the level of total DCX. Error bars are SD and a one way ANOVA with Dunnett's correction was used to compare each condition to the control cells transfected with GFP-DCX only. N= 3 independent experiments. *p* values of less than 0.05 are indicated in bold.

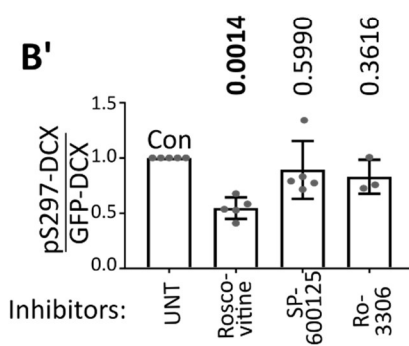
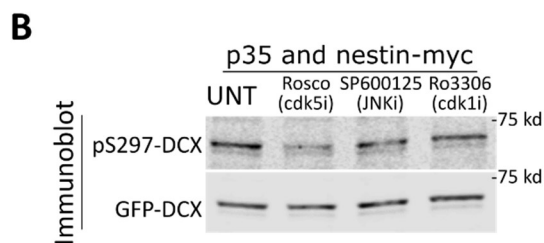
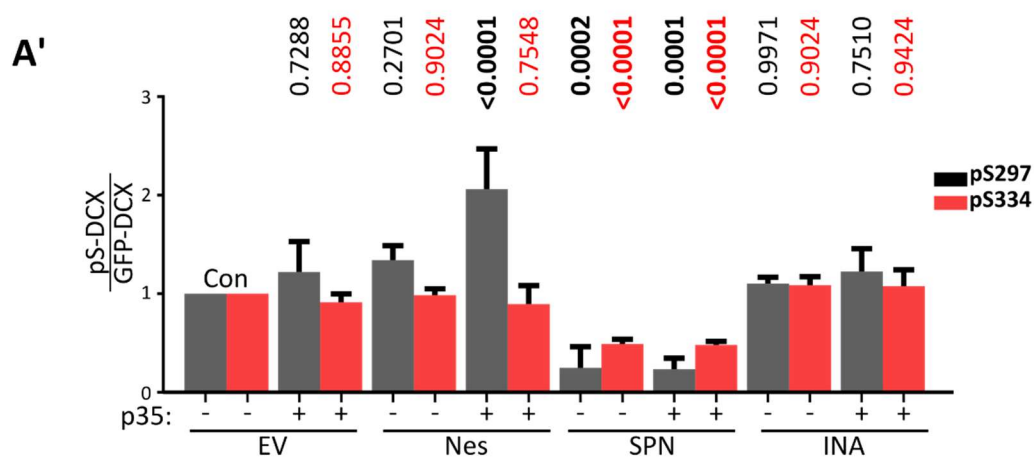
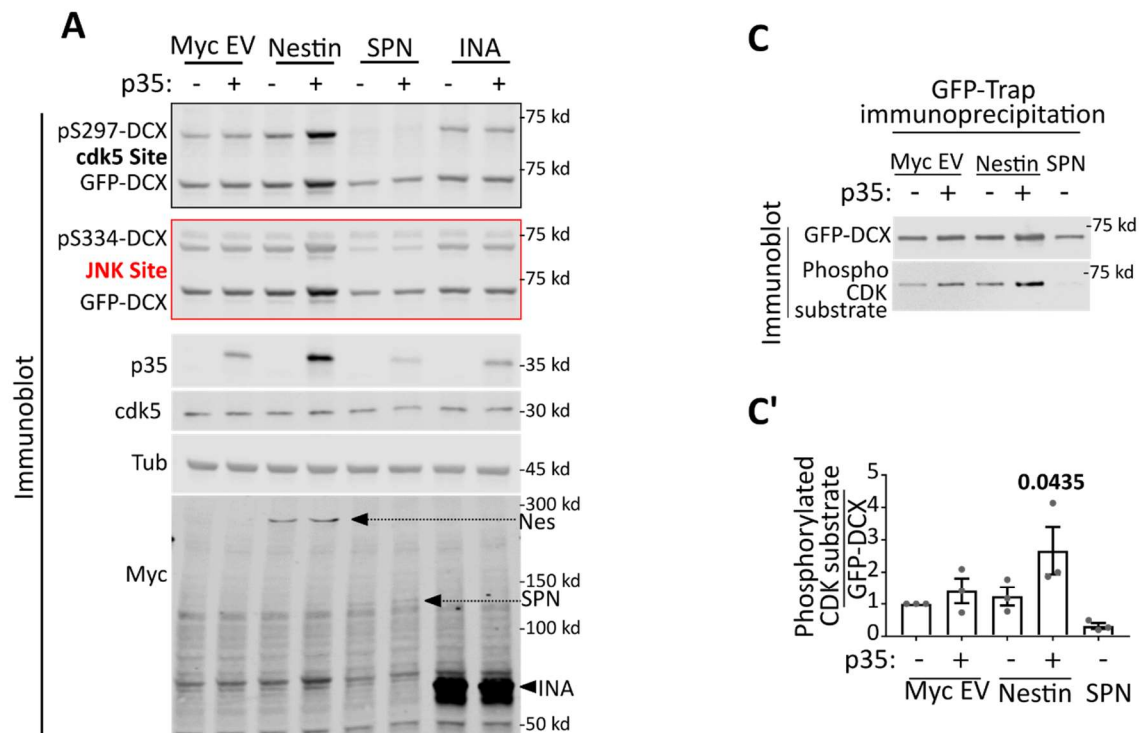
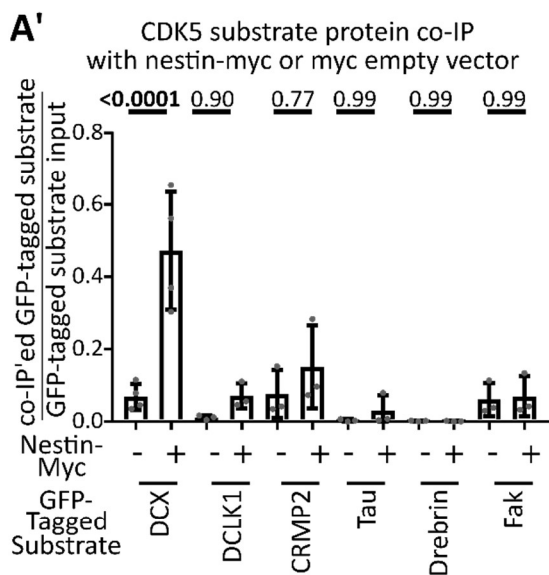
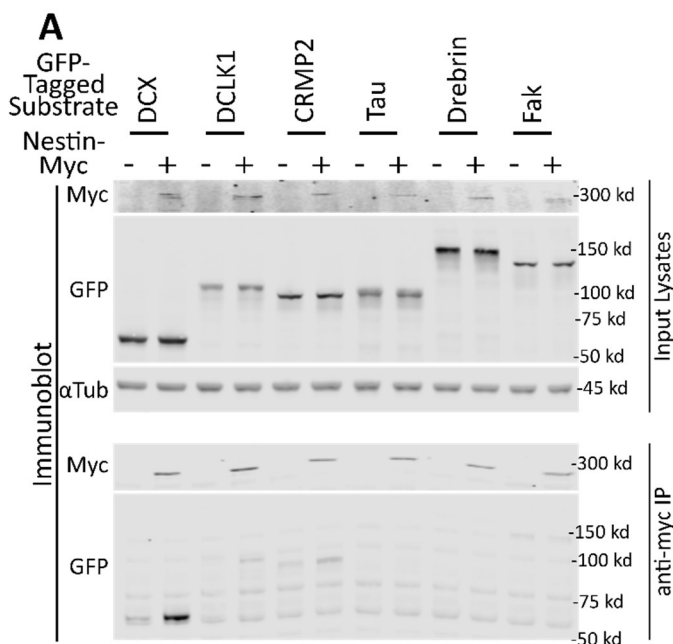


Figure 16: Nestin forms a complex specifically with DCX.

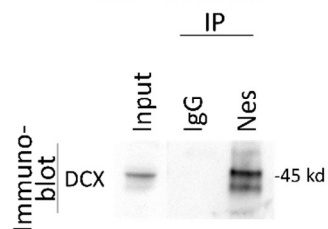
A. Candidate screen for Cdk5 substrates that interact with nestin by co-immunoprecipitation (co-IP). Six different GFP-tagged Cdk5 substrates were expressed with or without nestin-myc in HEK293 cells and subjected to immunoprecipitation with anti-myc antibody. An empty vector was used as a negative control. Top panel: Input lysates are shown. α -Tubulin is used as a loading control. Bottom panel: Anti-myc IPs are probed against myc or GFP. Only GFP-DCX co-IPs with nestin-myc. A'. Densitometry analysis of each co-IP'ed substrate relative to its input. Statistical comparisons (ordinary one-way ANOVA with Sidak's correction) were performed between the empty vector myc IP compared to nestin-myc IP. Errors bars are SD, n = at least 3 for each condition. P-values are indicated above the graph. *p* values of less than 0.05 are indicated in bold.

B - B'. IP of endogenous nestin and DCX complexes from brain. B. DCX co-IP with anti-nestin antibody from E17 rat brain compared to a control IgG. B'. Nestin co-IP with anti-DCX antibody from E17 rat brain compared to a control IgG. As a positive control, DCX IPs were probed against SPN. Drebrin, serves as a negative control.

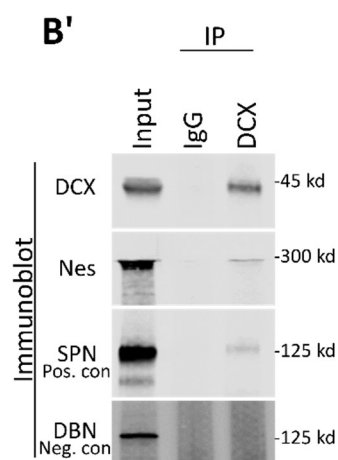
C. anti-DCX immunoprecipitation from 1DIV cortical E16 mouse neurons results in co-IP of nestin from WT neurons, but not from DCX knockout (null) neurons, demonstrating specificity of the IP. The double-headed arrow points at the band corresponding to nestin. No anti-DCX immunoreactivity is seen in the western blots of DCX null neurons compared to WT, also demonstrating specificity of the antibody.



B E17 rat brain



B'



C

E16 Mouse
Cortical neuron culture
1 DIV

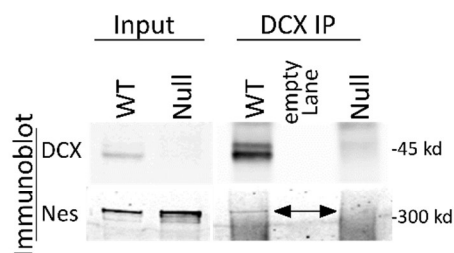


Figure 17: Nestin co-localizes with DCX-MT bundles.

A-E: Confocal images of COS-7 cells transfected with GFP-DCX + myc EV (A), GFP + Nes-myc (B), GFP-DCX + Nes-myc (C), YFP-tau + Nes-myc (D), and GFP-DCX + INA-myc (E). All cells are counterstained with GFP booster nanobody, anti-myc tag antibody, and antibody against endogenous vimentin, as labeled above each panel column. The transfected cell is outlined with a dotted line. Individual black and white images are shown for each channel separately, as well as merged images of the GFP/myc and myc/vimentin channels. Panel outlines of black and white images correspond to the color used in the composite images. Nestin is closely co-localized with vimentin in the perinuclear region, except when GFP-DCX is co-expressed which enriches nestin onto DCX MT bundles. Vimentin remains in the perinuclear region. Tau and α -internexin are additional negative controls.

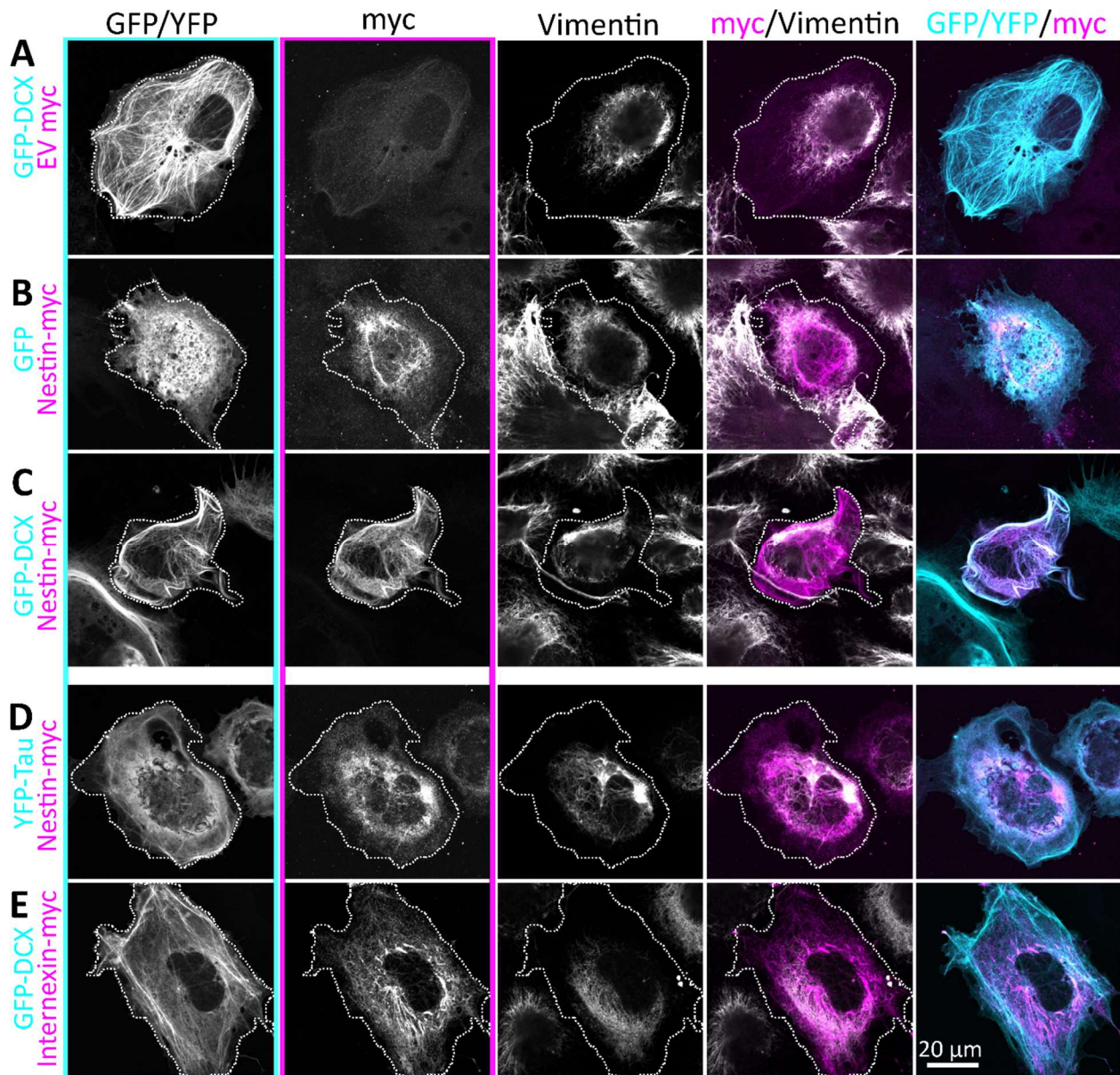


Figure 18: Nestin co-localizes with DCX in axons of newly born neurons *in vitro* and *in vivo*.

A. Confocal images of an E16 cortical mouse stage 3 neuron after 1 DIV culture, counterstained for endogenous DCX, nestin, and $\beta 3$ tubulin. DCX is enriched at the distal region of all neurites, whereas nestin immunostaining labels only the distal region of the growing axon (arrowhead), but not of the minor neurites.

B. Enhanced resolution confocal imaging of nestin in the distal region of an axon-together with DCX. Distally, some nestin filaments appear to extend into the central region of the growth cone and into some proximal filopodia (arrowhead).

C. Wide field immunofluorescence image of a coronal section of E16.5 mouse cortex to illustrate the sparse labeling of individual neurons achieved with knockin of HA-tag using CRISPR and IUE (*in utero* electroporation). In all panels, red arrowhead indicates the cell body that projects the HA/Nes/DCX positive growth cone. "*" marks the nestin positive growth cone, whereas # marks the nestin negative neuron (shown in D", E). The major cortical layers are labeled: VZ- ventricular zone, IZ- intermediate zone, CP- cortical plate. Antibody labeling is indicated in each panel. C'. Inset of square in C demonstrating HA-staining of a single stage 3 neuron with the entirety of its axon imaged in a confocal stack (maximum projection). The distal axon/growth cone is marked with a white arrowhead, and cell body with a red arrowhead.

D and D' panels are confocal images, and D" is an airyscan enhanced resolution image. D. High magnification zoom of the inset square of C' marked with * in C and C'. A single z-plane of each channel shown. D'. Orthogonal projection of the region indicated in the red dashed line of C". The red box outlines the relevant HA-labeled cell. D". High magnification Zeiss Airyscan confocal image equivalent of D.

E. High magnification zoom of the growth cone marked with "#" in C. Arrowheads point along the length of the axon, nestin is not detected in this growth cone.

F. Diagram of the experimental strategy to detect nestin and DCX in single growth cones in mouse cortex. E13.5 mouse cortex was electroporated *in utero* to sparsely introduce three HA-tags into β -actin (Actb-3xHA) by CRISPR. Brains were fixed at E16.5. The CRISPR strategy is depicted diagrammatically.

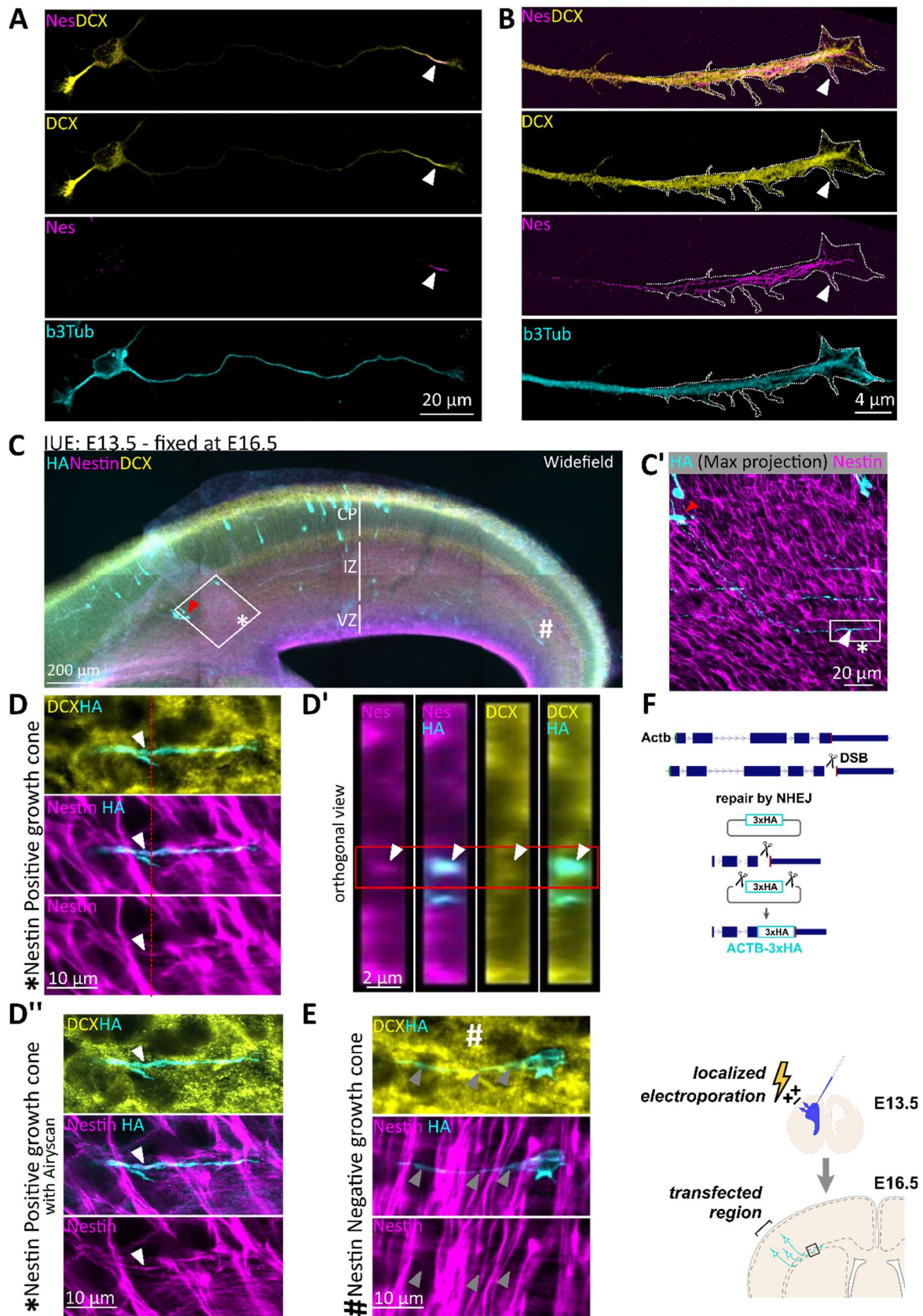


Figure 19: Nestin scaffolds Cdk5 and DCX to promote DCX phosphorylation.

A. Variable amounts of p35 plasmid (0, 1, 2, 4 μ g) were transfected to increase levels of p35 expression in the absence of nestin. In addition, nestin was co-expressed with 0 or 1 μ g p35 plasmid (+Nes lanes). GFP-DCX was expressed in every condition. Levels of pS297-DCX and pS334-DCX were determined by Western blotting. Levels of GFP-DCX, p35, Cdk5 are also assayed. A longer exposure of the p35 blot is shown to illustrate negligible levels of the proteolytic product p25 form of p35. A'. Densitometry analysis of A. Grey bars are ratio of pS297-DCX/total GFP-DCX, red bars are ratio of pS334-DCX/total GFP-DCX. Error bars are SD. Statistical analysis was one way ANOVA with Dunnet's correction. Significant pairwise p-values compared to control (Con) are indicated in black for pS297 and in red for pS334. All other pairwise comparisons to control were not significant and are not shown. N=4 independent experiments. *p* values of less than 0.05 are indicated in bold.

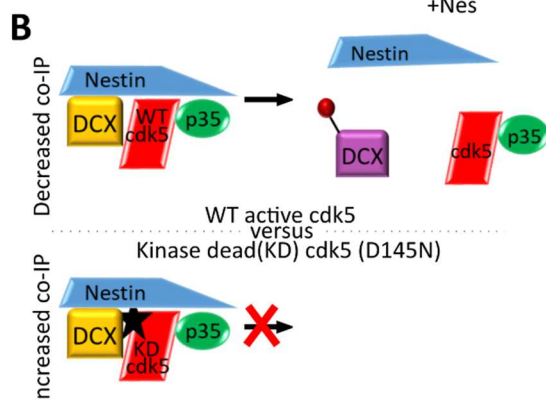
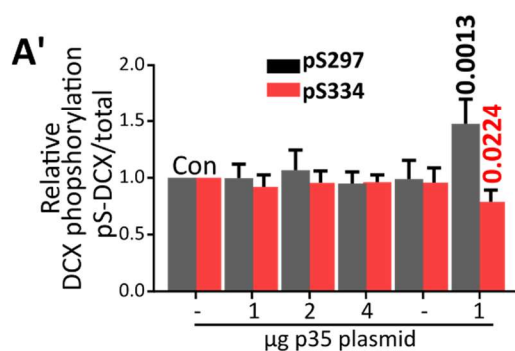
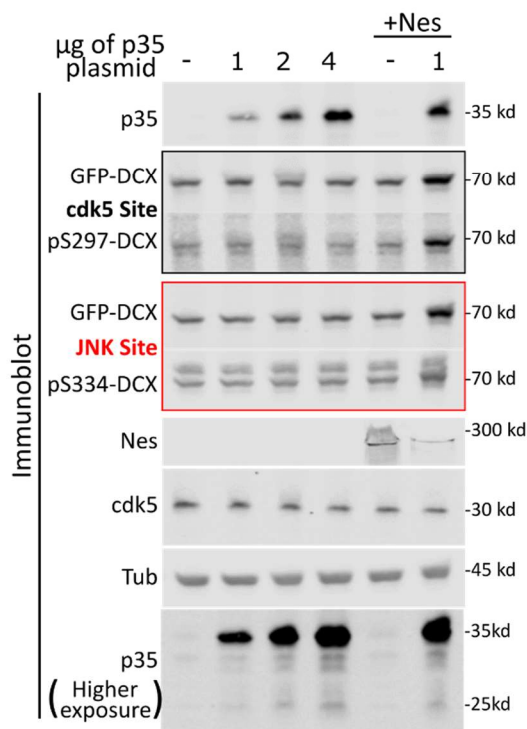
B. Experimental model for using the kinase dead (KD) Cdk5- D145N to trap substrate: If a quaternary complex of Cdk5/p35/DCX/nestin exists, the kinase-dead Cdk5 is predicted to trap all components of the complex which can now be co-IPed. WT Cdk5, on the other hand, more transiently associates with its substrate DCX and does not form a stable complex (as is typical for kinases and their substrates).

C. KD Cdk5 increases efficiency of nestin pulldowns for DCX. GFP-DCX and p35 was co-transfected with myc EV, Nes-myc, or INA-myc together with HA-Cdk5-WT or HA-Cdk5-KD, as indicated above the lanes, and IPed with anti-myc antibody. GFP-DCX inputs (top blot) were compared to amounts of immunoprecipitated GFP-DCX after anti-myc IPs (bottom two blots). C'. The amount of DCX after nestin IP is shown as a ratio of the co-IP to input DCX. HA-Cdk5-KD was compared to HA-Cdk5-WT after nestin IP. This ratio was set to 1 for Cdk5-KD. With Cdk5-KD, DCX is trapped in a stable complex with nestin. Error bars are SD, and statistics were unpaired t-test. N= 6 independent experiments. *p* values of less than 0.05 are indicated in bold.

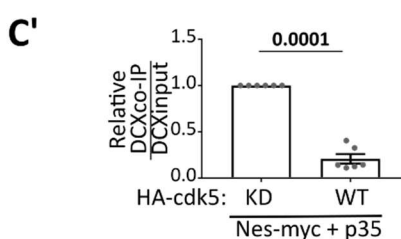
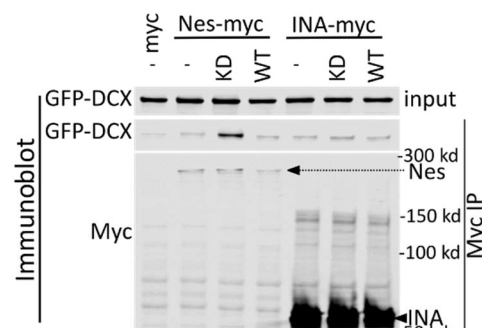
D. P35 co-IPs more DCX when nestin is co-expressed. Transfection conditions are indicated above each lane. HA-Cdk5-KD is expressed in each condition to stabilize the kinase/substrate/scaffold complex. Input levels in the lysate (left panel) are compared to levels of GFP-DCX IPed with anti-p35 antibody (right panel). Nestin increases the amount of DCX that co-IP's with p35. D'. Relative densitometry analysis of DCX in p35 co-IP compared to DCX in input. Error bars are SD, and statistical analysis was t-test with Welch's correction. N= 3 independent experiments.

E. Lambda (λ) phosphatase effectively reduces pS297 levels of GFP-DCX as detected in input lysates. Nestin-myc can co-IP more GFP-DCX when dephosphorylated with lambda phosphatase, compared to untreated samples containing phosphatase inhibitors (inhibs.). Binding was performed *in-vitro* using overexpression lysates. A representative blot (of 4 independent experiments) is shown.

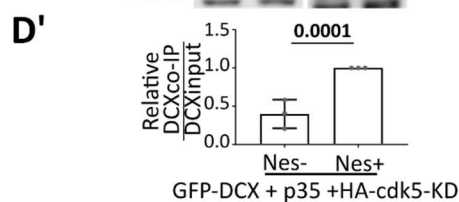
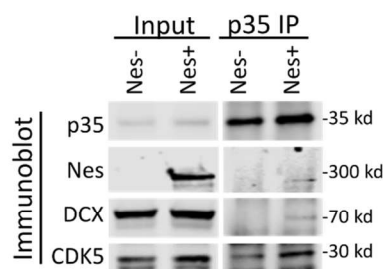
A DCX phosphorylation by cdk5 requires Nestin and is independent of p35 level



C Cdk5 activity dependent DCX and Nestin interaction



D Nestin increases DCX's interaction with p35 by co-IP



E

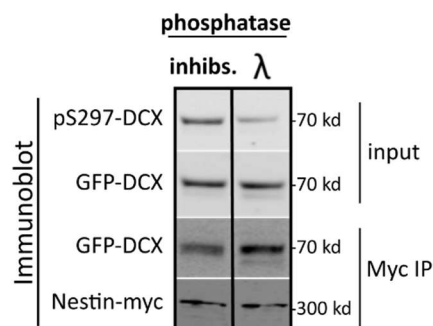


Figure 20: The T316D mutation in nestin affects p35/DCX binding and DCX phosphorylation, but not incorporation into vimentin filaments.

A. Point mutants in nestin (T316A - phospho dead or T316D - putative phospho mimetic) were tested for binding to p35, DCX, and vimentin by co-IP from HEK293 cells. Inputs (left blot) and corresponding co-immunoprecipitation of Vimentin, GFP-DCX, and p35 after anti-myc IP (right blot) are shown. T316D-nestin has greatly reduced levels of co-IP of p35 and DCX compared to WT nestin and T316A-nestin. Each mutant co-IPs vimentin similarly. [Note, the p35 and DCX/vimentin panels are combined from the same experiment, carried out from two different sets of plates of cells. The blots are qualitatively similar for both sets, and were combined into a single figure for simpler viewing.]

B. Nestin-dependent Cdk5-phosphorylation of DCX in HEK293 cells. B'. Densitometry quantification of the blot in B showing the relative levels of pS297-DCX phosphorylation with expression of each mutant. Each value represents the relative phosphorylation of DCX when expressed with nestin and p35, compared to just nestin expression. T316D-nestin does not augment p35/Cdk5-mediated DCX phosphorylation. Error bars are SD, and each condition was compared to WT nestin condition (one way ANOVA with Dunnett's correction). N= 3 independent experiments. Bold *p* values are less than 0.05 and are considered significant.

C-H. Confocal images of COS-7 cells transfected with GFP-DCX (C-E) or GFP (F-H) co-transfected with WT Nes-myc (C,F) or mutant nestin (T316A: D,G. T316D: E,H), as indicated. The transfected cell is outlined with a dotted line. Individual black and white channels are shown, as well as merges with GFP/myc and myc/vimentin channels. Outlines of black and white images correspond to the color used in the composite images. WT nestin and the 316A-nestin mutant co-localize with DCX MT bundles. However, nestin is associated with vimentin when expressed without DCX or when the DCX-binding deficient T316D-nestin is expressed, even in the presence of DCX.

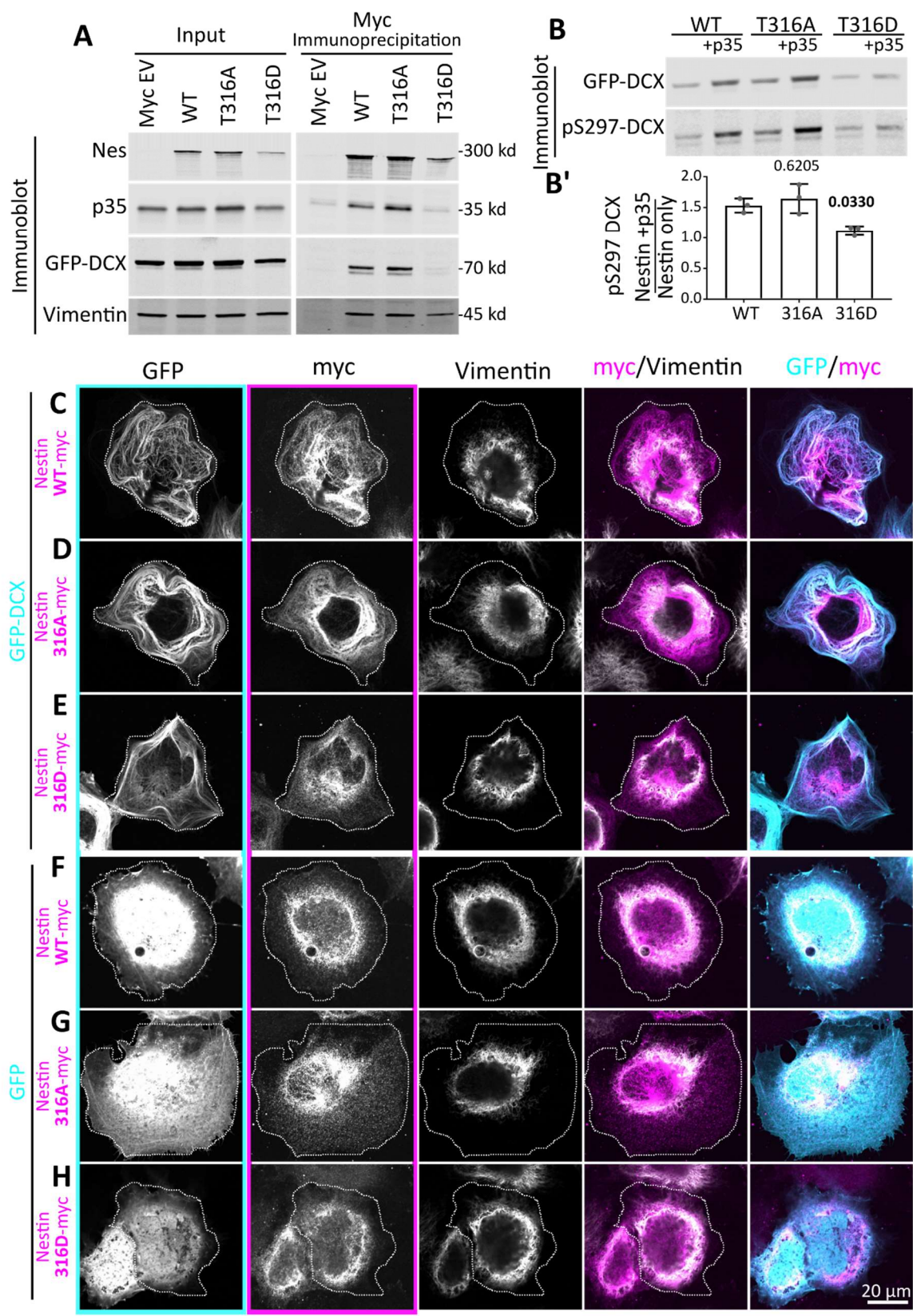


Figure 21: Binding to p35 and/or DCX is required for nestin's effect on growth cone size.

A. Representative images of DIV2 cortical neurons expressing nestin or T316-nestin mutants compared to empty vector control or INA-myc. β 3 tubulin and phalloidin were used to visualize MTs and F-actin, respectively. Axonal GCs are indicated with arrows, and secondary neurites (dendrites), are labeled with arrowheads. Brightness was adjusted for each image for easier viewing. Insets show transfected neurons, identified by GFP expression.

B, B', and B''. Quantification of neuronal morphology in neurons expressing different nestin constructs (as shown in A). N= 72 to 61 cells counted per condition in 3 different independent experiments. Data was analyzed with non-parametric Kruskal-Wallis test with Dunn's correction. Pairwise p-values are shown for comparisons to myc EV (control). WT nestin and T316A-nestin decrease growth cone area and filopodia number, but T316D-nestin does not. *p* values of less than 0.05 are indicated in bold.

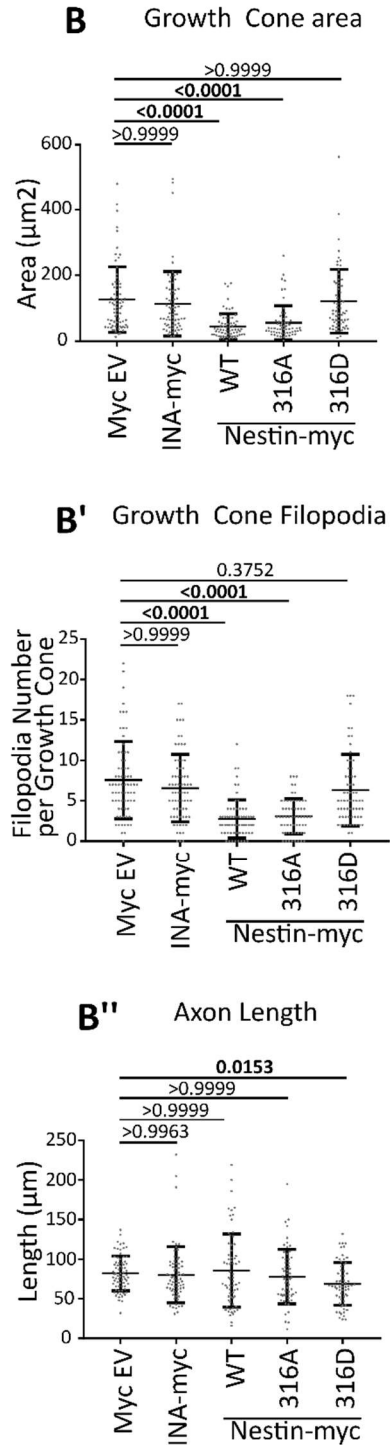
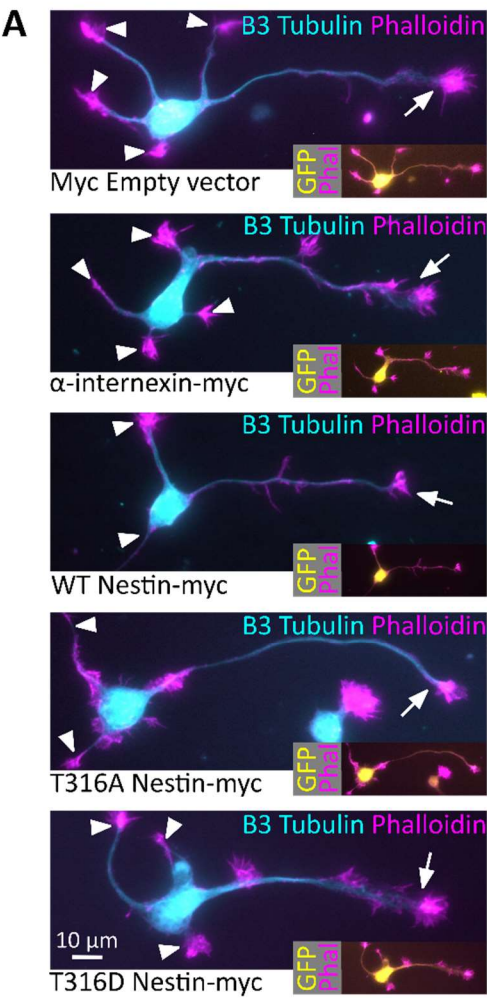


Figure 22: In the absence of DCX, nestin overexpression does not result in small growth cones.

A. Representative images of WT or DCX null E16 cortical neurons (as labeled) expressing Nes-myc with GFP or Nes-myc with GFP-DCX after 48 hours in culture. WT neurons transfected with Nes-myc show smaller axonal GCs (arrows) whereas DCX KO neurons transfected with nestin-myc do not show smaller GCs. When GFP-DCX is co-transfected into DCX KO neurons, GCs are smaller. Axon growth cones are indicated with arrows. The growth cones of secondary neurites (dendrites) were not considered and are indicated with arrowheads.

B', B'', B'''. Quantification of morphological characteristics. The background shading color behind the images in A correspond to the conditions shaded in the graphs B', B'', and B''' for easier interpretation. B', B'', and B''' shows the quantification of morphological measurements from transfected neurons: growth cone area (B'), filopodia number (B''), and axon length (B'''). Error bars are SD. Kruskal-Wallis non-parametric test was used. P-values are only shown for selected statistical comparisons to keep the graph less cluttered. N= 40 to 70 cells counted in 3 different independent experiments.

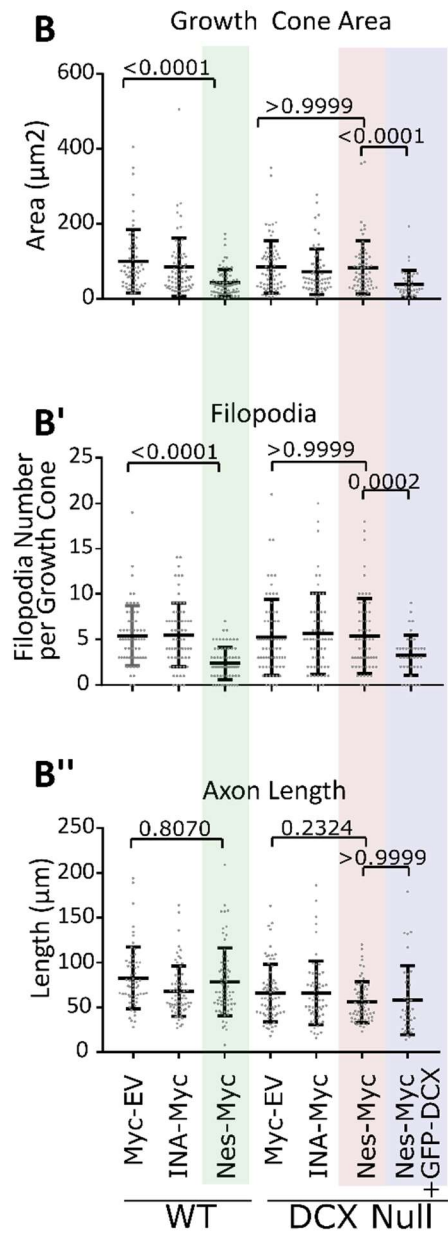
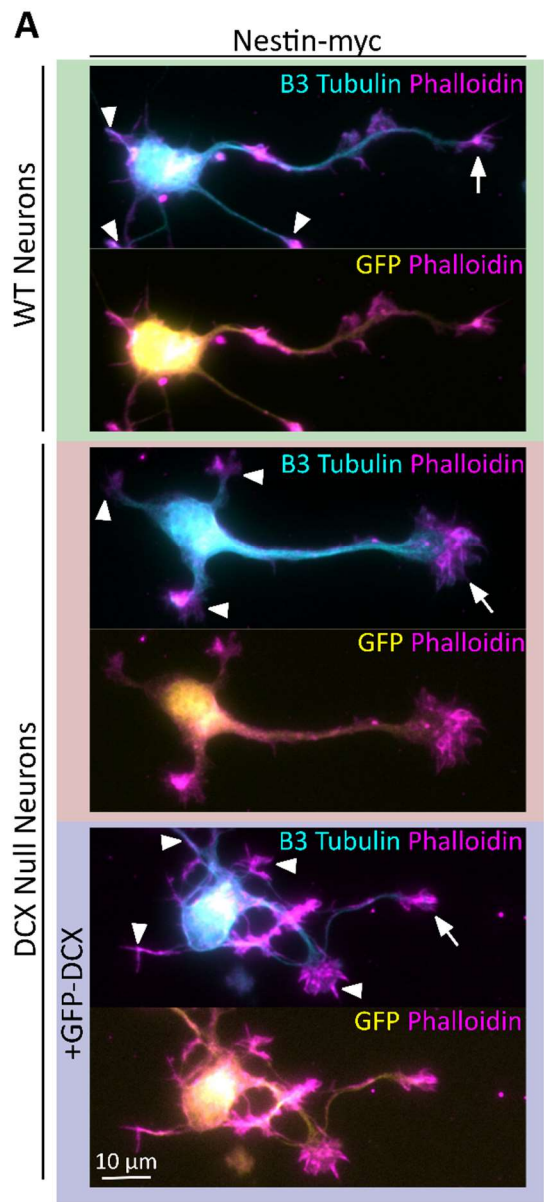


Figure 23: DCX is a Cdk5 substrate downstream of Sema3a, and DCX null neurons respond in a nestin independent manner.

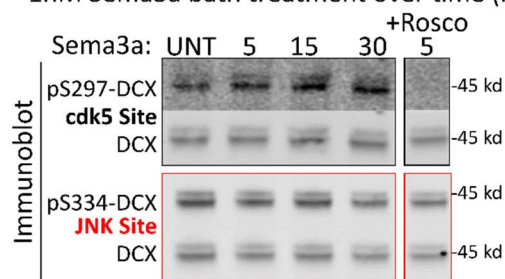
A. Sema3a treatment of 1DIV cultured mouse cortical E16 neurons increases DCX phosphorylation at S297, but not at S334. Rightmost lane: Neurons were treated with 1nM Sema3a for 5 min with pre-incubation of the cells with 10 μ M Roscovitine for 30 minutes. The inhibitor lane was from the same blot as the other lanes, but separated by intervening lanes which were removed. A'. Quantification of Sema3a time course. Blots in A were subjected to densitometry analysis, and the ratio of phospho-DCX signal relative to the total DCX is plotted. DCX phosphorylation at pS297, but not at pS334, begins quickly after Sema3a stimulation, and becomes significant at 15 and 30 minutes. Error bars are SD and statistical analysis was performed at each timepoint compared to untreated (UNT) with an ordinary one way ANOVA with Dunnett's correction. n=5 independent experiments. *p* values of less than 0.05 are indicated in bold.

A''. Quantification of Roscovitine sensitivity (rightmost lane in A). Each value was obtained from densitometry analysis of western blots, where the relative level of p-DCX was compared to total DCX. The values in the plot are a ratio of the relative phosphorylation after inhibitor (drug) treatment compared to no inhibitor treatment. Error bars are SD and statistical analysis was performed with a two-tailed unpaired t-test. N=5 independent experiments.

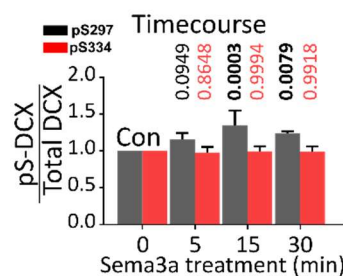
B,B',B''. Quantification of morphological characteristics of nestin-negative and nestin-positive neurons derived from WT or DCX null E16 cortex at 1DIV (stage 3). WT cells show nestin dependent decrease in growth cone size, while DCX null neurons do not. When treated with 1nM Sema3a for 5 minutes, filopodial retraction in WT neurons was dependent on nestin expression. In DCX null neurons, there was a filopodia decrease after Sema3a treatment in nestin positive and negative neurons (independent of nestin). Axon length was not significantly different in any condition. Error bars are SEM. B,B'. Statistical analysis was one way ANOVA with Sidak's multiple comparison correction with pairs tested shown. B''. Statistical analysis was one way ANOVA with Tukey's multiple comparison correction. N=4-5 independent experiments with 20-30 cells counted in each set. *p* values of less than 0.05 are indicated in bold.

C. Model for how nestin increases Cdk5-phosphorylation of DCX by scaffolding: in the absence of nestin (-Nestin; top) non-phospho-DCX is bound to microtubules and inefficiently phosphorylated by Cdk5/p35. In the presence of nestin (+ Nestin scaffold; bottom), DCX becomes associated with Cdk5/p35, increasing the efficiency of DCX phosphorylation. DCX phosphorylation results in dissociation of DCX from MTs, this allowing remodeling by additional factors (red bars). In this model, we also depict data from others that showed that the actin-associated SPN which scaffolds Protein Phosphatase 1 (PP1) potentially dephosphorylates DCX. In our model, the level of phospho-DCX is determined by the relative opposing activities of the two regulatory complexes nestin/Cdk5/p35 or SPN/PP1. However, in DCX null neurons (bottom half of the pane)l, nestin no longer has an effect on Sema3a sensitivity. Without DCX MT binding and stabilization, growth cones retract and are sensitive to Sema3a independent of nestin. Nestin-mediated enhancement of Sema3a sensitivity is thus lost in DCX null neurons.

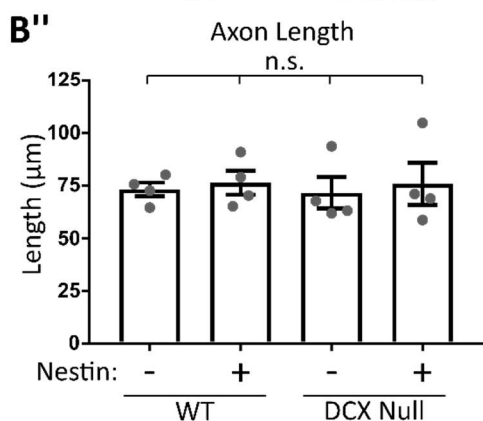
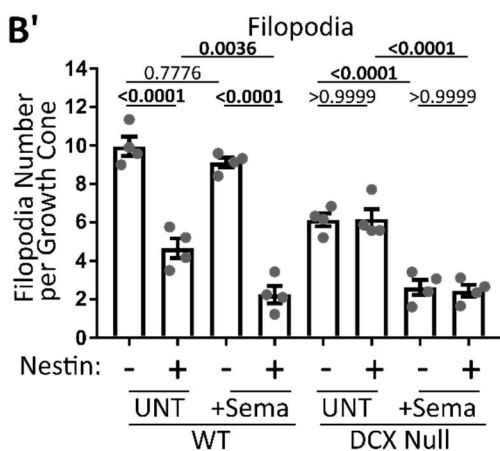
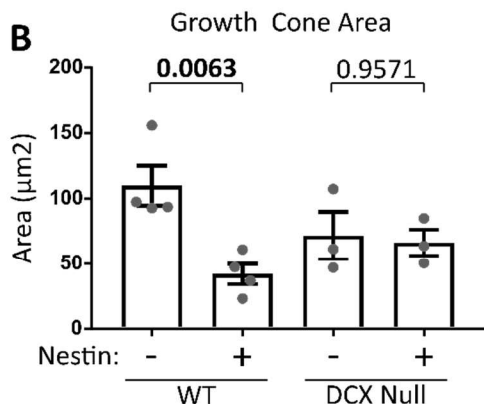
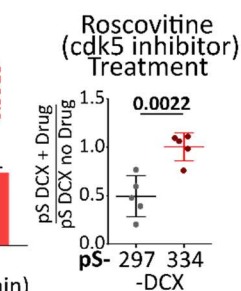
A 1DIV cortical mouse neurons
1nM Sema3a bath treatment over time (min)



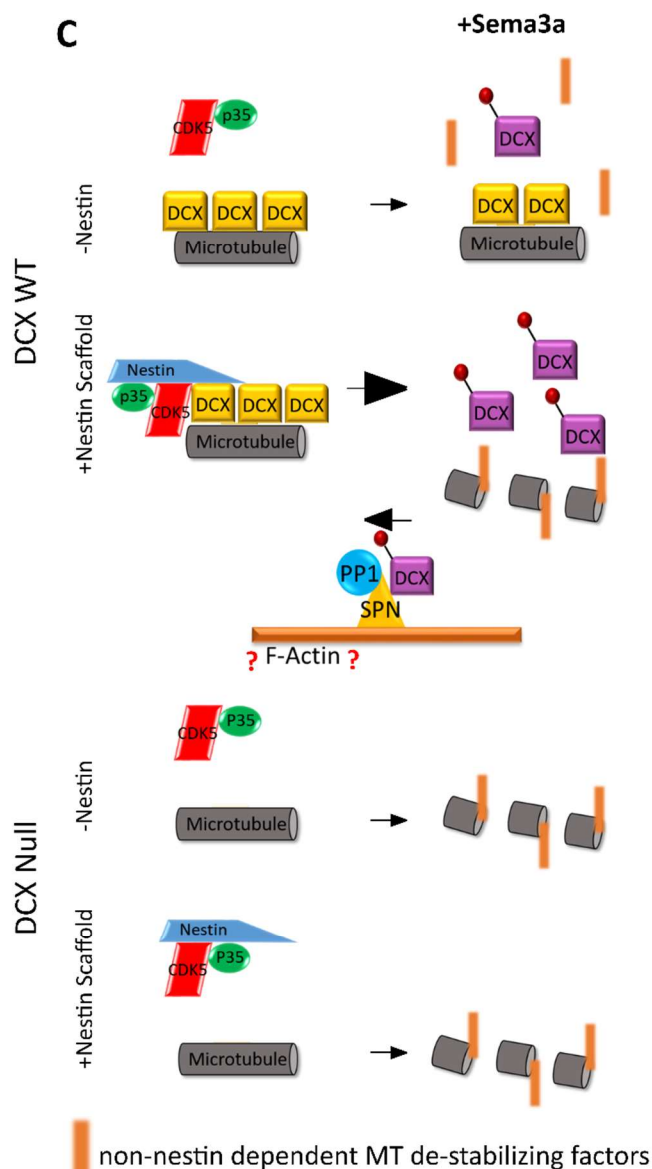
A'



A''



C



Chapter 4: Summary of major findings and Conclusion

4.1 Overview

The work done in this dissertation focuses on the role of the intermediate filament protein nestin in immature neurons, and how it can alter signaling pathways involving Cdk5 through the microtubule associated protein DCX. This study started initially with the serendipitous discovery of a complex between DCX and nestin from an unbiased screen of DCX binding partners (by co-IP) in rat brain. Since nestin is usually considered a marker of neural progenitors whereas DCX is a marker of postmitotic neurons, finding nestin as a potential binding partner of DCX was puzzling and counter to expectations in the field. I therefore first verified that nestin and DCX were co-expressed in the same cell. After initially verifying that low levels of nestin persisted in DCX positive immature neurons, I noticed that the growth cone morphology of nestin positive neurons differed from nestin negative neurons. Nestin negative neurons had larger growth cones- which is suggestive as a more stabilized skeleton (Kiss *et al.*, 2018) and phenocopies treatment of neurons with the microtubule stabilizing drug taxol (Gumy *et al.*, 2013). The best described function of nestin is regulating the kinase Cdk5, so I set out looking for Cdk5-dependent processes or substrates associated with the cytoskeleton in neurons that could be affected by nestin. The result was identifying a complex between DCX, nestin, and Cdk5 which acts as a scaffolding complex that selectively mediates phosphorylation of DCX, but not other Cdk5 substrates. I found that this complex is important in mediating nestin-dependent sensitivity to Sema3a by releasing the “brake” of DCX from its role in stabilizing microtubule to allow for cytoskeleton instability and filopodia retraction in growth cones following stimulation by Sema3a.

4.2 Nestin cell type expression, localization, and functional relevance

Nestin has commonly been used as an immunological marker for neural progenitor cells. We were thus surprised when we identified nestin as co-immunoprecipitating with DCX from embryonic rat brain, as DCX is not expressed in neural progenitor cells, but is expressed immediately after differentiation in the earliest stages of neuron maturation. I thus carried out careful immunostaining experiments using multiple antibodies to nestin and DCX in the earliest stages of mouse cortical neurons (Figure 6), from progenitors (cultured as neurospheres), to newly born neurons (only a matter of hours after differentiation). I confirmed that DCX was not expressed in neural progenitors (Figure7), but that low levels of nestin persisted in early stages of neuron differentiation (Figure 8). We could see this in differentiated mouse neural progenitors, in 1 day *in vitro* (DIV) mouse primary neuron cultures, and in neuronally differentiated human IPSC's in collaboration with Karen Litwa (Figure8). Furthermore, nestin appeared to be enriched in the distal region of axons (just as DCX was) but was absent from dendrites (unlike DCX which is in the distal region of axons and dendrites)(Figure 6). Chapter 2 characterizes these nestin-expressing neurons, and posits that nestin in neurons is functionally relevant. I thus hypothesized that nestin could be involved in axon-specific, DCX-dependent processes. Furthermore, I hypothesized that nestin would be involved in a Cdk5-dependent process, as nestin's best described function is regulating and interacting with Cdk5 and its activator p35, and DCX is a substrate of Cdk5 phosphorylation.

Initially, I decided to take advantage of the observation that at 1DIV, nestin was only expressed in around 60% of neurons. Thus, we could analyze nestin-dependent phenotypes within the same culture, by comparing nestin-positive with nestin-negative cells by analyzing after immunostaining for nestin. First of all, nestin did not appear to be associated with any specific cell type or layer, but appear to represent a stage that the majority (~ 60-70%) of neurons went through during maturation (Figure8). Nestin expression did not vary between two main pyramidal cell populations (which are cortical layer markers *in vivo*)- Satb2 (deeper layers) and Ctip1 (superficial layers), nor did nestin expression change when primary neurons were

prepared from different embryonic days- E14, E15, or E16 (not shown)- which represent neurons bound for deeper (Satb2-positive) or more superficial layers (Ctip2-positive), respectively (Figure7). The first phenotype noted was that nestin-positive growth cones were on average statistically smaller in area with fewer filopodia when compared to nestin-negative growth cones (Figure11). This was interesting, because previous studies of live imaging EB3- a microtubule tip tracking protein- had noted that smaller growth cones had more dynamic microtubules (more EB3 comets per area) compared to large growth cones (Kiss *et al.*, 2018). We therefore extrapolated from this study and inferred that nestin-positive (small) growth cones would have more dynamic microtubules, and nestin-negative (large) growth cones would have less dynamic microtubules. A separate study showed that taxol (a microtubule stabilizing drug) resulted in large growth cones (Gumy *et al.*, 2013), again suggesting that larger growth cones have more stable microtubules. The large growth cone phenotype derived from the endogenous variation in nestin expression was replicated using nestin specific siRNA's, confirming that this phenotype was related to the cells nestin expression.

Previous studies from other groups had firmly established that when DCX was bound to microtubules, they were stabilized, and depolymerized less often (Moore *et al.*, 2004, 2006; Tanaka, Finley F. Serneo, *et al.*, 2004; Bielas *et al.*, 2007; Moslehi, Ng and Bogoyevitch, 2017). Phenotypically, this suggested that nestin-negative growth cones have more DCX bound to microtubules. Binding of DCX to microtubules is regulated by phosphorylation by Cdk5, in that Cdk5-phosphorylated DCX has a decreased affinity and had less of an ability to stabilize microtubules than non-phosphorylated DCX (Tanaka, Finley F. Serneo, *et al.*, 2004; Bielas *et al.*, 2007). Therefore, I hypothesized that DCX would be less phosphorylated in the absence of nestin.

In order to test if nestin modulation of Cdk5 signaling might be important in neurons, I needed a physiological stimulus for Cdk5 activation. We chose Semaphorin3a to test on these cells because Semaphorin3a was known to signal through Cdk5 (Brown *et al.*, 2004; Uchida *et al.*, 2005; Ng *et al.*, 2013), and nestin could potentially modulating Cdk5 activity (Mohseni *et al.*, 2011; Yang *et al.*, 2011). I therefore decided to investigate if nestin modulated Sema3a responses. I observed that nestin-positive cells were more sensitive to the repulsive cue Semaphorin3a- such that a low dose of Sema3a for only 5 minutes resulted in significant growth cone filopodia retraction from nestin-positive cells, and no significant change in the number of growth cone filopodia of nestin-negative cells (Figure11). This phenotype was seen when the cells were negative for nestin by endogenous variation, or negative because of treatment with nestin targeting siRNA (Figure12). Thus, presence of nestin appeared to promote Cdk5 signaling downstream of Semaphorin3a, whereas absence of nestin did not. Many studies that characterized the responsiveness of cortical neurons to Semaphorin3a had noted that only about half of the neurons responded to the guidance cue (Dent, 2004). My work confirms this finding and implicates nestin as a contributor to this variation.

My work also provided counterevidence for the previous dogma in the field which had implied an absence of intermediate filaments from growth cones. Early reviews repeatedly claimed that actin and microtubules were the only cytoskeletal elements of concern for the study of axon guidance, and that intermediate filaments were not even present- however this was often mentioned as "data not shown"(Dent and Gertler, 2003). I, on the other hand, could detect intermediate filaments in the more proximal regions of the growth cone, and subsequent high resolution imaging could detect individual intermediate filaments projecting into the most distal regions of the growth cone and even some filopodia. Furthermore, the lack of strong phenotype from neurofilament knockout mice was used as evidence for the lack of involvement of intermediate filaments in axon guidance. However, it is worthwhile to note that consistently, neurofilament-L and -M knockout mice had 10-20% fewer axons in the ventral root- which was the primary region analyzed and very little characterization of the CNS or the cortex was performed on these mice (Jacomy *et al.*, 1999; Perrot *et al.*, 2008). In fact, individual axon

tracts were barely analyzed at all in these mice, and the fact of a viable mouse with a spinal cord and ventral roots was used as evidence for absence of a role for intermediate filaments in axon guidance. This was concluded even though knockout mice lacking the gold standard protein in axon guidance, netrin 1, also develop a spinal cord and ventral roots effectively, and only a subpopulation of axons are misprojected, whereas most brain structures develop normally when analyzed at a gross level (Bin *et al.*, 2015; Yung, Nishitani and Goodrich, 2015). Thus the early dismissal of a role for intermediate filaments in axon guidance was premature.

Earlier work also overstated the specificity of nestin expression exclusively in neural progenitor cells. I could detect nestin in early mouse, rat, and human neurons *in vitro*. I could also detect nestin in the axons of the cortices of embryonic mice. I should note here, that the first study (Hockfield and McKay, 1985) used to define nestin's discrete expression in neural stem cells was performed in 1985, with rather low resolution and sensitivity microscopy and labeling methods, and before the architecture of the developing CNS was fully understood. In addition, this study looked at the spinal cord only, but its findings have been extrapolated to apply to all part of the CNS. A subsequent study from 1994 (Dahlstrand, Lardelli and Lendahl, 1995b), looked at nestin mRNA, and is said to confirm the 1985 study, but the title of the study itself is, "Nestin mRNA expression *correlates* with the central nervous system progenitor cell state in many, but not all, regions of developing central nervous system" (emphasis mine). The study merely correlated peak nestin mRNA level with known periods of neurogenesis in crude whole brain mRNA extracts using RT-PCR. That is, a comparison between E15.5 whole mouse brain vs adult mouse brain. The higher level of nestin at E15.5 in whole brain mRNA extracts meant that nestin was correlated with neurogenesis- which was known to happen embryonically and not in adult brain. In addition, some (low magnification) *in situ* hybridizations were performed, which observed high nestin mRNA in the ventricular zone, but noted some lower levels of nestin mRNA in the intermediate zone- which is exactly where I see low levels of nestin protein in intermediate zone axons. Thus the field has been strongly adhering to nestin's exclusivity to neural progenitor cell despite only correlative evidence from over 25-35 years ago. It's about time that modern high resolution, high sensitivity methods were used to revisit the question.

4.3 Nestin selectively facilitates phosphorylation of DCX by Cdk5 through scaffolding

Chapter 3 of this dissertation provides mechanistic insight into nestin modulation of growth cone morphology and Semaphorin3a responsiveness, as well as provides additional evidence of nestin expression in axons *in vitro* and *in vivo*- using the latest techniques and high resolution microscopy. Chapter 2 had not yet provided any molecular link between DCX and nestin, and thus I proceeded in an unbiased manner, as we had no reason to think that there was a specific link only between nestin and DCX. I screened a number of known Cdk5 substrates that are known to be involved in the response to Sema3a in neurons. I used commercially available antibodies specific to Cdk5 phosphorylation sites of these proteins to see if nestin affected these substrates' phosphorylation by Cdk5. This assay was an "in-cell" kinase assay, where heterologous Hek293 cells were used to express the various constructs (Figure 14). These cells provided an ideal scenario, where they expressed Cdk5 endogenously, but had no Cdk5 activity because they did not express the Cdk5 activator p35. I found that for most Cdk5 substrates expression of p35 was sufficient to elicit a detectable and significant increase in phosphorylation by Cdk5, and that co-expression of nestin had not additional effect. DCX was the only Cdk5 substrate tested that did not have any significant increase in phosphorylation with the expression of p35, but co-expression of nestin significantly increased phosphorylation of DCX (Figure 14).

To address how nestin affected phosphorylation of DCX selectively, we immunoprecipitated nestin when co-expressed with the different Cdk5 substrates. Only DCX

co-immunoprecipitated with nestin, which could be confirmed with endogenous protein originating from embryonic mouse brain or 1DIV primary neuronal cultures (Figure 16). We identified a scaffolding mechanism, where nestin interacting with p35/Cdk5 and DCX simultaneously facilitated a robust kinase reaction- presumably by bringing kinase and substrate into close proximity with each other. Phosphorylation of DCX resulted in disassembly of the complex- and the complex could be hyper-stabilized using a kinase-dead version of Cdk5 (Figure19).

I constructed nestin mutants with putative phospho-mimetic (T to D) or phospho-dead (T to A) substitutions at threonine 316. This site had previously been shown to be involved in binding of nestin to Cdk5/p35. In our hands, we found that nestin-T316D had greatly reduced binding to p35, but surprisingly also to DCX. Additionally, nestin-T316D no longer promoted enhanced phosphorylation of DCX by Cdk5. Nestin-T316A retained its binding and phosphorylation promoting functions. However, both mutants retained their WT ability to interact with vimentin and incorporate into endogenous vimentin intermediate filament networks in heterologous Cos7 cells (Figure20). When expressed in WT neurons, I found that the T316D mutant failed to elicit changes in growth cone morphology (small growth cones) whereas both WT and nestin-T316A did (Figure21). These experiments suggesting that nestin binding to DCX was essential for the growth cone morphology modulation by nestin. In order to test this idea more directly, I used DCX knockout neurons. WT nestin failed to elicit any changes in morphology of DCX-null neurons, but the small growth cone phenotype could be rescued with a GFP-DCX rescue (Figure 22). Finally, I showed that unlike WT neurons, DCX null neurons did not show any nestin-dependent growth cone morphology differences, or filopodial retraction response to Semaphorin3a (Figure23). My results thus strongly suggest that DCX is downstream of nestin in the Sema3a pathway.

Finally, this chapter includes some high resolution imaging of nestin in the axons and growth cone of both *in vitro* and *in vivo* neurons (Figure18). The enhanced resolution images of *in vitro* neurons demonstrated how some apparent individual nestin containing filaments extended into peripheral regions of the growth cone, and even some filopodia. *In vivo*, I worked with a collaborator Kenneth Kwan and his student Jason Keil, who provided mouse brains that had HA tags knocked in to the actin locus using CRISPR technologies with *in utero* electroporation. This technique allowed sparse labeling of neuron not possible with conventional *in utero* electroporation strategies. We were thus able to image the entirety of an individual neuron from cell body to growth cone. We found, by enhanced resolution imaging (Airyscan), that nestin immunolabeling localized in the distal regions of the axon and growth cone of early neurons, at an equivalent stage as that identified in primary neuron culture.

4.4 Conclusion and future questions

This work identified a population of early neurons that express nestin in their axons, and functionally these neurons are more sensitive to the repulsive guidance cue Semaphorin3a. We found that expression of nestin selectively facilitated robust phosphorylation of DCX by Cdk5, but other Cdk5 substrates were not affected. Nestin specifically interacts with DCX, and increases its phosphorylation through kinase scaffolding, and acts as an adaptor protein for Cdk5 to interact with DCX. We find that nestin mutants that fail to increase DCX phosphorylation do not have the same morphological effects on neurons as WT nestin does, and that WT nestin does not affect DCX null neurons similarly to WT neurons. Finally, DCX null neurons are sensitive to Semaphorin3a in a nestin-independent manner.

This work advances several main overall concepts:

Higher resolution characterization of the temporal progression of intermediate filaments in the cortex: As discussed above, nestin has been and continues to be a commonly used distinguishing marker for neural progenitors. Many of these studies, using modern high sensitivity and resolution techniques but have relied on some rather dated studies using low

resolution and low sensitivity methods. Thus it is essential to update the details of nestin's expression to be better applied to these modern techniques.

Temporally expressed signaling modulators and axon guidance: Variance in guidance cue signaling is crucial in the brain, where there are many different axon targeting outcomes but a finite number of guidance cue signaling molecules. Thus some are reused in different brain regions, and a growth cone may have to respond differently in one brain region compared to another. This represents altered sensitivity to a guidance cue over an individual neuron's maturation. Nestin's expression profile and kinase signaling modulating activity provides this function to developing cortical neurons. Our antibody to the Cdk5 phosphorylation site on DCX failed to produce a consistent staining pattern by immunofluorescence, and I was thus not able to detect changes in DCX phosphorylation in individual neurons dependent on nestin expression in neurons. Perhaps antibodies made in the future to other phosphorylation sites on DCX can provide that capability. In addition, I was unable to manipulate nestin expression *in vivo*, using knockdown or overexpression of nestin constructs delivered by *in utero* electroporation. This proved to be beyond the technical realm of our lab, but work with collaborators in the future may provide the expertise needed to complete such experiments.

Intermediate filaments as signaling modulators: As discussed in the introduction in detail, intermediate filaments associate with and have the potential to modulate signaling molecules and cascade in many contexts. This study provides further evidence of nestin's function as a Cdk5 modulator. Previous work identified nestin as a modulator of Cdk5 in myoblasts, but a physiological substrate for nestin/Cdk5/p35 was not identified. My work provides the first identification of Cdk5-mediated phosphorylation changes in a physiological substrate, i.e. DCX. Not only does nestin modulate a kinase's activity, but it does so in a substrate-specific manner. This work may provide precedence for studies of other neuronal intermediate filaments and possible contributions of intermediate filaments to creating functional neuronal variability in responsiveness to physiological extracellular cues.

References

- Argiro A., Bunge M.B., Johnson, I. . T., Rapp, S. and Scott, B. (1984) 'Correlation between growth form and movement and their dependence on neuronal age', *The Journal of Neuroscience*, 4(12), pp. 3051–3062.
- Arner, E. *et al.* (2015) 'Transcribed enhancers lead waves of coordinated transcription in transitioning mammalian cells', *Science*, 347(6225), pp. 1010–1015.
- Bahi-Buisson, N. *et al.* (2013) 'New insights into genotype-phenotype correlations for the doublecortin-related lissencephaly spectrum.', *Brain : a journal of neurology*, 136(Pt 1), pp. 223–44. doi: 10.1093/brain/aws323.
- Ballatore, C., Lee, V. M. and Trojanowski, J. Q. (2007) 'Tau-mediated neurodegeneration in Alzheimer's disease and related disorders', *Nature*, (August). doi: 10.1038/nrn2194.
- Banker, G. A. and Cowan, W. M. (1977) 'Rat Hippocampal neurons in dispersed cell culture', *Brain Research*, 126(3), pp. 397–425.
- Baribault, H. *et al.* (1993) 'Mid-gestational lethality in mice lacking eratin 8', pp. 1191–1202.
- Barry, D. M. *et al.* (2007) 'New movements in neurofilament transport, turnover and disease', *Experimental Cell Research*, 3. doi: 10.1016/j.yexcr.2007.03.011.
- Battaglia, R. A. *et al.* (2019) 'Vimentin on the move : new developments in cell migration', *F1000 Research*, 7, pp. 1–10.
- Baucum, A. J. *et al.* (2010) 'Identification and Validation of Novel Spinophilin-associated Proteins in Rodent Striatum Using an Enhanced *ex Vivo* Shotgun Proteomics Approach', *Molecular & Cellular Proteomics*, 9(6), pp. 1243–1259. doi: 10.1074/mcp.M900387-MCP200.
- Baucum, A. J., Strack, S. and Colbran, R. J. (2012) 'Age-dependent targeting of protein phosphatase 1 to Ca²⁺/calmodulin-dependent protein kinase II by spinophilin in mouse striatum', *PLoS ONE*, 7(2). doi: 10.1371/journal.pone.0031554.
- Beher, O. Golden, J A. Mashimo, H. Schoen, F. Fishman, M. (1996) 'Semaphorin III is needed for normal patterning and growth of nerves, bones, and heart', *Nature*, 383(10), pp. 525–528.
- Bennett, G. S. (1987) 'Changes in Intermediate Filament Ccomposition During Neurogenesis', *Current Topics in Developmental Biology*, 21.
- Benson, D. L., Mandell J. W., Shaw G., B. G. (1996) 'Compartmentation of alpha-internexin and neurofilament triplet proteins in cultured hippocampal neurons', *Journal of Neurocytology*, 25(3), pp. 181–196.
- Bernal, A. and Arranz, L. (2018) 'Nestin - expressing progenitor cells : function , identity and therapeutic implications', *Cellular and Molecular Life Sciences*. Springer International Publishing, 75(12), pp. 2177–2195. doi: 10.1007/s00018-018-2794-z.
- Bernot, K. M., Lee, C. and Coulombe, P. A. (2005) 'A small surface hydrophobic stripe in the coiled-coil domain of type I keratins mediates tetramer stability', *Journal of Cell*

Biology, 168(6). doi: 10.1083/jcb.200408116.

Bielas, S. L. *et al.* (2007) 'Spinophilin Facilitates Dephosphorylation of Doublecortin by PP1 to Mediate Microtubule Bundling at the Axonal Wrist', *Cell*, 129(3), pp. 579–591. doi: 10.1016/j.cell.2007.03.023.

Bigler, R. L. *et al.* (2017) 'Messenger RNAs localized to distal projections of human stem cell derived neurons', *Scientific Reports*. Springer US, 7(1), pp. 1–11. doi: 10.1038/s41598-017-00676-w.

Bin, J. M. *et al.* (2015) 'Complete Loss of Netrin-1 Results in Embryonic Lethality and Severe Axon Guidance Defects without Increased Neural Cell Death Report Complete Loss of Netrin-1 Results in Embryonic Lethality and Severe Axon Guidance Defects without Increased Neural Cell Death', *CellReports*. The Authors, 12(7), pp. 1099–1106. doi: 10.1016/j.celrep.2015.07.028.

Bott, C *et al.* (2019) 'Nestin in immature embryonic neurons affects axon growth cone morphology and Semaphorin3a sensitivity', *MBOC*, 30(10), pp. 1214–1229. doi: 10.1091/mbc.E18-06-0361.

Bott, C.J. *et al.* (2019) 'Nestin selectively facilitates the phosphorylation of the Lissencephaly-linked protein doublecortin (DCX) by Cdk5/p35 to regulate growth cone morphology and Sema3a sensitivity in developing neurons', *Bioarxiv preprint*.

Bourgeois, F. *et al.* (2015) 'A critical and previously unsuspected role for doublecortin at the neuromuscular junction in mouse and human', *Neuromuscular Disorders*. Elsevier B.V., 25(6), pp. 461–473. doi: 10.1016/j.nmd.2015.01.012.

Boyne, L. J., Fischer, I. and Shea, T. B. (1996) 'Role of vimentin in early stages of neuritogenesis in cultured hippocampal neurons', *International Journal of Developmental Neuroscience*, 14, pp. 739–748. doi: 10.1016/S0736-5748(96)00053-6.

Bragina, L., Conti, F. and Duffy, K. R. (2018) 'Expression of Neurofilament Subunits at Neocortical Glutamatergic and GABAergic Synapses', 12(September), pp. 1–10. doi: 10.3389/fnana.2018.00074.

Bridges, S. N., Starr, D. A. and Fridolfsson, H. N. (2010) 'Interactions Between Nuclei and the Cytoskeleton Are Mediated by SUN-KASH Nuclear-Envelope Bridges', *Annual review of cell and developmental biology*, 26, pp. 421–444. doi: 10.1146/annurev-cellbio-100109-104037.Interactions.

Brown, A. (2013) 'Axonal Transport', in *Neuroscience in the 21st Century*, pp. 255–308. doi: 10.1007/978-1-4614-1997-6.

Brown, M. *et al.* (2004) 'α2-Chimaerin, Cyclin-Dependent Kinase 5/p35, and Its Target Collapsin Response Mediator Protein-2 Are Essential Components in Semaphorin 3A-Induced Growth-Cone Collapse', *The Journal of Neuroscience*, 24(41), pp. 8994–9004. doi: 10.1523/JNEUROSCI.3184-04.2004.

Brownlees, J. *et al.* (2002) 'Charcot – Marie – Tooth disease neurofilament mutations disrupt neurofilament assembly and axonal transport', 11(23), pp. 2837–2844.

Calderone, A. (2018) 'The Biological Role of Nestin (+) -Cells in Physiological and Pathological Cardiovascular Remodeling', *Frontiers in cell and developmental biology*,

6(February), pp. 1–14. doi: 10.3389/fcell.2018.00015.

Campbell, M. J. and Morrison, J. H. (1989) 'Monoclonal Antibody to Neurofilament Protein (SMI-32) Labels a Subpopulation of Pyramidal Neurons in the Human and Monkey Neocortex', 205, pp. 191–205.

Carcea, I. *et al.* (2010) 'Flotillin-Mediated Endocytic Events Dictate Cell Type-Specific Responses to Semaphorin 3A', *Journal of Neuroscience*, 30(45), pp. 15317–15329. doi: 10.1523/JNEUROSCI.1821-10.2010.

Cattaneo, E. and McKay, R. (1990) 'Proliferation and differentiation of neuronal stem cells regulated by nerve growth factor', *Nature*, 347(6295), pp. 762–5. doi: 10.1038/347762a0.

Chan, S., Peng, D. and Chiu, F. (1997) 'Heterogeneous expression of neurofilament proteins in forebrain and cerebellum during development : clinical implications for spinocerebellar ataxia', *Brain Research*.

Chang, L. and Goldman, R. D. (2004) 'Intermediate filaments mediate cytoskeletal crosstalk.', *Nature reviews. Molecular cell biology*, 5(8), pp. 601–13. doi: 10.1038/nrm1438.

Chen, G. *et al.* (2008) 'Semaphorin-3A guides radial migration of cortical neurons during development', *Nature Neuroscience*, 11(1), pp. 36–44. doi: 10.1038/nn2018.

Chen, H. L., Yuh, C. H. and Wu, K. K. (2010) 'Nestin is essential for zebrafish brain and eye development through control of progenitor cell apoptosis', *PLoS ONE*, 5(2). doi: 10.1371/journal.pone.0009318.

Cheng, F. *et al.* (2016) 'Vimentin coordinates fibroblast proliferation and keratinocyte differentiation in wound healing via TGF- β – Slug signaling', *PNAS*. doi: 10.1073/pnas.1519197113.

Cho, A. *et al.* (2016) 'An atypical Tropomyosin in Drosophila with intermediate filament-like properties', *Cell Reports*, 16(4), pp. 928–938. doi: 10.1186/s40945-017-0033-9.Using.

Chou, Y. *et al.* (2003) 'Nestin Promotes the Phosphorylation-dependent Disassembly of Vimentin Intermediate Filaments During Mitosis', 14(April), pp. 1468–1478. doi: 10.1091/mbc.E02.

Cochard, P. and Paulin, D. (1984) 'Initial expression of neurofilaments and vimentin in the central and peripheral nervous system of the mouse embryo *in vivo*', *J.Neurosci.*, 4(8), pp. 2080–2094. Available at: <http://www.ncbi.nlm.nih.gov/pubmed/0006432971>.

Colakoglu, G. and Brown, A. (2009) 'Intermediate filaments exchange subunits along their length and elongate by end-to-end annealing', *Journal of Cell Biology*, 185(5), pp. 769–777. doi: 10.1083/jcb.200809166.

Colucci-Guyon, E. *et al.* (1999) 'Cerebellar Defect and Impaired Motor Coordination in Mice Lacking Vimentin', *Glia*, 43(April 1998), pp. 33–43.

Crews, L. *et al.* (2011) 'Modulation of aberrant Cdk5 signaling rescues impaired neurogenesis in models of Alzheimer's disease.', *Cell death & disease*. Nature

Publishing Group, 2(2), p. e120. doi: 10.1038/cddis.2011.2.

Crino, P. B. and Eberwine, J. (1996) 'Molecular Characterization of the Dendritic Growth Cone: Regulated mRNA Transport and Local Protein Synthesis', *Neuron*, 17(6), pp. 1173–1187. doi: 10.1016/S0896-6273(00)80248-2.

Dahlstrand, J. *et al.* (1992) 'Characterization of the human nestin gene reveals a close evolutionary relationship to neurofilaments.', *Journal of cell science*, 103 (Pt 2, pp. 589–97. Available at: <http://www.ncbi.nlm.nih.gov/pubmed/1478958>.

Dahlstrand, J., Lardelli, M. and Lendahl, U. (1995a) 'Nestin mRNA expression correlates with the central nervous system progenitor cell state in many, but not all, regions of developing central nervous system', *Developmental Brain Research*, 84, pp. 109–129. doi: 10.1016/0165-3806(94)00162-S.

Dahlstrand, J., Lardelli, M. and Lendahl, U. (1995b) 'Nestin mRNA expression correlates with the central nervous system progenitor cell state in many, but not all, regions of developing central nervous system', *Developmental Brain Research*, 84(1), pp. 109–129. doi: 10.1016/0165-3806(94)00162-S.

Dang, P., Smythe, E. and Furley, A. J. W. (2013) 'TAG1 regulates the endocytic trafficking and signalling of the Semaphorin3A receptor complex', *Journal of Neuroscience*, 32(30), pp. 10370–10382. doi: 10.1523/JNEUROSCI.5874-11.2012.TAG1.

Dave, J. M. *et al.* (2013) 'Proteomic Profiling of Endothelial Invasion Revealed Receptor for Activated C Kinase 1 (RACK1) Complexed with Vimentin to Regulate Focal Adhesion Kinase (FAK) *', *The Journal of biological chemistry*, 288(42), pp. 30720–30733. doi: 10.1074/jbc.M113.512467.

Decimo, I. *et al.* (2011) 'Nestin- and doublecortin-positive cells reside in adult spinal cord meninges and participate in injury-induced parenchymal reaction.', *Stem cells (Dayton, Ohio)*, 29(12), pp. 2062–76. doi: 10.1002/stem.766.

Dehmelt, L., Halpain, S. (2007) 'Neurite outgrowth. A Flick of the wrist', *Current Biology*, 17(15), pp. 609–611. doi: 10.1016/j.cub.2007.05.038.

Dent, E. W. (2004) 'Netrin-1 and Semaphorin 3A Promote or Inhibit Cortical Axon Branching, Respectively, by Reorganization of the Cytoskeleton', *Journal of Neuroscience*, 24(12), pp. 3002–3012. doi: 10.1523/JNEUROSCI.4963-03.2004.

Dent, E. W. and Gertler, F. B. (2003) 'Cytoskeletal dynamics and transport in growth cone motility and guidance', *Neuron*, 40(2), pp. 209–227. doi: 10.1016/S0896-6273(03)00633-0.

Dent, E. W., Gupton, S. L. and Gertler, F. B. (2011) 'The growth cone cytoskeleton in axon outgrowth and guidance.', *Cold Spring Harbor perspectives in biology*, 3(3), pp. 1–39. doi: 10.1101/cshperspect.a001800.

Dey, A. *et al.* (2017) 'Electrophysiological and gene expression characterization of the ontogeny of nestin-expressing cells in the adult mouse midbrain', *Stem Cell Research*. The Authors, 23, pp. 143–153. doi: 10.1016/j.scr.2017.07.001.

Didonna, A. and Opal, P. (2019) 'The role of neurofilament aggregation in

neurodegeneration : lessons from rare inherited neurological disorders'. *Molecular Neurodegeneration*, 4, pp. 1–10.

Digilio, L. Yap, CC. Winckler, B. (2015) 'Ctip2-, Satb2-, Prox1-, and GAD65-Expressing Neurons in Rat Cultures: Preponderance of Single- and Double-Positive Cells, and Cell Type-Specific Expression of Neuron-Specific Gene Family Members, Nsg-1 (NEEP21) and Nsg-2 (P19)', *PloS one*, pp. 1–16. doi: 10.1371/journal.pone.0140010.

Dotti, C. G., Sullivan, C. a and Banker, G. a (1988) 'The establishment of polarity by hippocampal neurons in culture.', *The Journal of neuroscience : the official journal of the Society for Neuroscience*, 8(4), pp. 1454–1468. doi: 10.1016/0012-1606(89)90269-8.

E. Goldsmith, R. Akella, X. Min, T. Zhou, J. H. (2007) 'Substrate and Docking Interactions in Ser/Thr Protein Kinases Elizabeth', *Chemical Reviews*, 107(11), pp. 5065–5081. doi: 10.1021/cr068221w.Substrate.

Eckes, B. *et al.* (2000) 'Impaired wound healing in embryonic and adult mice lacking vimentin', *Journal of cell science*, 2462, pp. 2455–2462.

Ehlers, M. D. *et al.* (1998) 'Splice variant-specific interaction of the NMDA receptor subunit NR1 with neuronal intermediate filaments.', *The Journal of neuroscience*, 18(2), pp. 720–730.

Eriksson, J. E. *et al.* (2009) 'Introducing intermediate filaments: from discovery to disease', *The Journal of Clinical Investigation*, 119(7), pp. 1763–1771. doi: 10.1172/JCI38339.cells.

Farzanehfar, P. *et al.* (2017) 'Evidence of functional duplicity of Nestin expression in the adult mouse midbrain', *Stem Cell Research*. The Author(s), 19, pp. 82–93. doi: 10.1016/j.scr.2017.01.002.

Farzanehfar, P., Horne, M. K. and Aumann, T. D. (2017) 'An investigation of gene expression in single cells derived from Nestin-expressing cells in the adult mouse midbrain *in vivo*', *Neuroscience Letters*. Elsevier Ireland Ltd, 648, pp. 34–40. doi: 10.1016/j.neulet.2017.03.028.

Fliegner, K. H. *et al.* (1994) 'Expression of the Gene for the Neuronal Intermediate Filament Protein α -internexin Coincides With the Onset of Neuronal Differentiation in the Developing Rat Nervous System', 173, pp. 161–173.

Francis, F. *et al.* (1999) 'Doublecortin is a developmentally regulated, microtubule-associated protein expressed in migrating and differentiating neurons', *Neuron*, 23(2), pp. 247–256.

Friocourt, G. *et al.* (2003) 'Doublecortin functions at the extremities of growing neuronal processes', *Cerebral Cortex*, 13, pp. 620–626. doi: 10.1093/cercor/13.6.620.

Fu, X. *et al.* (2013) 'Doublecortin (Dcx) Family Proteins Regulate Filamentous Actin Structure in Developing Neurons', *The Journal of Neuroscience*, 33(2), pp. 709–721. doi: 10.1523/JNEUROSCI.4603-12.2013.

Galou, M. *et al.* (1997) 'The importance of intermediate filaments in the adaptation of tissues to mechanical stress: Evidence from gene knockout studies', *Biology of the Cell*, pp. 85–97.

Gan, Z. *et al.* (2017) 'Vimentin intermediate filaments template microtubule networks to enhance persistence in cell polarity and directed migration', *Cell Systems*, 3(3), pp. 252–263. doi: 10.1016/j.cels.2016.08.007.Vimentin.

Ge, W. *et al.* (2006) 'Coupling of cell migration with neurogenesis by proneural bHLH factors.', *Proceedings of the National Academy of Sciences of the United States of America*, 103(5), pp. 1319–24. doi: 10.1073/pnas.0510419103.

Geraldo, S. and Gordon-Weeks, P. R. (2009) 'Cytoskeletal dynamics in growth-cone steering.', *Journal of cell science*, 122(Pt 20), pp. 3595–604. doi: 10.1242/jcs.042309.

Germain, J. *et al.* (2013) 'Doublecortin knockout mice show normal hippocampal-dependent memory despite CA3 lamination defects.', *PloS one*, 8(9), p. e74992. doi: 10.1371/journal.pone.0074992.

Giese, K. P. (2014) 'Generation of the Cdk5 activator p25 is a memory mechanism that is affected in early Alzheimer's disease', 7(May), pp. 5–8. doi: 10.3389/fnmol.2014.00036.

Gillen, C. *et al.* (1995) 'Differentially Expressed Genes After Peripheral Nerve Injury', *Journal of neuroscience research*, 42, pp. 159–171.

Gleeson, J. G. *et al.* (1999) 'Doublecortin is a microtubule-associated protein and is expressed widely by migrating neurons', *Neuron*, 23(2), pp. 257–271.

Godsel, L. M., Hobbs, R. P. and Green, K. J. (2008) 'Intermediate filament assembly: dynamics to disease', *Cell*, 18(1), pp. 28–37. doi: 10.1016/j.tcb.2007.11.004.

Goldmann, W. H. (2018) 'Intermediate filaments and cellular mechanics', *Cell Biology International*, 42, pp. 132–138. doi: 10.1002/cbin.10879.

Goldstein, M. E., Sternberger, L. A. and Sternberger, N. H. (1983) 'Microheterogeneity ("neurotypy") of neurofilament proteins', *PNAS*, 80(May), pp. 3101–3105.

Grant, P. and Pant, H. (2000) 'Neurofilament protein synthesis and phosphorylation', *Journal of Neurocytology*, 872, pp. 843–872.

Gu, H. *et al.* (2002) 'Distribution of nestin immunoreactivity in the normal adult human forebrain', *Brain Research*, 943(2), pp. 174–180.

Gumy, L. F. *et al.* (2013) 'The Kinesin-2 Family Member KIF3C Regulates Microtubule Dynamics and Is Required for Axon Growth and Regeneration', *The Journal of Neuroscience*, 33(28), pp. 11329–11345. doi: 10.1523/JNEUROSCI.5221-12.2013.

Guo, K. H. *et al.* (2014) 'Postnatal development of nestin positive neurons in rat basal forebrain: Different onset and topography with choline acetyltransferase and parvalbumin expression', *International Journal of Developmental Neuroscience*. International Society for Developmental Neuroscience, 35, pp. 72–79. doi: 10.1016/j.ijdevneu.2014.03.004.

Helfand, B. T. *et al.* (2003) 'Rapid transport of neural intermediate filament protein', *Journal of cell science*. doi: 10.1242/jcs.00526.

Hemmati-Brivanlou, A., Mann, R. W. and Harland, R. M. (1992) 'A protein expressed in the growth cones of embryonic nerves defines a new class of intermediate filament

protein', *Neuron*, 9(3), pp. 417–428.

Hendrickson, M. L. *et al.* (2011) 'Expression of nestin by neural cells in the adult rat and human brain.', *PloS one*, 6(4), p. e18535. doi: 10.1371/journal.pone.0018535.

Henley, J. R. *et al.* (2004) 'Calcium mediates bidirectional growth cone turning induced by myelin-associated glycoprotein', *Neuron*, 44(6), pp. 909–916. doi: 10.1016/j.neuron.2004.11.030.

Herrmann, H. and Aebi, U. (2016) 'Intermediate Filaments : Structure and Assembly', *Cold Spring Harbor perspectives in biology*, 8(11), pp. 1–22.

Herrmann, H., Aebi, U. and Mu, M. E. (2004) 'Intermediate Filaments : Molecular Structure , Assembly Mechanism , and Integration Into Functionally Distinct Intracellular Scaffolds', *Annual Review of Biochemistry*, 73, pp. 749–789. doi: 10.1146/annurev.biochem.73.011303.073823.

Herrmann, H. and Strelkov, S. V. (2011) 'History and phylogeny of intermediate filaments: Now in insects', *BMC Biology*, 9, pp. 1–5. doi: 10.1186/1741-7007-9-16.

Hiscock, J. J., Mackenzie, L. and Willoughby, J. O. (1996) 'Fos induction in subtypes of cerebrocortical neurons following single picrotoxin-induced seizures', 738, pp. 301–312.

Hockfield, S. and McKay, R. D. (1985) 'Identification of major cell classes in the developing mammalian nervous system.', *The Journal of neuroscience : the official journal of the Society for Neuroscience*, 5(12), pp. 3310–3328.

Hoffman, P. N. *et al.* (1987) 'Neurofilament gene expression: A major determinant of axonal caliber', 84(May), pp. 3472–3476.

Hu, W. *et al.* (2016) 'Suppression of Nestin reveals a critical role for p38-EGFR pathway in neural progenitor cell proliferation', 7(52), pp. 87052–87063. doi: 10.18632/oncotarget.13498.

Huang, Y. *et al.* (2017) 'Nestin Serves as a Prosurvival Determinant that is Linked to the Cytoprotective Effect of Epidermal Growth Factor in Rat Vascular Smooth Muscle Cells', *Journal of biochemistry*, 146(October), pp. 307–315. doi: 10.1093/jb/mvp070.

Hughes, A. *et al.* (2014) 'Single-cell western blotting', *Nature Methods*, 11(7), pp. 455–464. doi: 10.1007/978-1-4939-2694-7_46.

Hyder, C. L. *et al.* (2008) 'Providing cellular signposts - Post-translational modifications of intermediate filaments', *FEBS Letters*, 582, pp. 2140–2148. doi: 10.1016/j.febslet.2008.04.064.

Hyder, C. L., Lazaro, G., Pylvänäinen, J. W., *et al.* (2014) 'Nestin regulates prostate cancer cell invasion by influencing the localisation and functions of FAK and integrins.', *Journal of cell science*, 127, pp. 2161–73. doi: 10.1242/jcs.125062.

Hyder, C. L., Lazaro, G., Pylvanainen, J. W., *et al.* (2014) 'Nestin regulates prostate cancer cell invasion by influencing the localisation and functions of FAK and integrins', *Journal of Cell Science*, 127, pp. 2161–2173. doi: 10.1242/jcs.125062.

Ip, J. P. K. *et al.* (2011) 'a 2-chimaerin controls neuronal migration and functioning of the cerebral cortex through CRMP-2', *Nature Neuroscience*. Nature Publishing Group,

15(1), pp. 39–47. doi: 10.1038/nn.2972.

Jacomy, H. *et al.* (1999) 'Disruption of Type IV Intermediate Filament Network in Mice Lacking the Neurofilament Medium and Heavy Subunits', *Journal of Neurochemistry*, pp. 972–984.

Jean, D. C., Baas, P. W. and Black, M. M. (2012) 'A novel role for doublecortin and doublecortin-like kinase in regulating growth cone microtubules.', *Human molecular genetics*, 21(26), pp. 5511–27. doi: 10.1093/hmg/dds395.

Jordan, B. A. *et al.* (2004) 'Identification and Verification of Novel Rodent Postsynaptic Density Proteins', *Molecular & Cellular Proteomics*, pp. 857–871. doi: 10.1074/mcp.M400045-MCP200.

Joshi, D., Inamdar, M. S. and Forscher, P. (2019) 'Rudhira / BCAS3 couples microtubules and intermediate filaments to promote cell migration for angiogenic remodeling', 30. doi: 10.1091/mbc.E18-08-0484.

K. Pennypacker, I. Fischer, P. L. (1991) 'Early in Vitro Genesis and Differentiation of Axons and Dendrites by Hippocampal Neurons Analyzed Quantitatively with Neurofilament-H and Microtubule-Associated Protein 2 Antibodies', *Experimental Neurology*, 111(Jan), pp. 25–35.

Kapitein, L. C. and Hoogenraad, C. C. (2015) 'Building the Neuronal Microtubule Cytoskeleton', *Neuron*. Elsevier Inc., 87(3), pp. 492–506. doi: 10.1016/j.neuron.2015.05.046.

Kaplan, A. *et al.* (2014) 'Switching Responses : Spatial and Temporal Regulators of Axon Guidance', *Molecular Neurobiology*, pp. 1077–1086. doi: 10.1007/s12035-013-8582-8.

Kaplan, P. *et al.* (1990) 'α-Internexin, a Novel Neuronal Intermediate Filament Protein , Precedes the Low Molecular Weight Neurofilament Protein (NF-L) in the Developing Rat Brain', *The Journal of Neuroscience*, 10(8), pp. 2735–2748.

Kappeler, C. *et al.* (2006) 'Branching and nucleokinesis defects in migrating interneurons derived from doublecortin knockout mice.', *Human molecular genetics*, 15(9), pp. 1387–400. doi: 10.1093/hmg/ddl062.

Karabinos, A. *et al.* (2001) 'Essential roles for four cytoplasmic intermediate filament proteins in *Caenorhabditis elegans* development.', *Proceedings of the National Academy of Sciences of the United States of America*, 98(14), pp. 7863–8. doi: 10.1073/pnas.121169998.

Kawauchi, T. (2014) 'Cdk5 regulates multiple cellular events in neural development, function and disease.', *Development, growth & differentiation*, 56(5), pp. 335–48. doi: 10.1111/dgd.12138.

Kent, C. B. *et al.* (2010) '14-3-3 Proteins Regulate Protein Kinase A Activity to Modulate Growth Cone Turning Responses', *The Journal of Neuroscience*, 30(42), pp. 14059–14067. doi: 10.1523/JNEUROSCI.3883-10.2010.

Khazaei, M. R. *et al.* (2014) 'Collapsin Response Mediator Protein 4 Regulates Growth Cone Dynamics through the Actin and Microtubule', 289(43), pp. 30133–30143. doi:

10.1074/jbc.M114.570440.

Kim, O.-J. *et al.* (2002) 'Neurofilament-M interacts with the D1 dopamine receptor to regulate cell surface expression and desensitization.', *The Journal of neuroscience : the official journal of the Society for Neuroscience*, 22(14), pp. 5920–30. doi: 20026596.

Kim, S. and Coulombe, P. A. (2007) 'Intermediate filament scaffolds fulfill mechanical, organizational, and signaling functions in the cytoplasm', *Genes and Development*, 21(13), pp. 1581–1597. doi: 10.1101/gad.1552107.

Kirkcaldie, M. T. K. *et al.* (2002) 'Neurofilament triplet proteins are restricted to a subset of neurons in the rat neocortex', 24.

Kiss, A. *et al.* (2018) 'Neuronal Growth Cone Size-Dependent and -Independent Parameters of Microtubule Polymerization', *Frontiers in Cellular Neuroscience*, 12(July), pp. 1–15. doi: 10.3389/fncel.2018.00195.

Kobayashi, H. *et al.* (2014) 'Phosphorylation of Cyclin-dependent Kinase 5 (Cdk5) at Tyr-15 Is Inhibited by Cdk5 Activators and Does Not Contribute to the Activation of Cdk5 *', *The Journal of biological chemistry*, 289(28), pp. 19627–19636. doi: 10.1074/jbc.M113.501148.

Koizumi, H. *et al.* (2006) 'Doublecortin maintains bipolar shape and nuclear translocation during migration in the adult forebrain.', *Nature neuroscience*, 9(6), pp. 779–86. doi: 10.1038/nn1704.

Kolodkin, A. L. and Tessier-Lavigne, M. (2011) 'Mechanisms and molecules of neuronal wiring: a primer.', *Cold Spring Harbor perspectives in biology*, 3(6). doi: 10.1101/cshperspect.a001727.

Kornreich, M. *et al.* (2015) 'Composite bottlebrush mechanics: α -internexin fine-tunes neurofilament network properties', *Royal Society of Chemistry*. Royal Society of Chemistry, 11, pp. 5839–5849. doi: 10.1039/c5sm00662g.

Köster, S. *et al.* (2015) 'Intermediate filament mechanics *in vitro* and in the cell: From coiled coils to filaments, fibers and networks', *Current Opinion in Cell Biology*, 32, pp. 82–91. doi: 10.1016/j.ceb.2015.01.001.

Kreis, S. *et al.* (2005) 'The intermediate filament protein vimentin binds specifically to a recombinant integrin $\alpha 2 / \beta 1$ cytoplasmic tail complex and co-localizes with native $\alpha 2 / \beta 1$ in endothelial cell focal adhesions', *Experimental Cell Research*, 305, pp. 110–121. doi: 10.1016/j.yexcr.2004.12.023.

Kreplak, L. *et al.* (2005) 'Exploring the Mechanical Behavior of Single Intermediate Filaments', *Journal of Molecular Biology*, pp. 569–577. doi: 10.1016/j.jmb.2005.09.092.

Kreplak, L., Aebi, U. and Herrmann, H. (2004) 'Molecular mechanisms underlying the assembly of intermediate filaments', *Experimental Cell Research*, 301, pp. 77–83. doi: 10.1016/j.yexcr.2004.08.021.

Kriz, J. *et al.* (2000) 'Electrophysiological properties of axons in mice lacking neurofilament subunit genes: disparity between conduction velocity and axon diameter in absence of NF-H', *Brain Research*, 885, pp. 32–44.

- Ku, N. *et al.* (2002) 'Keratin binding to 14-3-3 proteins modulates keratin filaments and hepatocyte mitotic progression', *PNAS*, 99(7), pp. 4373–4378.
- Ku, N., Liao, J. and Omary, M. B. (1998) 'Phosphorylation of human keratin 18 serine 33 regulates binding to 14-3-3 proteins', *The EMBO Journal*, 17(7), pp. 1892–1906.
- Kuo, L. T. *et al.* (2005) 'Effects of systemically administered NT-3 on sensory neuron loss and nestin expression following axotomy', *Journal of Comparative Neurology*, 482(4), pp. 320–332. doi: 10.1002/cne.20400.
- Landis, D. M. D. and Reese, T. S. (1983) 'Cytoplasmic Organization in Cerebellar Dendritic Spines', *The Journal of cell biology*, 97, pp. 1169–1178.
- Lariviere, R. C. and Julien, J. (2003) 'Functions of Intermediate Filaments in Neuronal Development and Disease', *Journal of Neurobiology*, 58(1), pp. 131–48. doi: 10.1002/neu.10270.
- Laser-Azogui, A. *et al.* (2015) 'Neurofilament assembly and function during neuronal development', *Current Opinion in Cell Biology*. Elsevier Ltd, 32(2), pp. 92–101. doi: 10.1016/j.ceb.2015.01.003.
- Leduc, C. and Manneville, S. E. (2017) 'Regulation of microtubule-associated motors drives intermediate filament network polarization', *The Journal of Cell Biology*.
- Lee, M. *et al.* (1993) 'Neurofilaments Are Obligate Heteropolymers In Vivo', *The Journal of cell biology*, 122(6), pp. 1337–1350.
- Lee, S. and Shea, T. B. (2014) 'The high molecular weight neurofilament subunit plays an essential role in axonal outgrowth and stabilization.', *Biology open*, 3(10), pp. 974–81. doi: 10.1242/bio.20149779.
- Lendahl, U., Zimmerman, L. B. and McKay, R. D. G. (1990) 'CNS stem cells express a new class of intermediate filament protein', *Cell*, 60(4), pp. 585–595. doi: 10.1016/0092-8674(90)90662-X.
- Leon, M. De *et al.* (1991) 'Identification of Transcriptionally Regulated Genes After Sciatic Nerve Injury', *Journal of neuroscience research*, 29, pp. 437–448.
- Leterrier, J. F. *et al.* (1996) 'Mechanical Effects of Neurofilament Cross-bridges', *The Journal of biological chemistry*, 271(26), pp. 15687–15694.
- Leung, C. L. *et al.* (2001) 'The BPAG1 locus: alternative splicing produces multiple isoforms with distinct cytoskeletal linker domains , including predominant isoforms in neurons and muscles', *JCB*, 154(4), pp. 691–697. doi: 10.1083/jcb.200012098.
- Levavasseur, F., Zhu, Q. and Julien, J. P. (1999) 'No requirement of α -internexin for nervous system development and for radial growth of axons', *Molecular Brain Research*, 69(1), pp. 104–112. doi: 10.1016/S0169-328X(99)00104-7.
- Liang, Z. *et al.* (2018) 'Nestin-mediated cytoskeletal remodeling in endothelial cells : novel mechanistic insight into VEGF-induced cell migration in angiogenesis', (22), pp. 349–358. doi: 10.1152/ajpcell.00121.2014.
- Liao, J. and Bishr, M. (1996) '14-3-3 Proteins Associate with Phosphorylated Simple Epithelial Keratins during Cell Cycle Progression and Act as a Solubility Cofactor', *The*

Journal of cell biology, 133(2), pp. 345–357.

Liem, R. K. H. (2019) 'Cytoskeletal Integrators : The Spectrin Superfamily', *Cold Spring Harbor perspectives in biology*.

Lin, W., Szaro, B. (1995) 'Neurofilaments Help maintain Normal Morphologies and Support Elongation of Neurites in *Xenopus laevis* Cultured Embryonic Spinal Cord Neurons', *The Journal of Neuroscience*, 15(December), pp. 8331–8344.

Lin, W. *et al.* (2005) 'Neurotransmitter Acetylcholine Negatively Regulates Neuromuscular Synapse Formation by a Cdk5-Dependent Mechanism', *Neuron*, 46(5), pp. 569–579. doi: 10.1016/j.neuron.2005.04.002.

Lin, W. and Szaro, B. G. (1996) 'Effects of Intermediate Filament Disruption on the Early Development of the Peripheral Nervous System of *Xenopus laevis*', *Developmental Biology*, 211(0251), pp. 197–211.

Lindqvist, J. *et al.* (2017) 'Nestin contributes to skeletal muscle homeostasis and regeneration', *Journal of cell science*, 130, pp. 2833–2842. doi: 10.1242/jcs.202226.

Lindqvist, J., Wistbacka, N. and Eriksson, J. E. (2016) *Studying Nestin and its Interrelationship with Cdk5*. 1st edn, *Methods in Enzymology*. 1st edn. Elsevier Inc. doi: 10.1016/bs.mie.2015.09.019.

Liu, J. *et al.* (2018) 'Nestin-expressing cell types in the temporal lobe and hippocampus: Morphology, differentiation, and proliferative capacity', *Glia*, 66(1), pp. 62–77. doi: 10.1002/glia.23211.

Lobsiger, C. S. *et al.* (2005) 'Altered axonal architecture by removal of the heavily phosphorylated neurofilament tail domains strongly slows superoxide dismutase 1 mutant-mediated ALS', *PNAS*, 102(29).

Lowery, J. *et al.* (2015) 'Intermediate Filaments Play a Pivotal Role in Regulating Cell Architecture and Function *', 290(28), pp. 17145–17153. doi: 10.1074/jbc.R115.640359.

Ma, Q. *et al.* (2012) 'PAK in Alzheimer disease , Huntington disease and X-linked mental retardation', *Cellular Logistics*, (June), pp. 117–125.

Mahammad, S. *et al.* (2013) 'Giant axonal neuropathy – associated gigaxonin mutations impair intermediate filament protein degradation', *The Journal of Clinical Investigation*, 123(5), pp. 1964–1975. doi: 10.1172/JCI66387DS1.

Manning, B. D. and Cantley, L. C. (2002) 'Hitting the Target : Emerging Technologies in the Search for Kinase Substrates', *Sci STKE*, 162(12), pp. 1–5.

Manuscript, A. (2007) 'Neurofilaments Switch between Distinct Mobile and Stationary States during Their Transport along Axons', *J Neurosci*, 27(3), pp. 507–516.

Menon, S. and Gupton, S. L. (2016) 'Building Blocks of Functioning Brain : Cytoskeletal Dynamics in Neuronal Development', in *International Review of Cell and Molecular Biology/International Review of Cell and Molecular Biology*. Elsevier Inc., pp. 183–245. doi: 10.1016/bs.ircmb.2015.10.002.

Messam, C. A. *et al.* (2002) 'Analysis of the temporal expression of nestin in human fetal brain derived neuronal and glial progenitor cells', *Developmental Brain Research*,

134(1–2), pp. 87–92. doi: 10.1016/S0165-3806(01)00325-X.

Messam, C. A., Hou, J. and Major, E. O. (1999) 'Coexpression of nestin in neural and glial cells in the developing human CNS defined by a human-specific anti-nestin antibody', *Experimental Neurology*, 161(2), pp. 585–596. doi: 10.1006/exnr.1999.7319.

Michalczyk, K. and Ziman, M. (2005) 'Nestin structure and predicted function in cellular cytoskeletal organisation', *Histology and Histopathology*, 20, pp. 665–671. doi: 665-671.

Miller, F. D. and Gauthier, A. S. (2007) 'Timing Is Everything: Making Neurons versus Glia in the Developing Cortex', *Neuron*, 54(3), pp. 357–369. doi: 10.1016/j.neuron.2007.04.019.

Miller, K. E. and Suter, D. M. (2018) 'An Integrated Cytoskeletal Model of Neurite Outgrowth', *Frontiers in Cellular Neuroscience*, 12(November), pp. 1–19. doi: 10.3389/fncel.2018.00447.

Mintz, C. D. *et al.* (2009) 'ERM proteins regulate growth cone responses to Sema3A', *J Comp Neurol*, 510(4), pp. 351–366. doi: 10.1002/cne.21799.ERM.

Mitew, S. *et al.* (2013) 'Neurites containing the neurofilament-triplet proteins are selectively vulnerable to cytoskeletal pathology in Alzheimer ' s disease and transgenic mouse models MATERIALS AND METHODS', 7(September), pp. 1–10. doi: 10.3389/fnana.2013.00030.

Mohseni, P. *et al.* (2011) 'Nestin is not essential for development of the CNS but required for dispersion of acetylcholine receptor clusters at the area of neuromuscular junctions.', *The Journal of neuroscience : the official journal of the Society for Neuroscience*, 31(32), pp. 11547–52. doi: 10.1523/JNEUROSCI.4396-10.2011.

Moore, C. A. *et al.* (2004) 'Mechanism of microtubule stabilization by doublecortin.', *Molecular cell*, 14(6), pp. 833–9. doi: 10.1016/j.molcel.2004.06.009.

Moore, C. a *et al.* (2006) 'Distinct roles of doublecortin modulating the microtubule cytoskeleton.', *The EMBO journal*, 25(19), pp. 4448–57. doi: 10.1038/sj.emboj.7601335.

Moslehi, M., Ng, D. C. H. and Bogoyevitch, M. A. (2017) 'Dynamic microtubule association of Doublecortin X (DCX) is regulated by its C-terminus', *Scientific Reports*. Springer US, 5245(7), pp. 1–11. doi: 10.1038/s41598-017-05340-x.

Murphy, J. M., Park, H. and Lim, S. S. (2016) 'FAK and Pyk2 in disease', *Frontiers in Biology*, 11(1), pp. 1–9. doi: 10.1007/s11515-016-1384-4.

Namba, T., Kibe, Y., Funahashi, Y., Nakamuta, S., Takano, T., Ueno, T., Shimada, A., Kozawa, S., Okamoto, M., Shimoda, Y., Oda, K., Wada, Y., Masuda, T., Sakakibara, A., Igarashi, M., Miyata, T., Faivre-Sarrailh, C., *et al.* (2014) 'Pioneering axons regulate neuronal polarization in the developing cerebral cortex', *Neuron*. Elsevier Inc., 81(4), pp. 814–829. doi: 10.1016/j.neuron.2013.12.015.

Namba, T., Kibe, Y., Funahashi, Y., Nakamuta, S., Takano, T., Ueno, T., Shimada, A., Kozawa, S., Okamoto, M., Shimoda, Y., Oda, K., Wada, Y., Masuda, T., Sakakibara, A., Igarashi, M., Miyata, T., Faivre-sarrailh, C., *et al.* (2014) 'Pioneering Axons Regulate Neuronal Polarization in the Developing Cerebral Cortex', *Neuron*. Elsevier Inc., 81(4), pp. 814–829. doi: 10.1016/j.neuron.2013.12.015.

- Narita, K. *et al.* (2014) 'Nestin regulates proliferation, migration, invasion and stemness of lung adenocarcinoma', *International Journal of Oncology*, 44(4), pp. 1118–1130. doi: 10.3892/ijo.2014.2278.
- Neradil, J. and Veselska, R. (2015) 'Nestin as a marker of cancer stem cells', *Cancer Science*, 106(7). doi: 10.1111/cas.12691.
- Ng, T. *et al.* (2013) 'Class 3 Semaphorin Mediates Dendrite Growth in Adult Newborn Neurons through Cdk5/FAK Pathway', *PLoS ONE*, 8(6), pp. 1–15. doi: 10.1371/journal.pone.0065572.
- Nishimura, Y. V *et al.* (2014) 'Cdk5 and its substrates, Dcx and p27 kip1, regulate cytoplasmic dilation formation and nuclear elongation in migrating neurons', *Development*, 141(18), pp. 3540–3550. doi: 10.1242/dev.111294.
- Nixon, R. A. and Shea, T. B. (1992) 'Dynamics of neuronal intermediate filaments: A developmental perspective', *Cell Motility and the Cytoskeleton*, 22(2), pp. 81–91. doi: 10.1002/cm.970220202.
- Nosten-Bertrand, M. *et al.* (2008) 'Epilepsy in Dcx knockout mice associated with discrete lamination defects and enhanced excitability in the hippocampus.', *PloS one*, 3(6), p. e2473. doi: 10.1371/journal.pone.0002473.
- Ohshima, T. *et al.* (1996) 'Targeted disruption of the cyclin-dependent kinase 5 gene results in abnormal corticogenesis, neuronal pathology and perinatal death', 93(October), pp. 11173–11178.
- Omary, M. B. *et al.* (2006) "Heads and tails" of intermediate filament phosphorylation: multiple sites and functional insights', *Trends in Biochemical Sciences*, 31(7). doi: 10.1016/j.tibs.2006.05.008.
- Omary, M. B. (2009) "IF-pathies": a broad spectrum of intermediate filament – associated diseases', *The Journal of Clinical Investigation*, 119(7). doi: 10.1172/JCI39894.1756.
- Omary, M. B., Coulombe, P. A. and Mclean, W. H. I. (2004) 'Intermediate Filament Proteins and Their Associated Diseases', pp. 2087–2100.
- Osborn, M., Franke, W. and Weber, K. (1980) 'Direct demonstration of the presence of two immunologically distinct intermediate-sized filament systems in the same cell by double immunofluorescence microscopy', *Experimental Cell Research*, 125, pp. 37–46.
- Ouda, L., Druga, R. and Syka, J. (2012) 'Distribution of SMI-32-immunoreactive neurons in the central auditory system of the rat', pp. 19–36. doi: 10.1007/s00429-011-0329-6.
- Pacey, L. *et al.* (2006) 'Neural Stem Cell Culture: Neurosphere generation, microscopical analysis and cryopreservation', *Nature Protocol Exchange*. Nature Publishing Group. Available at: <http://dx.doi.org/10.1038/nprot.2006.215>.
- Pallari, H.-M. and Eriksson, J. E. (2006) 'Intermediate filaments as signaling platforms.', *Science's STKE: signal transduction knowledge environment*, 2006(366), p. pe53. doi: 10.1126/stke.3662006pe53.

- Pallari, H. *et al.* (2011) 'Nestin as a regulator of Cdk5 in differentiating myoblasts', *Molecular biology of the cell*, 22, pp. 1539–1549. doi: 10.1091/mbc.E10-07-0568.
- Paramio, J. M. and Jorcano, J. L. (2002) 'Beyond structure: Do intermediate filaments modulate cell signalling?', *BioEssays*, 24(9), pp. 836–844. doi: 10.1002/bies.10140.
- Park, D. *et al.* (2010) 'Nestin is required for the proper self-renewal of neural stem cells', *Stem Cells*, 28(12), pp. 2162–2171. doi: 10.1002/stem.541.
- Perlini, L. E. *et al.* (2015) 'Synapsin III acts downstream of Semaphorin 3A/Cdk5 signaling to regulate radial migration and orientation of pyramidal neurons *in vivo*', *Cell Reports*, 11(2), pp. 234–248. doi: 10.1016/j.celrep.2015.03.022.
- Perlson, E. *et al.* (2004) 'Differential Proteomics Reveals Multiple Components in Retrogradely Transported Axoplasm After Nerve Injury', *Molecular & Cellular Proteomics*, pp. 510–520. doi: 10.1074/mcp.M400004-MCP200.
- Perlson, E. *et al.* (2005) 'Vimentin-Dependent Spatial Translocation of an Activated MAP Kinase in Injured Nerve', 45, pp. 715–726. doi: 10.1016/j.neuron.2005.01.023.
- Perlson, E. *et al.* (2006) 'Vimentin Binding to Phosphorylated Erk Sterically Hinders Enzymatic Dephosphorylation of the Kinase', pp. 938–944. doi: 10.1016/j.jmb.2006.09.056.
- Perrot, R. *et al.* (2008) 'Review of the Multiple Aspects of Neurofilament Functions , and their Possible Contribution to Neurodegeneration', *Mol Neurobiol*, 38, pp. 27–65. doi: 10.1007/s12035-008-8033-0.
- Perrot, R. and Eyer, J. (2009) 'Neuronal intermediate filaments and neurodegenerative disorders', *Brain Research Bulletin*, 80(4–5), pp. 282–295. doi: 10.1016/j.brainresbull.2009.06.004.
- Perry, E. K. *et al.* (2012) 'Neurogenic abnormalities in Alzheimer's disease differ between stages of neurogenesis and are partly related to cholinergic pathology', *Neurobiology of Disease*, 47(2), pp. 155–162. doi: 10.1016/j.nbd.2012.03.033.
- Petrovic, M. and Schmucker, D. (2015) 'Axonal wiring in neural development: Target-independent mechanisms help to establish precision and complexity', *Bioessays*, 37(Sep), pp. 996–1004. doi: 10.1002/bies.201400222.
- Pilz, D. T. *et al.* (1998) 'LIS1 and XLIS (DCX) mutations cause most classical lissencephaly , but different patterns of malformation', 7(13), pp. 19–22.
- Potokar, M. *et al.* (2010) 'Intermediate Filaments Attenuate Stimulation-Dependent Mobility of Endosomes / Lysosomes in Astrocytes', *Glia*, 1219(April), pp. 1208–1219. doi: 10.1002/glia.21000.
- Poulain, F. E. and Sobel, A. (2007) 'The “ SCG10-Like Protein ” SCLIP is a novel regulator of axonal branching in hippocampal neurons , unlike SCG10', 34, pp. 137–146. doi: 10.1016/j.mcn.2006.10.012.
- Pramparo, T. *et al.* (2010) 'Novel embryonic neuronal migration and proliferation defects in Dcx mutant mice are exacerbated by Lis1 reduction.', *The Journal of neuroscience : the official journal of the Society for Neuroscience*, 30(8), pp. 3002–12. doi:

10.1523/JNEUROSCI.4851-09.2010.

Rammensee, S., Janmey, P. A. and Bausch, S. . (2007) 'Mechanical and structural properties of *in vitro* neurofilament hydrogels', *European Biophysics Journal*, pp. 661–668. doi: 10.1007/s00249-007-0141-7.

Rani, S. B. *et al.* (2006) 'Expression of nestin - a stem cell associated intermediate filament in human CNS tumours', *Indian Journal of Medical Research*, (September), pp. 269–280.

Rao, M. V *et al.* (2002) 'Gene replacement in mice reveals that the heavily phosphorylated tail of neurofilament heavy subunit does not affect axonal caliber or the transit of cargoes in slow axonal transport', *Journal of Cell Biology*, pp. 681–693. doi: 10.1083/jcb.200202037.

Rao, M. V *et al.* (2011) 'The Myosin Va Head Domain Binds to the Neurofilament- L Rod and Modulates Endoplasmic Reticulum (ER) Content and Distribution within Axons', *PloS one*, 6(2). doi: 10.1371/journal.pone.0017087.

Ratnam, J. and Teichberg, V. I. (2005) 'Neurofilament-light increases the cell surface expression of the N -methyl- D -aspartate receptor and prevents its ubiquitination', pp. 878–885. doi: 10.1111/j.1471-4159.2004.02936.x.

Reimer, R. *et al.* (2009) 'Nestin modulates glucocorticoid receptor function by cytoplasmic anchoring.', *PloS one*, 4(6), p. e6084. doi: 10.1371/journal.pone.0006084.

Ren, Y. and Suter, D. M. (2016) 'Increase in Growth Cone Size Correlates with Decrease in Neurite Growth Rate', 2016, pp. 20–22.

Robert, A. *et al.* (2015) 'Vimentin filament precursors exchange subunits in an ATP-dependent manner', 2015. doi: 10.1073/pnas.1505303112.

Robert, A., Hookway, C. and Gelfand, Vladimir I. (2016) 'Intermediate filament dynamics: What we can see now and why it matters', *BioEssays*, 38(3), pp. 232–243. doi: 10.1002/bies.201500142.

Robert, A., Hookway, C. and Gelfand, Vladimir I (2016) 'Intermediate filament dynamics: What we can see now and why it matters', *BioEssays*, pp. 232–243. doi: 10.1002/bies.201500142.

Romito-DiGiacomo, R. R. *et al.* (2007) 'Effects of Alzheimer's disease on different cortical layers: the role of intrinsic differences in Abeta susceptibility.', *The Journal of neuroscience : the official journal of the Society for Neuroscience*, 27(32), pp. 8496–504. doi: 10.1523/JNEUROSCI.1008-07.2007.

Roy, S. *et al.* (2000) 'Neurofilaments are transported rapidly but intermittently in axons: implications for slow axonal transport.', *Journal of Neuroscience*, 20(18), pp. 6849–61. doi: 20/18/6849 [pii].

Ruediger, T. *et al.* (2013) 'Integration of opposing Semaphorin guidance cues in cortical axons', *Cerebral Cortex*, 23(3), pp. 604–614. doi: 10.1093/cercor/bhs044.

Sahlgren, C. M. *et al.* (2001) 'Mitotic reorganization of the intermediate filament protein nestin involves phosphorylation by cdc2 kinase.', *The Journal of biological chemistry*,

276(19), pp. 16456–63. doi: 10.1074/jbc.M009669200.

Sahlgren, C. M. *et al.* (2003) 'Cdk5 Regulates the Organization of Nestin and Its Association with p35', *Molecular and cellular biology*, 23(14), pp. 5090–5106. doi: 10.1128/MCB.23.14.5090.

Sahlgren, C. M. *et al.* (2006) 'A nestin scaffold links Cdk5/p35 signaling to oxidant-induced cell death.', *The EMBO journal*, 25(20), pp. 4808–19. doi: 10.1038/sj.emboj.7601366.

Sakakibara, A. and Hatanaka, Y. (2015) 'Neuronal polarization in the developing cerebral cortex', *Frontiers in Neuroscience*, 9(April), pp. 1–10. doi: 10.3389/fnins.2015.00116.

Sanghvi-shah, R. and Weber, G. F. (2017) 'Intermediate Filaments at the Junction of Mechanotransduction, Migration, and Development', *Frontiers in cell and developmental biology*, 5(September), pp. 1–19. doi: 10.3389/fcell.2017.00081.

Sapir, T. *et al.* (2000) 'Doublecortin mutations cluster in evolutionarily conserved functional domains.', *Human molecular genetics*, 9(5), pp. 703–712. doi: 10.1093/hmg/9.5.703.

Sasaki, S. *et al.* (2005) 'Complete Loss of Ndel1 Results in Neuronal Migration Defects and Early Embryonic Lethality', *Molecular and cellular biology*, 25(17), pp. 7812–7827. doi: 10.1128/MCB.25.17.7812.

Sasaki, Y. *et al.* (2002) 'Fyn and Cdk5 mediate Semaphorin-3A signaling, which is involved in regulation of dendrite orientation in cerebral cortex', *Neuron*, 35(5), pp. 907–920. doi: 10.1016/S0896-6273(02)00857-7.

Schaar, B. T., Kinoshita, K. and McConnell, S. K. (2004) 'Doublecortin Microtubule Affinity Is Regulated by a Balance of Kinase and Phosphatase Activity at the Leading Edge of Migrating Neurons', *Neuron*, 41(2), pp. 203–213.

Schlaepfer, W. W. (1974) 'Calcium-induced degeneration of axoplasm in isolated segments of rat peripheral nerve', *Brain Research*, 69, pp. 203–215.

Sharma, P. *et al.* (2019) 'Intermediate Filaments as Effectors of Cancer Development and Metastasis: A Focus on Keratins, Vimentin, and Nestin', *Cells*, 8, pp. 1–21.

Shaw, G., Banker, G., Weber, K. (1985) 'An immunofluorescence study of neurofilament protein expression by developing hippocampal neurons in tissue culture', *European Journal of Cell Biology*, 39(1), pp. 205–216.

Shea, T. B. and Beermann, M. L. (1999) 'Neuronal intermediate filament protein alpha-internexin facilitates axonal neurite elongation in neuroblastoma cells', *Cell motility and the cytoskeleton*, 43(4), pp. 322–333. doi: 10.1002/(SICI)1097-0169(1999)43:4<322::AID-CM5>3.0.CO;2-B [pii]r10.1002/(SICI)1097-0169(1999)43:4<322::AID-CM5>3.0.CO;2-B.

Shea, T. B., Beermann, M. L. and Fischer, I. (1993) 'Transient Requirement for Vimentin in Neuritogenesis: Intracellular Delivery of Anti-Vimentin Antibodies and Antisense Oligonucleotides Inhibit Neurite Initiation But Not Elongation of Existing Neurites in Neuroblastoma', *Journal of neuroscience research*, 76, pp. 66–76.

- Shen, Q. *et al.* (2002) 'Asymmetric Numb distribution is critical for asymmetric cell division of mouse cerebral cortical stem cells and neuroblasts.', *Development (Cambridge, England)*, 129, pp. 4843–4853.
- Shetty, R. *et al.* (2018) 'Rudhira / BCAS3 is essential for mouse development and cardiovascular patterning', pp. 1–12. doi: 10.1038/s41598-018-24014-w.
- Shi, Yang *et al.* (2008) 'Ndel1 Controls the Dynein-mediated Transport of Vimentin during Neurite Outgrowth', *The Journal of biological chemistry*, 283(18), pp. 12232–12240. doi: 10.1074/jbc.M710200200.
- Shim, K. S. and Lubec, G. (2002) 'Drebrin, a dendritic spine protein, is manifold decreased in brains of patients with Alzheimer ' s disease and Down syndrome', *Neuroscience I*, 324, pp. 209–212.
- Shin, E. *et al.* (2013) 'Doublecortin-like kinase enhances dendritic remodelling and negatively regulates synapse maturation.', *Nature communications*. Nature Publishing Group, 4(4), p. 1440. doi: 10.1038/ncomms2443.
- Shinmyo, Y. *et al.* (2015) 'Draxin from neocortical neurons controls the guidance of thalamocortical projections into the neocortex', *Nature Communications*. Nature Publishing Group, 6, pp. 1–13. doi: 10.1038/ncomms10232.
- Shmueli, A. *et al.* (2006) 'Site-specific dephosphorylation of doublecortin (DCX) by protein phosphatase 1 (PP1)', *Molecular and Cellular Neuroscience*, 32(1–2), pp. 15–26. doi: 10.1016/j.mcn.2006.01.014.
- Shupp, A., Casimiro, M. C. and Pestell, R. G. (2017) 'Biological functions of Cdk5 and potential Cdk5 targeted clinical treatments', *Oncotarget*, 8(10), pp. 17373–17382.
- Sibbe, M. *et al.* (2007) 'Development of the corticospinal tract in Semaphorin3A- and cd24-deficient mice', *Neuroscience*, 150, pp. 898–904. doi: 10.1016/j.neuroscience.2007.10.007.
- Singh, K. K. *et al.* (2010) 'Dixdc1 is a critical regulator of disc1 and embryonic cortical development', *Neuron*. Elsevier Ltd, 67(1), pp. 33–48. doi: 10.1016/j.neuron.2010.06.002.
- Smith, A., Gervasi, C. and Szaro, B. G. (2006) 'Neurofilament content is correlated with branch length in developing collateral branches of *Xenopus* spinal cord neurons', *Neuroscience Letters*, 403(3), pp. 283–287. doi: 10.1016/j.neulet.2006.04.055.
- Soellner, P., Quinlan, R. A. and Franke, W. W. (1985) 'Identification of a distinct soluble subunit of an intermediate filament protein : Tetrameric vimentin from living cells', *PNAS*, 82(December), pp. 7929–7933.
- Sonavane, P. R. *et al.* (2017) 'Mechanical and signaling roles for keratin intermediate filaments in the assembly and morphogenesis of *Xenopus* mesendoderm tissue at gastrulation', *Development*, 144, pp. 4363–4376. doi: 10.1242/dev.155200.
- Steinert, P. M. *et al.* (1999) 'A High Molecular Weight Intermediate Filament-associated Protein in BHK-21 Cells Is Nestin, a Type VI Intermediate Filament Protein', *Journal of Biological Chemistry*, 274(14), pp. 9881–9890. doi: 10.1074/jbc.274.14.9881.

- Steinert, P. M., Marekov, L. N. and Parry, D. A. D. (1999) 'Molecular Parameters of Type IV alpha-Internexin and Type IV-Type III alpha-Internexin-Vimentin Copolymer Intermediate Filaments', *The Journal of Biological Chemistry*, 274(3), pp. 1657–1666.
- Sternberger, N. H., Sternberger, L. A. and Ulrich, J. (1985) 'Aberrant neurofilament phosphorylation in Alzheimer disease', *PNAS*, 82(June), pp. 4274–4276.
- Su, P.-H. *et al.* (2013) 'Identification and cytoprotective function of a novel nestin isoform, Nes-S, in dorsal root ganglia neurons.', *The Journal of biological chemistry*, 288(12), pp. 8391–404. doi: 10.1074/jbc.M112.408179.
- Sumio, T. *et al.* (1996) 'Visualization of Slow Axonal Transport In Vivo', *Science*, 273(5276), pp. 784–788.
- Szaro, B. E. N. G. *et al.* (1991) 'Inhibition of Axonal Development After Injection of Neurofilament Antibodies Into a *Xenopus Zaevis* Embryo', *Journal of Comparative Neurology*, 585, pp. 576–585.
- Tamariz, E. and Varela-echavarría, A. (2015) 'The discovery of the growth cone and its influence on the study of axon guidance', *Frontiers in Neuroanatomy*, 9(May), pp. 1–9. doi: 10.3389/fnana.2015.00051.
- Tanaka, T., Serneo, Finley F., *et al.* (2004) 'Cdk5 Phosphorylation of Doublecortin Ser297 Regulates Its Effect on Neuronal Migration', *Neuron*, 41(2), pp. 215–227.
- Tanaka, T., Serneo, Finley F., *et al.* (2004) 'Lis1 and doublecortin function with dynein to mediate coupling of the nucleus to the centrosome in neuronal migration.', *The Journal of cell biology*, 165(5), pp. 709–21. doi: 10.1083/jcb.200309025.
- Telley, L. *et al.* (2016) 'Sequential transcriptional waves direct the differentiation of newborn neurons in the mouse neocortex', *Science*, 351, pp. 1443–6. doi: 10.1126/science.aad8361.
- Terry-Lorenzo, R. T. *et al.* (2000) 'Neurofilament-L is a protein phosphatase-1-binding protein associated with neuronal plasma membrane and post-synaptic density', *Journal of Biological Chemistry*, 275(4), pp. 2439–2446. doi: 10.1074/jbc.275.4.2439.
- Thonel, A. *et al.* (2010) 'Protein Kinase CZ Regulates Cdk5/p25 Signaling during Myogenesis', *Molecular biology of the cell*, 21, pp. 1426–1434. doi: 10.1091/mbc.E09.
- Toivola, D. M. *et al.* (2005) 'Cellular integrity plus: Organelle-related and protein-targeting functions of intermediate filaments', *Trends in Cell Biology*, 15(11), pp. 608–617. doi: 10.1016/j.tcb.2005.09.004.
- Tojima, T., Itofusa, R. and Kamiguchi, H. (2014) 'Steering neuronal growth cones by shifting the imbalance between exocytosis and endocytosis.', *The Journal of neuroscience : the official journal of the Society for Neuroscience*, 34(21), pp. 7165–78. doi: 10.1523/JNEUROSCI.5261-13.2014.
- Toth, C. *et al.* (2008) 'Ndel1 promotes axon regeneration via intermediate filaments', *PLoS ONE*, 3(4). doi: 10.1371/journal.pone.0002014.
- Tsukada, M. *et al.* (2005) 'Doublecortin association with actin filaments is regulated by neurabin II', *The Journal of biological chemistry*, 280(3), pp. 11361–8. doi:

10.1074/jbc.M405525200.

Tsukada, M., Prokscha, A. and Eichele, G. (2006) 'Neurabin II mediates doublecortin-phosphorylation on actin filaments', *Biochemical and Biophysical Research Communications*, 343(3), pp. 839–847. doi: 10.1016/j.bbrc.2006.03.045.

Tzivion, G., Luo, Z. and Avruch, J. (2000) 'Calyculin A-induced Vimentin Phosphorylation Sequesters 14-3-3 and Displaces Other 14-3-3 Partners in Vivo', 275(38), pp. 29772–29778. doi: 10.1074/jbc.M001207200.

Uchida, A. *et al.* (2018) 'Live-cell imaging of neurofilament transport in cultured neurons', (614), pp. 21–90. doi: 10.1016/bs.mcb.2015.07.001.Live-cell.

Uchida, A., Alami, N. H. and Brown, A. (2009) 'Tight Functional Coupling of Kinesin-1A and Dynein Motors in the Bidirectional Transport of Neurofilaments', *Molecular biology of the cell*, 20, pp. 4997–5006. doi: 10.1091/mbc.E09.

Uchida, A. and Brown, A. (2004) 'Arrival, Reversal, and Departure of Neurofilaments at the Tips of Growing Axons', *Molecular Biology of the Cell*, 15(September), pp. 4215–4225. doi: 10.1091/mbc.E04.

Uchida, Y. *et al.* (2005) 'Semaphorin3A signalling is mediated via sequential Cdk5 and GSK3 β phosphorylation of CRMP2 : implication of common phosphorylating mechanism underlying axon guidance and Alzheimer ' s disease', pp. 165–179. doi: 10.1111/j.1365-2443.2005.00827.x.

Ulloa, L. *et al.* (1994) 'Microtubule-associated protein MAP1B showing a fetal phosphorylation pattern is present in sites of neurofibrillary degeneration in brains of Alzheimer's disease patients', *Molecular Brain Research*, 26, pp. 113–122.

Vickers, J. C. and Costat, M. (1992) 'The Neurofilament Triplet Is Present In Distinct Subpopulations of Neurons in the Central Nervous System of the Guinea-Pig', *Neuroscience*, 49(1), pp. 73–100.

Vita, G. *et al.* (1998) 'DP116, talin, vinculin and vimentin immunoreactivities following nerve transection', *Clinical Science and Neuropathy*, 9(4), pp. 697–702.

Vitriol, E. a. and Zheng, J. Q. (2012) 'Growth Cone Travel in Space and Time: The Cellular Ensemble of Cytoskeleton, Adhesion, and Membrane', *Neuron*. Elsevier Inc., 73(6), pp. 1068–1080. doi: 10.1016/j.neuron.2012.03.005.

Wagner, O. I. *et al.* (2003) 'Mechanisms of Mitochondria – Neurofilament Interactions', *The Journal of Neuroscience*, 23(27), pp. 9046–9058.

Wakamatsu, Y. *et al.* (2007) 'Transitin, a nestin-like intermediate filament protein, mediates cortical localization and the lateral transport of Numb in mitotic avian neuroepithelial cells', *Development*, 134(13), pp. 2425–2433. doi: 10.1242/dev.02862.

Walker, K. L. *et al.* (2001) 'Loss of neurofilaments alters axonal growth dynamics.', *The Journal of neuroscience : the official journal of the Society for Neuroscience*, 21(24), pp. 9655–66. doi: 21/24/9655 [pii].

Walker, T. L. *et al.* (2007) 'The Doublecortin-Expressing Population in the Developing and Adult Brain Contains Multipotential Precursors in Addition to Neuronal-Lineage

Cells', *The Journal of Neuroscience*, 27(14), pp. 3734–3742. doi: 10.1523/JNEUROSCI.5060-06.2007.

Walters, G. B. *et al.* (2018) 'MAP1B mutations cause intellectual disability and extensive white matter de fi cit', *Nature communications*, (2018). doi: 10.1038/s41467-018-05595-6.

Wang, J. *et al.* (2017) 'A Nestin – Cyclin-Dependent Kinase 5 – Dynamin- Related Protein 1 Axis Regulates Neural Stem / Progenitor Cell Stemness via a Metabolic Shift', *Stem Cells*, 36, pp. 589–601.

Wang, J. *et al.* (2019) 'Nestin regulates cellular redox homeostasis in lung cancer through the Keap1â€Nrf2 feedback loop', *Nature Communications*. Springer US, pp. 1–17. doi: 10.1038/s41467-019-12925-9.

Wang, L. *et al.* (2000) 'Rapid movement of axonal neurofilaments interrupted by prolonged pauses', *Nature Cell Biology*, 2(March), pp. 137–141.

Wang, L., Monsma, P. C. and Brown, A. (2013) 'Severing and end-to-end annealing of neurofilaments in neurons'. doi: 10.1073/pnas.1221835110.

Wang, X., Sterne, G. R. and Ye, B. (2014) 'Regulatory mechanisms underlying the differential growth of dendrites and axons', *Neuroscience Bulletin*, 30(4), pp. 557–568. doi: 10.1007/s12264-014-1447-3.

Weber, G., Bjerke, M. and DeSimone, D. (2013) 'A mechanoresponsive cadherin-keratin complex directs polarized protrusive behavior and collective cell migration', *Developmental Cell*, 22(1), pp. 104–115. doi: 10.1016/j.devcel.2011.10.013.A.

Wei, L. *et al.* (2007) 'Nestin small interfering RNA (siRNA) reduces cell growth in cultured astrocytoma cells', 6, pp. 0–9. doi: 10.1016/j.brainres.2007.11.026.

Wilhelmsson, U. *et al.* (2019) 'Nestin Regulates Neurogenesis in Mice Through Notch Signaling From Astrocytes to Neural Stem Cells', *Cerebral Cortex*, pp. 1–17. doi: 10.1093/cercor/bhy284.

Williamson, R. *et al.* (2014) 'CRMP2 Hyperphosphorylation is Characteristic of Alzheimer ' s Disease and not a Feature Common to Other Neurodegenerative Diseases', *Journal of Alzheimer's Disease*, 27, pp. 615–625. doi: 10.3233/JAD-2011-110617.

Wynshaw-Boris, A. *et al.* (2010) 'Lissencephaly: Mechanistic insights from animal models andpotential therapeutic strategies', *Seminars in Cell and Developmental Biology*, 21(8), pp. 823–830. doi: 10.1016/j.semcdb.2010.07.008.Lissencephaly.

Xie, Z., Samuels, B. A. and Tsai, L. H. (2006) 'Cyclin-dependent kinase 5 permits efficient cytoskeletal remodeling - A hypothesis on neuronal migration', *Cerebral Cortex*, 16, pp. 64–8. doi: 10.1093/cercor/bhj170.

Xue, X. and Yuan, X. (2010) 'Nestin is essential for mitogen-stimulated proliferation of neural progenitor cells', *Molecular and Cellular Neuroscience*. Elsevier Inc., 45(1), pp. 26–36. doi: 10.1016/j.mcn.2010.05.006.

Yabe, J. T. *et al.* (2001) 'The Predominant Form in Which Neurofilament Subunits

Undergo Axonal Transport Varies During Axonal Initiation , Elongation , and Maturation', 83(September 2000), pp. 61–83.

Yabe, J. T. *et al.* (2003) 'Regulation of the Transition From Vimentin to Neurofilaments During Neuronal Differentiation', *Cell Motility and the Cytoskeleton*, 56(March), pp. 193–205. doi: 10.1002/cm.10137.

Yabe, J. T., Pimenta, A. and Shea, T. B. (1999) 'Kinesin-mediated transport of neurofilament protein oligomers in growing axons', *Journal of cell science*, 3814, pp. 3799–3814.

Yam, P. T. *et al.* (2012) '14-3-3 Proteins Regulate a Cell-Intrinsic Switch from Sonic Hedgehog-Mediated Commissural Axon Attraction to Repulsion after Midline Crossing', *Neuron*, pp. 735–749. doi: 10.1016/j.neuron.2012.09.017.

Yamada, K. M., Spooner, B. S. and Wessells, N. K. (1970) 'Axon Growth: Roles of Microfilaments and Microtubules', *Proceedings of the National Academy of Sciences*, 66(4), pp. 1206–1212. doi: 10.1073/pnas.66.4.1206.

Yamamoto, N., Tamada, A. and Murakami, F. (2003) 'Wiring of the brain by a range of guidance cues', *Progress in Neurobiology*, 68(Dec), pp. 393–407.

Yan, S. *et al.* (2016) 'Nestin regulates neural stem cell migration via controlling the cell contractility', *International Journal of Biochemistry and Cell Biology*, 78, pp. 349–360. doi: 10.1016/j.biocel.2016.07.034.

Yan, Y. *et al.* (2001) 'Mouse nestin protein localizes in growth cones of P19 neurons and cerebellar granule cells', *Neuroscience Letters*, 302, pp. 89–92. doi: 10.1016/S0304-3940(01)01664-0.

Yan, Y. (2005) 'Neurofilament Polymer Transport in Axons', *Journal of Neuroscience*, 25(30), pp. 7014–7021. doi: 10.1523/JNEUROSCI.2001-05.2005.

Yang, J. *et al.* (2011) 'Nestin negatively regulates postsynaptic differentiation of the neuromuscular synapse.', *Nature neuroscience*, 14(3), pp. 324–30. doi: 10.1038/nn.2747.

Yap, C. C. *et al.* (2012) 'Doublecortin (DCX) mediates endocytosis of neurofascin independently of microtubule binding.', *The Journal of neuroscience : the official journal of the Society for Neuroscience*, 32(22), pp. 7439–53. doi: 10.1523/JNEUROSCI.5318-11.2012.

Yap, C. C. *et al.* (2016) 'Different Doublecortin (DCX) Patient Alleles Show Distinct Phenotypes in Cultured Neurons', *Journal of Biological Chemistry*, 291(52), pp. 26613–26626. doi: 10.1074/jbc.M116.760777.

Yap, C. C. *et al.* (2018) 'A dominant dendrite phenotype caused by the disease-associated G253D mutation in doublecortin (DCX) is not due to its endocytosis defect', *Journal of Biological Chemistry*, 293(12), pp. 18890–18902. doi: 10.1074/jbc.RA118.004462.

Yuan, A. *et al.* (2003) 'Neurofilament Transport In Vivo Minimally Requires Hetero-Oligomer Formation', 23(28), pp. 9452–9458.

- Yuan, A. *et al.* (2006) 'α-Internexin Is Structurally and Functionally Associated with the Neurofilament Triplet Proteins in the Mature CNS', *Journal of Neuroscience*, 26(39), pp. 10006–10019. doi: 10.1523/JNEUROSCI.2580-06.2006.
- Yuan, A. *et al.* (2009) 'Neurofilaments Form a Highly Stable Stationary Cytoskeleton after Reaching a Critical Level in Axons', 29(36), pp. 11316–11329. doi: 10.1523/JNEUROSCI.1942-09.2009.
- Yuan, A. *et al.* (2012) 'Peripherin Is a Subunit of Peripheral Nerve Neurofilaments : Implications for Differential Vulnerability of CNS and Peripheral Nervous System Axons', *Neurobiology of Disease*, 32(25), pp. 8501–8508. doi: 10.1523/JNEUROSCI.1081-12.2012.
- Yuan, A. *et al.* (2015) 'Neurofilament Subunits are Integral Components of Synapses and Modulate Neurotransmission and Behavior In Vivo Aidong', *Mol Psychiatry*, 20(8), pp. 986–994. doi: 10.1038/mp.2015.45.Neurofilament.
- Yuan, A. *et al.* (2018) 'Neurofilament light interaction with GluN1 modulates neurotransmission and schizophrenia-associated behaviors', *Translational Psychiatry*. Springer US. doi: 10.1038/s41398-018-0194-7.
- Yuan, A. and Nixon, R. A. (2016) 'Specialized roles of neurofilament proteins in synapses: Relevance to neuropsychiatric disorders', *Brain Research Bulletin*. Elsevier Inc., 126, pp. 334–346. doi: 10.1016/j.brainresbull.2016.09.002.
- Yuan, A. and Rao, M. V (2012) 'Neurofilaments at a glance', *J Cell Sci*, 125(14), pp. 3257–3263. doi: 10.1242/jcs.104729.
- Yuan, A., Rao, M. V and Nixon, R. A. (2017) 'Neurofilaments and Neurofilament Proteins in Health and Disease'.
- Yung, A. R., Nishitani, A. M. and Goodrich, L. V (2015) 'Phenotypic analysis of mice completely lacking netrin 1', *Development*, pp. 3686–3691. doi: 10.1242/dev.128942.
- Zhang, J. *et al.* (2017) 'Nestin expression involves invasiveness of esophageal carcinoma and its downregulation enhances paclitaxel sensitivity to esophageal carcinoma cell apoptosis', 8(39), pp. 65056–65063.
- Zhang, Y. *et al.* (2018) 'Nuclear Nestin deficiency drives tumor senescence via lamin A/C-dependent nuclear deformation', *Nature Communications*. Springer US, 9(1), pp. 1–14. doi: 10.1038/s41467-018-05808-y.
- Zhao, Z. *et al.* (2014) 'Nestin positively regulates the Wnt/β-catenin pathway and the proliferation, survival and invasiveness of breast cancer stem cells.', *Breast cancer research : BCR*, 16, p. 408. doi: 10.1186/s13058-014-0408-8.
- Zhou, J. *et al.* (2013) 'Axon position within the corpus callosum determines contralateral cortical projection', *Proceedings of the National Academy of Sciences*, 110, pp. E2714–23. doi: 10.1073/pnas.1310233110.
- Zhu, J. *et al.* (2011) 'The nestin-expressing and non-expressing neurons in rat basal forebrain display different electrophysiological properties and project to hippocampus The nestin-expressing and non-expressing neurons in rat basal forebrain display different electrophysiology', *BMC Neuroscience*. BioMed Central Ltd, 12(1), p. 129. doi:

10.1186/1471-2202-12-129.

Zhu, Q. (1997) 'Delayed Maturation of Regenerating Myelinated Axons in Mice Lacking Neurofilaments', *Experimental Neurology*, 316(148), pp. 299–316.

Appendix 1: Different doublecortin (DCX) patient alleles show distinct phenotypes in cultured neurons: evidence for divergent loss-of-function and “off-pathway” cellular mechanisms.

Adapted from: Yap, C. C., Digilio, L., McMahon, L., Roszkowska, M., Bott, C. J., Kruczek, K., & Winckler, X. B. (2016). Different Doublecortin (DCX) Patient Alleles Show Distinct Phenotypes in Cultured Neurons. *Journal of Biological Chemistry*,

Introduction

DCX is a neuronal microtubule (MT)-binding protein with many roles in neurodevelopment. In humans, DCX is a major locus for X-linked lissencephaly (1-3) presenting with cortical, hippocampal, and cerebellar defects, and defects in major axon tracts (4-7). Much effort has thus been directed at understanding the molecular and cellular bases for this disease, with a particular focus on DCX-dependent defects in MT assembly and bundling. Experiments using a DCX knockout mouse, or double knockouts with the related genes DCLK1 and DCLK2 (8-14), or overexpression approaches (15) all argue strongly that DCX does in fact play important roles in neurodevelopmental processes. The best-studied defects are in neuronal migration in cortex (14, 16) and in hippocampus (17, 18). Axon and dendrite defects have also been described (6, 10, 17). For instance, dendrites in hippocampal pyramidal neurons are simplified in adult DCX KO mice (17). Dendrite growth is also impaired in cortical neurons cultured from DCLK1/DCX double knockout embryos (8). Furthermore, sh-mediated knockdown of DCX in cultured rat neurons led to reduction of dendrite complexity (15) (but see (19)). These knockout phenotypes are attributed to the required regulation of MTs by DCX. The converse is also true: overexpression of DCX increases dendrite complexity (15), further supporting a role for DCX in modulating dendrite elaboration. Similarly, overexpression of DCLK1 increases dendrite complexity (20).

DCX is also found in complexes with other proteins, including the actin-associated protein spinophilin (spn) (21), the clathrin adaptors AP-1 and AP-2 (22), and the cell adhesion molecule neurofascin (23), suggesting additional roles for DCX. These interactions were mapped to regions C-terminal of the MT-binding sites (Figure 1A). In fact, we previously discovered that DCX promotes the endocytosis of neurofascin independent of MT binding (24), but dependent on binding to clathrin adaptors via the C-terminal YLPL motif (Yap et al., in preparation). Among the known DCX patient alleles, some have mutations in the N-terminal MT-binding domain and lack MT binding whereas others have truncated C-termini and thus retain MT binding (Figure 1A). It is not known whether both classes of DCX patient alleles impair dendrite growth equally.

The available knock-out mouse model for DCX presents considerable challenges in terms of molecular characterization of DCX alleles. In particular, the phenotypes reported for DCX KO mice are very subtle and often transient, presumably because of redundancy with DCLK1 and DCLK2 (8, 11, 14, 18). Double knockout mice for DCX and DCLK1, on the other hand, do have profound neurodevelopmental defects, but show poor viability and difficulty breeding (9, 10), making them a challenging and expensive model for carrying out DCX mutant analysis. It is likely for these technical reasons that very little analysis is currently available about how DCX patient mutants behave in neurons. To

circumvent these technical barriers, we decided to take advantage experimentally of the observation that DCX can enhance dendrite growth when overexpressed (15). We thus used dendrite enhancement by DCX expression as an assay for wild type DCX function, using previously described MT binding-competent and MT binding-deficient mutants (25-27). All of these alleles were originally identified in Lissencephaly patients (2, 28, 29). We found that DCX alleles that retain MT-binding but lack the C-terminal regions (required for spn and AP adaptor binding) are defective for dendrite growth promotion (i.e. loss-of-function alleles) but to differing degrees. In particular, truncation mutants that retained MT- and spn-binding and lacked only the extreme C-terminus were less impaired than shorter truncation mutants that retained only MT binding. In addition, we found, surprisingly, that one of the mutations caused a cellular stress response in neurons through aggregate formation. These aggregates were ubiquitinated and were included in autophagosomes. Neurons thus likely upregulated degradative responses to clear the aggregates. Failure to efficiently clear the aggregates may lead to eventual cellular dysfunction and even death. This allele thus engaged an “off-pathway” response that was not usually activated by DCX and could be classified as “neomorph” by this criterion.

We report here an *ex vivo* overexpression approach as an experimentally efficient way for a first-pass screening of multiple DCX alleles in neurons. In particular, we dissected the cellular phenotypes of several DCX patient mutations in neurons and discovered that distinct DCX patient alleles caused dysfunction by different cellular mechanisms. This approach resulted in generating new hypotheses. The next step will be to take the insights generated and test their implications in a more physiological, *in vivo* context in the future. In addition, more of the published alleles need to be screened in neuronal cultures in order to further delineate other possible cellular pathways in which DCX alleles are deficient or in which “off-pathway” events occur for some alleles.

Results

The functions of DCX have been investigated on multiple levels, from biophysical (using purified proteins) to cellular (mostly in non-neuronal cells) to tissue level (using knockout models). Taking mechanistic discoveries from an *in vitro* binding assay straight into the whole animal is - more often than not - impossible or not informative, especially for DCX, a human disease gene for which the KO mouse does not fully phenocopy the human pathology. One reason for this lack of phenocopy is likely the small size of the murine cortex, coupled to redundancy with other genes in the same family. Furthermore, since the DCX gene is on the X-chromosome, it cannot be determined from the inheritance pattern whether or not any given human DCX patient allele is loss-of-function. Therefore, important new insights might be gained by expression analysis of DCX mutants in cultured neurons as an initial step. We thus decided to initiate an investigation of neuronal effects for a number of DCX alleles that had previously only been studied in non-neuronal cells or *in vitro*. We chose to investigate a cellular process that was known to be affected by DCX in cultured neurons, namely dendrite growth. Since we can read out the activity of WT DCX with this assay by increased dendrite growth, we can ask which patient alleles are loss-of-function alleles and then correlate their molecular binding activities with their lack of/ or altered function.

The C-terminus of DCX is required for DCX-mediated increase in dendrite complexity.

WT DCX was previously shown to increase dendrite complexity in cultured neurons (15). Freshly dissociated rat cortical neurons from E18 embryos were electroporated prior to plating with plasmids encoding GFP (as control) or WT DCX and the number of dendrites intersecting a concentric circle (diameter of 30 μm) was counted at 5 days *in vitro* (DIV 5) (Figure 1B). This measurement corresponds to a simplified Scholl analysis since dendrites are still short at these times in culture. In agreement with previous reports, we found that expression of WT DCX led to a significant increase in dendrite complexity compared to expressing GFP as a control (Figure 1C,D). The traced examples shown in Figure 1C were chosen to represent the 50th percentile of each data set. We next asked if the C-terminus was necessary for DCX-mediated dendrite complexity using the DCX truncations DCX-303X and DCX-272X (Figure 1A), which corresponded to published patient alleles. DCX-272X expression did not increase dendrite complexity, in contrast to expression of WT-DCX (Figure 1C,D). DCX-303X was still partially active and increased dendrite complexity compared to DCX-272X, but was less potent than WT DCX (Figure 1C,D). The DCX C-terminus was thus necessary for promoting dendrite growth.

DCX patient truncations DCX-303X and DCX-272X associate with microtubules.

The MT-binding domain of DCX has been mapped by multiple labs and resides in the DC repeat regions of the N-terminus of DCX (see Figure 1A). A truncated DCX (DC repeats 1 and 2: DCX1-247) still bound to microtubules *in vitro* (27), and both DCX-303X and DCX-272X contain all of the DC repeats. In order to confirm in our own hands the ability of the DCX C-terminal truncations to associate with microtubules inside cells, we used a cell-based detergent extraction assay, previously established by others (26, 27). WT DCX has been established by multiple labs (including ours) to remain associated with MTs by this stringent cell-based assay. This assay is thus well suited to determine if DCX mutants are still principally able to associate with microtubules in cells (see Experimental Procedures).

We quantified the ability of the two truncation mutants to remain associated with microtubules in transfected cells, compared to GFP as a negative control and WT DCX as a positive control. COS cells were transfected with GFP, WT DCX, DCX-303X, or DCX-272X. Lamin-cherry was co-transfected to mark transfected cells after detergent extraction. After 24 hours, one coverslip was fixed directly (“unextracted”) and one coverslip was extracted in detergent in microtubule-stabilizing buffer BRB-80 (“extracted”) for each construct. The mean intensity of DCX in transfected cells was then quantified. For GFP, ~90% of the GFP signal was extractable (Figure 2A,B,F) whereas WT DCX intensity was barely diminished by detergent extraction, demonstrating that WT DCX remained bound to microtubule networks under these extraction conditions (Figure 2C,F). Similarly to WT DCX, DCX-303X (Figure 2D) and DCX-272X (Figure 2E) were still clearly able to associate with MTs (Figure 2F), again in agreement with previous observations that the microtubule-binding domain is entirely contained within the DC repeats (26, 27).

Spinophilin binding capacity is partially impaired in DCX-272X, but not DCX-303X.

Since DCX-272X was not active in dendrite growth promotion even though it still associated with microtubules, we wondered if binding to another protein via the more C-terminal domain (missing in the truncated DCX-272X) might be required for full activity. The actin-binding protein spinophilin (spn) had been identified as a binding partner of

DCX and co-expression with spn reportedly recruited DCX increasingly onto the F-actin network (21). In our hands, WT-DCX was also recovered in anti-myc immunoprecipitations when myc-spn was co-expressed in COS cells, but not in controls lacking myc-spn (Figure 3A). When DCX was expressed in COS cells, it co-localized strikingly with MTs, but not with F-actin (phalloidin stain) (Figure 3B). In contrast, when DCX was co-expressed with spn in COS cells, DCX was distributed on both MTs and F-actin (Figure 3C). The boxed region of these quadruple-stained cells is shown in combinations of three channels in Figure 3D to make the dual co-localization with distinct MTs (arrowhead) and F-actin (arrows) easier to appreciate.

Since MTs and F-actin occupy largely overlapping spaces in COS cells, visualizing DCX pools on spn-containing F-actin structures was challenging. We thus determined if DCX was able to co-localize with spn in neurons where spn was greatly enriched in the actin-rich filopodia off the sides of dendrites and could thus be clearly distinguished from the MT-rich dendritic shaft. When DCX was expressed with spn, DCX strongly stained the dendrite shaft, but DCX staining could also be observed in MT-poor, actin/spn-rich dendritic filopodia (Figure 3E), suggesting that a subpopulation of DCX was able to enter actin-rich surface structures. DCX-272X also entered spn-rich dendritic filopodia (Figure 3F). We were unable to clearly quantify if it occurred to a similar extent as WT DCX because expression levels varied from cell to cell after the transient transfections. We thus turned to a more quantifiable assay to determine the spn binding capacity of DCX and the DCX truncations, namely co-immunoprecipitations.

The binding site for spn on DCX had been coarsely mapped previously. One paper reported no spn binding of DCX-246X (21) and another reported that the second DC repeat (aa 170-260) is sufficient for binding (6). Also, a point mutation at position 57 (F57L) was shown to completely abrogate spn co-immunoprecipitation, as did mutations at positions 331 and 334 (32). The required DCX sequences for spn binding are thus still not completely elucidated. Furthermore, DCX-272X had not previously been tested for spn binding. Consistently less myc-spn was immunoprecipitated with FLAG-DCX-272X (Figure 3G,H), indicating reduced binding (~50%) of spn to the truncated DCX-272X. We then tested the spn binding of FLAG-DCX-303X by co-immunoprecipitation. DCX-303X showed no statistically significant decrease in spn co-immunoprecipitation compared to WT-DCX (Figure 3G,H). We note that the total expression levels of WT DCX, DCX-303X, and DCX-272X were not different, indicating that the truncated C-termini did not affect stability of the DCX truncations. Our data contrasted somewhat with the conclusions of Bielas et al (2007), which was obtained with purified bacterially expressed fragments *in vitro* and who reported that spn binding ability was entirely contained within the N-terminal residues up to aa 260 (second DC repeat). Our data in contrast place important residues contributing to spn binding between residues 272 and 303. Our observations showed that the ability of DCX truncations to support dendrite growth correlated with their ability to bind to spn and that MT binding was not sufficient.

DCX-246X accumulates in the nucleus and is unstable.

Next, we generated DCX-246X (Figure 1A), also a patient allele, which was predicted to have no spn binding capacity based on previous reports (21), but retain MT binding. We confirmed MT association of DCX-246X (Figure 4A). Unexpectedly, DCX-246X was recovered at very low levels in the lysates that we had prepared for the purpose

of immunoprecipitation, making it impossible for us to test spn binding by that assay. Since MTs usually are depolymerized in lysates prepared on ice, we wondered if DCX-246X remained associated with other Triton-insoluble material, such as nuclei or intermediate filaments, and was thus spun out and discarded in the pre-clear step. We therefore transfected HEK293T cells with FLAG-DCX-246X, incubated them on ice to depolymerize MTs completely, and fractionated a soluble fraction (containing cytosolic protein, tubulin and MT-associated proteins) and an insoluble fraction (containing nuclei and intermediate filaments) (Figure 4B). As expected, tubulin (tub) was entirely found in the soluble fraction and vimentin (vim) was found overwhelmingly in the pellet fraction. Unlike WT DCX and FLAG-DCX-272X, FLAG-DCX-246X was expressed at low levels overall, and about 30% of it pelleted with nuclei and intermediate filaments into the insoluble pellet.

To assess the ability of DCX-246X to associate with spn with an alternative approach, we expressed it in either COS cells or neurons, as in Figure 3. In striking contrast to WT DCX (shown in Figure 3), DCX-246X co-localized strikingly with MTs, but not with spn/F-actin in extracted COS cells (Figure 4C). The partitioning of DCX-246X away from actin-rich structures was even more obvious in neurons where it was overwhelmingly excluded from actin/spn-rich protrusions off dendrite shafts (Figure 4D). These results were consistent with the spn mapping to DCX previously published by Tsukada et al. (2003).

When we evaluated the distribution of FLAG-DCX-246X with MTs and spn/actin without extraction in COS cells (Figure 4E), no co-localization with spn was apparent (see zoomed-in panels), but co-localization with MTs was extensive. Surprisingly, we observed accumulation of FLAG-DCX-246X on or in the nucleus in many cells. Z-stacks through the cell revealed that FLAG-DCX-246X appeared to be contained within the nucleus and not just peripherally associated with the nuclear envelope (Figure 4F). When we expressed DCX-246X in neurons for 24 hours, we frequently observed that FLAG-DCX-246X accumulated in the nucleus as well (Figure 4G), similar to our observations in unextracted COS cells.

When we tested whether DCX-246X still supported dendrite growth, we could only find a total of two neurons expressing FLAG-DCX-246X after five days of expression in three separate experiments (on 6 coverslips total). In contrast, we routinely recovered 200-1000 transfected cells per coverslip for WT DCX. The low number of DCX-246X expressing neurons could be due to the low levels of expression, as suggested by the observed instability of DCX-246X in COS cell lysates. Alternatively, the low number of DCX-246X expressing neurons could be due to their increased death. In order to distinguish between these two possibilities, we co-transfected DCX-246X with soluble GFP. Since the co-transduction rate is >80%, we could determine if few transfected neurons survived, suggesting death, or if GFP-expressing neurons were plentiful but lacking DCX-246X immunoreactivity, suggesting low expression. We recovered a large number of GFP-expressing neurons which were not immuno-positive for DCX-246X. These observations argued that transfected cells were not overwhelmingly dying and that DCX-246X was not stably expressed for five days. We note that in older neurons (transfected at DIV8 for 24 hours; Figure 4G) transfected neurons were detectable on each coverslip, albeit at much lower numbers compared to transfected WT DCX. We conclude that DCX-246X is an unstable protein.

DCX alleles DCX-R89G and DCX-R59H do not associate with MTs and are loss of function alleles.

We then made two DCX alleles that are reportedly deficient for MT binding, DCX-R89G and DCX-R59H. As expected, DCX-R89G staining is lost after detergent extraction (Figure 5A,B). DCX-R59H also showed greatly reduced MT association (Figure 5B). We noted that in many cells, DCX-R59H could be observed in detergent-insoluble aggregates (see below), and it was usually the fluorescence associated with these aggregated puncta that contributed the remaining DCX-R59H intensity in the measurements of extracted cells, rather than DCX-R59H remaining clearly associated with a microtubule network. We did not observe such aggregates with DCX-R89G.

We then tested if DCX-R89G and DCX-R59H were functional with respect to increasing dendrite complexity (as in Figure 1). Neither DCX-R89G nor DCX-R59H increased dendrite complexity compared to WT DCX control (Figure 5C). We noted one striking difference between DCX-R89G and DCX-R59H in the dendrite growth experiments, namely that we observed more than an order of magnitude fewer DCX-R59H expressing neurons after 5 days, compared to WT DCX and DCX-R89G. This was not due to problems with the plasmid per se since we observed comparable numbers of transfected COS cells for all the plasmids used, including DCX-R59H.

In order to more fully characterize the molecular binding properties of these two patient alleles, we also tested them for spn binding by co-immunoprecipitation. We saw somewhat lower levels of complex formation for DCX-R89G (Figure 5D,E), but the difference was not statistically significant compared to WT DCX binding. The failure of DCX-R89G to promote dendrite growth was therefore likely due to its inability to bind MTs. We could not determine the capacity of DCX-R59H to bind to myc-spn since DCX-R59H showed extremely high levels of non-specific binding to anti-myc-agarose conjugated beads (probably due to aggregation) which made interpretation of co-immunoprecipitations dubious. Our data so far suggest that DCX loss-of-function can result from loss of MT binding (DCX-R89G) or loss of spn binding (DCX-272X), and that different DCX patient alleles thus act via different cellular loss-of-function mechanisms. In addition, our data demonstrate that neither MT binding nor spn binding of DCX are sufficient for full function.

In order to corroborate the immunoprecipitation experiments, we then tested if association of DCX-R89G with spn could be demonstrated in cells. We thus repeated the COS cell detergent extraction (shown in Figure 5A) except that myc-spn was co-transfected with DCX-R89G. DCX-R89G was now detergent-resistant (Figure 5F) and remained prominently associated with spn and F-actin. Myc-spn co-expression was thus sufficient to impart detergent resistance onto DCX-R89G (compare Figure 5A to Figure 5F), consistent with its lacking MT binding but retaining spn binding. Consistent with these observations, DCX-R89G also entered actin-rich, MT-poor spines in dendrites of transfected neurons (Figure 5G).

The MT-binding deficient R59H patient allele forms cytoplasmic aggregates.

As previously noted, DCX-R59H was present in detergent-resistant cytoplasmic aggregates in detergent-resistant COS cells (Figure 6A). When myc-spn was co-expressed with DCX-R59H in COS cells and then detergent-extracted, much of the DCX-

R59H remained detergent-resistant in clear alignment with spn/actin-rich structures (Figure 6B). DCX-R59H can thus still bind to spn, but tends towards formation of insoluble cytoplasmic aggregates.

When we expressed DCX-R59H in DIV8 neurons for shorter times (24 hours), expressing neurons were easily found, but in many of them (about 50%) DCX-R59H was in cytoplasmic aggregates in dendrites and soma (Figure 6C). Some of these aggregates appeared to contain MAP2 and actin (Figure 6D2, D4; arrows) although the majority of MAP2 and F-actin was still distributed normally in soma and dendrites. In order to better visualize if expression of DCX-R59H affected the distribution of the actin cytoskeleton, we co-transfected mRuby-LifeAct (Figure 6E) or myc-spn (Figure 6F). Aggregates of DCX-R59H were highly co-localized with Ruby-LifeAct, arguing that the aggregates included F-actin, but the overall distribution of Ruby-LifeAct was still normal, and it distributed prominently to actin-rich protrusions off the dendrite shaft (Figure 6E). As shown above, myc-spn was found in dendritic protrusion off the shaft as well as in dendrite tips (Figure 6F1). In those neurons where DCX-R59H was not found in aggregates, DCX-R59H greatly co-localized with myc-spn in actin-rich dendritic protrusions, consistent with its ability to bind spn (Figure 6F2). Myc-spn distribution appeared undisturbed in these cells. In those neurons where DCX-R59H was found in aggregates, myc-spn localization was profoundly changed and co-localized completely with DCX-R59H aggregates in the dendrite shaft (Figure 6F3). Virtually none of the myc-spn remained in actin-rich dendritic protrusions off the shaft, indicating that DCX-R59H sequestered most, if not all, myc-spn in the cytoplasmic aggregates in the dendrite shaft. Of all the DCX alleles we tested (WT, DCX-303X, DCX-272X, DCX-R89G, DCX-R59H), DCX-R59H was the only one that formed aggregates and disrupted the distribution of other cytoskeletal elements. DCX-R59H thus has off-pathway effects and might manifest as an “off-pathway/neomorph” allele at the subcellular level.

Cytoplasmic aggregates of DCX-R59H contain Hsp70, ubiquitin and markers of autophagosomes.

Cytoplasmic aggregates of misfolded proteins are a common finding in multiple neurodegenerative disease. All cells, including neurons, possess cellular machinery to recognize and dispose of misfolded cytoplasmic proteins. Many misfolded proteins are recognized by Hsp70, tagged with ubiquitin, and ultimately degraded by the proteasome or in autophagosomes to maintain proteostasis and health. We therefore asked if cytoplasmic aggregates of DCX-R59H contained Hsp70, ubiquitin, or markers of autophagosomes (p62 and LC3) (Figure 6G). We observed clear co-localization of DCX-R59H aggregates with Hsp70 and ubiquitin (Figure 6G1, G2). Cytoskeletal components (MAP2, Figure 6G1; spn, Figure 6G2) were found in the same aggregates. These observations argue that when DCX-R59H misfolded in neurons, it was recognized by the Hsp70/ubiquitination machinery and tagged for degradation. Co-localization of DCX-R59H aggregates was also apparent with p62 and LC3 (Figure 6G3-5), but not with all of the aggregates. Neurons expressing DCX-R59H aggregates thus contain autophagosomes filled with ubiquitinated proteins and DCX-R59H. In addition, neurons containing DCX-R59H aggregates showed disruption of normal cytoskeletal organization which might contribute to neuronal dysfunction for this particular allele.

Discussion

Cortical malformations are recovered in the human populations at a surprisingly high rate and can be familial or arise spontaneously de novo (1-3, 28). One manifestation of cortical malformation is subcortical band heterotopia (SBH) and lissencephaly (LIS; smooth brain). A recent extensive study on human patients with SBH found that 100% of familial SBH is caused by mutations in the X-linked gene DCX. For de novo mutations, DCX mutations account for 50-80% of cases (28). Both DCX-linked SBH (in females) and DCX-linked LIS (in males) are likely caused by neuronal migration defects, but axon outgrowth and guidance defects have also been reported. In the hippocampus, lamination defects as well as dendrite defects are found in the DCX null mouse (17), and the hippocampus is affected in some of the human patients (4). For patients with SBH and LIS, intellectual disability and epilepsy are common and are likely due to a combination of misplaced neurons in the cortex and in the hippocampus, defects in major axon tracts (such as the corpus callosum), and connectivity problems due to misplaced neurons and defective dendrite growth. Even though many nonsense and missense mutations of DCX are known and more are continuously added to the list, the molecular and cellular defects for most of them are still only incompletely understood.

In this work, we analyzed and correlated the cellular and molecular characteristics of several DCX patient alleles. Our work led to the following conclusions and new insights:

- 1) Loss-of-function of DCX can arise from either loss of MT binding, or loss of C-terminal binding regions.

- 2) Sequences in the C-terminus of DCX (past the MT binding domains contained in the DC repeats) are required for full DCX function. These C-terminal sequences are necessary for full spn binding, AP-2 binding, as well as contain several regulatory phospho-sites.

- 3) Since DCX-303X shows only partial loss of function, absence of the phospho-sites (past residue 303) do not give strong phenotypes for dendrite elaboration.

- 4) DCX246X is an unstable protein that aberrantly accumulates in the nucleus.

- 5) One patient alleles (DCX-R59H) forms aggregates that activate autophagy. Neurons containing these aggregates show disrupted cytoskeletal components. We thus suggest that DCX-R59H can act as a cellular “off-pathway”/possibly neomorph allele.

Our findings lead to the suggestion that cellular pathology caused by different DCX patient alleles are due to either loss-of-function (lof) or off-pathway/potentially neomorph mechanisms (summarized in Table 1). Given recent discoveries of the importance of DCX and DCLK1 in regeneration (33), a full understanding of the importance of different domains of DCX has translational significance in addition to the relevance for neurodevelopment and for neurodevelopmental disorders.

DCX lof alleles for dendrite growth can map to MT binding or to C-terminal binding domain.

We identified several DCX patient alleles that show complete (DCX-R89G, DCX-272X) or partial (DCX-303X) loss-of-function phenotypes when assayed for DCX-mediated increases in dendrite complexity (Table 1). We then carried out binding analysis as well as localization studies to further characterize the molecular defects of these alleles. DCX-R89G is deficient in MT-binding, and its inability to support dendrite growth thus argues decisively that MT-binding by DCX is required.

Since both DCX272X and DCX303X show robust MT association in cells, their inability to support increased dendrite growth is not due to loss of MT association, but demonstrates that MT association is not sufficient for DCX function. Rather, binding interactions or regulatory phosphorylation sites (or both) contained in the C-terminus of DCX are required as well for full DCX function. One candidate for an additional necessary binding partner of DCX is spn, which we show here to bind less efficiently to DCX-272X. We propose that the partial loss of spn binding contributes to the lof phenotype of DCX-272X. DCX-303X, on the other hand, still binds normally to spn as well as to MTs, but is lacking the clathrin adaptor AP binding site (YLPL) (22) as well as a number of regulatory phosphorylation sites (34, 35). DCX-303X behaves as a hypomorph in our assay, suggesting that AP-binding might be additionally required for full DCX function. We previously showed that DCX promotes the endocytosis of a cell adhesion molecule (24), but further work is needed to explore which endocytic cargo might require DCX for trafficking in order to support dendrite elaboration.

Other work previously suggested that MT-binding is not sufficient for all roles of DCX. For example, a patient mutation in the linker between the two DC repeats (W146C) binds MTs, but not the MT motor KIF1A. DCX-146C fails to rescue normal *in vitro* morphogenesis after DCX knock-down (9), suggesting important functions for DCX in regulating MT motors in addition to MT polymerization and bundling. We would like to note that DCX null neurons initially stall in a multipolar morphology after leaving the ventricular zone and show defects in taking on the normal bipolar morphology of migratory neurons (14, 36). This early morphological transition is distinct from dendrite formation of neurons at DIV5, the process we are analyzing in this work. We also note that the dendrite defect is apparent in culture and thus likely not a consequence of aberrant migration and neuronal positioning, as has been suggested for dendrite morphology defects in the hippocampus (17).

Another example is DCX-S47R. The DCX-S47R mutant still binds to MTs but does not support migration of neural progenitors in an *in vitro* migration assay (37) and mislocalizes to the soma in neurons (9). The S47 site is phosphorylated by PKA and has been implicated in regulating actin via binding of the GEF Asef2 (37). A role for spn was not tested for this mutant. DCX-272X does not restore normal actin distribution in DCX null cultured neurons (10), again suggestive for a role of the spn binding interaction and/or additional C-terminal sequences playing important functional roles. Interestingly, DCX-303X shows complete loss of function in terms of migration from an *in vitro* aggregate of cerebellar granule neurons (38), whereas in our work we see only a partial defect for dendrite growth. It might thus be the case that clathrin adaptor binding is differentially required for distinct cellular DCX-mediated processes (migration vs dendrite growth). This possibility will be further examined in the future.

On the flip side, our experiments also demonstrate that binding interactions mediated by the C-terminus are not sufficient for full DCX function in the absence of MT binding. DCX-R89G can still bind spn (Figure 5) as well as the clathrin adaptor AP-2 (Yap, unpublished observations). It also still contains all phospho-sites but it nevertheless does not support the increase in dendrite complexity we see for WT DCX. These observations suggest a model for multifunctional roles of DCX, including (but not limited to) MT binding, spn binding, and/or clathrin adaptor binding (Table 1).

The patient allele DCX-R59H causes off-pathway effects at the cellular level.

Our experiments furthermore clearly demonstrate that not all DCX patient alleles are loss-of-function (lof) or hypomorph alleles. DCX-R59H not only does not support increased dendrite complexity, but additionally leads to cytoplasmic aggregates. Consistent with our interpretation that DCX-R59H misfolds and aggregates, the R59 side chain was shown to be partially buried, and a substitution at R59 (R59L) resulted in changed folding (25). We propose that neurons expressing DCX-R59H show manifestations of activated degradative pathways aimed at degrading DCX-R59H aggregates. The aggregates are positive for Hsp70, consistent with misfolded protein, become ubiquitinated, and many of them contain LC3 and p62, indicative of autophagosome formation. We speculate that neurons expressing DCX-R59H upregulate stress pathways to increase autophagy of accumulated DCX-R59H and its increased clearance. In addition, it is possible that the aggregates have some detrimental side effects since aggregates of DCX-R59H contain several components of the cytoskeleton, such as actin and MAP2. Most strikingly, though, they accumulate spn, a known binding partner of DCX. We speculate that DCX-R59H might thus impair the functions of other cytoskeletal elements as an “off-pathway” effect. Recent characterization of DCX mutations identified DCX-R59H as one of the more severe alleles in patients (28) and one that is only identified de novo. Interestingly, a small percentage of patients (~15%) show microcephaly (28). A subset of DCX alleles might thus cause some excess cell death in patients, but more work will be required to explore this idea.

Experimental Procedures

Reagents:

Antibodies:

Anti-DCX: Cell Signaling (rabbit polyclonal against N-terminus) #4604, lot:3, recognizes a single band at 45kD from fetal rat brain.

Abcam (rabbit polyclonal, against the C-terminus), #18724, lot: GR55971-1, recognizes a single band at 45kD from mouse brain lysate

Anti-FLAG: Sigma Flag F7425 (rabbit polyclonal)- lot # 064M4757V;
mouse #F1804, lot: SLBJ4607V

Anti-GFP: Molecular Probes (mouse) #A11120, lot: 877587,
Cell signaling (rabbit monoclonal), #2956S, lot: 4, recognizes a single band at 27kD from HCC827 cell lysate,
GFP booster (Chromotek)

Anti-tubulin: Sigma (mouse DM1a),
Santa Cruz (rat monoclonal yol1/34 Lot. G0714)

Anti-Vimentin: Bioss (rabbit BS-0756R Lot. No. 9A23M41). (1:5000 WB)

Anti-c-myc: Santa Cruz # SC-40 (mouse 9E10 Lot. B0614 and rabbit polyclonal A-14 #SC789 Lot H0114),

Bethyl (agarose conjugated goat polyclonal)

F-actin: Phalloidin 647 (Molecular Probes), #A22287.

Anti-MAP2: chicken antibody. EnCor Biotechnology (RRID: AB_2138173). This antibody shows a single band on western blots from rat and mouse brain lysates (EnCor).

Anti-Hsp70: BD biosciences (mouse), #610607, lot: 4114835, a single band at 70KD on WB from Hela cell lysate

Anti-ubiquitin (P4D1): UBPBio (mouse), #Y3011, lot: Y30142195, recognizes mono and polyubiquitinated proteins.

Anti-p62: American Research products (guinea pig), #03-GP62-C, lot: 406626B, a single band at 62KD on WB from A431 cell lysate.

Anti-spinophilin: Abcam (rabbit), #ab50184, lot: GR4937-5.

Secondary antibodies: Alexa-dye coupled antibodies (Molecular Probes) were used for Immunofluorescence. For Licor Odyssey Western blots, Jackson ImmunoResearch antibodies were used: Donkey anti mouse (680) #715-625-151, Donkey anti rabbit (790) #711-655-152, Donkey anti rat (680) #712-625-153 at 1:30,000.

Plasmids:

DCX plasmid: mouse wild type DCX-GFP and FLAG-DCX from (21, 24).

Lamin-cherry: Bryce Paschal (UVA)

GFP: Clontech

mRFP-LC3: Tamotsu Yoshimori (Addgene)

mRubyLifeAct: Ruby-lifeact was a gift from R. Wedlich-Soldner (Max-Planck Institute of Biochemistry, Germany)

GFP-spinophilin: Ora Bloom (Fordham University)

myc-spinophilin: Lawrence Brass (UPenn)

mcherry: Clontech

Generation of DCX mutants.

Point mutations: were introduced using Site-directed Quick change mutagenesis kit from Stratagene. All mutations were confirmed by sequencing. Multiple versions of WT and mutant DCX constructs were created, fused with either GFP, myc-, or FLAG-tags. No differences in behaviors were apparent, and the most convenient tag was used in different experiments.

Neuronal cultures. Neuronal cultures were prepared from E18 rat hippocampi, as approved in the institutional ACUC protocol #3422. Hippocampi from all pups in one litter were combined and thus contained male and female animals. Cells were plated on poly-L-lysine coated coverslips and incubated with DMEM medium with 10% horse serum. After 4h, the cells were transferred into serum-free medium supplemented with B27 (GIBCO BRL) and cultured for 9-12 DIV (days *in vitro*). Transfections were carried out with Lipofectamine 2000. Alternatively, neurons were electroporated (BTX Harvard apparatus) after dissociation and then cultured for 5 days.

COS and HEK293 cells were maintained in DMEM+10% fetal bovine serum, and all transfections were conducted using Lipofectamine 2000 (Invitrogen) according to the manufacturer's protocol.

Immunocytochemistry. Cells were fixed in 2% paraformaldehyde/3% sucrose/PBS in 50% conditioned medium at room temperature for 30 minutes, quenched in 10 mM glycine/PBS for 10 minutes. The fixation conditions used do not introduce holes into the overwhelming majority of cells (30). Coverslips were then blocked in 5% horse serum/1%

BSA/PBS \pm 0.05% TritonX-100 for 30 minutes. Antibodies were diluted in 1% BSA/PBS and incubated for 1-2 hours. Coverslips were mounted in Prolong Gold mounting medium and viewed on a Zeiss Z1-Observer with a 40x objective (EC Plan-Neofluar 40x/0.9 Pol WD=0.41). Apotome structures illumination was used for most images for better resolution. Images were captured with the Axiocam 503 camera using Zen software (Zeiss) and processed identically in Adobe Photoshop. No non-linear image adjustments were performed. Imaris software (Bitplane) was used for determining Pearson coefficients and 3D-voxel representations.

Detergent extractions: Detergent extractions of live cells were carried out in BRB80 buffer (80 mM Pipes, 1 mM $MgCl_2$, 1 mM EGTA, pH 6.8) with 0.3% Triton X-100 at 37°C for 3 minutes (24, 25, 31). Cells were washed twice in BRB80 buffer and fixed.

Soluble/insoluble protein sample preparation: Low passage 293 cells plated overnight at 80% confluency in 10% FBS DMEM were transfected with 8 μ g Flag-DCX WT, DCX-246X, DCX-R89G, or DCX-R59H and 14 μ l Lipofectamine 2000. After 48 hrs, adherent cells were washed with ice cold PBS, and lysed/scraped off the plate with a rubber policeman into 1ml IP buffer (50mM Tris pH 7.4, 150mM NaCl, 1mM $MgCl_2$, 1% NP-40, 1mM PMSF, 1mM DTT, 1x Halt protease + phosphatase inhibitor cocktail.) Cell lysates were recovered from the dish and mechanically lysed with 3 passages through a 28 gauge needle syringe. Lysates were rotisseriesed at 4°C 1 hr, followed by centrifugation at 21,000 RCF 20min 4°C. Supernatants were removed and diluted into 4X Laemmli sample buffer and boiled. Pellets were washed with 500 μ l IP buffer, rotisseriesed 30 min, and centrifuged at 21,000 RCF 20 min 4°C. The supernatant was aspirated and the pellet dissolved in 2X Laemmli buffer. Equivalent samples of both soluble and insoluble protein sample were used for western blotting.

Immunoprecipitations: One 10-cm culture dish COS7 cells per sample were transfected with either 7.5 μ g Flag-DCX construct alone or 5 μ g myc-spinophilin plus 5 μ g Flag-DCX construct with 2.5 μ l Lipofectamine2000/ μ g DNA. Cells were generally split in the morning then transfected about 6 hours later. Media was changed the next day. Cells were lysed on day two in lysis buffer (20mM Hepes, pH 7.4, 2 mM EDTA, 2 mM EGTA, 100 mM NaCl, 10 mM NaF, 1 mM PMSF (added just before use), 1% Triton X100, Roche protease inhibitor cocktail used at 1X (Roche 11 873 580 001). Lysates were pre-cleared with control agarose beads (Pierce Control Agarose resin (Thermo Scientific #26150)) overnight and then incubated with Goat anti c-myc agarose 0.45 μ g/ μ l (S-190-104). Beads were washed several times and then boiled and separated on PAGE gel. After transfer to nitrocellulose blots were probed for myc-spinophilin with c-Myc (9E10) Santa Cruz #sc-40 (Mouse, 1:2000) and Flag-DCX with Sigma #F7425 (Rabbit, 1:2000) followed by LI-COR fluorescent secondary antibodies (1:20000) and imaged on a LI-COR Odyssey fluorescence imager. Internal data produced by Licor showed that their Odyssey infrared imaging system (used in this study) has a greater than 4000-fold linear range compared to 250-fold for chemiluminescence. For the IPs, band intensity determined from the Licor was corrected to the input (total lysate) and then normalized to WT DCX.

Dendrite quantification: Dendrites were quantified on images of transfected cells fixed on DIV5 and counterstained with DCX antibody. Since dendrites were short at this time point, a simplified Scholl analysis was used where the number of intersecting dendrites was counted at two concentric rings only, one with a diameter of 30 μm and one of 60 μm . The 30 μm measurements are reported in the figure.

Statistical analysis: Statistical analysis was carried out using Graphpad Prism software. Data sets were first evaluated as parametric vs. non-parametric. Non-parametric data sets were analyzed using Mann-Whitney U test, parametric data sets were analyzed with student's t-test or ANOVA followed by posthoc test. For dendrite measurements, three repeats using independent cultures were quantified with >50 cells counted per condition. The exact number of cells is indicated in the figure legend for each graph. For co-immunoprecipitations, statistical analysis of the DCX-spinophilin co-IP data was carried out with Graphpad Prism software. For each replication individual lanes on the western blots were corrected to the expression levels in the cell lysates, then normalized to the WT control. Significance was evaluated in Prism using the Wilcoxon signed-rank test.

Abbreviations list

DCX – doublecortin on the X-chromosome; MT – microtubule; DIV – days *in vitro*; WT – wild type; KO – knockout; DN – dominant-negative; Lof – loss of function; Spn – spinophilin/neurabinII

Acknowledgments:

We are grateful to Drs. Gregor Eichele, Dorothy Schafer, Lawrence F. Brass, and Ora Bloom for generously providing crucial reagents. We thank all members of the Winckler Laboratory and Dr. Judy Liu (National Children's Hospital) for constructive engagement throughout the duration of this work and critical reading of the manuscript. This work was supported by NIH grant R01NS081674 (to BW).

Conflict of Interest: The authors declare no competing financial interests.

Author Contributions: CCY and BW conceived and coordinated the study and wrote the paper. CCY created tagged DCX versions and made the DCX mutants. LD and CCY designed, performed and analyzed the dendrite (Figure 1C,D; Figure 5C) and MT binding experiments (Figure 2; Figure 4A; Figure 5B). LPM designed, performed and analyzed the spn co-IP experiments (Figure 3A,G,H; Figure 5D,E) and carried out the Imaris analysis (Figure 4F). CB designed, performed and analyzed the cell fractionation experiment in Figure 4B. CCY designed, performed and analyzed the neuronal expression experiments (Figure 3E,F; Figure 4D,G; Figure 5G) as well as the COS cell extraction experiments \pm myc-spn expression (Figure 4 C,E,F; Figure 5A,F) and all the experiments in Figure 6. KK and MR initiated the experiments for dendrite measurements (Figure 1B). CCY, BW, CB, LD and LPM contributed to figure preparation. All authors reviewed the results and approved the final version of the manuscript.

Table 1: Summary of phenotypes of DCX alleles and proposed mechanism of pathology

DCX allele	Molecular phenotypes	Sub-Cellular phenotypes	phenotype lof/gof for dendrites	Pathological mechanism proposed
WT	MT binding: yes Spn binding: yes AP2 binding: yes many phospho-sites	none	Wild type	NA
303X	MT binding: yes Spn binding: yes AP2 binding: no loss of multiple phospho-sites	None noted	lof/ hypomorph	Interactions with extreme C-terminal needed (AP2, phosphorylation)
272X	MT binding: yes Spn binding: 50% reduced AP2 binding: no loss of multiple phospho-sites	None noted	lof/ amorph	Full spn binding needed. Interactions with extreme C-terminal needed (AP2, phospho)
246X	MT binding: yes Spn binding: no AP2 binding: no loss of multiple phospho-sites	Nuclear accumulation, low expression.	No cells expressed the protein. ND.	Protein is unstable. Nuclear accumulation might also have negative effects on cells.
R89G	MT binding: no Spn binding: yes AP2 binding: yes	Present in actin-rich protrusions, but not on MTs	lof/ amorph	MT binding required, Spn binding not sufficient
R59H	MT binding: no Spn binding: yes AP2 binding: yes	Cytoplasmic aggregates consistent with misfolding, increased autophagy in many cells. Disruption of actin, MAP2 and spn.	Off-pathway/ possibly neomorph	Loss of MT binding. In addition, other cytoskeletal elements are disrupted which might cause additional "off-pathway" pathology.

References

1. Dixon-Salazar, T. J., and Gleeson, J. G. (2010) Genetic regulation of human brain development: lessons from Mendelian diseases. *Annals of the New York Academy of Sciences*. **1214**, 156–167
2. Friocourt, G., Marcorelles, P., Saugier-veber, P., Quille, M.-L., Marret, S., and Laquerrière, A. (2010) Role of cytoskeletal abnormalities in the neuropathology and pathophysiology of type I lissencephaly. *Acta Neuropathol*. **121**, 149–170
3. Liu, J. S. (2011) Molecular genetics of neuronal migration disorders. *Curr Neurol Neurosci Rep*. **11**, 171–178
4. Kappeler, C., Dhenain, M., Phan Dinh Tuy, F., Saillour, Y., Marty, S., Fallet-Bianco, C., Souville, I., Souil, E., Pinard, J. M., Meyer, G., Encha-Razavi, F., Volk, A., Beldjord, C., Chelly, J., and Francis, F. (2007) Magnetic resonance imaging and histological studies of corpus callosal and hippocampal abnormalities linked to doublecortin deficiency. *J. Comp. Neurol*. **500**, 239–254
5. Koizumi, H., Tanaka, T., and Gleeson, J. G. (2006) Doublecortin-like kinase functions with doublecortin to mediate fiber tract decussation and neuronal migration. *Neuron*. **49**, 55–66
6. Bielas, S. L., Serneo, F. F., Chechlac, M., Deerinck, T. J., Perkins, G. A., Allen, P. B., Ellisman, M. H., and Gleeson, J. G. (2007) Spinophilin Facilitates Dephosphorylation of Doublecortin by PP1 to Mediate Microtubule Bundling at the Axonal Wrist. *Cell*. **129**, 579–591
7. Tanaka, T. (2006) The Doublecortin and Doublecortin-Like Kinase 1 Genes Cooperate in Murine Hippocampal Development. *Cerebral Cortex*. **16**, i69–i73
8. Deuel, T. A. S., Liu, J. S., Corbo, J. C., Yoo, S.-Y., Rorke-Adams, L. B., and Walsh, C. A. (2006) Genetic interactions between doublecortin and doublecortin-like kinase in neuronal migration and axon outgrowth. *Neuron*. **49**, 41–53
9. Liu, J. S., Schubert, C. R., Fu, X., Fourniol, F. J., Jaiswal, J. K., Houdusse, A., Stultz, C. M., Moores, C. A., and Walsh, C. A. (2012) Molecular basis for specific regulation of neuronal Kinesin-3 motors by doublecortin family proteins. *Mol Cell*. **47**, 707–721
10. Fu, X., Brown, K. J., Yap, C. C., Winckler, B., Jaiswal, J. K., and Liu, J. S. (2013) Doublecortin (dcx) family proteins regulate filamentous actin structure in developing neurons. *Journal of Neuroscience*. **33**, 709–721
11. Kerjan, G., Koizumi, H., Han, E. B., Dubé, C. M., Djakovic, S. N., Patrick, G. N., Baram, T. Z., Heinemann, S. F., and Gleeson, J. G. (2009) Mice lacking doublecortin and doublecortin-like kinase 2 display altered hippocampal neuronal maturation and spontaneous seizures. *Proc Natl Acad Sci USA*. **106**, 6766–6771
12. Jean, D. C., Baas, P. W., and Black, M. M. (2012) A novel role for doublecortin and doublecortin-like kinase in regulating growth cone microtubules. *Human Molecular Genetics*. **21**, 5511–5527
13. Friocourt, G., Liu, J. S., Antypa, M., Rakic, S., Walsh, C. A., and Parnavelas, J. G. (2007) Both doublecortin and doublecortin-like kinase play a role in cortical interneuron migration. *Journal of Neuroscience*. **27**, 3875–3883
14. Pramparo, T., Youn, Y. H., Yingling, J., Hirotune, S., and Wynshaw-Boris, A.

- (2010) Novel embryonic neuronal migration and proliferation defects in Dcx mutant mice are exacerbated by Lis1 reduction. *Journal of Neuroscience*. **30**, 3002–3012
15. Cohen, D., Segal, M., and Reiner, O. (2008) Doublecortin Supports the Development of Dendritic Arbors in Primary Hippocampal Neurons. *Dev Neurosci*. **30**, 187–199
 16. Bai, J., Ramos, R. L., Ackman, J. B., Thomas, A. M., Lee, R. V., and Loturco, J. J. (2003) RNAi reveals doublecortin is required for radial migration in rat neocortex. *Nat Neurosci*. **6**, 1277–1283
 17. Bazelot, M., Simonnet, J., Dinocourt, C., Bruel-Jungerman, E., Miles, R., Fricker, D., and Francis, F. (2012) Cellular anatomy, physiology and epileptiform activity in the CA3 region of Dcx knockout mice: a neuronal lamination defect and its consequences. *European Journal of Neuroscience*. **35**, 244–256
 18. Corbo, J. C., Deuel, T. A., Long, J. M., LaPorte, P., Tsai, E., Wynshaw-Boris, A., and Walsh, C. A. (2002) Doublecortin is required in mice for lamination of the hippocampus but not the neocortex. *Journal of Neuroscience*. **22**, 7548–7557
 19. Baek, S. T., Kerjan, G., Bielas, S. L., Lee, J. E., Fenstermaker, A. G., Novarino, G., and Gleeson, J. G. (2014) Off-Target Effect of doublecortin Family shRNA on Neuronal Migration Associated with Endogenous MicroRNA Dysregulation. *Neuron*. **82**, 1255–1262
 20. Shin, E., Kashiwagi, Y., Kuriu, T., Iwasaki, H., Tanaka, T., Koizumi, H., Gleeson, J. G., and Okabe, S. (2013) Doublecortin-like kinase enhances dendritic remodelling and negatively regulates synapse maturation. *Nature Communications*. **4**, 1440–14
 21. Tsukada, M., Prokscha, A., Oldekamp, J., and Eichele, G. (2003) Identification of neurabin II as a novel doublecortin interacting protein. *Mech Dev*. **120**, 1033–1043
 22. Friocourt, G. (2001) Doublecortin Interacts with μ Subunits of Clathrin Adaptor Complexes in the Developing Nervous System. *Molecular and Cellular Neuroscience*. **18**, 307–319
 23. Kizhatil, K., Wu, Y.-X., Sen, A., and Bennett, V. (2002) A new activity of doublecortin in recognition of the phospho-FIGQY tyrosine in the cytoplasmic domain of neurofascin. *Journal of Neuroscience*. **22**, 7948–7958
 24. Yap, C. C., Vakulenko, M., Kruczek, K., Motamedi, B., Digilio, L., Liu, J. S., and Winckler, B. (2012) Doublecortin (DCX) Mediates Endocytosis of Neurofascin Independently of Microtubule Binding. *Journal of Neuroscience*. **32**, 7439–7453
 25. Kim, M. H., Cierpicki, T., Derewenda, U., Krowarsch, D., Feng, Y., Devedjiev, Y., Dauter, Z., Walsh, C. A., Otlewski, J., Bushweller, J. H., and Derewenda, Z. S. (2003) The DCX-domain tandems of doublecortin and doublecortin-like kinase. *Nat. Struct. Biol*. **10**, 324–333
 26. Sapir, T., Horesh, D., Caspi, M., Atlas, R., Burgess, H. A., Wolf, S. G., Francis, F., Chelly, J., Elbaum, M., Pietrokovski, S., and Reiner, O. (2000) Doublecortin mutations cluster in evolutionarily conserved functional domains. *Human Molecular Genetics*. **9**, 703–712
 27. Taylor, K. R., Holzer, A. K., Bazan, J. F., Walsh, C. A., and Gleeson, J. G. (2000) Patient mutations in doublecortin define a repeated tubulin-binding domain. *J Biol*

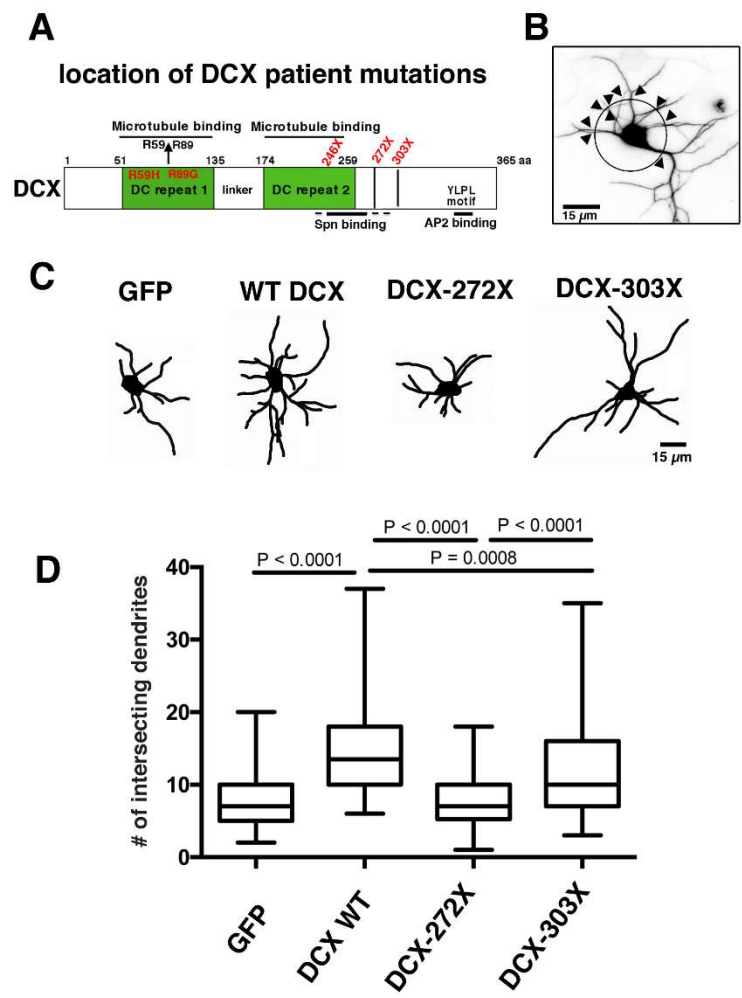
- Chem.* **275**, 34442–34450
28. Bahi-Buisson, N., Souville, I., Fourniol, F. J., Toussaint, A., Moores, C. A., Houdusse, A., Yves Lemaitre, J., Poirier, K., Khalaf-Nazzal, R., Hully, M., Louis Leger, P., Elie, C., Boddaert, N., Beldjord, C., Chelly, J., Francis, F., SBH-LIS European Consortium (2013) New insights into genotype-phenotype correlations for the doublecortin-related lissencephaly spectrum. *Brain*. **136**, 223–244
 29. Gleeson, J. G., Minnerath, S. R., Fox, J. W., Allen, K. M., Luo, R. F., Hong, S. E., Berg, M. J., Kuzniecky, R., Reitnauer, P. J., Borgatti, R., Mira, A. P., Guerrini, R., Holmes, G. L., Rooney, C. M., Berkovic, S., Scheffer, I., Cooper, E. C., Ricci, S., Cusmai, R., Crawford, T. O., Leroy, R., Andermann, E., Wheless, J. W., Dobyns, W. B., and Walsh, C. A. (1999) Characterization of mutations in the gene doublecortin in patients with double cortex syndrome. *Ann Neurol.* **45**, 146–153
 30. Wisco, D., Anderson, E. D., Chang, M. C., Norden, C., Boiko, T., Fölsch, H., and Winckler, B. (2003) Uncovering multiple axonal targeting pathways in hippocampal neurons. *The Journal of Cell Biology.* **162**, 1317–1328
 31. Sapir, T., Horesh, D., Caspi, M., Atlas, R., Burgess, H. A., Wolf, S. G., Francis, F., Chelly, J., Elbaum, M., Pietrokovski, S., and Reiner, O. (2000) Doublecortin mutations cluster in evolutionarily conserved functional domains. *Human Molecular Genetics.* **9**, 703–712
 32. Santra, M., Zhang, X., Santra, S., Jiang, F., and Chopp, M. (2006) Ectopic Doublecortin Gene Expression Suppresses the Malignant Phenotype in Glioblastoma Cells. *Cancer Research.* **66**, 11726–11735
 33. Nawabi, H., Belin, S., Cartoni, R., Williams, P. R., Wang, C., Latremolière, A., Wang, X., Zhu, J., Taub, D. G., Fu, X., Bin Yu, Gu, X., Woolf, C. J., Liu, J. S., Gabel, C. V., Steen, J. A., and He, Z. (2015) Doublecortin-Like Kinases Promote Neuronal Survival and Induce Growth Cone Reformation via Distinct Mechanisms. *Neuron.* **88**, 704–719
 34. Shmueli, A., Gdalyahu, A., Sapoznik, S., Sapir, T., Tsukada, M., and Reiner, O. (2006) Site-specific dephosphorylation of doublecortin (DCX) by protein phosphatase 1 (PP1). *Mol Cell Neurosci.* **32**, 15–26
 35. Gdalyahu, A., Ghosh, I., Levy, T., Sapir, T., Sapoznik, S., Fishler, Y., Azoulai, D., and Reiner, O. (2004) DCX, a new mediator of the JNK pathway. *EMBO J.* **23**, 823–832
 36. Loturco, J. J., and Bai, J. (2006) The multipolar stage and disruptions in neuronal migration. *Trends in Neurosciences.* **29**, 407–413
 37. Toriyama, M., Mizuno, N., Fukami, T., Iguchi, T., Toriyama, M., Tago, K., and Itoh, H. (2012) Phosphorylation of doublecortin by protein kinase A orchestrates microtubule and actin dynamics to promote neuronal progenitor cell migration. *Journal of Biological Chemistry.* **287**, 12691–12702
 38. Tanaka, T. (2004) Lis1 and doublecortin function with dynein to mediate coupling of the nucleus to the centrosome in neuronal migration. *The Journal of Cell Biology.* **165**, 709–721

Figure 1: The C-terminus of DCX is required for DCX-mediated increase in dendrite complexity.

(A) Diagram of the domain structure of DCX indicating the two DC repeats. DC repeat 1 binds to microtubules. DC repeat 2 binds to tubulin dimers. Microtubule bundling requires both repeats. The locations of the DCX patient alleles used in this work are indicated in red.

(B) Cortical neurons in culture were electroporated prior to plating with DCX or DCX mutants (as labeled), and the number of intersecting dendrites with a circle at 30 μm diameter was determined five days later (DIV5). Size bar = 15 μm .

(C,D) Three independent experiments were carried out in separate cultures, and one representative experiment is shown for WT DCX, DCX-272X and DCX-303X. (C) shows example tracings of neurons representing the 50th percentile of the quantification in (D). The number of cells quantified in (D) was: 84 cells for GFP, 84 cells for WT DCX, 95 cells for DCX-303X, 84 cells for DCX-272X. WT DCX and DCX-303X led to statistically significant increase in dendrite complexity compared to GFP controls (using Mann-Whitney test, *** $P < 0.0001$), but DCX-303X was less potent than WT DCX (*** $P = 0.0008$). The same results were obtained in all three independent experiments.



Yap et al. Figure 1

Figure 2: *DCX patient truncations DCX-303X and DCX-272X associate with microtubules.*

(A-E) COS cells were transfected with lamin-cherry to mark transfected cells and with WT DCX or DCX mutants. Cells were either fixed directly or after live detergent extraction in microtubule-stabilizing buffer to determine the ability of DCX and its mutants to remain associated with microtubules.

(A-B) GFP is cytosolic in unextracted cells (A) but completely extracted in detergent (B). WT DCX (C), DCX-303X (D), and DCX-272X (E) all remain associated with detergent-insoluble cytoskeleton. Inserts show high co-localization on microtubules.

(F) Quantification of the fluorescence intensity remaining after extraction normalized to non-extracted cells expressing the same construct. The fluorescence of 50-60 cells was quantified for each condition.

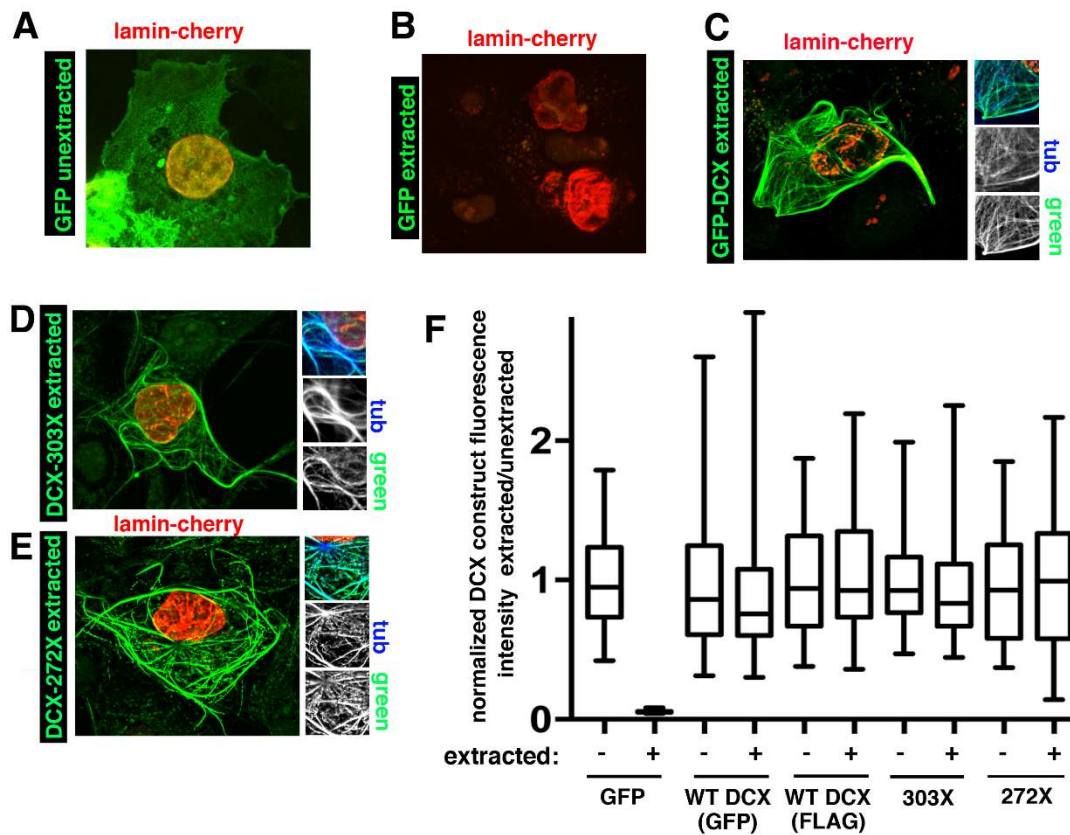


Figure 3: *Spinophilin binding capacity is partially impaired in DCX-272X, but not DCX-303X.*

(A) COS cells were transfected with FLAG-DCX and were either co-transfected with myc-spn (+) or not (-). Immunoprecipitations were performed with an anti-myc antibody and blots probed for the presence of myc-spn and FLAG-DCX. A co-immunoprecipitating DCX band was only observed when myc-spn was co-expressed.

(B) COS cells transfected with WT DCX show extensive co-localization with MTs, but no co-alignment with F-actin.

(C,D) WT DCX was retained prominently on MTs as well on some spn/actin containing structures in COS cells co-expressing DCX and spn. The region indicated with arrows is rich in F-actin and spn, but not MTs. The region indicated with an arrowhead is rich in MTs, but not spn or F-actin. Both contain DCX. This is in striking contrast to the COS cell shown in (B) which does not co-express spn. The inset (D) shows a zoomed-in regions (boxed in C) with the four channels shown in combinations of three markers. A tracing of MTs and F-actin is included for easier comparison of WT DCX staining pattern. The region indicated with arrows is rich in F-actin and spn, but not MTs. The region indicated with an arrowhead is rich in MTs, but not spn or F-actin. Both contain DCX.

(E,F) Co-localization of WT DCX (E), and DCX-272X (F) with spn-enriched protrusions off the dendrite shaft.

(G,H) Myc-spn was co-transfected into COS cells together with WT DCX (lane 1), DCX-272X (lane 2) or DCX-303X (lane 3). DCX-272X was recovered less abundantly after anti-myc immunoprecipitations compared to WT DCX or DCX-303X. One representative experiment is shown in (G). The average and individual data points of several independent immunoprecipitation experiments is shown in (H), normalized to WT DCX (set to 1.0). Error bar indicates 95% confidence interval. $p=0.016$ for DCX-272X ($n=7$), $p=0.94$ for DCX-303X ($n=6$) using Wilcoxon test.

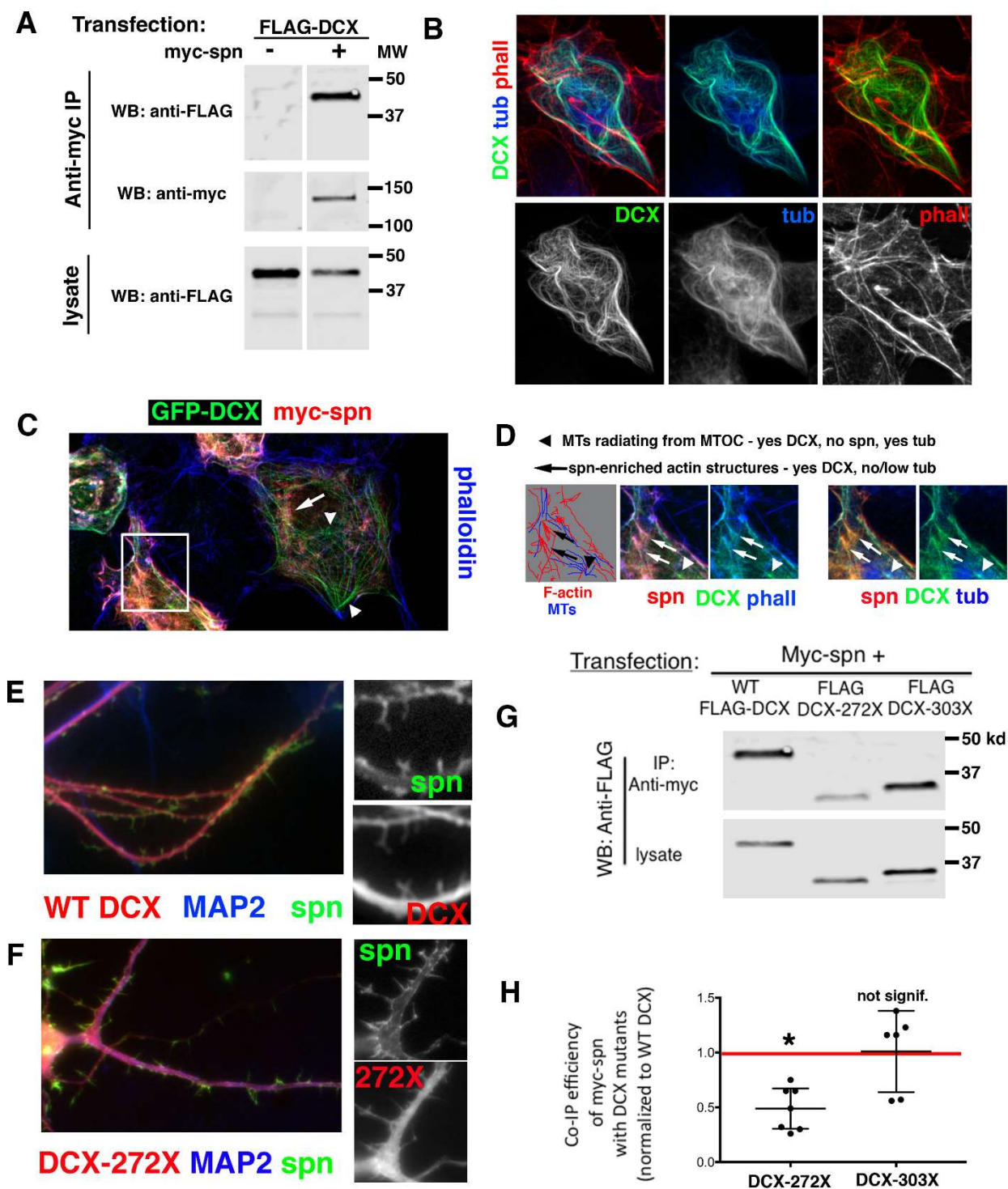


Figure 4: *DCX-246X accumulates in the nucleus and is unstable.*

(A) Quantification of MT association of DCX-246X in detergent-extracted COS cells (details as in Figure 2).

(B) HEK293T cells were transfected with WT FLAG-DCX, FLAG-DCX-246X, or FLAG-DCX-272X. Cells were incubated on ice to disassemble microtubules and then lysed in detergent. The washed insoluble pellet (containing nuclei and intermediate filaments) and the soluble fraction were collected and probed for FLAG, tubulin (tub) and vimentin (vim). All of the tubulin was found in the soluble fraction whereas vimentin was found in the pellet. All of the DCX proteins with the exception of DCX-246X were completely soluble in the absence of assembled microtubules. DCX-246X, on the other hand, was found at lower levels overall and about one third of it pelleted with nuclei and intermediate filaments.

(C) COS cells were transfected with myc-spn and DCX-246X and cells extracted in detergent in microtubule stabilizing buffer. DCX-246X was detergent-resistant and localized prominently with microtubules but not with spn/actin. Single channels are shown in the zoomed-in panels below.

(D) Co-expression of DCX-246X (red) and myc-spn (green) in neurons. MAP2 is counterstained in blue. DCX-246X is restricted to the microtubule-dense dendrite shaft and does not enter spn-enriched protrusions off the dendrite shaft.

(E) COS cells were transfected with GFP-spn (green) and FLAG-DCX-246X (red) and fixed without detergent extraction. DCX-246X was found prominently on microtubules but not on spn-decorated actin structures. Small panels on the right show each individual channel of a zoomed in region as well as tracings for easier comparison. In addition, prominent nuclear association is seen in many cells.

(F) COS cells were transfected with FLAG-DCX-246X and lamin-cherry and imaged with structured illumination microscopy (Zeiss Apotome), taking z-stacks. The bottom and middle sections of the z-stack are shown. DCX-246X is found on cytoplasmic microtubules but also diffusely inside the nucleus. The lamin-cherry channel was used to segment the voxel space corresponding to the nucleus of a different cell. DCX-246X could be seen clearly contained within the nuclear voxel space.

(G) DIV8 neurons were transfected with GFP (green) and FLAG-DCX-246X (red) and counterstained for MAP2 (blue). About half of the transfected cells show prominent nuclear accumulation of DCX-246X with only faint staining of dendrites.

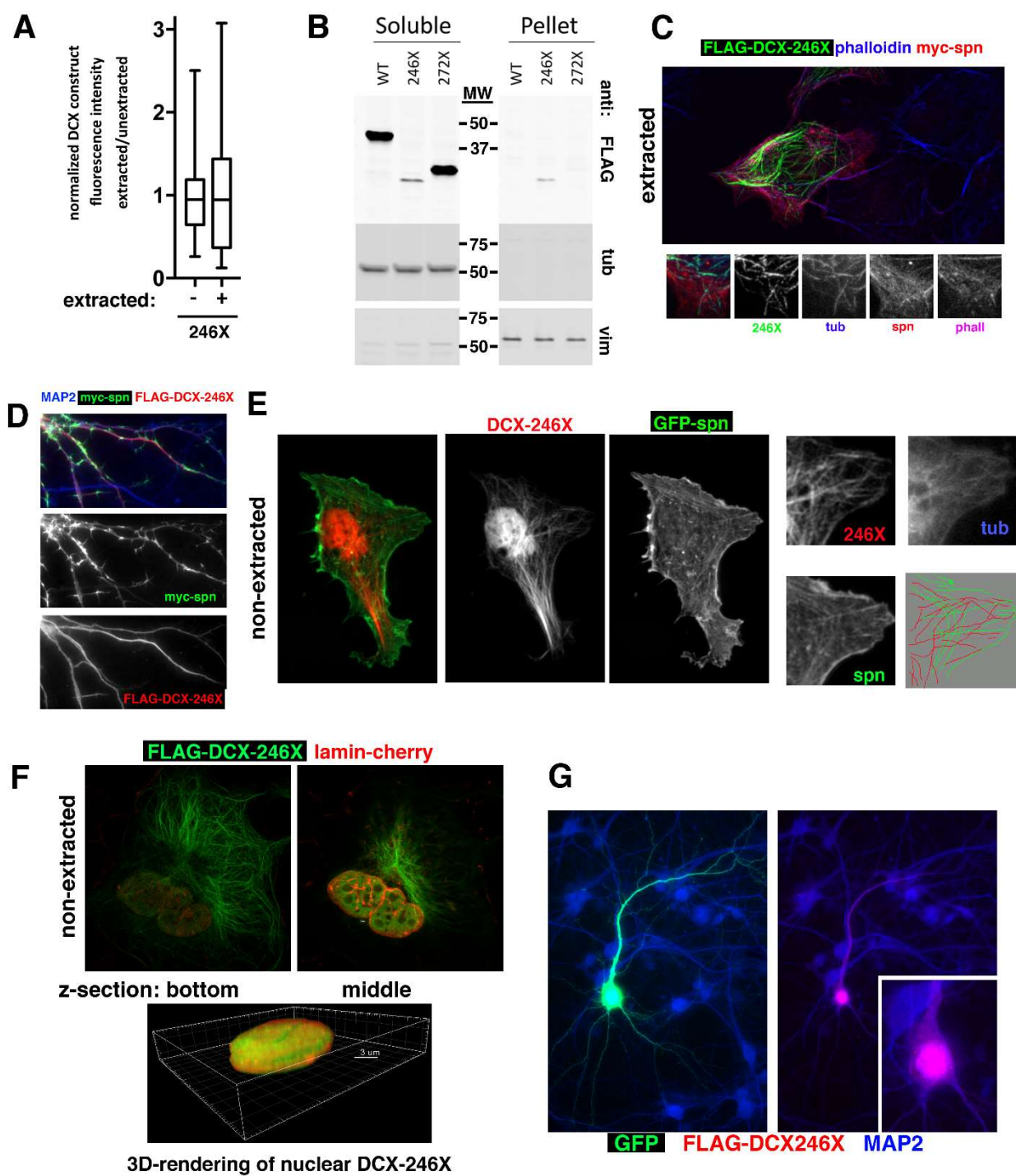


Figure 5: *DCX* alleles *DCX-R89G* and *DCX-R59H* do not associate with MTs and are loss of function alleles.

(A,B) In-cell MT association was assessed as in Figure 2 for DCX-R89G and DCX-R59H. DCX-R89G was completely detergent-extracted (A). Quantification is shown in (B) for 50-60 cells.

(C) Cortical neurons in culture were electroporated prior to plating with DCX or DCX mutants (as in Figure 1), and the number of intersecting dendrites with a circle at 30 μ m diameter was determined five days later (DIV5). Three independent experiments were carried out in separate cultures, and one representative experiment is shown in (C) for WT DCX, DCX-R89G and DCX-R59H. The number of cells quantified in this experiment was: 58 cells for GFP, 61 cells for WT DCX, 34 cells for DCX-R59H, 48 cells for DCX-R89G. Only WT DCX led to statistically significant increase in dendrite complexity compared to GFP controls (using Mann-Whitney test, **** $P < 0.0001$). The same outcomes were obtained in all three independent experiments.

(D,E) Myc-spn was co-transfected into COS cells together with WT DCX (lane 1), or DCX-R89G (lane 2). The average of four independent immunoprecipitation experiments is shown in (E). Error bar indicates sem. One representative experiment is shown in (D) from the same blot with an intervening irrelevant lane removed.

(F) COS cells were transfected with myc-spn and DCX-R89G and cells extracted in detergent in microtubule stabilizing buffer. Unlike in panel (A), DCX-R89G was detergent-resistant in the presence of co-expressed myc-spn and localizes prominently to spn/actin structures.

(G) DCX-R89G (red) was able to associate with spn/actin-rich protrusions (green) off the dendrite shaft in neurons.

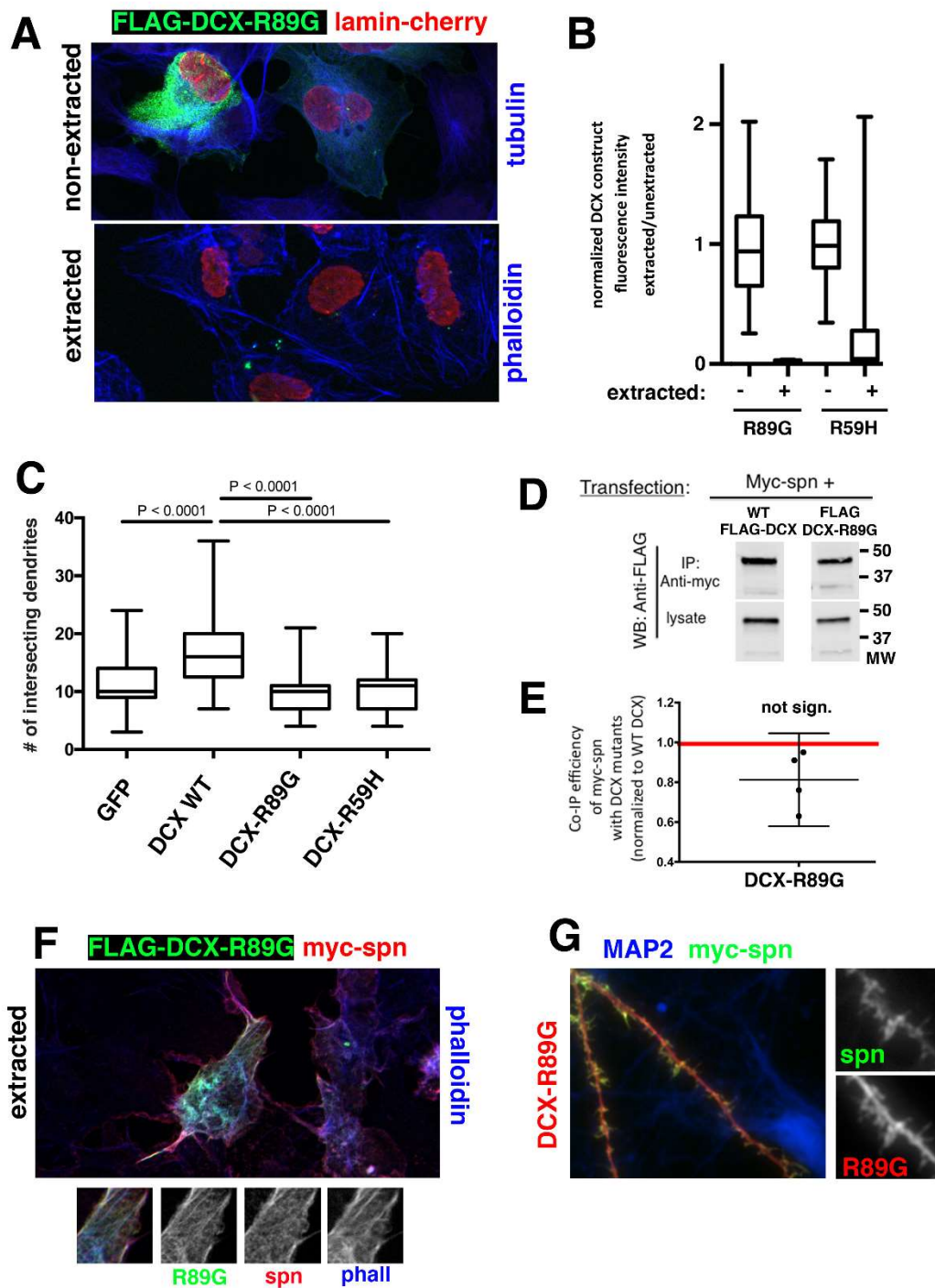


Figure 6: The DCX-R59H patient allele forms cytoplasmic aggregates enriched in spn, HSP70, ubiquitin and autophagosome proteins.

(A) DCX-R59H forms detergent-resistant cytoplasmic aggregates in COS cells. A1 is a merged image of the individual channels shown in A2-4.

(B) In COS cells co-expressing myc-spn, DCX-R59H becomes detergent-resistant and co-localizes strikingly with F-actin and spn. This suggests that DCX-R59H retains spn binding. B1 is a merged image of the individual channels shown in B2-4.

(C,D) DCX-R59H forms cytoplasmic aggregates in DIV8 neurons which contain some MAP2 and actin (C). D shows single channel close-ups of soma for DCX-R59H (D1), MAP2 (D2) and phalloidin (blue in D3 and D4). Arrows point at location of DCX-R59H aggregates.

(E) Ruby-LifeAct (red) decorates F-actin rich structures at the tip and off the shaft of dendrites (E'). This pattern is not disrupted by DCX-R59H containing cytoplasmic aggregates (E", green), but each aggregate contains some Ruby-LifeAct. MAP2 is counterstained in blue.

(F) Localization of myc-spn (red) in DIV8 neurons in the absence of DCX-R59H (F1), in the presence of non-aggregated DCX-R59H (F2), and in the presence of aggregated DCX-R59H (F3). DCX-R59H localizes to spn-enriched dendritic protrusions when not aggregated (F2), but disrupts the off-shaft localization of myc-spn when aggregated, pulling it completely into cytoplasmic aggregates in the dendritic shaft (F3). MAP2 is counterstained in blue.

(G) DIV8 neurons were transfected with DCX-R59H (green) and fixed 24 hours later. They were counterstained with antibodies to endogenous MAP2 (blue) and hsp70 (red) (G1), endogenous spn (blue) and ubiquitin (red) (G2), endogenous p62 (red) and ubiquitin (blue) (G3).

(G4-5) In order to visualize autophagosomes, neurons were transfected with DCX-R59H (green) and RFP-LC3 (red) and fixed after 24 hours. Cells were additionally stained against endogenous ubiquitin (blue) (G4) or endogenous p62 (blue) (G5).

Arrows point at DCX-R59H containing cytoplasmic aggregates.

